

H4. SMR/1247
Lecture Note: 24

**WORKSHOP ON PHYSICS OF
MESOSPHERE-STRATOSPHERE-TROPOSPHERE
INTERACTIONS WITH SPECIAL EMPHASIS ON MST
RADAR TECHNIQUES**

(13 - 24 November 2000)

METEORS AS TOOLS FOR ATMOSPHERIC RESEARCH

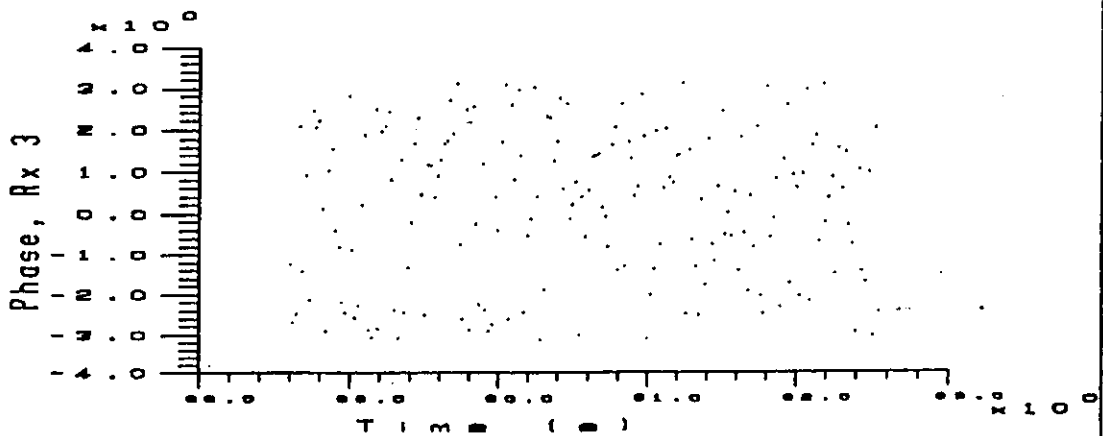
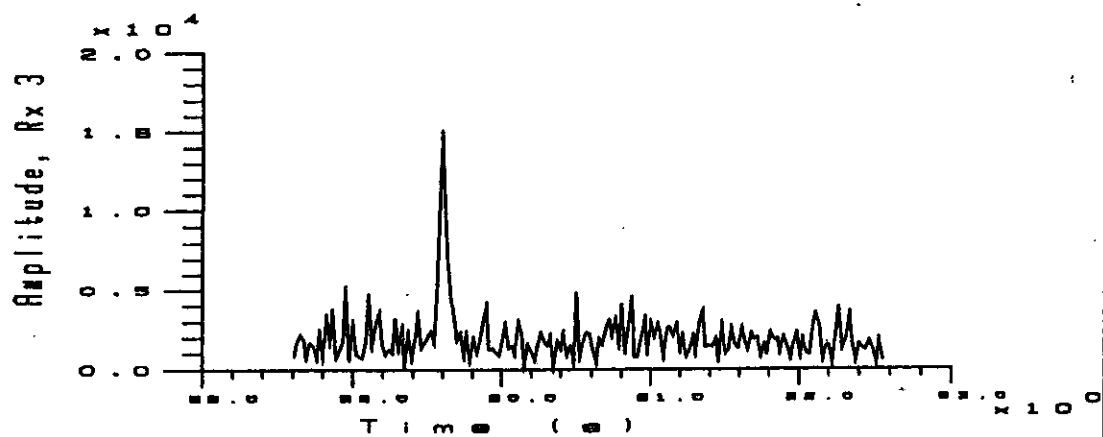
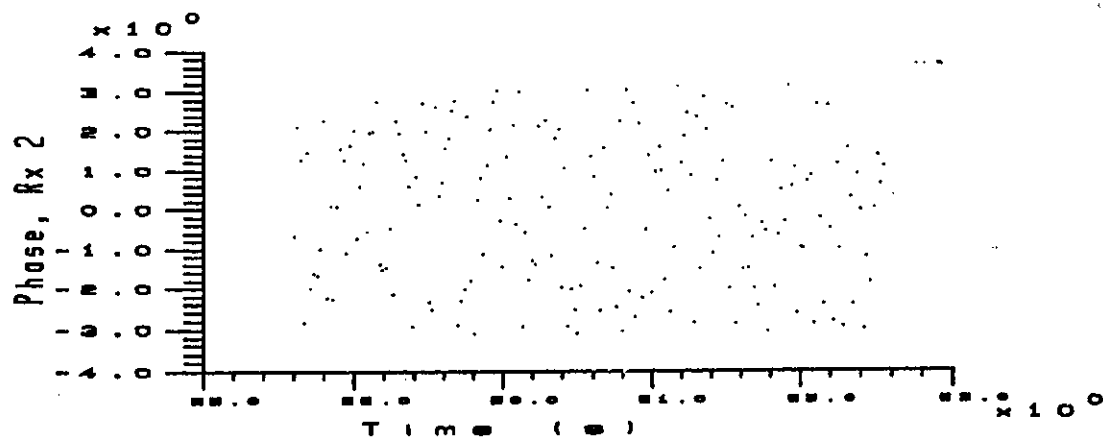
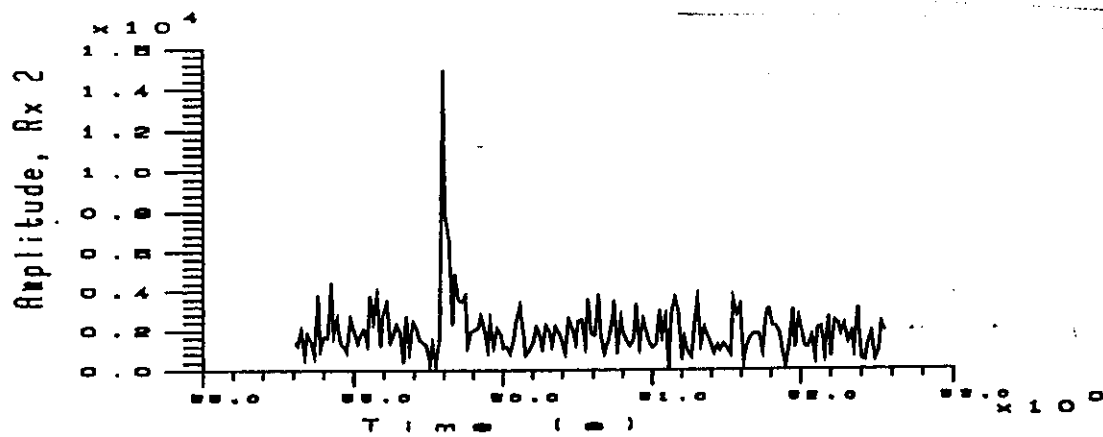
Prof. W. K. Hocking

Dept. of Physics
University of Western Ontario
London, Ontario
CANADA

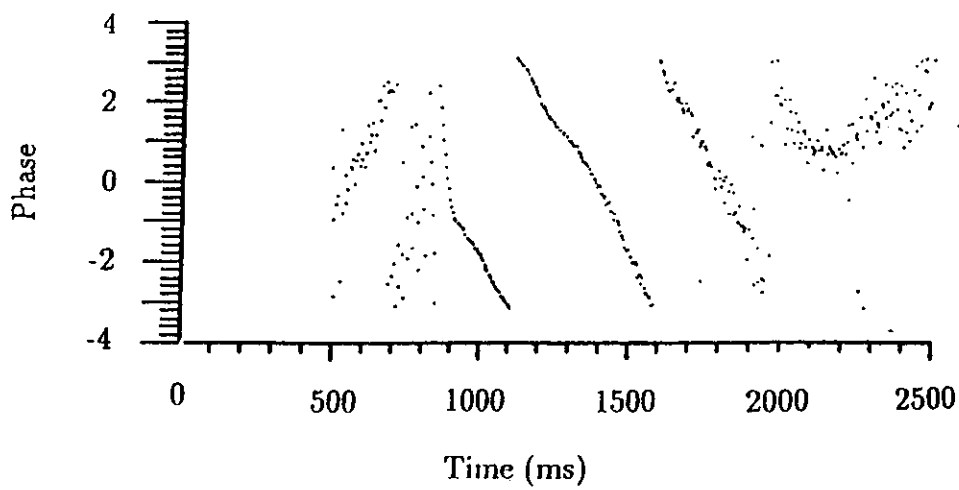
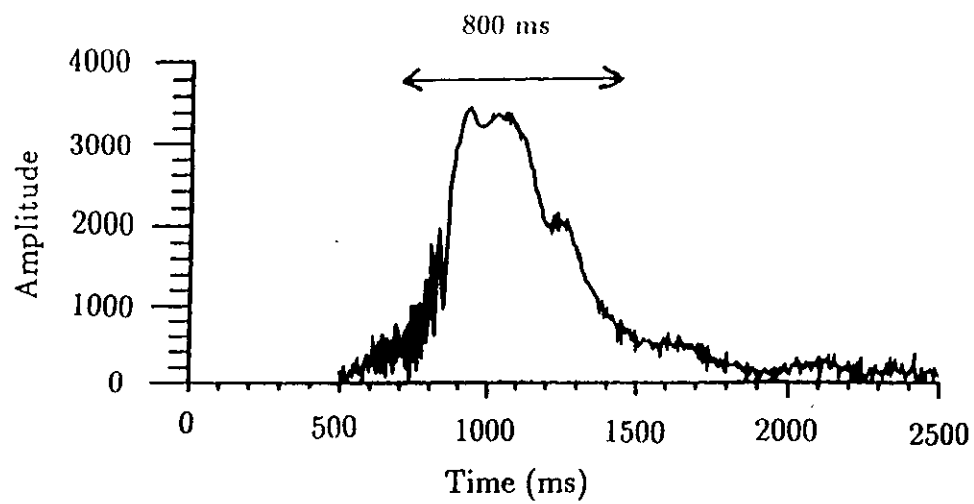
Meteors as tools for atmospheric research

- ref... McKinley.

- small fragments of sand and dust (and occasionally larger) entering the Earth's atmosphere at speeds of $12-72 \text{ km s}^{-1}$.
 - vapourize the air around them and form ionized trails
 - radio-waves incident upon the trail are reflected (totally or partially), and therefore can be used as a means to identify and track the trails.
 - characterized according to the number of electrons per unit length along the trail - the so-called line-density, q . e.g. line density of 10^{10} electrons per metre corresponds to a mass of 10^{-6} grams and a velocity V of 35 m s^{-1} .
 - another important parameter is the zenithal maximum ionization, q_z , where $q_z = q/(\cos\chi)$ and χ is the zenithal angle of the meteor.
 - may be overdense ($q > 10^{15} \text{ m}^{-1}$) or underdense ($q < 10^{13} \text{ m}^{-1}$) meteors.
- Note that whilst one might initially expect the "break" between the two modes to be frequency dependent, this is not true - turns out $\S 0$ because the trail diameter is small enough that evanescent electromagnetic waves generated in the trail in the case of critical reflection compensate for the fact that one might normally expect a frequency dependence).
- underdense meteors show fast rise time ($< 0.1 \text{ s}$), generally exponential decay, and lifetimes less than about 0.4 s . Overdense ones often show an oscillatory type of decay, and have lifetimes exceeding 0.4 s - up to even tens of seconds.
 - To be detected, the meteor trail must be orientated perpendicular to the vector from the radar to the trail (monostatic radar). It is possible for a trail to form at some other angle and then be twisted by the wind so that some portion of it is specularly reflecting. In such cases the rise-time is often more than 0.1 s .

Under dense meteor

321



Over dense melodic

Sources of meteors.

- Debris floating around the solar system - particularly remnants of long-gone comets or asteroids.
 - two main types - sporadic and showers.
- showers are increased occurrence of meteor activity, due to clusters of meteoric material in moderately tightly clustered orbits which are probably recently destroyed comets or asteroids. The Earth's orbit intersects these orbits, and leads to increased meteor activity.
- sporadic meteors were once considered to be meteoric debris drifting randomly in the solar system. They occur all the time.
- The meteor activity generally peaks at around 6 am in the morning, and this was previously assumed to be due to the fact that at this time of day the Earth is moving into its surrounding solar system environment and therefore encounters more meteors (see diagram) (it essentially collides with the meteors). Objects coming from behind must move faster than the Earth in order to catch up to it.
- BUT recent research (e.g. Jones^{Brown} 1994) has shown that even these "sporadic" meteors belong to (very ancient and spread-out) meteor streams, presumably due to very old comets or asteroids which broke up a long time ago. Indeed this also accounts for why there often seems to be a secondary maximum in the mid afternoon. (see over)

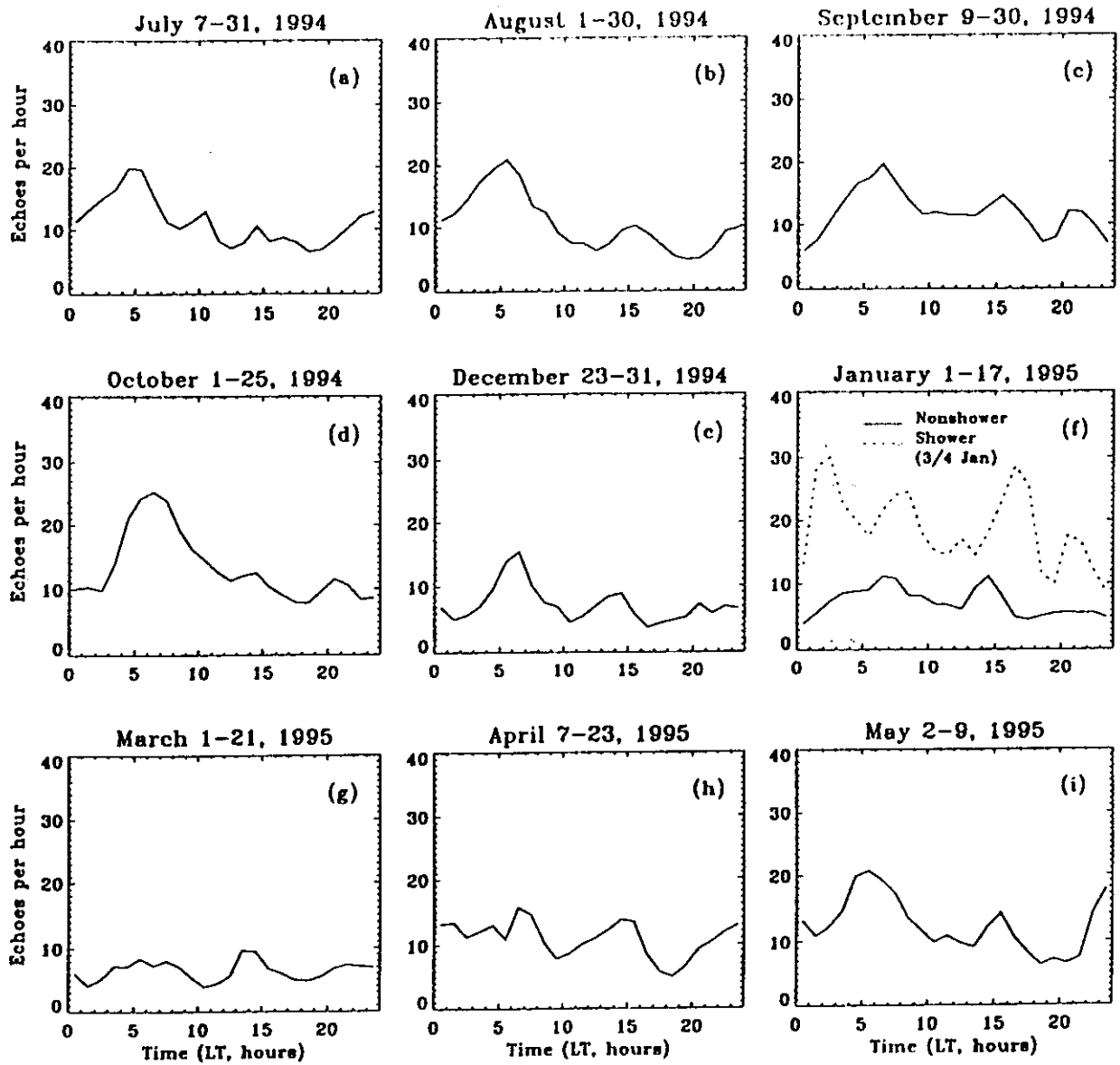
Typical meteor count rates with the CLOVAR (a typical meteor radar situated at London Ontario) are shown over the page, together with information about meteor showers. Note that the system was not optimized - much higher count rates are possible with an optimized system. Note also that the seasonal variations may be contaminated by system modifications which were periodically applied to improve the system.

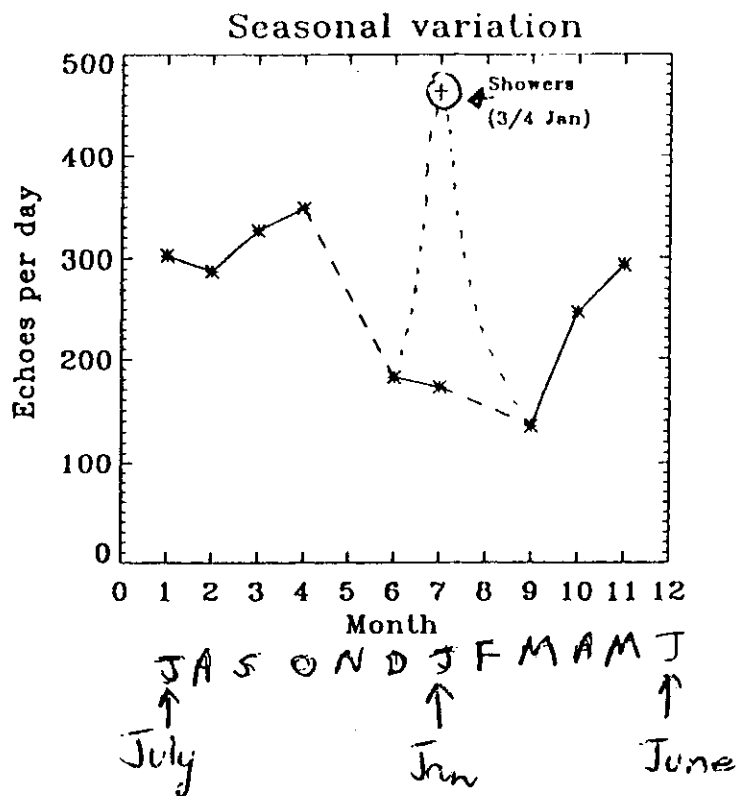
TABLE 40. PRINCIPAL METEOR SHOWERS

Shower	Epoch		Radiant		Notes
	Normal limits	Max.	R.A.	Dec.	
			h m °	°	
Quadrantids	Jan 1-5	Jan 4	15 28 (232)	+ 50	Medium speed. Blue. Many faint meteors.
*Corona Australids	Mar. 14-18	Mar. 16	16 20 (245)	- 48	
Lyrids (April)	Apr. 19-24	Apr. 21	18 08 (272)	+ 32	Fast moving. Brilliant.
η -Aquarids	May 1-8	May 5	22 24 (336)	0	Very fast. Persistent trains.
Lyrids (June)	Jun. 10-21	Jun. 15	18 32 (278)	+ 35	Blue.
*Ophiuchids	Jun. 17-26	Jun. 20	17 20 (260)	- 20	
Capricornids	Jly 10-Aug. 15	Jly 25	21 00 (315)	- 15	Yellow. Very slow.
δ -Aquarids	Jly 15-Aug. 15	Jly 28	22 36 (339)	- 17	Slow. Long paths.
			22 36 (339)	0	
*Piscis Australids	Jly 15-Aug. 20	Jly 30	22 40 (340)	- 30	
α -Capricornids	Jly 15-Aug. 25	Aug. 1	20 36 (309)	- 10	Yellow.
ϵ -Aquarids	Jly 15-Aug. 25	Aug. 6	22 32 (338)	- 15	
			22 04 (331)	- 6	
Perscids	Jly 25-Aug. 18	Aug. 12	03 04 (046)	+ 58	Very fast. Fragmenting.
κ -Cygnids	Aug. 18-22	Aug. 20	19 20 (290)	+ 55	Bright. Exploding.
Orionids	Oct. 16-27	Oct. 21	06 24 (096)	+ 15	Very fast. Persistent trains.
Taurids	Oct. 10-Dec. 3	Nov. 1	03 28 (052)	+ 14	Slow. Brilliant.
			03 36 (054)	+ 21	
Leonids	Nov. 15-19	Nov. 17	10 08 (152)	+ 22	Very fast. Persistent trains.
*Phenicids	—	Dec. 4	01 00 (015)	- 55	
Geminids	Dec. 7-15	Dec. 14	07 28 (112)	+ 32	White.
Ursids	Dec. 17-24	Dec. 22	14 28 (217)	+ 78	

*Visible in southern hemisphere only.

(Norton's star atlas)





VB affected by changes in
 optimization + variations
 in local noise levels
 (esp. Dec, March)

The factors which determine the amplitude of a radar echo from an underdense meteor trail during the formation and initial evolution of that train have been reviewed (amongst others) by Greenhow and Hall [1955]; Greenhow and Newfeld [1955]; Greenhow and Hall [1960]; McKinley, 1961; Olsson-Steel and Elford [1987], Thomas et al [1988], and Steel and Elford [1991]. The main factors which cause the attenuation in echo amplitude are (1) the initial radius of the trail (2) the finite meteor velocity effect and (3) ambipolar diffusion. The attenuation factors given throughout in this section are those describing the attenuation in amplitude rather than in power.

The initial meteor trail with radius r_0 , (usually defined as the half-amplitude half-width of the electron density distribution assumed to be Gaussian), will reduce the returned echo amplitude relative to complete reflection by a factor

$$\alpha_r = \exp\left(\frac{-4\pi^2 r_0^2}{\lambda^2}\right) \quad (7.2)$$

where λ is the radar wavelength [e.g., Baggaley, 1970]. This initial radius is thought to be due to the fact that the evaporating meteoric species initially have forward velocities close to the translational velocity of the meteor (which is in the 12-72 km/s range), this being about two orders of magnitude higher than the diffusive velocities of atmospheric species in the meteor region [Greenhow and Hall, 1960; McKinley, 1961]. The meteor trail is therefore formed with a certain radius and this arises essentially instantaneously. The initial radius of the meteor trail, r_0 , in the 80-120 km height range is approximated by [Baggaley, 1980, 1981]:

$$\log_{10} r_0 = 0.019h - 1.92 + \log_{10}\left(\frac{V}{40}\right) \quad (7.3)$$

where h is the height in km and V is the meteor velocity in km/s; r_0 is then in m. As an example, if $V = 40$ km/s and $h = 88$ km (this height is taken as an example in this section because we shall see later that height distributions of the meteors peak around 88 km), then $r_0 = 0.56$ m and so for $\lambda = 7.375$ m (as in our case) the initial radius attenuation factor α_r is 0.8, while at $h = 110$ km, $\alpha_r = 0.2$. Considering only the initial radius effect, it can therefore be seen that a 7.375 m wavelength meteor radar has a very low probability of detecting any meteors forming above about 110 km.

(Some of this text refers specifically to LLORAR, a 40.68 MHz radar system)

The second factor to be considered is the effect of the finite meteor velocity [Kaiser, 1953]. The radio echo is dominated by the contribution of the first Fresnel zone of the trail, which the meteor takes a finite time to cross. If, by the time the meteor has reached the end of this zone, the trail has diffused to reach a width comparable to the wavelength, then the

echo amplitude will be severely attenuated. Clearly this effect depends upon the length of this zone, $2 \left(\frac{R\lambda}{2}\right)^{\frac{1}{2}}$, where R is the meteor range from the observatory site [e.g., Greenhow and Hall, 1960]. Note that $\left(\frac{R\lambda}{2}\right)^{\frac{1}{2}}$ is the radius of the first Fresnel zone. The attenuation in echo amplitude is then given by a factor

$$\alpha_V = \exp\left[-16\pi^2\left(\frac{D}{V}\right)\left(\frac{R}{2\lambda^3}\right)^{\frac{1}{2}}\right] \quad (7.4)$$

where D (m^2s^{-1}) is the ambipolar diffusion coefficient [McKinley, 1961]. Thus, although the first Fresnel zone increases in length with wavelength, in fact the finite velocity effect is reduced by using a longer wavelength. It should be noted that the finite velocity effect has the opposite trend to the initial radius effect; at any particular height the former is more severe for slower meteors. Note also that α_V approaches unity as V becomes very large. According to McDaniel and Mason [1973], the ambipolar diffusion is related to the zero field reduced mobility K by the expression:

$$D = 6.39 \times 10^{-2} \frac{T^2 K}{p} \quad (7.5)$$

where typically $K = 2.2 \times 10^{-4} \text{ m}^2\text{s}^{-1}\text{V}^{-1}$ and the temperature T (K) and pressure p (Pa) are functions of the height h (km). Using the U.S. Standard Atmosphere D is approximated over the height range 80-125 km by [Thomas et al., 1988]:

$$\log_{10} D = 0.0758h - 6.51 \quad (7.6)$$

As an example, if $h = 88$ km, then $D = 1.45 \text{ m}^2\text{s}^{-1}$ and so for $V = 40$ km/s, $\lambda = 7.375$ m and $R = 130$ km, we find $\alpha_V = 0.93$. At 110 km, λ_V is dramatically reduced to about 0.04. This shows that detectable echo amplitudes at 7.375 m radar wavelength are generally fairly unlikely above 100 km. It should be noted that, on occasions, larger temperature gradients are found in the meteor region and the relationship between $\log_{10} D$ and h is then no longer linear.

Another influence, (although of little importance here), is that meteors forming at heights of ≤ 78 km have a decreased probability of detection due to the rapid loss of ionization due to the transfer of charge from atomic oxygen ions, with molecular ions being formed [Jones, 1975; Baggaley, 1978, 1979]. At all heights, but especially in the lower regions, wind distortion of trails can lead to the non-observation of many meteors, or the multiple observation of some trails due to glinting as sections of the trail are blown into orientations which are orthogonal to the radar beam [McKinley, 1961; McIntosh, 1969].

The ionized trail dissipates by ambipolar diffusion, turbulence and chemical and ionic processes. Diffusion dominates for a few seconds while turbulence is the chief mechanism for trails lasting 30 s or more. Once the meteor trail has formed, the expansion of the column of ions and electrons due to radial diffusion causes the returned echo amplitude to decay exponentially with time in the manner

$$A = A_0 \exp\left(\frac{-t}{\tau_d}\right) \quad (7.7)$$

where A_0 is the initial amplitude and A is the amplitude after time t . The echo decay time constant τ_d is given by

$$\tau_d = \frac{\lambda^2}{16\pi^2 D} \quad (7.8)$$

which defines the duration to $1/e$ of the initial amplitude. Note that τ_d depends only upon the wavelength and diffusion coefficient [e.g., Herlofson, 1948]. Thus at a given λ and D the echoes from all underdense trails decay with the same time constant. Echoes from underdense trails are therefore referred to as 'decay-type-echoes' [Phillips, 1969]. As an example, if $h = 88$ km, $D = 1.45 \text{ m}^2\text{s}^{-1}$ and $\lambda = 7.375$ m the decay time constant is 0.24 s. Underdense trails at observable heights therefore have durations of about a few tenths of a second. In contrast to 88 km, at 110 km height the time decay constant is reduced to about 5 ms and trails become very difficult to detect unless the radar wavelength is increased. For example, at $\lambda = 50$ m and $h = 110$ km, the time decay constant has increased to about 0.24 s. It is noteworthy that for wavelengths below 15 m (or frequencies above 20 MHz) the decay time is short compared to the time taken for the wind to distort the trail from its initial straight line. However at long wavelengths (or low frequencies, e.g., 2 MHz) this is no longer the case and most trails are bent from a straight line (or deformed by wind shear) during the life time of the echo. Thus the exponential decay in strength of an echo has fluctuations due to focusing and defocusing superimposed on it, and it becomes difficult to determine the decay time constant.

It is interesting to note that if the pulse repetition frequency (prf, number of pulses per second) of the radar is low, then it is possible that fast-decaying echoes are less likely to be seen by the radar. That is rapid diffusion of the trail occurs between pulses so that the first observed echo is attenuated by this effect, making meteor detection less likely [Steel and Elford, 1991]. In addition, if the prf is low the long duration of the echoes (because of the long decay time constant) does lead to confusion between new meteor echoes, drifting meteor trails, and patches of sporadic E-region ionization. Thus an attenuation factor incorporating the effect of diffusion during the inter-pulse period is necessary. This factor is given by Steel

and Elford [1991]:

$$\alpha_d = \exp\left(\frac{-16\pi^2 D}{\lambda^2(\text{prf})}\right) \quad (7.9)$$

where the prf is in Hz. This assumes that the trail is formed just after the instant of passage of a transmitted pulse; a more precise expression for a particular experiment would be dependent upon the exact meteor recognition criteria used (*e.g.*, single pulse return above some threshold, two successive pulses, a running average, etc) [Steel and Elford, 1991] (also see Section 7.2.2).

The resultant effect of a trail's initial radius, finite velocity of formation and diffusion, is a significant attenuation of the radar echo so that an effective 'ceiling' of about 110 km occurs for observations at 40.68 MHz (corresponds to 7.375 m wavelength). Thus, the average echo height of meteors becomes a function of frequency.

[Hall, 1960; Thomas et al., 1988]

The individual attenuations from equations (7.2), (7.4), and (7.9) give a total attenuation in the returned amplitude from an underdense meteor trail of:

$$\alpha = \alpha_r \alpha_v \alpha_d \quad (7.11)$$

[*e.g.*, Steel and Elford, 1991]. Figure 7.1 ^{not shown.} shows the attenuation factors for our 40.68 MHz radar frequency. (The method of data collection is described in Section 7.2 of the current chapter.) The values of the four α 's are plotted as functions of height at three velocities (20, 40, 60 km/s). The pulse repetition frequency used was 1100 Hz (sometimes we use 2143 Hz, see Section 7.2.1), as in the actual data collection. The range used in the computation was $R = 130$ km since data were collected in the 78-110 km height region; we have assumed $\theta = 53^\circ$, where θ is the angle from zenith (this will be discussed shortly, see Section 7.2.4). At $V = 20$ km/s, the finite velocity effect α_v dominates the net attenuation and $\alpha = 0.5$ at $h \approx 96$ km; but at $V = 40$ km/s, the initial radius term α_r has taken control and $\alpha = 0.5$ at ~ 95 km; at $V = 60$ km/s, the initial radius term totally dominates and $\alpha = 0.5$ at ~ 90 km. This clearly indicates that the radar is insensitive to high velocity underdense meteors.

The initial echo power in watts, from underdense reflection, assuming the initial trail radius to be much smaller than the wavelength employed, is given by the radar equation



Distribution of meteors as a function of height determined with a 2 MHz radar.

Note that the meteor max is at ~ 104 km, showing that the ^(normal) maximum of the count rate at $\sim 88-90$ km is a function of the radar frequency (see shortly)

Olsson-Steel & Elford, JATP, 49, 243, (1987)

Height distribution of radio meteors

255

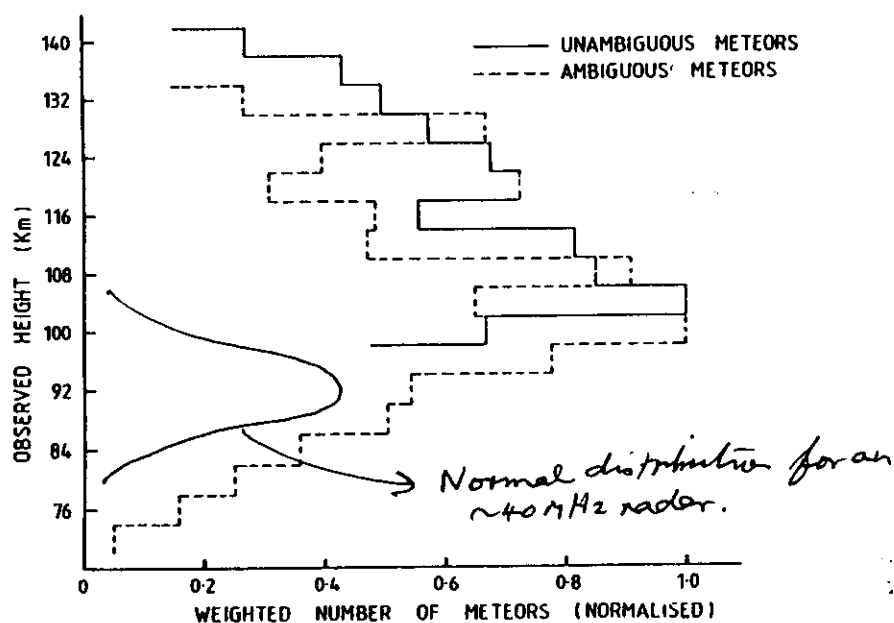


Fig. 4. The true height distributions of meteors to radio magnitude +7 observed at 2 MHz, obtained from the data sets shown in Fig. 3 by correcting for height-selection effects.

[McKinley, 1961; Thomas et al., 1988; Steel and Elford, 1991]

$$P_r = 2.5 \times 10^{-32} \left(\frac{\lambda}{R} \right)^3 P_t G_t G_r q^2 \quad (7.12)$$

where λ is the radar wavelength, R is the echo range, P_t is the transmitted power, G_t and G_r the gains with respect to an isotropic antenna of the transmitting and receiving systems respectively. The above attenuation factors mean that the expression (7.12) for the initial echo power must be modified to become:

$$P_r = 2.5 \times 10^{-32} \left(\frac{\lambda}{R} \right)^3 P_t G_t G_r \alpha^2 q^2 \quad (7.13)$$

7.1.4 Radar detection of meteors at low frequency

Most meteor radars have customarily been operated at radio frequencies of around 20-60 MHz (5-15 m wavelengths) in order to avoid problems associated with reflection or absorption of the radio wave in the ionosphere. It is suggested that the 'missing mass' in the $10^{-6} - 10^{-2}$ g range of interplanetary material might be held in a faint, high velocity component which could be undetected since it ablates at high altitude [Hughes, 1978]. Hughes [1978] argued that only 3-4 % of the meteoric mass incident upon the upper atmosphere in the $10^{-6} - 10^{-2}$ g range is being detected by conventional radio meteor techniques. This would imply that the vast majority of meteoric material is deposited into the atmosphere above 100 km, having important ramifications for the aeronomy and other branches of the atmospheric sciences. The existence of such high velocity, low mass meteors would also be significant in relation to the origin and evolution of the meteoroidal complex in the solar system.

Conventional meteor radars, operating at wavelengths of around 5-15 m (20-60 MHz frequency), are unable to detect high altitude meteors due to the wavelength dependent echo ceiling (see Section 7.1.3). The diameter (or width) of an underdense ionized trail increases monotonically with height in the 80-140 km region due to the increase in the molecular mean free path with diminishing air density. Consequently, a rapid growth with height occurs both in the initial radius of a forming trail and also in its rate of expansion due to the mechanism of ambipolar diffusion during the finite time required for the meteor to traverse the central (first) Fresnel zone of the radar (so-called finite velocity effect, also see Section 7.1.3). The echo ceiling begins to act at heights for which the diameter of a trail approaches the dimensions of an appreciable fraction of the wavelength, when destructive interference between waves reflected from the front and back of the trail's cylindrical cross-section causes increasing attenuation of the backscattered signal.

Use of meteor trails for atmospheric studies

It is generally believed that meteor trails, once formed, drift with the neutral wind. Nevertheless, one must be cautious - above 100 km the effects of electric and magnetic fields may make this assumption questionable. Kaiser (1969) have investigated this theoretically and have found that generally the trails do drift with the neutral wind for heights below 95 km, and *provided that the trail is aligned at least 2° away from the direction of the Earth's magnetic field.*

Generally pulsed radars should be used for meteor work - in past years CW systems have been used, and heights determined by decay times, but this is crude and unreliable.

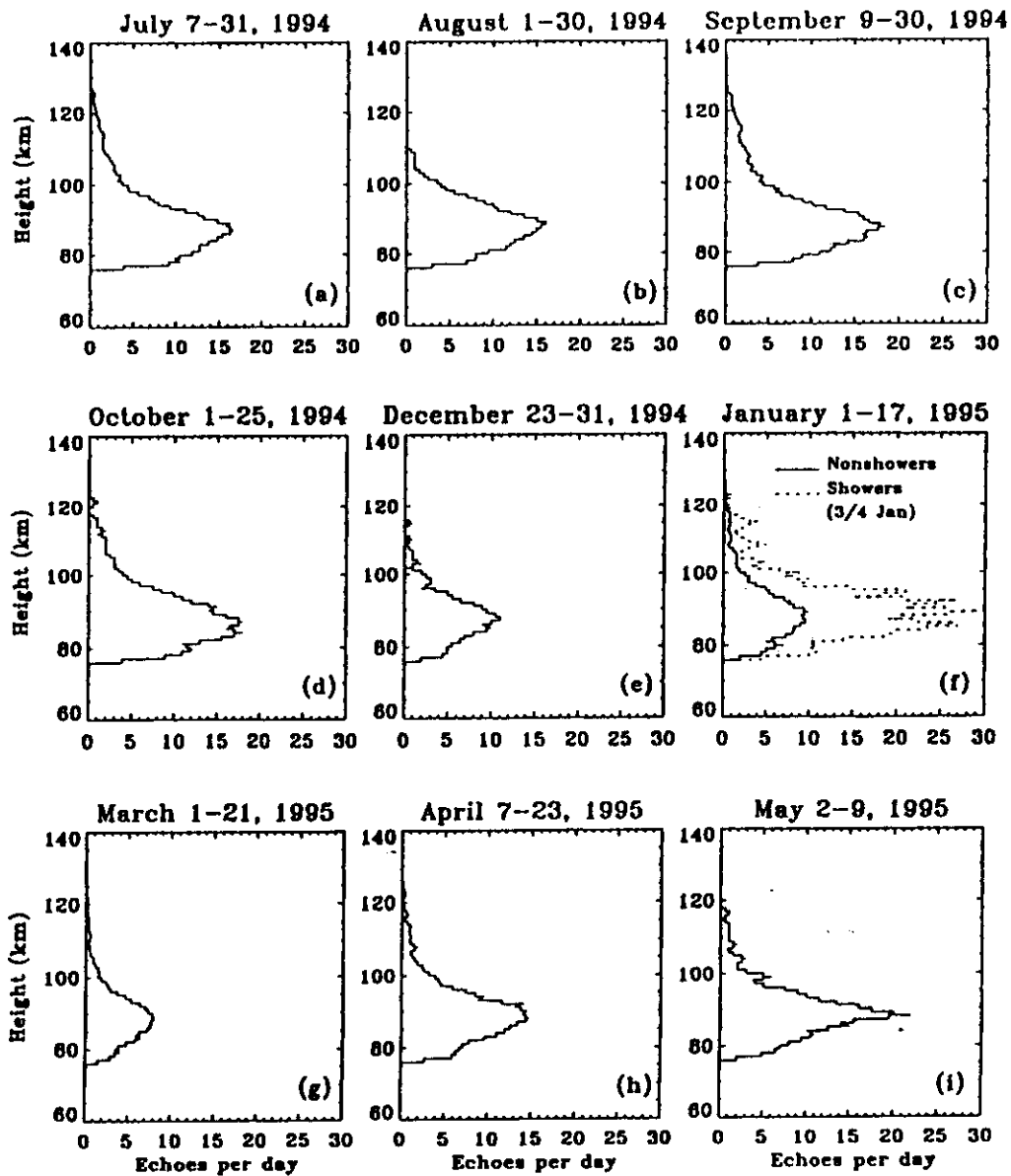
The optimum frequency range is 15 - 60 MHz. Meteors are certainly detectable at lower frequencies (and to higher heights, as seen), but are much harder to detect because they are often hidden in the normal D-region scatter.


In this frequency range ^(15-60 MHz), the meteor count rate generally peaks at about 88-92 km altitude - see attached diagram.

Sometimes secondary maxima are detected higher up, during certain showers (e.g. Leonids, Orionids).

Height distribution for a 40 MHz radar

333



CLOVAR 
(UWO motion)

Typical radar configurations

- Two main types of instruments

(a) Narrow beam (b) Interferometer

(a) Narrow beam Doppler this category is simple - high gain antennas pointed to particular directions of sky, and standard Doppler procedures used to obtain radial velocities (e.g. MEDAC (Avery), Cervera and Reid, Radio Sci., 1995).

Major problem with this method is the possibility of large meteors being detected in the sidelobes - the user is not aware that these meteors are not in the main beam and therefore obtains an erroneous radial velocity.

Nevertheless, majority of meteors do appear to lie in the main beam.

(b) Interferometry In this procedure, one transmits on a moderately isotropic beam, and receives using spaced antennas on the ground (at least 3). Phase differences of the signals received by the receiving antennas are used to determine the location of the meteor in the sky.

This procedure is to some extent superior, but some care is needed.

(i) The spacing of the antenna must be chosen carefully. If a spacing in excess of $\lambda/2$ is used, there are ambiguities of direction of arrival (see diagram over page)

(ii) If the antennas are closer together than about λ , then antenna coupling can be severe and introduce biases into the phase differences between antennas. An antenna spacing of $\lambda/2$ should NEVER be used.

(iii) These two apparently conflicting requirements are resolved in one of two ways
- either one uses moderately high gain receiver antennas (e.g. multi-element Yagi's)
(eliminate grating lobes) OR

- one uses extra antennas to help remove the ambiguities.

Most systems adopt the former approach. At the University of Western Ontario, the CLOVAR radar uses the former, although it is not optimized. It is able to unambiguously resolve 70% of all meteor echoes for details, see talk later on in this workshop).

An even better arrangement is to use 5 antennas spaced as shown in the diagram on the attached diagram (courtesy of Prof. Jim Jones, UWO).

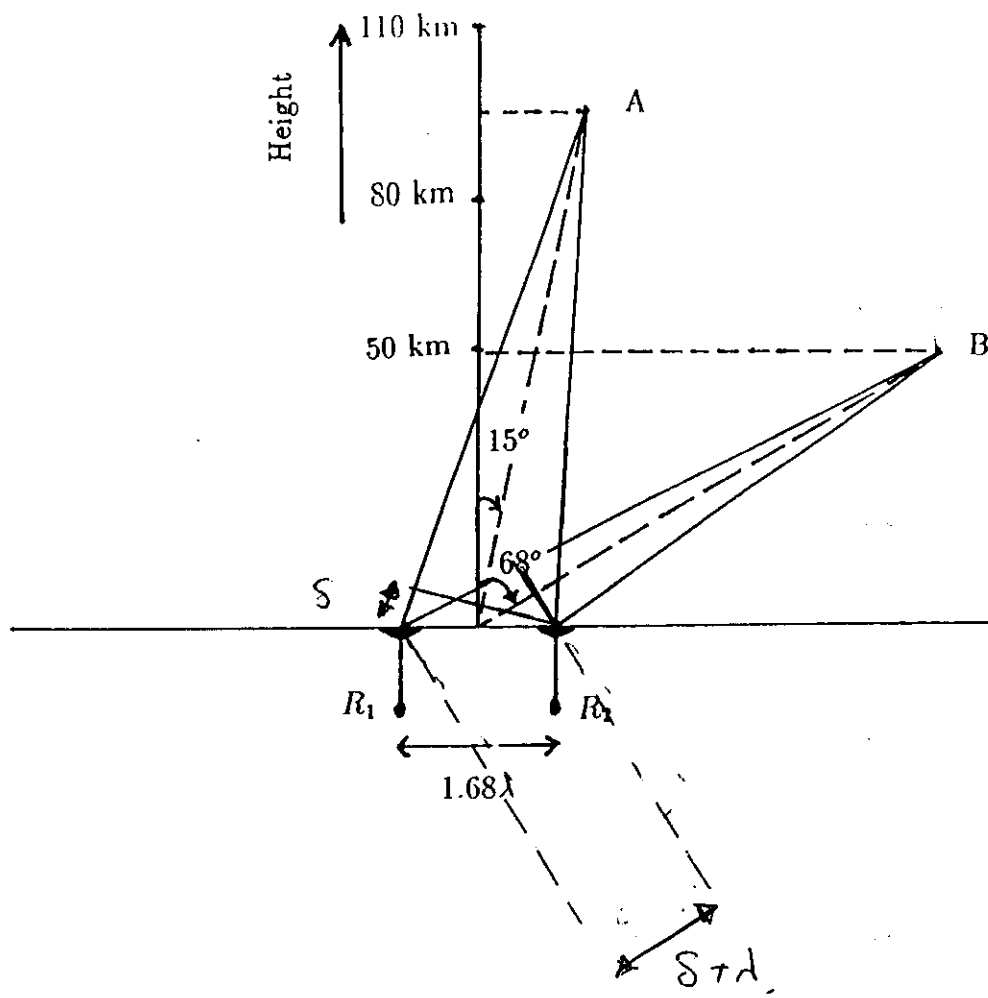
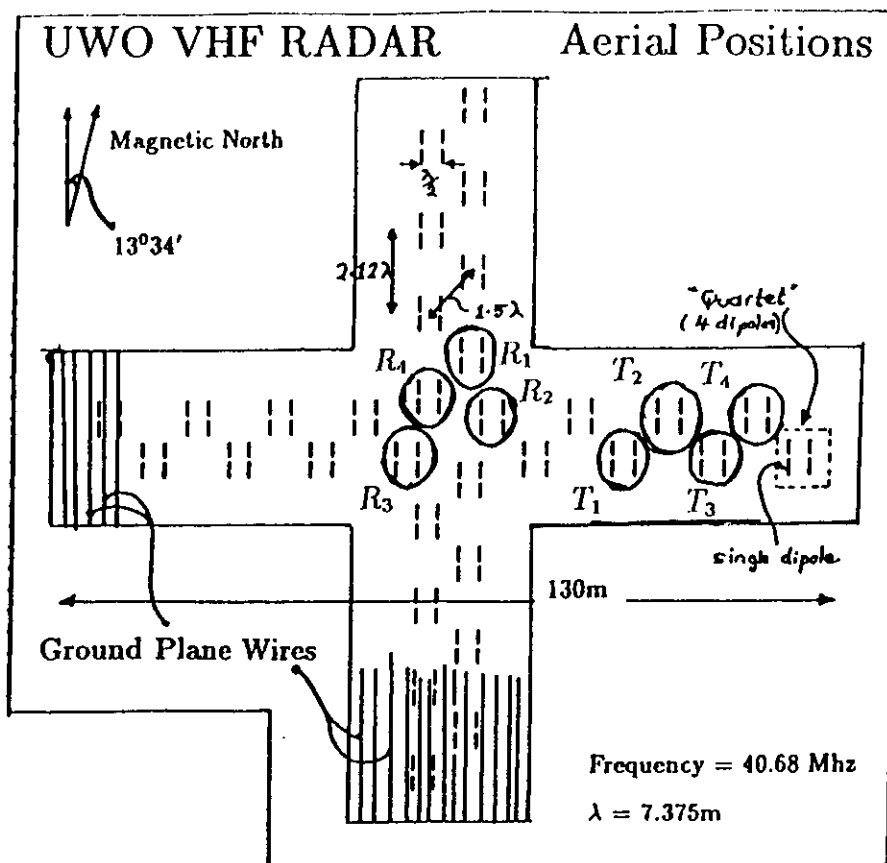
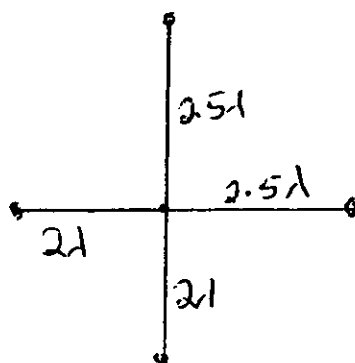


Illustration of angular ambiguity.



Rx antennas used with CLOVAR.



OPTIMUM Rx SPACING USED BY JIM JONES,
UWO.

Detection algorithms

Detection algorithms vary from author to author, but generally involve looking for periods when the amplitude “leaps” above the background signal and then dies out. I will not dwell on this matter - it is an issue for individual experimenters to deal with. However, as an example, part of the algorithm used with the CLOVAR is described over the page.

One also need to ensure that the PRF's are kept less than about 1100 Hz , so that the meteors are not range-aliased (unless special precautions are taken).

7.2.2 Meteor detection algorithm

Meteor echoes are detected in the following manner. The meteor detection algorithm basically just searches for a place where 2 successive amplitude points exceed a threshold value compare to the mean noise level (fast-rising signals) of the time series. After several trial and error tests, it turns out that if the average amplitude of the pair of successive points exceeds 3σ , where σ is the root-mean-square amplitude over a length of 2.5 s of data, then amplitudes following these initial 2 larger successive peaks are examined, and if a large amplitude points last for long enough (i.e. not impulsive spikes), then the corresponding interval in the time series is identified as being a possible meteor. It is also required that no secondary peaks occur in a region up to 2.5 s after the original large amplitudes. There is evidence of overdense echoes which can last up to 10's of seconds, but it was decided to use the time interval of 2.5 s in order to eliminate false detections such as aircraft (see later), random noise, etc. in the meteor detection procedure. Once the meteor is detected the algorithm also checks a few points back from the maximum amplitude of the location of the meteor trail to test whether the echo is characterized by a rapid initial rise in amplitude, followed by small amplitude fluctuations. This procedure successfully rejected the data if there was any beating (the reason for this is that, generally, overdense echoes have very long lifetimes, and the trail can be distorted by the wind field, possibly producing multiple reflection points whose scattered signals beat with each other) present in the echo, or any other irregularities (e.g., two meteors observed within a short time interval) present due to trail distortion. After several tests, it turns out that the maximum amplitude is reached frequently within $\frac{1}{10}$ s, and it was decided to use this value as a reliable time limit in the meteor detection procedure. Any slowly rising echo is rejected by the program. This procedure successfully rejected the long meteors, aircraft, E-region echoes (e.g. sporadic E) and possible turbulence scatter. Studies of several hundred meteor observations using this algorithm show it is a reliable discriminator of meteors.

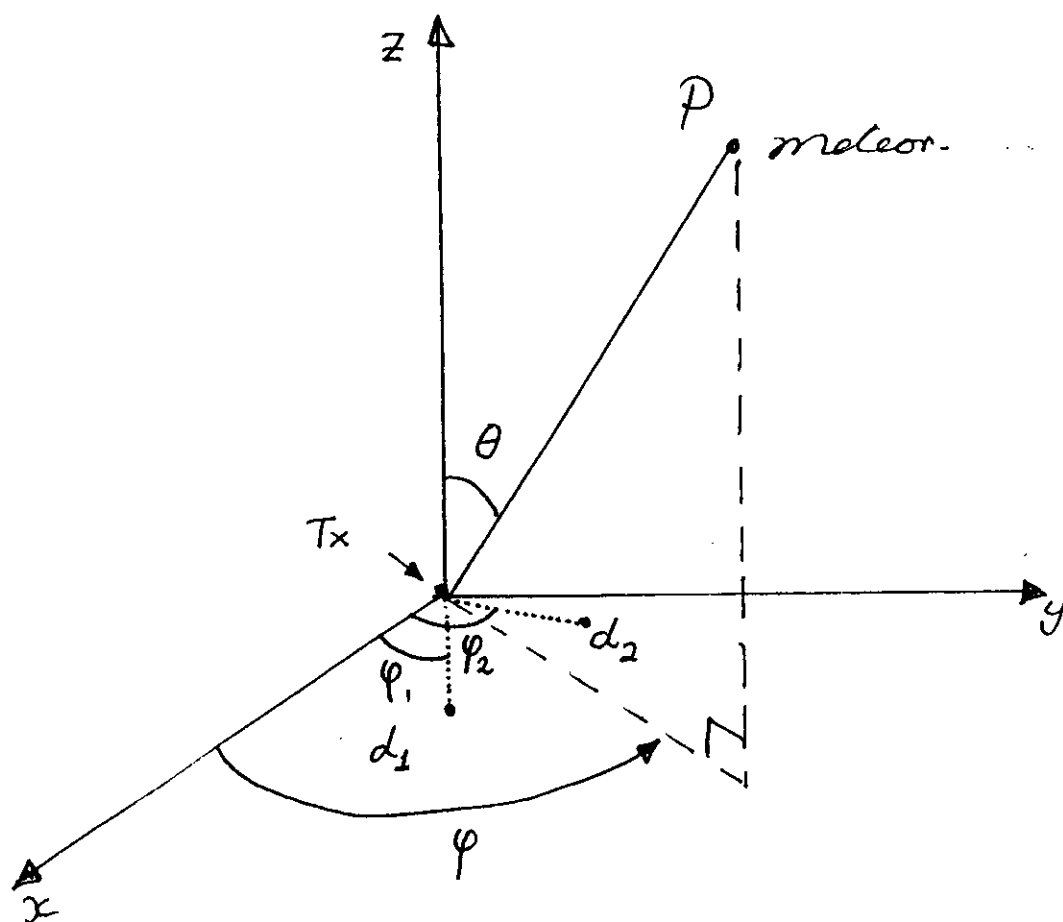
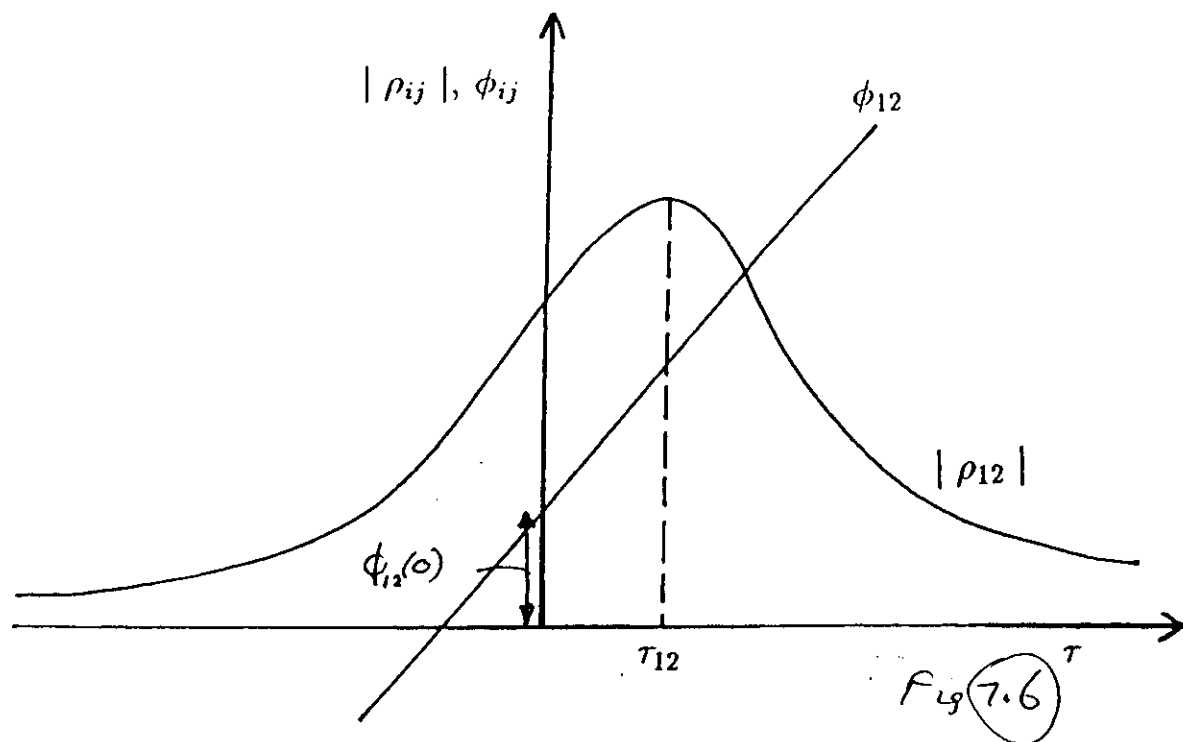
For comparison with the above time scales, a 40 km/s ($\approx \frac{2\sqrt{RN/2}}{v}$) meteor at range 130 km (maximum range used in our case) takes $\sim 0.03 \text{ s}$ to cross the first Frèsnel zone, so that the rise of the echo is comparatively rapid. All rise times would be less than 0.1 s , corresponding to a meteor velocity of 12 km/s . The decay time constants for $\lambda = 7.374 \text{ m}$ are $\sim 1.36 \text{ s}$ at 78 km , $\sim 0.24 \text{ s}$ at 88 km , and $\sim 0.04 \text{ s}$ at 110 km (see also Section 7.1.3). Therefore, the meteor echo must persist for $\geq 1.46 \text{ s}$ to be recognized in the $78\text{--}110 \text{ km}$ height range. The data interval of 2.5 s is considered to be a good choice. ~~The sampling time interval~~

Interferometry procedures and mean wind determinations for meteor winds

The basic ideas implicit in meteor measurements are similar to those used in IDI, with some subtle differences.

One finds the cross-correlation between the complex data recorded on each receiver, and then uses the phases differences at zero lag to deduce the angle of arrival. The rate of change of phase gives the radial velocity. When more than 3 receiver antennas are used, consistency checks are possible which allow further validation that we truly have a meteor.

The procedures used with the CLOVAR radar are described over the page.



R

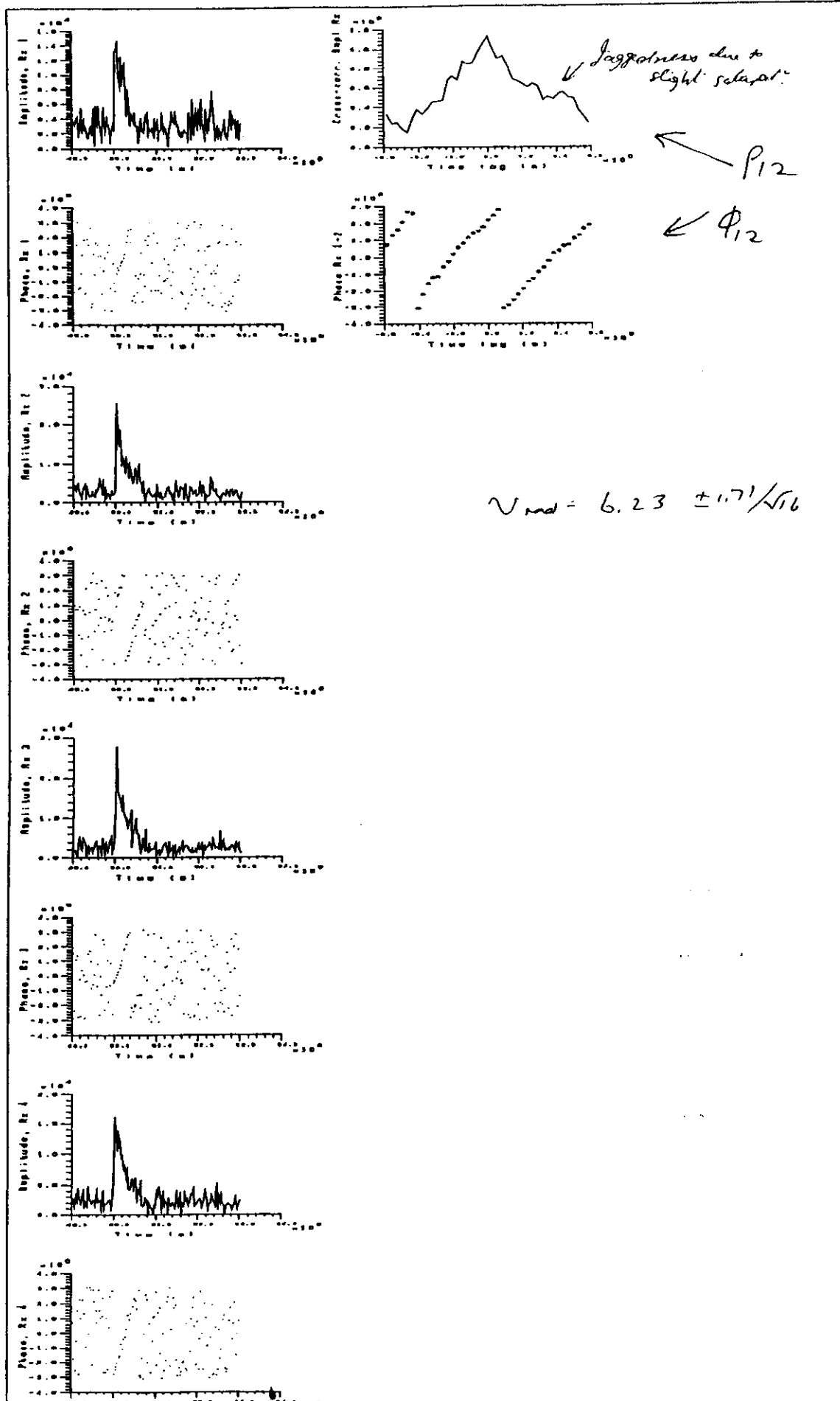
ME940711.ABU

(ABU 0711.psf)

3

341

A Real Sample!



7.2.8 Phase and radial velocity determination procedure

We have adapted the complex cross correlation method to measure the phase differences between the receiving antennas in order to determine the echo arrival angle, and have used both the complex auto and cross correlation methods to measure the rate of change of the relative phase in order to determine the radial velocity of the meteor trail. This radar interferometer method is sketched in Figure 7.7. When we apply the interferometric technique with two receiving antennas R_1 and R_2 , we can compute the complex cross correlation function of the signals measured at R_1 and R_2 (Figure 7.6). The cross correlation function of signals measured at one receiving antenna R_1 ($i = 1$) and the other receiving antenna R_2 ($j = 2$) is

$$\rho_{ij}(\tau) = |\rho_{ij}(\tau)| e^{i\phi_{ij}(\tau)} \quad (7.22)$$

where τ is the temporal displacement, $|\rho_{ij}(\tau)|$ is the amplitude, and $\phi_{ij}(\tau)$ is the phase of the cross correlation function. The phase $\phi_{ij}(0)$ at zero lag ($\tau = 0$) yields the phase difference between the receiving antennas and can be related to the mean angle of arrival of the backscattered signal (see equation (7.16)). The radial velocity, V_R , is determined by measuring the time derivative of the phase near zero lag from both the auto and cross correlation functions. The equation (7.21) can be re-written as:

$$V_R = -\frac{\lambda}{4\pi} \frac{d\phi_{ij}}{d\tau} \quad (7.23)$$

We have used $\phi_{ij}(\tau)$ at $\tau = -1, 0, 1$ to measure the rate of change of phase. In order to measure the rate of change of phase, we used all combinations of i ($i = 1, 4$) and j ($j = 1, 4$).

We avoided the duplicated combinations such as $\phi_{12}(1) = \phi_{21}(-1)$, $\phi_{11}(-1) = -\phi_{11}(1)$,...etc. In all, there are 32 independent combinations of phase values to determine the rate of change of phase; as seen later, if there is too much variability between these various estimates then we reject the meteor.

7.2.9 The echo arrival angle

Our intended interferometer antenna configuration is given by Figure 7.7. The echo arrival angle is measured with a 4 antenna interferometer. The direction of the echo is obtained by comparison of the phase of the echo signal at four receiving antennas. A set of possible directions is obtained from the receiving antennas R_1 , R_2 , and R_3 , while the antenna R_4 is sited for optimum resolution of the ambiguity. The point P represents the specular reflection point of a meteor trail which is drifting in the direction of (θ, ψ) with respect to $(0,0)$; where θ and ψ represent the zenith and azimuth angles. The positive azimuth angle is measured in the anti-clockwise direction from eastward direction (x-axis).

The unit vector giving the direction of the specular reflection point can be written as

$$\vec{I}_R = \sin \theta \cos \psi \vec{i} + \sin \theta \sin \psi \vec{j} + \cos \theta \vec{k} \quad (7.24)$$

where \vec{i} , \vec{j} , and \vec{k} unit vectors in the x, y, and z directions. The position vector of the receiving antenna R_1 is given by

$$\vec{R}_1 = d_1 \cos \psi_1 \vec{i} + d_1 \sin \psi_1 \vec{j} + 0 \vec{k} \quad (7.25)$$

Therefore, the phase of the signal received at R_1 with respect to $(0,0)$ is given by:

$$\phi_1 = \frac{2\pi}{\lambda} (\vec{R}_1 \cdot \vec{I}_R) \quad (7.26)$$

substituting (7.24) and (7.25) into (7.26), after some manipulations, one obtain

$$\phi_1 = \left(\frac{2\pi}{\lambda}\right) d_1 \cos(\psi - \psi_1) \sin \theta \quad (7.27)$$

Similarly, the phases of the signals received at R_2 and R_3 are:

$$\phi_2 = \left(\frac{2\pi}{\lambda}\right) d_2 \cos(\psi - \psi_2) \sin \theta \quad (7.28)$$

$$\phi_3 = \left(\frac{2\pi}{\lambda}\right) d_3 \cos(\psi - \psi_3) \sin \theta \quad (7.29)$$

where d_1 , d_2 , and d_3 are distances of the receivers R_1 , R_2 , and R_3 relative to $(0,0)$. $\{\psi_{i=1,3}\}$ represent the azimuth angle, which are directly known, measured from the x-axis (east).

Now, consider 2 receivers at $R_1 (d_1, \phi_1)$ and $R_2 (d_2, \phi_2)$. Then the relevant phase difference between these receivers is:

$$\phi_{12} = \phi_2 - \phi_1 \quad (7.30)$$

i.e.

$$\phi_{12} = \frac{2\pi \sin \theta}{\lambda} [d_2 \cos(\psi - \psi_2) - d_1 \cos(\psi - \psi_1)] \quad (7.31)$$

Note that ϕ_{12} means the phase of the signal received at antenna 2 leads that received at antenna 1. However, it actually works more easily to use the expansion of the above equation. Therefore we get:

$$\phi_{12} = \frac{2\pi \sin \theta}{\lambda} [d_2 \cos \psi \cos \psi_2 + d_2 \sin \psi \sin \psi_2 - d_1 \cos \psi \cos \psi_1 - d_1 \sin \psi \sin \psi_1] \quad (7.32)$$

Similarly, the phase difference between receivers R_1 and R_3 is:

$$\phi_{13} = \frac{2\pi \sin \theta}{\lambda} [d_3 \cos \psi \cos \psi_3 + d_3 \sin \psi \sin \psi_3 - d_1 \cos \psi \cos \psi_1 - d_1 \sin \psi \sin \psi_1] \quad (7.33)$$

Note that

$$\phi_{12} + \phi_{23} + \phi_{31} = 0 \quad (7.34)$$

So, there is no useful extra information in the ϕ_{23} term except for subsequent error checking. ϕ_{12} and ϕ_{13} are determined by computing the complex cross correlation of the signals measured at receivers (R_1, R_2) and (R_1, R_3) respectively, as described in Section 7.2.8. It is convenient to express the equations (7.32) and (7.33) in the matrix form. Thus we must solve the simple matrix equation

$$[A] \underline{x} = \underline{b} \quad (7.35)$$

i.e.

$$\begin{bmatrix} \frac{2\pi}{\lambda}(d_2 \cos \psi_2 - d_1 \cos \psi_1) & \frac{2\pi}{\lambda}(d_2 \sin \psi_2 - d_1 \sin \psi_1) \\ \frac{2\pi}{\lambda}(d_3 \cos \psi_3 - d_1 \cos \psi_1) & \frac{2\pi}{\lambda}(d_3 \sin \psi_3 - d_1 \sin \psi_1) \end{bmatrix} \begin{pmatrix} \sin \theta \cos \psi \\ \sin \theta \sin \psi \end{pmatrix} = \begin{pmatrix} \phi_{12} \\ \phi_{13} \end{pmatrix} \quad (7.36)$$

where ϕ_{12} , ϕ_{13} , and $[A]$ are known, Therefore we can solve ~~for~~ \underline{x} using a matrix inversion method, i.e.

$$\underline{x} = [A]^{-1} \cdot \underline{b} \quad (7.37)$$

Thus we obtain

$$x_1 = \sin \theta \cos \psi \quad (7.38)$$

$$x_2 = \sin \theta \sin \psi \quad (7.39)$$

and then

$$\sin^2 \theta = \chi_1^2 + \chi_2^2, \text{ giving } \theta = \sin^{-1} \sqrt{\chi_1^2 + \chi_2^2} \quad (7.40)$$

We can determine ψ by substituting θ into equation (7.38) or (7.39)

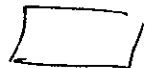
$$\Rightarrow \psi = \arccos\left(\frac{\chi_1}{\sin \theta}\right) \quad \text{or} \quad \arcsin\left(\frac{\chi_2}{\sin \theta}\right) \quad (7.41)$$

or dividing the equation (7.39) by (7.38) we can deduce

$$\psi = \arctan\left(\frac{\chi_2}{\chi_1}\right) \quad (7.42)$$

The arrival of the echo angle (θ, ψ) is thus readily determined. We determined such (θ, ψ) combinations for all measured phase differences ϕ_{ij} , and also for other combinations of ϕ_{ij} involving addition and subtraction of 2π . This sometimes lead to 2 or more possible "acceptable" angles. We then turned to receiver R_4 to help resolve these ambiguity, and in 70 % of all cases it was possible to produce an unambiguous meteor location.

The accuracy of the zenith angle determination is essentially depend upon the error in the phase determination. For each meteor the zenith angle of the reflection point was calculated from the mean phase difference between the receivers, averaged over 6 independent estimations (using the combinations of 4 receiving antennas). After several tests, we decided to limit the deviation in phase difference (i.e. $\phi_{ij(i \neq j)} - \phi(ave)$) to be $< 35^\circ$, which then turns out to be a reliable criteria. The experimental uncertainty in zenith angle is therefore $\leq 3^\circ$. The spread in possible zenith angles for each meteor was used in conjunction with the range to find the possible spread in heights. The average spread was ± 3.2 km, due to the phase uncertainty. Thus the range error due to the pulse length ($13.33 \mu s$ pulse resulting in a range uncertainty of 2 km) is also significant, giving a total uncertainty in height of about ± 3.8 km for individual meteors. It is therefore not productive to bin the resultant individual meteor height values into divisions finer than ~ 3 km.



Determination of the winds

Once we have collected a large number of radial velocities, it is necessary to use these data to determine zonal and meridional winds. Usually this is done by clustering the radial velocities into groups - say one-hour bins, and 3 km height bins. Then a least-squares fitting procedure must be applied to determine mean wind components for this height-time bin. An example of the type of analysis which is often applied is shown ^{below} over the page - this is the procedure used at London, Ontario.

Other variations include the Groves analysis, in which similar binning is done, but the data are forced to fit to a polynomial function in height. Generally one uses a cubic fit, but other orders are also possible.

7.2.10 Wind components over the whole sky

Now R , θ , and ψ form a three dimensional coordinate system which we transform to a Cartesian system, where x-axis is east, y-axis is north, and z-axis is vertical. The scattering point parameters are then sorted by altitude and time bin. Since an off-zenith point at 85 km height might be detected in the, say, 94 km range gate, a considerable regrouping of the points takes place at this point in the analysis. The main procedure for regrouping of the points in the analysis can be explained as follows... *etc.*

Significant diurnal variation in the meteor echo rate is observed (see Section 7.3.2) with the largest echo rate occurring during the early mornings hours when the meteor fluxes were large and minimum values in the evening hours when the fluxes were small. When both the height distribution and hourly rates are considered, it is clear that it is difficult to make up a continuous time series of wind velocities for altitudes close to the top (about 100 km) and bottom (about 80 km) of the meteor region (see also Section 7.3.1). Therefore a weekly or monthly study of the mean winds and tidal oscillations using the vector average of the daily mean values (similar to chapter 3), irrespective of the time of the day, would be biased. To eliminate the possible bias due to the diurnal variation of the echo rate values in winds, we adapted the so-called 'superposed epoch' analysis to estimate the mean winds and tidal oscillations. In such a case, recordings may be *binned* in the same hour of the day over several days. There are two options to perform the time-averaging of the data. We use either 1-hour or 2-hour bins of data. The basic procedure can be explained as follows for recording the data in 1-hour bins. The wind values during each hourly (local time) bins (2330-0030, 0030-0130, 0130-0230, ..., 2230-2330 LT) for all the days in each month are grouped together and a least-squares fitting procedure is applied to all these radial velocities to obtain the hourly mean values, and the resulting time series are taken to represent the 24 hourly mean values for the equivalent day of the month. In a similar fashion, the data can be grouped into 2-hour bins (2300-0100, 0100-0300, 0300-0500, ..., 2100-2300 LT), and the resulting time series are taken to represent the 12 two-hour mean values for the equivalent day of the month. It should be noted here that the 1-hour bins are allowed to overlap ± 15 minutes on either end into adjacent intervals, and the 2-hour bins are allowed to overlap ± 30 minutes. These "overlapping intervals" ensure that the winds are moderately smooth as a function of height and time. One of the main objectives of this study is to compare the winds and tides (i.e. long period oscillations) with the MF radar using the SA technique. Therefore it is not unreasonable to force a certain degree of continuity upon the data (this will be further discussed in the following chapter).

All echoes used in the analysis were distributed in heights between 77 and 130 km, with 85% of them lying between 80 and 100 km. The vertical structure of the winds and tides are established by dividing the recorded data into 6 height groups. The height groups used were 78-84 km, 83-87 km, 86-90 km, 89-93 km, 92-97 km, and 96-102.5 km for the central heights of 82 km, 85 km, 88 km, 91 km, 94 km, and 98 km respectively. Note that the winds are moderately smoothed as a function of height. We have grouped the echoes according to this sequence for 2 reasons. 1) It increases the number of points to do the fitting. 2) It



gives a height resolution similar to the MF system; it somewhat simulates the pulse used in the MF case, where the pulse width is ~ 3 km but spreads out to $\sim \pm 4$ km. It should be noted that for the discussion of mean winds and tides, only the height region 82-98 km is considered (Chapter 8); for the discussion of echo rates and selection efficiency the height region 77-130 km is used (Section 7.3).

(not included)

Next we want to calculate the mean apparent motion of the scattering points. For each scattering point we initially determined the Doppler frequency, so the scalar value of the radial velocity of each scatterer can be calculated from the equation (7.19) as

$$V_{Ri} = \frac{c}{2f} f_{di} \quad (7.43)$$

where $i = 1, 2, 3, \dots, N$, where N is the number of scattering points identified at height z and the time bin Δt .

Having previously determined the location of each scattering point, we can now write the vector radial velocity as

$$\vec{V}_{Ri} = V_{Ri} \vec{I}_{Ri} \quad (7.44)$$

where \vec{I}_{Ri} is a unit vector in the radial direction passing through the i th point, and is given by

$$\vec{I}_{Ri} = l_i \vec{i} + m_i \vec{j} + n_i \vec{k} \quad (7.45)$$

where l_i , m_i , and n_i are the direction cosines of the i th scattering point, given by

$$l_i = \sin \theta_i \cos \psi_i \quad (7.46)$$

$$m_i = \sin \theta_i \sin \psi_i \quad (7.47)$$

$$n_i = \cos \theta_i \quad (7.48)$$

Now let the mean wind field vector is described by

$$\vec{V}_m = u\vec{i} + v\vec{j} + w\vec{k} \quad (7.49)$$

where u , v , and w are the zonal, meridional, and vertical components of the wind field, respectively. Three scattering points are sufficient (in principle!) to determine the three unknown components of the motion. With more than three points we can calculate a least-squares fit to the scattering point parameters as follows. V_{Ri} is simply the projection of the mean wind vector onto the radar's (unit) line-of-sight vector \vec{I}_{Ri} . Since

$$V_{Ri} = \vec{V}_m \cdot \vec{I}_{Ri} \quad (7.50)$$

for all i if the least-squares fit is perfect, the residual is given by

$$\epsilon^2 = \sum_{i=1}^N [(ul_i + vm_i + wn_i) - V_{Ri}]^2 \quad (7.51)$$

The best estimates for u , v , and w are those values for which ϵ^2 is smallest. Differentiating ϵ^2 with respect to u , v and w and setting these derivatives equal to zero, we obtain the three equations

$$\frac{\partial \epsilon^2}{\partial u} = \frac{\partial \epsilon^2}{\partial v} = \frac{\partial \epsilon^2}{\partial w} = 0 \quad (7.52)$$

which gives

$$u \sum l_i^2 + v \sum l_i m_i + w \sum l_i n_i = \sum V_{Ri} l_i \quad (7.53)$$

$$u \sum l_i m_i + v \sum m_i^2 + w \sum m_i n_i = \sum V_{Ri} m_i \quad (7.54)$$

$$u \sum l_i n_i + v \sum m_i n_i + w \sum n_i^2 = \sum V_{Ri} n_i \quad (7.55)$$

For any set of measurements (l_i, m_i, n_i) , these simultaneous equations for u , v , and w can be solved to find the best estimates for u , v , and w .

When calculating apparent motions vector, we use 2 other selection criteria. First we reject points that lie within 12° of zenith, since errors in these points cause large errors in the calculated horizontal motion. Second we reject points when $|V_{Ri}(\text{measured}) - V_{Ri}(\text{calculated})| > 30$ m/s. $V_{Ri}(\text{calculated})$ is found in the following way. First, we do a first rough estimate of (u, v, w) without any rejection. Then we do a second run through, and use ^{the} previously calculated (u, v, w) as first guess to determine an estimation value for the radial velocity - which we call $V_{Ri}(\text{calculated})$. If $|V_{Ri}(\text{measured}) - V_{Ri}(\text{calculated})| > 30$ m/s then the measured value, $V_{Ri}(\text{measured})$, is rejected as an outlier. After rejecting the worst outliers of $V_{Ri}(\text{measured})$, a list of 'new' (u, v, w) estimates are determined, and subsequently used for the tidal analysis. Note that

$$V_\sigma = \sqrt{\left(\frac{\sum_{i=1}^N [V_{Ri}(\text{measured}) - V_{Ri}(\text{calculated})]^2}{N} \right)} \quad (7.56)$$

represents a sort of a measure of the 'residuals'. They are typically ~ 5 - 20 m/s, which is to be expected, since they represent the effects of gravity wave fluctuations (see Chapter 5). The meteor region is characterized by a wide wave motion spectrum and is generally turbulent. Chapter 5 shows that gravity wave (GW) fluctuations are typically several times the fluctuation due to the tides, and $V_{rms} \sim 30$ m/s (V_{rms} = root-mean-square value). Bearing in mind that on the average the zenith angle is typically $\sim 30^\circ$ off vertical, we expect the the residuals to be $\sim 0.5 \times V_{rms}(\text{GW}) \sim 15$ m/s or so. Therefore, taking 30 m/s

(not included)

as a limit value is not unreasonable. It might be thought that the residuals would be largest for those time bins (1-hour or 2-hour bin) containing the smaller numbers of meteor echoes, but this is not so. In general the greatest scatter occurs for those time bins where the wind speed^{*} direction is changing most rapidly.

In our discussion of the statistical analysis of data, we have so far discussed only observations of three variables (eastward, northward, and vertical). However, we allow the following 3 options to deduce the wind field using the least-squares fitting procedure. (1) Do a fit to a 3-D wind field (eastward, northward, and vertical); the one discussed in the previous section. (2) Do a fit to a 2-D wind field; this wind analysis method assumes the vertical wind to be zero (this is a valid assumption as the vertical wind velocity is on average 1-2 orders of magnitude less than the horizontal wind velocity), and simply project the line-of-sight component onto the horizontal plane. This problem is a special case of our three-variable method, i.e. a very straightforward generalization of our three-variable method discussed above, and can be solved in a similar way. Therefore, the mathematical details of this analysis will not further be discussed in this section. (3) Obtain the eastward wind using only the meteors to the east and west. After several trial tests, it turns out that options (1) and (2) work especially well if the meteors are symmetrically distributed about the sky, and (2) seems superior. The case (3) is a useful option when there are a majority of meteors in the east and west.

In the present study, the variation of wind velocity with height and time is also determined by a least-squares fitting analysis developed by Groves [1959]. This method allows variations in temporal behaviour of the wind, with periods of 24, 12, and 8 hours. In addition, the amplitude and phase of each periodic component and amplitude and direction of the prevailing components are allowed a polynomial variation with height. Groves analysis has been used by several groups [e.g., Rossiter, 1971; Stubbs and Vincent, 1973; Roper, 1965, 1975, 1978; Aso et al., 1979, 1980; Tsuda et al., 1980].

Meteor techniques have been especially used to test out the validity of MF spaced antenna measurements in the upper atmosphere.

A sample comparison is presented - but such comparisons are on-going and will no doubt be discussed in the workshop to follow this session.

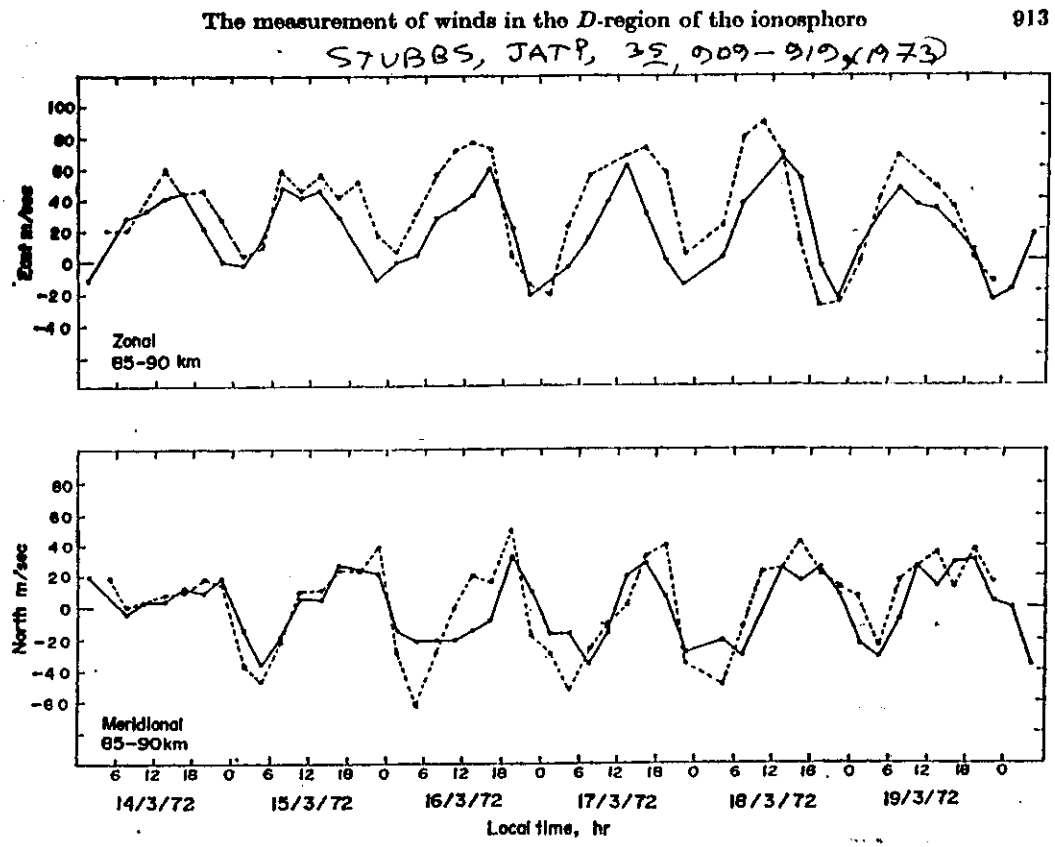


Fig. 2. A 6-day comparison of ionospheric drifts (full lines) and meteor radar wind estimates (broken lines) with each discrete point representing a 3-hourly average.

Measurements of ^{temperature} turbulence ~~and~~ using meteor trails

Some final comments on the use of meteor trails.

- (1) The decay time of meteor can sometimes be used to determine temperature ^{see MAP handbook}
- (2) Roper (~1960) ₁₉₆₅ & subsequently Fellous & Fregal ^{handbook}

(MAP handbook vol 2, p323) have used multiple receiver stations to detect transmitted pulses which have reflected off 3 (closely spaced) different parts of the meteor trail. They then used the 3 different estimates of radial velocity at these 3 points on the trail to determine the transverse velocity structure functions. This then allowed them to deduce the turbulent energy dissipation rate ϵ .

$$(D_{tt} = \frac{4}{3} C_v^2 \epsilon^{\frac{2}{3}} r^{\frac{2}{3}}.)$$

(Fellous & Fregal actually used 2 transmitters and one receiver site, but the principle is the same - see attached diagram).

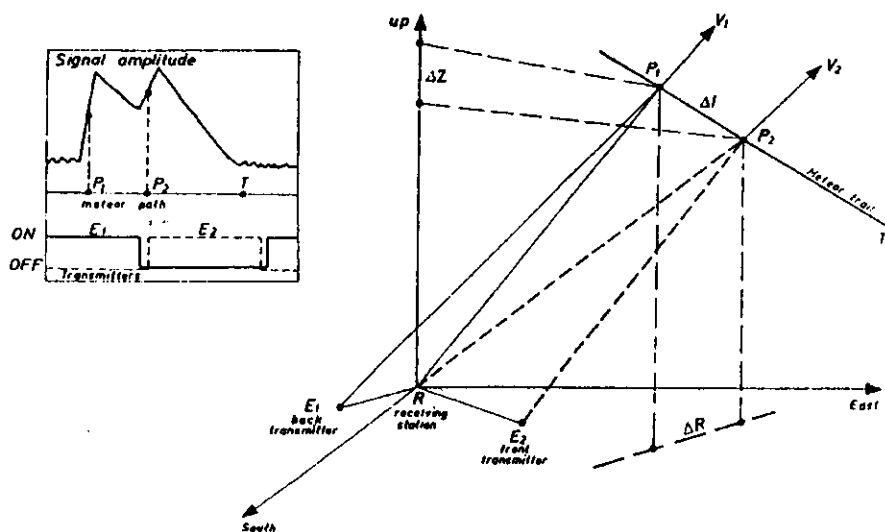


Figure 1. Geometrical representation of experimental set up.

Meteors

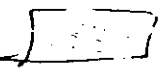
— some references
(Compiled by T. Thayaparan)

References

- [1] Adams, G. W., J. W. Brosnahan, and D. P. Edwards, The imaging Doppler interferometer: data analysis, *Radio Sci.*, 20, 1481-1492, 1985.
- [2] Appleton, E. V., and M. A. F. Barnett, On some direct evidence for downward atmospheric reflection of electric rays, *Proc. Roy. Soc., A* 109, 621-641, 1925.
- [3] Aso, T., T. Tsuda, and S. Kato, Meteor radar observations at Kyoto university, *J. Atmos. Terr. Phys.*, 41, 517-525, 1979.
- [4] Aso, T., T. Tsuda, Y. Takashima, R. Ito, and S. Kato, Observations of lower ionospheric wind by the Kyoto meteor radar, *J. Geophys. Res.*, A 1, 177-184, 1980.
- [5] Avery, S. K., A. C. Riddle, and B. B. Balsley, The Poker Flat, Alaska, MST radar as a meteor radar, *Radio, Sci.*, 18, 1021-1027, 1983.
- [6] Awe, O., The fading of radio waves weakly scattered at vertical incidence from heights near 90 km, *J. Atmos. Terr. Phys.*, 21, 142-156, 1961.
- [7] Baggaley, W. J., On the variation of the ambipolar diffusion coefficient with height, *Planet. Space Sci.*, 18, 1836-1842, 1970.
- [8] Baggaley, W. J., and E. M. Poulter, The radio meteor wind facility at Christchurch, New Zealand, *J. Atmos. Terr. Phys.*, 40, 941-943, 1978.
- [9] Bills, R. E., C. S. Gardner, and S. J. Franke, Na Doppler/ Temperature Lidar: Initial mesopause region observations and comparison with the Urbana medium frequency radar, *J. Geophys. Res.*, 90, D12, 22701-22707, 1991.
- [10] Booker, H. G., Turbulence in the ionosphere with applications to meteor trails, radio star, scintillations, auroral radar echoes, and other phenomena, *J. Geophys. Res.*, 61, 673-705, 1956.
- [11] Briggs, B. H., Ionospheric drifts, *J. Atmos. Terr. Phys.*, 39, 1023-1033, 1977.
- [12] Bronshten, V. A., *Physics of meteoric phenomena*, Reidel, Dordrecht, 1983.
- [13] Brown, N., Radio echoes from meteor trains at a frequency of 1.98 MHz, *J. Atmos. Terr. Phys.*, 38, 83-87, 1976.
- [14] Cervera, M. A., and Reid, I. M., Comparison of simultaneous wind measurements using colocated VHF meteor radar and MF spaced antenna radar systems, *Radio Sci.*, 30, 1245-1261, 1995.
- [15] Clark, R. R., Meteor wind data for global comparisons, *J. Atmos. Terr. Phys.*, 40, 905-911, 1978.

- [16] Davies, J. G., and C. D. Ellyett, The diffraction of radio waves from meteor trails and the measurement of meteor velocities, *Phil. Mag.*, (7) 40, 614-626, 1949.
- [17] Elford, W. G., and D. S. Robertson, Measurements of winds in the upper atmosphere by means of drifting meteor trails, *J. Atmos. Terr. Phys.*, 4, 271-284, 1953.
- [18] Elford, W. G., A Study of winds between 80 and 100 km in medium latitudes, *Planet. Space Sci.*, 1, 94-101, 1959.
- [19] Elford, W. G., and D. Olsson-Steel, The height distribution of radio meteors: observations at 6 MHz, *J. Atmos. Terr. Phys.*, 50, 811-818, 1988.
- [20] Farley, D. T., H. M. Ierke, and B. G. Fejer, Radar interferometry: A new technique for studying plasma turbulence in the ionosphere, *J. Geophys. Res.*, 86, 1467-1472, 1981.
- [21] Felgate, D. G., A. N. Hunter, S. P. Kingsley, and H. G. Muller, Comparative studies of E-region ionospheric drifts and meteor winds, *Planet. Space Sci.*, 23, 389-400, 1975.
- [22] Fellous, J. L., R. Bernard, M. Glass, M. Massebeuf, and A. Spizzichino, A study of the variations of atmospheric tides in the meteor zone, *J. Atmos. Terr. Phys.*, 37, 1511-1524, 1975.
- [23] Fraser, G. J., The measurement of atmospheric winds at altitudes of 64-120 km using ground-based radio equipment, *J. Atmos. Sci.*, 22, 217-218, 1965.
- [24] Fraser, G. J., Seasonal variation of southern hemisphere mid-latitude winds at altitudes 70-100 km, *J. Atmos. Terr. Phys.*, 30, 707-719, 1968.
- [25] Fraser, G. J., and A. Kochanski, Ionospheric drifts from 64-108 km altitudes at Birdlings Flat, *J. Geophys. Res.*, 26, 675-687, 1970.
- [26] Geller, M. A., S. A. Bowhill, and G. C. Hess, A description of the university of Illinois meteor radar system and some first results, *J. Atmos. Terr. Phys.*, 39, 15-24, 1977.
- [27] Glass, M., R. Bernard, J. L. Fellous, and M. Massebeuf, The French meteor radar facility, *J. Atmos. Terr. Phys.*, 40, 923-931, 1978.
- [28] Golley, M. G., and Rossiter, D. E., Some tests of methods of analysis of ionospheric drift records using an array for 89 aeriels, *J. Atmos. Terr. Phys.*, 32, 1215-1233, 1970.
- [29] Greenhow, J. S., Characteristics of radio echoes from meteor trails: the behaviour of the electron trails after formation, *Proc. Phys. Soc.*, 65, 169-181, 1952.
- [30] Greenhow, J. S., Systematic wind measurements at altitudes of 80-100 km using radio echoes from meteor trails, *Philos. Mag.*, 45, 471-490, 1954.
- [31] Greenhow, J. S., and E. L. Neufeld, The diffusion of ionized meteor trails in the upper atmosphere, *J. Atmos. Terr. Phys.*, 6, 133-140, 1955.
- [32] Greenhow, J. S., and J. E. Hall, ———, *J. Atmos. Terr. Phys.*, 5, 109, 1955.
- [33] Greenhow, J. S., and E. L. Neufeld, Height variation of upper atmospheric winds, *Philos. Mag. Ser.*, 8, 1, 1157-1171, 1956.

- [34] Greenhow, J. S., and J. E. Hall, The importance of initial trail radius on the apparent height and number distributions of meteor echoes, *Mon. Not. R. Astr. Soc.*, 121, 183-196, 1960.
- [35] Greenhow, J. S., and E. L. Neufeld, Winds in the upper atmosphere, *Quart. J. Roy. Meteorol. Soc.*, 87, 472-489, 1961.
- [36] Gregory, J. B., and D. T. Rees, Wind profiles to 100 km near 53° N during 1969, *J. Atmos. Sci.*, 1079-1082, 1971.
- [37] Grossi, M. D., R. B. Southworth, and S. K. Rosenthal, Radar observations of meteor winds above Illinois, *Thermospheric circulation*, The MIT Press, Massachusetts, 205-248, 1972.
- [38] Groves, G. V., A theory for determining upper atmosphere winds from radio observations on meteor trails, *J. Atmos. Terr. Phys.*, 16, 344-356, 1959.
- [39] Herlofson, N., The theory of meteor ionization, *Phys. Soc. Rep. Prog. Phys.*, 11, 444-454, 1948.
- [40] Hocking, W. K., The University of Western Ontario VHF atmospheric radar, Solar-terrestrial energy program, *Proceedings of the sixth workshop on technical and scientific aspects of MST radar*, SCOSTEP Secretariat NOAA, Boulder, Colorado, 349-356, 1993.
- [41] Hughes, D. W., *Cosmic dust*, McDonnell, J. A. M., ed., Wiley, Chichester, 123, 1978.
- [42] Ierick, H. M., and J. Röttger, Mesospheric measurements of irregularity patches using a 3 antenna interferometer, *Handbook for MAP*, Vol. 14, Scostep Secretariat, University of Illinois, Urbana, 174-178, 1984.
- [43] Jones, J., On the decay of underdense radio meteor echoes, *Mon. Not. R. Astr. Soc.*, 173, 637-646, 1975.
- [44] Jones, J., B. A. McIntosh, M. Scmek, Ozone and the duration of overdense radio meteors, *J. Atmos. Terr. Phys.*, 52, 253-258, 1990.
- [45] Jones, J., and P. Brown, The radiant distribution of sporadic meteors., *Planet. Space Sci.*, 42, 123-126, 1994.
- [46] Kaiser, T. R., Radio echo studies of meteor ionization, *Adv. Phys. (Phil. Mag. Supp.)* 2, 495-544, 1953.
- [47] Kaiser, T. R., W. M. Pickering, and C. D. Watkins, Ambipolar diffusion and motion of ion clouds in the earth's magnetic field, *Planet. Space Sci.*, 17, 519-552, 1969.
- [48] Kingsley, S. P., H. G. Muller, L. Nelson, and A. Scholefield, Meteor winds over Sheffield (53° N, 2° W), *J. Atmos. Terr. Phys.*, 40, 917-922, 1978.
- [49] Kraus, J. D., *Radio astronomy*, McGraw-Hill, New York, 1966.
- [50] Kudeki, E., P. K. Rastogi, and F. Sürücü, Systematic errors in radar wind estimation: Implications for comparative measurements, *Radio Sci.*, 28, 169-179, 1992.
- [51] Labitzke, K., A. H. Manson, J. J. Barnett, and M. Corney, Comparison of geostrophic and observed winds in the upper mesosphere over Saskatoon, Canada, *J. Atmos. Terr. Phys.*, 49, 987-997, 1987.



- [52] Lloyd, N., A. H. Manson, D. J. McEwen, and C. E. Meek, A comparison of middle atmospheric dynamics at Saskatoon (52° N, 107° W) as measured by a medium-frequency radar and a Fabry-Perot interferometer, *J. Geophys. Res.*, 95, D6, 7653-7660, 1990.
- [53] Lysenko, I. A., A. D. Orlyansky, and Yu. I. Portnyagin, A study of the wind regime at an altitude of about 100 km by the meteor radar method *Phil. Trans. R. Soc. Lond.*, A 271, 601-610, 1972.
- [54] Lysenko, I. A., Yu. I. Portnyagin, K. Sprenger, K. M. Greisiger, and R. Schminder, Results of a comparison between radar meteor wind measurements and simultaneous lower ionosphere drifts measurements in the same area, *J. Atmos. Terr. Phys.*, 34, 1453-1444, 1972.
- [55] Manning, L. A. O., O. G. Villard, and A. M. Peterson, Meteoric echo study of upper atmospheric winds, *Proc. Inst. Radio. Engrs.*, 38, 877-883, 1953.
- [56] Manning, L. A. O., The initial radius of meteoric ionization, *J. Geophys. Res.*, 63, 81-196, 1958.
- [57] Mawrey, R. S., and A. D. Broadhurst, Comparison of predicted and measured detection rates of meteor signals, *Radio Sci.*, 28, 415-427, 1993.
- [58] McDaniel, E. W., and E. A. Mason, *Mobility and diffusion of ions in gases*, John Wiley, New York, 1973.
- [59] McIntosh, B. A., The effect of wind shear on the decay constant of meteor echoes, *Can. J. Phys.*, 47, 1337-1341, 1969.
- [60] McKinley, D. W. R., and P. M. Millman, A phenomenological theory of radar echoes from meteors, *Proc. Inst. Radio Engrs.*, 37, 364-375, 1949.
- [61] McKinley, D. W. R., *Meteor science and engineering*, McGraw-Hill, New York, 1961.
- [62] Muller, H. G., Atmospheric tides in the Meteor zone, *Planet. Space Sci.*, 14, 1253-1272, 1966.
- [63] Muller, H. G., Wind shears in the meteor zone, *Planet. Space Sci.*, 16, 61-90, 1968.
- [64] Muller, H. G., Simultaneous observations of meteor winds and ionospheric drifts, *J. Atmos. Terr. Phys.*, 30, 701-706, 1968.
- [65] Muller, H. G., The Sheffield meteor wind experiment, *Quart. J. R. Met. Soc.*, 96, 195-213, 1970.
- [66] Muller, H. G., and S. P. Kingsley, Long period meteor wind oscillations, *J. Atmos. Terr. Phys.*, 36, 1933-1943, 1974.
- [67] Muller, H. G., R. L. Havill, V. E. Comley, and P. C. J. Hill, A study of meteor winds from two locations in the British Isles, *J. Atmos. Terr. Phys.*, 57, 979-993, 1995.
- [68] Olsson-Steel, D., and W. G. Elford, The height distribution of radio meteors: observations at 2 MHz, *J. Atmos. Terr. Phys.*, 49, 243-258, 1987.
- [69] Phillips, E., Wind structure from the amplitude fluctuations in persistent radio meteor echoes, *Planet. Space Sci.*, 17, 553-559, 1969.

- [70] Phillips, A., A. H. Manson, C. E. Meek, and E. J. Llewellyn, A long-term comparison of middle atmosphere winds measured at Saskatoon (52° N, 107° W) by a medium-frequency radar and a Fabry-Perot interferometer, *J. Geophys. Res.*, 99, D6, 12923-12935, 1994.
- [71] Pfister, W., The wave-like nature of inhomogeneities in the E-region, *J. Atmos. Terr. Phys.*, 33, 999-1025, 1971.
- [72] Poulder, E. M., and W. J. Baggaley, Radiowave scattering from meteor ionization, *J. Atmos. Terr. Phys.*, 39, 757-768, 1977.
- [73] Poulder, E. M., and W. J. Baggaley, The application of radio-wave scattering theory to radio-meteor observations, *Planet. Space sci.*, 26, 969-977, 1978.
- [74] Poulder, E. M., Winter motions in the southern hemisphere meteor region, *J. Atmos. Terr. Phys.*, 42, 661-672, 1980.
- [75] Poole, L. M. G., The Grahamstown all-sky meteor radar, *J. Atmos. Terr. Phys.*, 50, 585-590, 1988.
- [76] Poole, L. M. G., Characteristics of the mesospheric two day wave as observed at Grahamstown (33.3° S, 26.5° E), *J. Atmos. Terr. Phys.*, 52, 259-268, 1990.
- [77] Reddi, C. R., K. Rajeev, and R. Ramkumar, Annual and semiannual temperature oscillations at the mesopause levels over Trivandrum (8.5° N, 78° E), *J. Geophys. Res.*, D5, 8925-8931, 1993.
- [78] Reid, I. M., MF Doppler and spaced antenna radar measurements of upper middle atmospheric winds, *J. Atmos. Terr. Phys.*, 50, 117-134, 1988.
- [79] Rees, D., H. G. Muller, and S. P. Kingsley, Comparative wind measurements in the lower thermosphere using rocket trail and meteor radar techniques, *J. Atmos. Terr. Phys.*, 38, 365-370, 1976.
- [80] Reid, G. C., The influence of electric fields on radar measurements of winds in the upper mesosphere, paper presented at URSI Symposium, Fairbanks, Alaska, August 1982.
- [81] Robertson, D. S., D. T. Liddy, and W. G. Elford, Measurement of winds in the upper atmosphere by means of drifting meteor trails, *J. Atmos. Terr. Phys.*, 4, 255-270, 1953.
- [82] Roper, R. G., The semidiurnal tide in the lower thermosphere, *J. Geophys. Res.*, 71, 5746-5748, 1966.
- [83] Roper, R. G., The measurement of meteor winds over Atlanta (34° N, 84° W), *Radio Sci.*, 10, 363-369, 1975.
- [84] Roper, R. G., Winds from the Atlanta (34° N, 84° W) radio meteor wind facility, *J. Atmos. Terr. Phys.*, 40, 891-894, 1978.
- [85] Rossiter, D. E., A comparison of ionospheric drifts with radio meteor measurement of the neutral wind, *Aus. J. Phys.*, 23, 103-117, 1970.
- [86] Royrvik, O., VHF radar signals scattered from the equatorial mesosphere, *Radio Sci.*, 18, 1325-1335, 1983.

- [87] Röttger, J., and R. A. Vincent, VHF radar studies of tropospheric velocities and irregularities using spaced antenna techniques, *Geophys. Res. Lett.*, 5, 917-920, 1978.
- [88] Röttger, J., and P. Czechowsky, Tropospheric and stratospheric wind measurements with the spaced antenna drifts technique and the Doppler beam swinging technique using a VHF radar, Preprint, 19th Conf. on radar meteorology of Am. Met. Soc., Miami, FL, USA, 15-18 Apr., 577-584, 1980.
- [89] Röttger, J., Investigations of lower and middle atmosphere dynamics with spaced antenna drift radars, *J. Atmos. Terr. Phys.*, 43, 277-292, 1981.
- [90] Röttger, J., The capabilities of VHF radar for meteorological observations, Preprint of Nowcasting Symposium, Third scientific assembly of international association of meteorology and atmospheric physics, Hamburg, Germany, 17-21 Aug. 1981.
- [91] Röttger, J., Techniques for measurements of horizontal and vertical velocities: Determination of horizontal and vertical wavelengths of gravity waves, *Handbook for MAP*, Vol. 9, SCOSTEP Secretariat, Dep. Elec. Computer Eng., Univ. of Il. Urbana, 150-163, 1983.
- [92] Spizzichino, A., Meteor trail radar winds over Europe, *Thermospheric circulation*, The MIT Press, Massachusetts, 205-248, 1972.
- [93] Sprenger, K., and Schminder, R., Results of ten years ionospheric drift measurements in the L.F. range, *J. Atmos. Terr. Phys.*, 30, 183-199, 1967.
- [94] Sprenger, K., and Schminder, R., On the significance of ionospheric drift measurements in the L. F. range, *J. Atmos. Terr. Phys.*, 30, 693-700, 1968.
- [95] Sprenger, K., and Lysenko, I. A., The significance and interpretation of ionospheric drift measurements in the low frequency range, *Phil. Trans. R. Soc.*, A271, 473-484, 1972.
- [96] Steel, D. I., and W. G. Elford, The height distribution of radio meteors: comparison of observations at different frequencies on the basis of standard echo theory, *J. Atmos. Terr. Phys.*, 53, 409-417, 1991.
- [97] Stohl, J., Seasonal variation in the radiant distribution of meteors, *Physics and dynamics of meteors*, Physics and dynamics of meteors (edited by L. Kresak and P. M. Millman), Reidel, Dordrecht, 298-303, 1968.
- [98] Stubbs, T. J., The measurement of winds in the D-region of the ionosphere by the use of partially reflected radio waves, *J. Atmos. Terr. Phys.*, 35, 909-919, 1973.
- [99] Stubbs, T. J., and R. A. Vincent, Studies of D-region drifts during the winters of 1970-72, *Aus. J. Phys.*, 26, 645-660, 1973.
- [100] Sugar, G. R., Radio propagation by reflection from meteor trails, *proc. IEEE*, 52, 116-136, 1964.
- [101] Sürücü, F., S. J. Franke, and E. Kudeki, On the influence of specular reflections in MF radar wind measurements, *Radio Sci.*, 30, 1229-1244, 1995.
- [102] Taylor, J. R., An introduction to error analysis, University science books, Mill valley, California, USA.

- [103] Tetenbaum, D., S. K. Avery, and A. C. Riddle, Observations of mean winds and tides in the upper mesosphere during 1980-1984, using the Poker Flat, Alaska, MST radar as a meteor radar, *J. Geophys. Res.*, 91, D13, 14539-14555, 1986.
- [104] Thomas, R. M., P. S. Whitham, and W. G. Elford, Response of high frequency radar to meteor backscatter, *J. Atmos. Terr. Phys.*, 50, 703-724, 1988.
- [105] Thomas, R. M., Detection by HF radar of the Eta Aquarid meteor shower, *Planet. Space Sci.*, 37, 837-846, 1989.
- [106] Tsuda, T., T. Aso, Y. Takashima, R. Ito, and S. Kato, Meteor radar observations at Kyoto in two C.T.O.P. periods, *J. Atmos. Terr. Phys.*, 42, 461-469, 1980.
- [107] Tsuda, T., J. Tanil, T. Aso, and S. Kato, Lunar tides at meteor heights, *Geophys. Res. Lett.*, 8, 191-194, 1981.
- [108] Vincent, R. A., T. J. Stubbs, R. H. O. Pearson, K. H. Lloyd, and C. H. Low, A comparison of partial reflection drifts with winds determined by rocket techniques - I, *J. Atmos. Terr. Phys.*, 39, 813-821, 1977.
- [109] Vincent, R. A., and Röttger, Spaced antenna radar observations of tropospheric velocities and irregularities, *Radio Sci.*, 15, 319-335, 1980.
- [110] Vincent, R. A., P. T. May, W. K. Hocking, W. K. Elford, W. G. Candy, and B. H. Briggs, First results with the Adelaide VHF radar: Spaced antenna studies of tropospheric winds, *J. Atmos. Terr. Phys.*, 49, 353-366, 1987.
- [111] Wang, S. T., D. Tetenbaum, B. B. Balsley, R. L. Obert, S. K. Avery, and J. P. Avery, A meteor echo detection and collection system for use on VHF radars, *Radio Sci.*, 23, 46-54, 1988.
- [112] Ward, W., Private communication.
- [113] Whitehead, J. D., W. R. From, K. L. Jones, and P. E. Monro, Measurements of movements in the ionosphere using radio reflections, *J. Atmos. Terr. Phys.*, 45, 345-351, 1983.
- [114] Woodman, R. F., Inclination of the geomagnetic field measured by an incoherent scatter technique, *J. Geophys. Res.*, 76, 178-184, 1971.
- [115] Wohlleben, R., and H. Mattes, *Interferometrie in radioastronomie und radartechnik*, Vogel-Verlag, Wurzburg.
- [116] Wright, J. W., The interpretation of ionospheric radio drift measurements - I. Some results of experimental comparisons with neutral wind profiles, *J. Atmos. Terr. Phys.*, 30, 919-930, 1968.
- [117] Wright, J. W., M. Glass, and A. Spizzichino, The interpretation of ionospheric radio drift measurements - VII. Direct comparisons of meteor radar winds and kinesiometer measurements: mean and random motions, *J. Atmos. Terr. Phys.*, 38, 713-729, 1976.



PERGAMON

ATP 1262

7-8-2000

Journal of Atmospheric and Solar-Terrestrial Physics 000 (2000) 000-000

Journal of
ATMOSPHERIC AND
SOLAR-TERRESTRIAL
PHYSICS

www.elsevier.nl/locate/jastp

Real-time determination of meteor-related parameters utilizing modern digital technology

W.K. Hocking^{a,*}, B. Fuller^b, B. Vandepeer^b^aMardoc Inc., London, Ont., Canada N6G 4N4^bGenesis Software Pty. Ltd., Adelaide, Australia

Received 7 September 1999; accepted 30 January 2000

Abstract

Modern fast digitization techniques and computer methods have been combined with both new and old theoretical approaches to permit construction of a new class of meteor radar. This radar can simultaneously stream data into memory, detect occurrences of meteors, and determine the location of meteor trails (range and angle), as well as find their radial drift speeds and decay times. The meteor entrance speeds as the meteors enter the atmosphere can also be determined. These parameters may then be used to deduce meteor fluxes, as well as winds, temperatures and diffusion coefficients at altitudes of 80–100 km. This information can also be used to deduce source positions of meteor shower radiants. Some of these capabilities are very new, especially the ability to measure atmospheric temperatures at ~ 90 km altitude. © 2000 Elsevier Science Ltd. All rights reserved.

Keywords: ■ ■ ■ Meteors, Atmosphere, Astronomy, radar, interferometry.

1. Introduction

Meteor studies have a long history, and the field was particularly active prior to the mid-1970s. These studies were made to determine both information about the meteors themselves, and also to learn about the atmosphere in which they burn up. Many of the earlier astronomical results have been described by McKinley (1961), and some of the atmospheric results have been described in a special MAP handbook (Roper, 1987). An excellent, and more recent review, is given by Ceplecha et al. (1998).

During the 1980s and early 1990s, the incidence of new meteor research, especially for atmospheric applications, diminished. This was in part due to the retirement of some active researchers, and also because, to some extent, new possible advances were limited by inadequate technology. Many of the previous studies used photographic film, or somewhat primitive computer detection algorithms, and some of the research was manpower intensive. Computer algorithms

were restricted in their capabilities and often “non-meteor” echoes could not be adequately discriminated from true meteor echoes. There was also, in the atmospheric community, a perception that middle atmosphere wind measurements could best be made with other techniques such as spaced antenna studies (e.g. Briggs, 1980, 1984; Hocking et al., 1989) and VHF Doppler radars (Woodman, 1985; Zrnic, 1979; Hocking, 1997b). One notable exception was the work of Avery et al. (1983, 1989), who used narrow beam VHF radars to undertake meteors studies, but because the radars were often optimized for MST VHF studies, the meteor detection rates were often low. Tsuda et al. (1987, 1995) also carried out meteor studies in this time frame.

The availability of fast digitization devices, and high-speed personal computers with large memory buffers, changed this situation. It was now possible to use multi-tasking operating systems like UNIX on personal computers, and simultaneously stream data to memory and analyze it “on the fly”. Furthermore, very detailed meteor selection and analysis algorithms were now possible, permitting very high rejection probabilities for lightning, E-region echoes, impulsive RF interference, auroral echoes, and so forth. Procedures which once required manual intervention and

* Corresponding author. Tel.: +1-519-657-7822; fax: +1-519-657-7822.

E-mail address: mardoc-inc@home.com (W.K. Hocking).

CH/Visage Communications Inc.

Revised
1981

took hours or days to perform on large data sets, could now be performed in real time. Newer, more sensitive detection algorithms were also possible.

Meteor radars have generally used either narrow beams (Avery et al., 1983) or, more commonly, interferometric techniques. The interferometric techniques generally utilize wider beams. In the limit, beams which are almost isotropic can be used, and these are capable of seeing meteors over the whole sky (the so-called “all-sky” systems). Interferometric techniques use phase information recorded at the receiving antennas to determine meteor locations, whereas narrow-beam systems rely on the assumption that most meteors detected occurred somewhere in the main beam of the radar. In regard to the interferometric method, one other limitation of earlier meteor studies was that these systems often used receiving antennas spaced only a half-wavelength apart, and the coupling between these antennas could be severe (up to ~ -10 dB). This therefore produced biases in the phases measured by the antennas, and so produced errors in location of the meteors. Improvements to this design were only forthcoming in the 1990s. Hocking and Thaya-paran (1997) used four antennas spaced by typically 1.5–3 wavelengths, whilst Jones and Webster (1992), and subsequently Hocking (1997a) used a 5-antenna system with minimum antenna spacing of 2 wavelengths. The latter system has been analyzed for coupling effects by Jones et al. (1998). The availability of these new antenna arrangements improved the reliability of meteor systems.

Finally, two other phenomena caused a regeneration of interest in meteor studies. The first was the imminent arrival of the Leonids meteor storm in 1998/1999 (e.g. see Brown et al., 1997, 1998b; Brown, 1999), and the second was the possibility of meteor damage to satellites. These events produced a renewed interest from the astronomical and military communities.

It was within this environment of renewed interest, and significantly improved technology, that the SKiYMET radar was developed.

2. Radar objectives

The purposes behind the construction of the SKiYMET radar were multiple. It was intended that a system be developed which could acquire data at the highest possible rate, and simultaneously perform many different analyses. The ability to run continuously and unattended was also an important requirement. The system was designed to employ interferometry, using optimal receiver antenna spacings, and was also designed to be an all-sky system. This is in contrast to many earlier radars which transmitted their power into moderately narrow beams aligned at low elevation angles. The system was also designed to operate at very high pulse repetition frequencies (PRFs) — up to 2000 Hz and higher. This was a new development for routine meteor studies, since systems in the past often used PRFs of 600 Hz and

less. These higher PRFs would allow the system to be used to determine parameters previously not amenable to standard meteor radar studies, such as meteor entrance speeds. Use of such a high PRF, however, suffered from one limitation — the aliasing range was small. For example, if the PRF is 2143 Hz, the aliasing range is 70 km. Thus, in principle, it would be impossible to resolve whether a meteor had a range of say 65, 135, 205 km, etc. This limitation, however, is easily resolved. Because it is known that the vast majority of meteors burn up in the altitude range between 70 and 110 km, and because the angular location (azimuth and elevation) are well known from interferometry, it is possible in most cases to use this information to determine the true range unambiguously.

Other special requirements of the new design included very detailed real-time meteor echo discrimination algorithms, as well as various forms of on-line “post-detection” software, including determination of middle atmosphere winds (80–100 km altitude), mapping of radiant sources during shower conditions, and determination of ambipolar diffusion coefficients and temperatures. Determination of diffusion coefficients (Tsutsumi et al., 1994) and temperatures (Hocking et al., 1997; Hocking, 1999a) are in fact very recent developments. It was also intended that the radar could measure meteor entrance speeds (e.g. Cervera et al., 1997), and substantial developments have been implemented here to permit real-time determinations. The system is also sufficiently flexible that new developments can be incorporated into the system where appropriate.

A persistent and underlying philosophy has been to ensure that, as much as possible, the data acquisition and analysis are fully integrated onto a single platform. Off-line analysis is reduced because much of the data reduction is performed in real time. Results of the on-line analysis can be obtained with relative ease. At the same time, the raw data associated with any events of possible significance are stored to file in real time, and so are accessible to the user should further detailed analysis be required.

In the following sections, the implementation of these objectives will be described. Following that, examples of typical outputs will be discussed and displayed.

3. Hardware

The system hardware comprises antennas, cables, a transmitter and a receiving/digitizing unit. The antenna layout is illustrated in Fig. 1, where the five receiving antennas are arranged in the form of an asymmetric cross, with arms of lengths of either 2 wavelengths or 2.5 wavelengths, as shown. The location of the transmitter antenna is not critical, although it should not be too close to any of the receivers. Each receiving antenna is connected to a separate receiver with cables of equal phase-length — typically 70 m or so. Systems generally operate at a fixed frequency which is selected by the user, but is normally in the range from 20 to

SKiYMET antenna ground plan

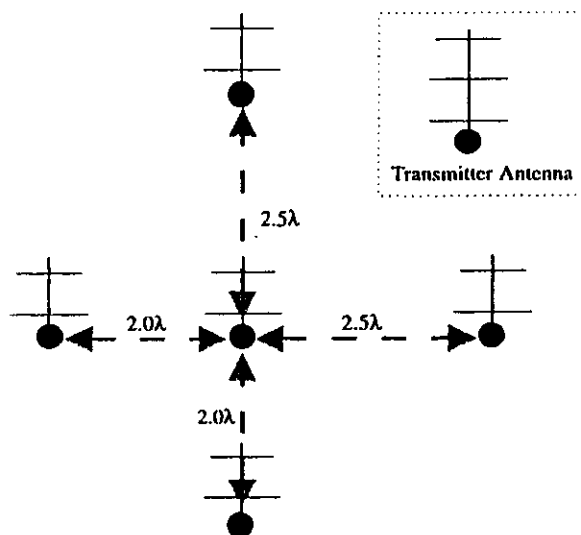


Fig. 1. Plan view of the antenna arrangement for the radar system. The location of the transmitter antenna is not critical and can be placed in any convenient location. The receiving antennas all need to be in a horizontal plane. The symbol λ represents the radar wavelength.

50 MHz. The transmitter antenna is connected to the transmitter with low loss cable. It is also possible, in cases of very long receiver-antenna cables, to place pre-amplifiers at the antennas to enhance the signal for transmission back to the receivers.

The transmitter is a solid state unit comprising (typically) six 1 kW modules, although larger numbers of modules can be used. It is supplied by Tomco Electronics Pty. Ltd. of Australia. It is physically compact, being approximately a cube in shape, and having a length of about 60 cm per side. The peak power transmitted is generally 6 kW, and a selection of pulses are available. They may have a variety of shapes, including Gaussian, square, and square pulses with shaped tapering on the ends. Pulse lengths can also be selected, and can vary from a few hundred metres up to several kilometres. Generally an effective pulse length of about 2 km is the most common choice. The transmitter also includes protection against excessive standing-wave ratios and over-heating.

The next hardware unit to consider is called the Radar Data Acquisition System (RDAS). This unit includes five identical receivers, each connected to a separate antenna, which are then interfaced to a digitization system. It also contains the "Frequency Synthesizer Unit" (FSU), which provides various reference frequencies for the transmitter and receivers. The whole system is in turn driven by a personal computer running under a FreeBSD UNIX operating system. Many parameters can be selected under computer

control, including filter bandwidths: up to four different filters may be chosen. Typical base-band filter half-widths are 25, 50, 125 and 250 kHz. For a 2 km pulse, the 25 kHz filter approximately optimizes the signal-to-noise ratio. Other selectable parameters include pulse length, pulse shape, pulse repetition frequency, receiver gain (up to 122 dB), sampling interval, and number of coherent integrations. The system also contains a large self-diagnostic capability, enabling thorough checks on the system functionality.

The use of a UNIX operating system is an important advantage. It enables fast and efficient multi-tasking, and also makes it easy to link the system to modems and the Internet. The multi-tasking capability makes it possible to stream the data into memory on a continuous basis, while at the same time analyzing the incoming data for the occurrence of meteor echoes. This minimizes the system "blind-time", so that the system is able to detect several thousand useful meteor echoes per day. The data are then written to hard disk. It is possible to store all data to disk, for detailed studies at a later time, or to record only the raw data associated with individual detections. It is most common to use the latter option. Typically, the data stored are ~~for 1 s before~~ ^{for 1 s before} the meteor occurrence, and 3 s afterwards, at the range of detection. These data are then further analyzed to determine meteor range, angular location, height, strength of backscatter, lifetime, radial drift velocity (and its error), and meteor entrance speeds (where possible). This processing once again takes advantage of the multi-tasking capabilities of the UNIX environment, so that the processing can proceed independently while the radar continues to acquire new data. A wide variety of determinations are then possible, such as upper atmosphere wind speeds, temperatures in the meteor region, ambipolar diffusion coefficients, pressure in the meteor region, and locations of shower radiant. A flow chart describing the interactions between the various units, the data acquisition, and the software algorithms, is shown in Fig. 2.

In the following sections, we will describe the various software algorithms in some detail. We will begin with the initial detection software, and then progress to the higher level analyses.

4. Detection algorithms

One of the most important tasks performed by the SKiYMET software is meteor detection and discrimination. In the following sections, these algorithms will be outlined.

Meteor detection is performed with two successive processes. The first algorithm in the meteor identification sequence is termed the "detector", and this performs a "first-pass" examination of the in-phase and quadrature time series, identifies potential meteors for further analysis, and stores the data associated with them to data files, which we shall call "Preliminary Event Files" (PEVs). These files typically include 1 s of raw data prior to the meteor

SKiYMET Hardware and Software Flow Diagram

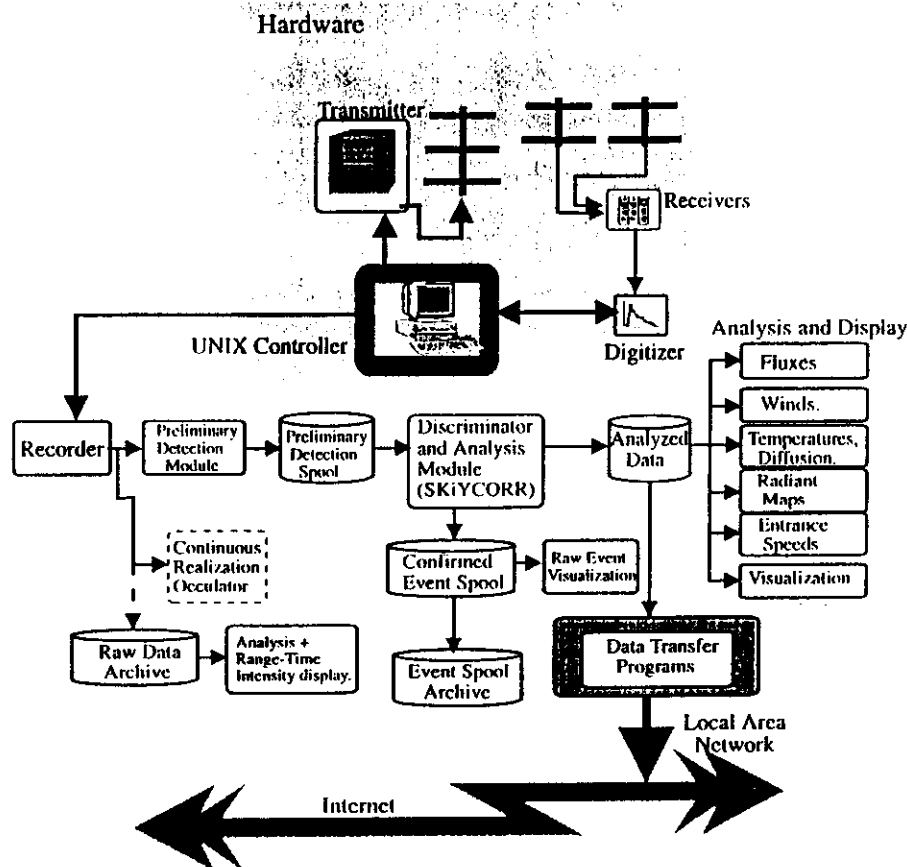


Fig. 2. Flow chart showing the interaction between and within the various hardware and software components of the system.

peak, and 3 s after it, at the range at which the meteor was detected. As a rule, this results in a reduction of storage space by a factor of about 100 (or more) relative to that which would have resulted if all data were stored.

The second-stage analysis (termed “skiycorr”) re-examines these same meteors, but in much greater detail, and confirms them as meteors where possible. This strategy has been adopted so that the first-stage software (detector) has simpler tests to perform and so requires only minimal tasks to undertake during the initial detection. In cases of extremely high data rates, the detector is therefore not encumbered by more stringent tests. The second-stage (confirmation) program then analyzes these “PEV” files, but the time constraints for it are not so severe. Analysis is performed in the background, with the first-stage detector always having the highest priority. The confirmation program analyzes the PEVs whenever there is spare time on the machine. As a rule, with modern computers this second-stage analysis actually completes within seconds of the data acquisition, but in principle it is possible that it could lag the initial

detection by any length of time. Thus, if there are bursts of meteor activity, the first-stage detector can function most efficiently for detection, and the second-stage confirmation can proceed at a later time when the meteor activity has diminished.

4.1. First-stage detection

One of the most difficult processes in the meteor analysis sequence is simply the task of finding meteor echoes and discriminating them from other short-duration signals. The features which distinguish meteors (or at least underdense meteors) include their relatively short duration, their rapid onset, and their quasi-exponential decay time. Once detected, it is relatively simple to perform cross- and auto-correlation functions on them, but the initial detection can be quite difficult, especially if the meteor signal is weak. Therefore, various signal-to-noise improvements are necessary for this initial stage of detection. The “detector” performs the following tests.

eg. see Jones, 1975

Step 1. First, the in-phase and quadrature components are averaged in time bins, thereby implementing a (temporary) coherent integration on each receiver. This is in addition to any coherent integration which has already been performed at the digitization stage. Typically, we average over a sequence of 2–4 points in length (where the actual value is user-specified). The number should be selected in such a way that the integration time is substantially less than the period of the fastest oscillations expected due to the radial drift of the meteor trails. For a PRF of 2144 Hz (which is very common), with an initial coherent integration of 4, an extra (temporary) coherent integration of 2–4 points is a very reasonable number.

Step 2. Next, the amplitude of the signal on each receiver is determined from the in-phase and quadrature averages determined above, and then the program incoherently averages the amplitudes across all five receivers. This optimizes our signal for initial detection purposes. We use the incoherent average across receivers, rather than the coherent one, because a coherent average may well sum to zero, or a small value, since the phases on all five receivers are different. Then, the magnitude of each such sum is compared to the mean value of the amplitude in the previous “ n ” points, where the value of n is user-determined and is typically of the order of 10 or 20. If the current value significantly exceeds the standard deviation of the previous n points, then the point is considered as a possible meteor. If this is not so, the program proceeds to the next point. The meaning of “significant” is user-defined — the user specifies a number which represents the multiple of standard deviations by which the peak must exceed the standard deviation of the previous points. If the point does satisfy this criterion, then a flag is set to indicate a possible meteor. The next point is then examined; it is necessary that this must also exceed the noise floor by the above-specified multiple. If this is not so, the “meteor-present” flag is turned off. If the next point also satisfies this test, the program proceeds to further tests. Individual large spikes usually relate to lightning, or impulsive interference, and if these occur, they can be removed and replaced by the average of the value on either side. This latter process can be selected at the user’s discretion.

Step 3. It is now necessary to proceed to further tests, in order to determine if the signal is truly a meteor. It is therefore determined whether the large value really does rise abruptly out of the noise. If the rise is slow, the data are rejected as aircraft, or E-region echoes, or some other type of contaminant. It is also necessary to ensure that the echo is reasonably short lived (typically less than 2 or 3 s). For example, aircraft generally take a few seconds (typically 10 or more) to pass through the beam so the signal is tested to see if it has returned to “normal” after about 3 s. If this is so, the signal is more likely to be a real meteor, so the test progresses to checking that the mean amplitude level has returned to a value comparable to the noise level within typically 3 s of the peak. This procedure also helps eliminate other slowly fading events such as ionospheric echoes.

However, this test alone is insufficient to ensure that the signal is indeed a real meteor. It is also necessary to check that the meteor suddenly “turns on” and that the mean level for the cluster of three successive points at a location 0.3 s prior to peak does not have a mean value which exceeds the previously assigned trigger level. This effectively constraints the rise time to 0.3 s or less.

Experience has also shown that lightning can be a nuisance, both in the form of lightning-induced RF interference and radar scatter from lightning plasma trails. If these appear in the time series as individual amplitude spikes, they can be removed using the spike-rejection algorithms previously discussed. However, the duration of the lightning signals often exceeds the interpulse period, and their effect can be found on several successive pulses. When this occurs, the signals tend to show substantial amplitude variation throughout their lifetime, rather than the moderately smooth decay associated with meteors. This is true for both RF interference and scatter from lightning plasma-tubes. Other forms of signal also exist which alternate up and down in amplitude on time scales of a few tenths of a second, and these also need to be eliminated. All of these types of echoes can be eliminated with the following test.

Step 4. The data are searched for occurrences where the amplitude fluctuates up and down as a function of time in the 900 ms following the peak, using the following algorithm. First, the place where the amplitude has fallen to 0.3 times the peak value at the initial meteor onset is located. Next, the meteor echo amplitude beyond this point is examined to determine whether the amplitude rises to above 0.7 times the initial amplitude. If this occurs, it is assumed that the echo has non-meteor characteristics. As a consequence, the signal is rejected. This algorithm has proved very effective at removing lightning as well as other non-meteor echoes such as sporadic E-region reflections (which tend to show substantial amplitude variability). It does have the disadvantage that occasionally deeply fading oscillatory over-dense meteor echoes may be rejected, but this likelihood can be accommodated by adjusting the depth of the fading permitted (i.e. the values of 0.3 and 0.7 as previously discussed). This procedure will also remove signals associated with over-dense meteor trails, but since these are only a small percentage of the total number of meteors, the loss is not too significant. The rejection of a great many false echoes more than compensates for the few over-dense meteors which may be rejected by this algorithm.

Step 5. Despite the care taken in these tests, experience has shown that non-meteor events can occasionally slip through, and therefore there is one more important test which can be applied. This test also rejects very weak meteors which cannot be used because their signal-to-noise ratio is too small to allow their locations to be determined. The actual test involves forming the cross-correlation function between all pairs of antennas and examining the variance of the rate-of-change of phase of these correlation functions. When the standard deviation of the rate-of-change

of phase at zero lag is found across all receiver-pair combinations, a very useful decision-making parameter is obtained. If the value is small, it is relatively certain that we have a good meteor, while if the value is large, it is likely that the “signal” is in fact very noisy and should be discarded. The division between a “large” and “small” standard deviation must be determined by the user, but visual examination of many meteors has permitted us to determine that a value of about 6 m/s (where the rate of change of phase has been converted to a radial drift velocity) is reasonable. However, in the detector algorithm, the parameter can be user-defined. Indeed in some cases, values of up to 12 m/s are accepted, so that even some very weak meteors will not be rejected. More rigorous tests are applied in the following, second-stage detector, program, which will be discussed shortly. It should be noted that the cross-correlation function, rather than the autocorrelation function, is used, since the autocorrelation function has a troublesome noise-spike at zero lag which can complicate calculations. The cross-correlation function is less contaminated by such spikes.

The above tests have been found to be very effective in removing non-meteor echoes. As an example, during a recent meteorological storm, 4000 echoes due to lightning were recorded and were initially accepted as meteors; yet after running through these final two identification processes, it was found that there were only 10 left. About six of these were real meteors, and the other four were lightning spikes superimposed on simultaneous short-lived aircraft occurrences. This is a relatively rare event, and four such “false detections” in the course of a day’s worth of meteors represents a very small error rate. However, it is emphasized that these detection criteria can be controlled, to some extent, by the user. Some parameters are adjustable, and some tests can be turned on or off. Often the criteria are relaxed so that a higher percentage of “doubtful” signals are accepted. This is done so that these echoes can be visualized with the various graphics packages available; it is often a good idea to be able to investigate “doubtful meteors” from time to time, in order to keep a visual check on the rejection criteria. It must be remembered that all these detections will still be subjected to a much more rigorous series of tests in the second-stage confirmation program, so false detections will be removed there. Indeed, the criteria used in that program even allowed removal of the four curious lightning-cases “left over” in the discussion above.

Step 6. Finally, if an echo is detected and passes all of these tests, the data associated with this echo ~~is~~^{are} saved to a PEV file. In particular, a 4-s data stream containing all of the in-phase and quadrature components for each receiver is saved, where the data stream starts 1 s prior to the peak of the meteor, and finishes 3 s after the peak, at the range of detection. Data are not stored at the resolution used for the tests discussed earlier, but rather at the (much higher) temporal resolution of the original data acquisition specifications.

4.2. Second-stage analysis: meteor confirmation

4.2.1. Data storage and general strategy

The second stage of identification and confirmation can now begin. The program name used for these studies is “skycorr”. It is possible to run this analysis in parallel with the first-stage detector, with this new program identifying new 4-s records and analyzing them as soon as the detector has produced them. However, it is also possible to save all 4-s files and analyze them at a later time. The purpose of this program is two-fold. First, it is used to further subject the original meteor-detections to more rigorous testing, to be sure that the “possible meteors” really are valid meteors. Files which pass these tests are written to new files called “Confirmed Event” files (CEVs). Then, secondly, it is used to determine the location of the meteors in the sky (zenith, azimuth and range), and then perform other calculations such as determinations of decay times, radial velocities, and entrance speeds. The results of these analyses (including meteor trail drift velocities) are then written to an ASCII text file for further study. Once again, these analysis procedures will be described in a sequential manner.

Before applying these tests, it is important to register the intrinsic phase delays between the antenna/receiver combinations. These delays must be known in order for the algorithm to determine meteor positions. They arise from a variety of factors, but are mainly due to receiver delays, since all cables are generally cut to equal phase lengths, and all receiving antennas are identical. As a rule these phase delays are measured at the time of installation, and also at regular subsequent intervals. They are stored to file, from which the skycorr program can read them as required. We have found that the receivers are very stable with respect to time, and drift by only a few degrees over the course of a year. Nevertheless, regular phase checks are highly advised.

Skycorr repeats some of the steps in the detector, but with more aggressive rejection criteria. Some new tests have also been added and these will be discussed in due course. It also has the option to include its own “spike-rejection” criteria, which can be used either to supplement that used in the detector, or to replace it entirely.

The confirmation program, skycorr, then begins to search for meteors within each 4-s record produced by the detector. The 4-s PEV files also contain some header information which tells the skycorr program where (within the 4-s record) to look for the meteor. Following this, skycorr performs a double-check of the position of the meteor peak. This check begins with a search of the incoherently averaged data points, seeking out pairs of points which stand out above the noise, just as in the detector, but with more stringent acceptance criteria.

Once a possible meteor has been accurately located, a series of more thorough tests then ensues. Some of these repeat algorithms used in the first stage of detection, but with more stringent parameters. However, the majority of these tests are new. They are listed below. It should be noted that

some of the tests may not seem especially “stringent”. This is true, and it is a deliberate strategy, with the intent being to apply many tests of a modest nature throughout the program, rather than one or two extreme tests. When combined, our tests then make a powerful discriminator of meteor echoes.

4.2.2. Second-stage tests

The tests performed in “skycorr” are now described.

Step 1. Three separate data intervals of width 0.25 s are isolated at the following locations. The first interval is found at the very start of the record (usually 1.0 s prior to the meteor peak, and therefore covering a range from 1.0 to 0.75 s prior to the peak). The second interval is chosen just prior (0.35–0.1 s) to the peak. The third is found starting 0.7 s after the peak. The root-mean-square (RMS) values of the incoherently averaged data within these three bins are then found and compared. The largest RMS (root-mean-square) value of these is selected and is compared to the value of the peak of the meteor (where the peak value has been found after applying both the coherent and incoherent integrations described earlier). It is required that this peak value exceed the largest RMS value within the other three bins by at least a factor of two. (It is worth noting that when the incoherent amplitude averages are formed, the mean value is offset from zero by an amount which can substantially exceed the standard deviation of the amplitudes. This offset is removed from all the data before any tests are performed, and it is especially important to be aware of this for the above tests.) A factor of two may not seem large, but is sufficient to eliminate cases where the “peak” detected by the detector turns out to be little more than a noise burst.

Step 2. The next step involves cross-correlating the data on the different channels prior to the meteor peak. In this case, rather than requiring high levels of correlation, low levels are sought, so it can be determined that the meteor truly has occurred suddenly. This therefore takes advantage of one of the most unique features of meteors – the fact that meteor signals rise very rapidly out of the noise. This test successfully removes cases of moderate E-region reflections which are persistently present but which suddenly increase in strength, for example, because the data prior to the sudden increase are still correlated. It is also a very good way to remove aircraft contributions which somehow passed through the earlier tests. Specifically, the variance of the rate of change of phase of the cross-correlation functions between all pairs of antennas is examined near zero lag. The test is very similar to the cross-correlation procedure described earlier for the detector, but in this case small values are rejected because this indicates highly correlated data just prior to the meteor. In reality, the rates of change of phase are converted to radial drift velocities (the units of which are m/s) and those cases in which the standard deviation for the mean is less than 2.0 m/s are rejected.

Step 3. Following step 2, the same type of tests are applied yet again, but on this occasion the interval of time used includes that in which the meteor occurred. In this case, data

which are well correlated are sought. A data bin of typically 1.0–2.0 s is used, depending on the meteor duration, and cross-correlation functions are formed between all pairs of receivers. It has been found that data are acceptable if the standard deviation of the mean radial drift velocity is less than 5.5 m/s. This has been determined largely by the visual inspection of many hundreds of meteors, and this test works well for radar frequencies above 30 MHz. Larger values are acceptable for lower frequencies.

If the data passes all of the above tests, an acceptable meteor has been identified; if not, the data are rejected and ignored and the program passes on to examine the next 4-s data set.

5. Meteor parameters

The next step is to determine parameters which describe the meteor and its plasma trail. These are found in the skycorr program, after the meteor has been confirmed. Clearly, the peak amplitude and the lifetime are easily found – the latter is determined by finding the time for the cross-correlation function to fall to 0.5 times its value at zero lag.

One of the most important pieces of information is, of course, the location of the meteor in the sky. This is found by comparing phase differences of the meteor signal at zero time lag in the cross-correlation functions, after compensation for any intrinsic phase differences between the receivers. These phase differences may then be inverted to determine a direction of arrival of the reflected radio wave by standard interferometric techniques (e.g. Roettger and Ierke, 1985; Larsen and Roettger, 1991; Larsen et al., 1992). The novel interferometric antenna arrangement shown in Fig. 1 removes (in principle) any angular ambiguities. However, if the meteor signal-to-noise ratio is poor (leading to errors in the phase determinations), it can happen on occasion that the program cannot decide between two possible meteor positions in the sky. If this occurs, both options are saved, and the meteor is assigned an “ambiguity level” which specifies the number of acceptable angular positions. All this information is saved to the final output file so that the subsequent user can decide whether to employ this information or not. In general, only a small percentage of meteors show such angular ambiguities.

At this juncture, there is another calculation which needs to be made, and this is the determination of the height of the meteor. If the range is known, this is relatively trivial, since the angle from zenith may be used to determine the height. The curvature of the Earth is allowed for in this calculation. However, there are times when this calculation is more complicated; this occurs if the pulse repetition frequency of the system exceeds 1500 Hz. Such high PRFs are often used to enhance the signal-to-noise ratio, and also to permit determination of quantities which require higher temporal resolution (such as calculation of meteor entrance velocities).

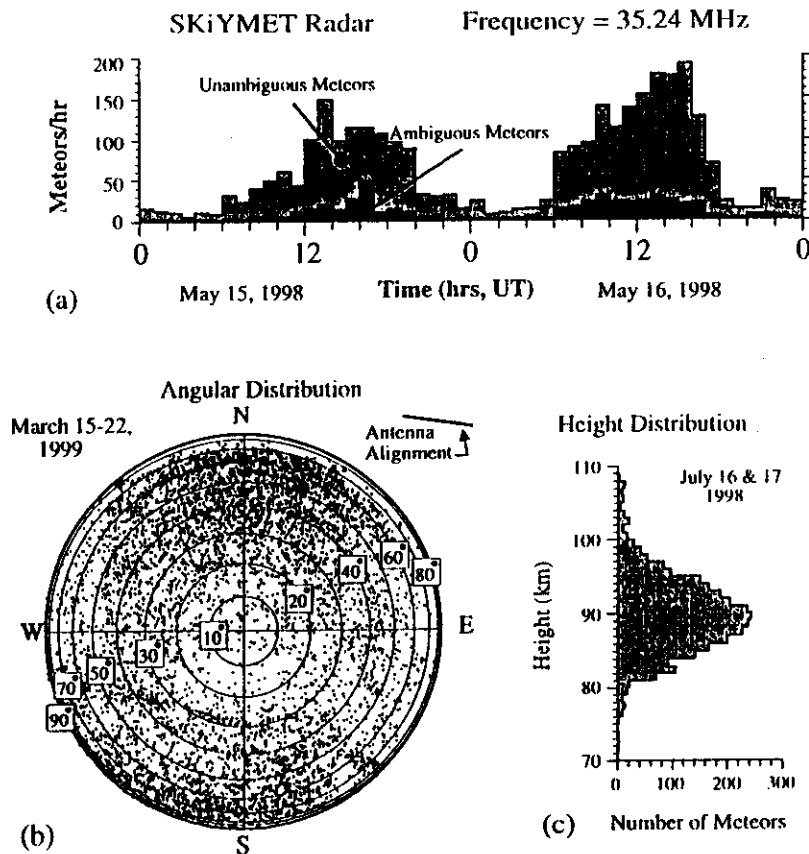


Fig. 3. Displays of typical flux data produced by the radar. (a) Typical meteor count rates as a function of time of day over a period of two days. A pronounced diurnal cycle is apparent, although the day-to-night variation is not always this severe. (b) Typical azimuthal and zenithal distribution of several thousand meteors, taken with a system in New Mexico. Note that the excess of meteors to the north and south are due to the antenna alignment. If crossed antennas are used, the distribution becomes more rotationally symmetric. (c) Typical height distribution of the meteors recorded with the radar.

6.2. Upper middle-atmosphere winds

Upper atmosphere winds have always been a main-stay of radio-meteor research. Measurements of this parameter are accomplished by measuring the radial velocity of every meteor detected, and then combining these measurements in an all-sky manner to determine upper level winds. In the case of SKiYMET, radial velocities are determined within *skiyccor* by using both auto- and cross-correlation functions associated with meteor detections, and using the rate of change of phase near zero lag to determine the radial velocity. All possible cross correlations between all signals from all five receiving antennas are used, as well as the auto-correlation functions on each receiver, and then the average is taken. The standard deviation for the mean is also found. This latter parameter is used as an estimate for the error, and is also stored with the radial velocity for subsequent analysis. If, however, the standard deviation for the mean is excessively large (typically greater than 5.5 m/s — see previously) then

the “meteor” is rejected entirely.

The on-line all-sky least-squares fitting routine currently assumes a uniform wind $\mathbf{u} = (u, v, w)$ and then minimizes the quantity

$$\sum_i [(\mathbf{u} \cdot \mathbf{r}_i'' - v_i)]^2, \quad (1)$$

where i refers to the meteor number in a specified height and time window. Typically, such a window would cover a height region of 3–4 km, and a duration of about 1.5 h. Such windows are stepped at time steps of 1 h, and height steps of 3 km. The vector \mathbf{r}_i'' is a unit vector pointing from the radar to the i th meteor trail. The value v_i is the measured radial velocity, and $\mathbf{u} \cdot \mathbf{r}_i''$ is a dot-product.

In the simplest case, it is assumed that $w = 0$; in more complex cases, it is possible to also assume that there are gradients as a function of position in the sky. The SKiYMET radar produces an on-line solution of Eq. (1) for the special case that $w = 0$, but provides all the relevant information

If a high PRF is used, it is possible that the meteor will be range-aliased. For example, a PRF of 2144 Hz (a commonly used value) produces an aliasing range of ~ 70 km, so a meteor at 150 km range appears at a range of 10 km. Likewise meteors at 80 km range, or 220 km range also appear at 10 km. SKiYMET therefore determines all possible ranges from which the meteor might have come, and then uses this information to determine possible heights of the meteor. Ranges which do not produce a height in the region 70–110 km (where these limits can be user-specified) are rejected. In the majority of cases (except for the lowest elevation angles), this procedure produces only one possible range, thus allowing unambiguous location of the meteor. In cases where there are range ambiguities, the “ambiguity level” is increased to reflect this fact, and the possible range-angle combinations are printed to file. Thus, these are still available to subsequent users should they be needed.

The final parameter which is determined is the speed at which the meteor entered the atmosphere. Determination of this parameter is not always possible, but when it can be determined, it represents very important information. The details about this determination will be given later.

Finally, the data are written to two files. One is a binary file, and the other is a text file. This dual option offers some extra security against file deletion, and also permits users to use either as input for subsequent analyses. The following data are written to file. First, the date and time are given (year, month, day, hour, minute, second, and millisecond). Then a unique identifier is given which allows the user to identify the 4-s record which holds the raw data (CEV file) for this meteor; this can be useful if the user wishes to go back and examine the raw data associated with the meteor in more detail. Following this, the range and height of the meteor are listed. Then the mean radial drift velocity and its associated error for the mean are written. Following this are the angle from zenith, and the azimuth angle anti-clockwise from due East. The next parameter is the ambiguity level — if this is 1, the data are unambiguous, whilst if it is greater than 1 then there exists the possibility that the meteor has been wrongly located. In the case of ambiguous echoes, other possible locations will be suggested in the lines immediately preceding or following the current line. Following this, a value representing the phase errors between antenna pairs is stored. This is found by determining the phase differences which should exist between all antenna pairs for the specified meteor location, and then finding the difference between the actual value and this “theoretical” value. The largest such difference is then recorded. This can sometimes be used to resolve between several possible ambiguous meteor locations. The next parameter is a 2-digit number which specifies which antenna pair has this maximum phase error. Other important parameters which are written to file include the meteor amplitude (digital units), the meteor decay time, and the meteor entrance speed into the atmosphere (if available).

6. Scientific measurements

We now turn to consideration of the scientific parameters deduced in the analyses. Some of these are determined in SKiYMET, but the system also includes other algorithms which accept the output of SKiYMET and determine higher level information, which relates to the essential science produced by the radar. The SKiYMET radar affords measurements of a variety of parameters, including both “traditional” ones, and some very new capabilities. Of the “traditional” ones, meteor fluxes, upper atmosphere winds and ambipolar diffusion coefficients are the most predominant, while newer parameters include absolute measurements of atmospheric temperature and pressure, as well as astronomical quantities like meteor entrance speeds and radiant mapping. In the following subsections, we will describe the various techniques used to determine and demonstrate their application. It is not possible to describe each technique in detail, but we will present a brief overview, and refer the reader to more detailed articles where appropriate.

6.1. Meteor fluxes

Perhaps the simplest parameter to measure with a radar of this type is meteor fluxes. In its simplest form, this consists simply of “counting” meteor occurrences. However, in order to be useful for astronomy purposes, it is important to make certain adjustments. Firstly, it is necessary to compensate for angular biases in detection rates. Such biases occur due to radar polar diagram effects, range effects, and atmospheric effects. The strengths of the meteor echoes should be converted to more useful parameters like particle mass. In order to do this, it is necessary to utilize the meteor amplitude, and use the known transmitted power, receiver gains and efficiencies, range effects and atmospheric effects, ~~and such conversions~~. Atmospheric biases include angle of entry effects. For example, meteors tend to be detected more commonly at angles beyond 25° from zenith, and rather more rarely from overhead. The meteor echo strength varies proportionally to the meteor range to the power of -3 . Examples of the types of calculations involved in these conversions can be found in Brown and Jones (1995) and Brown et al. (1998a, b), and references therein.

The SKiYMET software does not do these conversions directly, since the determinations are best done on a site-dependent basis, but it does provide all the information needed to do such conversions. Information which is supplied includes echo amplitude, range, zenith angle, and azimuth. Fig. 3 shows plots of typical meteor fluxes (before correction) and typical angular and height distributions. Notice that in this case there is a preponderance of meteors in two directions: this arises because the antennas which were used were planar Yagi antennas. If crossed antennas are used, fed with a 90° phase difference, this asymmetry disappears, and options exist to use such antennas with the SKiYMET system.

→ ic
(scribble)

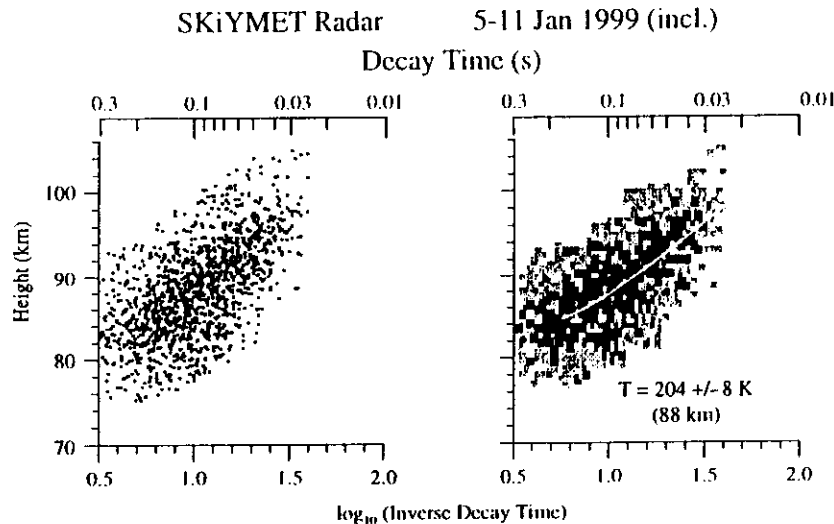


Fig. 4. Typical graphs of decay times vs. height produced by a SKiYMET radar. The graph on the left shows a scatter plot of individual meteors, while that on the right shows a density plot for the same data. The density shades are not given in absolute units since only the relative densities are important for the curve fitting. A best-fit fourth-order polynomial is shown as the white line in the right-hand side graph.

for the user to apply more sophisticated least-squares fitting algorithms should they so choose.

There is one more recommended process which should be applied in meteor winds determinations, which is also applied with the on-line SKiYMET determinations. This is a double-iteration of Eq. (1). In this process, Eq. (1) is first applied to all data in the specified time- and space-bin, to produce (u, v, w) . Then, for each meteor, the radial velocity which should have been observed, assuming that the true mean wind was indeed (u, v, w) , is determined. This is then compared to the actual measured radial velocity. If this difference exceeds some user-specified value (typically 30 or 40 m/s) then this meteor velocity is rejected as an outlier. This rejection value does not need to be specified too carefully — its purpose is simply to remove truly errant radial speeds. Then, Eq. (1) is repeated, but only using meteors which pass the above test. This procedure tends to “clean up” the data. It does not necessarily mean that rejected meteors are erroneous measurements, but rather that they are not typical of the “average” conditions in the sky at the time. They could, for example, come from a region and time where there were large, short-lived perturbations in the wind fields. Such events are often deserving of further study, but such investigations must be left to the scientists using the instruments. For first-order estimates of the mean wind, they are best ignored.

It is also useful to store the value of $\{[\sum_i (v_{m(i)} - v_o)^2]/N\}^{1/2}$, where N is the total number of points, $v_{m(i)}$ is the model radial velocity determined for the i th meteor assuming that the meteor’s angular location has been correctly located and that the mean wind is correctly specified by (u, v, w) , and v_o is the measured radial velocity for this

meteor. This parameter is called the “residual”, and gives a measure of fluctuations of the wind speeds about the mean. It serves as a crude indicator of gravity wave and turbulence strengths.

Because the wind speed is a somewhat common parameter, and has been determined with many previous radars, we will not present graphical examples here. Examples can be found in Hocking and Thayaparan (1997), among others.

6.3. Ambipolar diffusion coefficients, temperatures and pressures

Another fundamental parameter that is produced by meteor signal analyses is the decay time of the amplitude. The time for the amplitude to fall to one-half of the peak amplitude is given by

$$\tau_{1/2} = (\lambda^2 \ln 2) / (16\pi^2 D_a), \quad (2)$$

where D_a is called the ambipolar diffusion coefficient and λ is the radar wavelength. Studies of D_a have been undertaken by several authors (e.g. Tsutsumi et al., 1994; Nakamura et al., 1997). It has been shown (e.g. Jones and Jones, 1990; Hocking, 1999a) that the ambipolar diffusion coefficient is related to the atmospheric temperature (T) and pressure (P) at the height of the meteor trail by

$$D_a = K_a T^2 / P, \quad (3)$$

where K_a is a constant. A graph of the logarithm of the inverse-decay-time as a function of height is a monotonically increasing function with substantial scatter. An example is shown in Fig. 4. By fitting a polynomial to plots like this as a function of height, Hocking et al. (1997) were able

Temperatures at ~75N

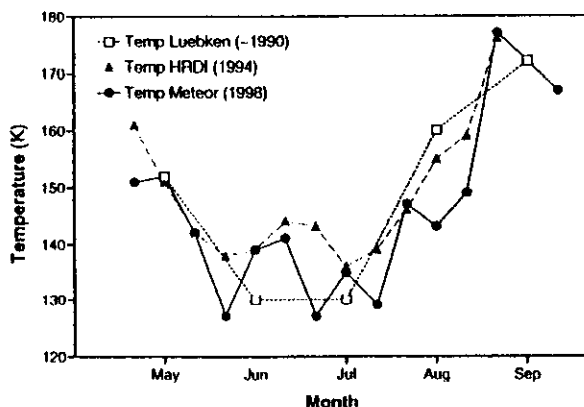


Fig. 5. Temperatures measured by a SKiYMET-like radar at Resolute Bay in northern Canada, and compared to other methods, during the summer time.

to produce reasonable estimates of T^2/P as a function of height and month, which compared moderately well with the COSPAR International Reference Atmosphere (CIRA). However, because of errors in the CIRA pressures, it was not possible to use these estimates to produce accurate absolute temperatures. However, by using a different approach, which involves a scale-height analysis of D_0 , Hocking (1999a) was able to deduce absolute temperatures at the height of peak meteor count rates, and this process required no knowledge of the atmospheric pressure. This procedure appears to be robust, and Fig. 5 shows an example of temperatures measured at Resolute Bay, in northern Canada, compared to other reference measurements. After determination of absolute temperatures, and determination of T^2/P from Eq. (2), it is also possible to derive absolute pressures at this same height. Determination of pressures is a very novel capability which is rare in almost any ground-based instrument.

SKiYMET radars are capable of all these calculations, and have already produced a large number of measurements of these quantities at a variety of sites. Detailed studies using these results will be forthcoming in future publications. It should be especially noted that the meteor radar operates throughout both day and night, and this gives the system the ability to study tidal temperature oscillations. For example, by superposing decay times from common hours throughout a full month, a composite day can be produced, with temperatures determined for each hour of the day. Harmonic fitting can then be applied, to give diurnal and semidiurnal temperature tides. This opens new possibilities for studies of atmospheric tides which have previously not been available, since many of the instruments which have produced mesopause-level temperatures in the past have been optical in nature, and could not operate outside of cloud-free, moon-free, night-time conditions.

6.4. Radiant location

In astronomical studies of meteor activity, a common requirement is determination of the sources of meteors. Meteors can be either sporadic, or shower, types. In the former case, they tend to come from a broad range of locations in the sky, while in the latter case they come from a single radiant. Although it is not possible to determine the radiant of any individual meteor using the SKiYMET radar, it is nonetheless possible to determine locations of radiants when many meteors have a common origin. This can be done in the following way.

When a meteor enters the atmosphere, it is seen by the radar if it produces a plasma trail which is aligned perpendicular to a vector originating from the radar and pointing to the meteor trail. Thus, there is a "great circle" in the sky, centered around the radar, along which ~~meteors~~ can be detected. Conversely, if a meteor trail is detected at a particular azimuth and zenith angle, then it is known that the meteor radiant must have been at some point on another great circle aligned perpendicularly to the vector from the radar to the trail. The exact location of the source on this great circle is unknown. However, the great circle can easily be plotted in celestial equatorial co-ordinates. If we now turn to another meteor, it also has its own great circle of "possible radiants", and this can be plotted. It will generally differ from that of the first meteor. Such great circles can be plotted in celestial equatorial co-ordinates for every meteor detected. This requires compensation for the time of day of the detection, as well as compensation for latitude and longitude, but it is not a difficult procedure. If there were a significant single source of meteors in the sky (as during a meteor shower), then many of these great circles will cross at a common right-ascension and declination, and this point will indicate the source of the shower.

This procedure has been automated with the SKiYMET radar, and Fig. 6 shows two examples of this procedure. The first shows a typical situation when there is no dominant source in the sky. It can be seen that there is a broad region which is slightly stronger than its surroundings, but the region is diffuse. Such diffuse "sources" are common for the case where the sporadic background is the main origin of most meteors. The second shows the case when there is a strong meteor source in the sky, and it correctly locates the position of the shower radiant to within 3° . More detailed analysis allows even better localization. Other versions of similar algorithms have been presented by Jones and Morton (1982) and Jones and Brown (1993, 1994).

It should be emphasized that even in the case of sporadic meteors, the SKiYMET radar gives useful information about the distribution of meteors. Studies using SKiYMET-like radars are already underway to further understand both meteor sources and this diffuse background (e.g. see Brown et al., 1998a,b). Accurate location of radiant sources, and studies of the sporadic background, are therefore both areas

A meteor
from
meteor
radiant

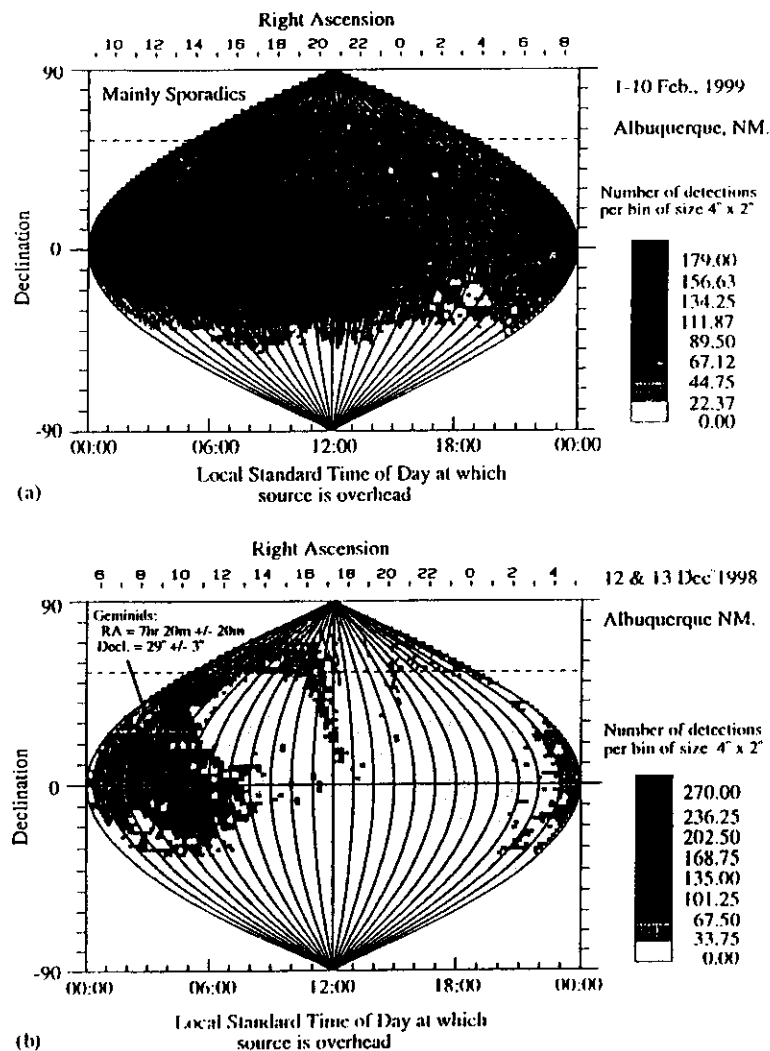


Fig. 6. (a) Results of “radiant mapping” determinations for data from early February, 1999. This is a period when there are no major sources in the sky, so that this is a typical case for a sporadic background of meteors. Note that the abscissa uses two scales — one is the right ascension, the other is the time of day at which radiant (if any) is overhead. To use this axis, apply the scales to the equator, then follow the curved lines of right ascension to (or from) the appropriate declination. (b) Results of “radiant mapping” determinations for data from December 12 to 13, 1998. This is a period when the Geminids stream was the major source in the sky. Notice that the strongest density is at the point indicated by the circle in the top left-hand corner. The correct value for the location of the Geminids, according to the Norton’s Star Atlas (Norton, 1973), is RA = 7 h 28 min, Decl. = +32°. This agrees with the value determined by the analysis to within the error quoted on the figure. It should be emphasized that the errors shown arise because of our choice of grid size — higher accuracy is indeed possible (to about 1.5° or better) if smaller grids are used. We have chosen to use the coarser resolution because this graph emulates a real-time display on the system. Use of a smaller grid size produces software which is too slow for on-line implementation, but can certainly be applied off-line.

where the SKiYMET radar is making, and will continue to make, significant contributions.

6.5. Meteor entrance speeds

Meteors enter the atmosphere with speeds in the range of typically 10–100 km/s. There are therefore at least two

speeds associated with a meteor trail. One speed is the drift of the trail as it is blown around by the atmospheric wind, but there is also a second. This latter speed is the speed at which the head of the meteor moves through the atmosphere, and it is very similar to the speed of entry of the meteor into the atmosphere. Whilst it is common to measure the drift speed due to the wind, it is also possible, although more difficult, to measure the speed

of the head of the echo. This determination can be undertaken as follows.

If a meteor trail being formed in the atmosphere is illuminated by radio waves impinging from a direction perpendicular to the direction of alignment of the trail, then a Fresnel diffraction pattern is produced at the radar by the backscattered radio waves. This pattern sweeps past the radar (as the front of the trail proceeds to move forward) with the speed of the incident meteoroid which formed the trail. This pattern has a well-known shape, which is similar to that formed when light is diffracted around a sharp edge (e.g. Hecht and Zajac, 1974, p. 386). By measuring the complex amplitude as a function of time, it is possible to measure the speed of the pattern past the radar, and thence that of the meteor itself. It should be emphasized that this diffraction pattern first appears before the meteor signal peaks in amplitude, and persists after the peak. In the past, the amplitude oscillation occurring just after the peak has been used to measure the meteor speeds (e.g. McKinley, 1961), and more recently Cervera et al. (1997) have used the phase oscillations prior to the peak. The SKiYMET radar is unique in that it employs both these parts of the signal time series, and uses them to determine the entrance speed. The determination is fully automated. We will not describe the method in full detail here; it is discussed in much more detail by Hocking (1999b). However, we will demonstrate some results produced by the SKiYMET radar.

Fig. 7 shows a sequence of typical distributions of meteor speeds measured with a SKiYMET radar near Adelaide, Australia. The maximum speeds are around 40 km/s, but this is a limitation of the sampling strategy used, rather than the technique itself. In this case, we used a PRF of 2144 Hz, and a 4-point coherent integration. Higher speeds can be measured if less coherent integrations are used. The basic shape is broadly similar from one time interval to the next, but there are also some subtle differences. One difference of note is that there is a secondary peak at speeds of 7–8 km/s, and this peak shows a temporal variation. This is the speed which dust and debris would have in orbit around the Earth, and so it is possible that these points could be due to space debris falling into the atmosphere, or dust from a diffuse cloud orbiting the Earth. This particular group of meteoroids deserve much further study.

On occasions, there is an extra feature which shows in these graphs, and that is the presence of a narrow “spike” of velocities superimposed on the general shape. This arises when meteor showers are present and dominant. The speed associated with such spikes is that of the entrance speeds of meteors from the shower, and there is usually only a very small spread in values. Indeed, it appears (from multi-frequency comparisons of the same meteors) that the method can determine the speeds to accuracies of less than 0.5 km/s. By combining information about entrance speeds, and radiant determinations, it is possible to determine the orbits of meteor streams. This is very important knowledge for meteor astronomers, since it allows them to associate

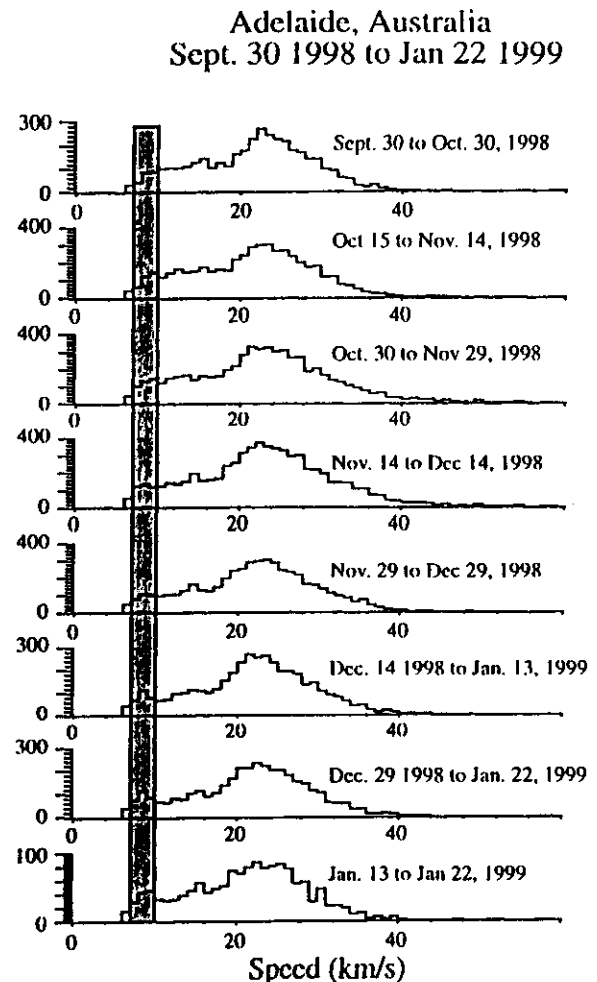


Fig. 7. Typical distributions of the entrance speeds of meteors as they enter the atmosphere, for a PRF of 2144 Hz, and a 4-point coherent integration. Speeds of around 7–8 km/s are highlighted. These data were produced at a site called Delamere, near Adelaide, Australia, but similar graphs have also been produced at other sites.

particular meteor streams with particular comets. An outstanding example of this appears in the paper by Arlt et al. (1999), where a study of the June Bootids meteor shower was able to prove for the first time that this meteor stream was associated with a comet called Pons-Winnecke. Such studies are relatively simple with the SKiYMET radar.

7. Conclusions

We have demonstrated how, by combining new technology and both old and new concepts in meteor physics, it has been possible to develop a new generation of meteor radar. The principles used in meteor selection, and examples of applications of the data, have been demonstrated. Examples

have included both atmospheric and astronomical application of this instrument.

8. Uncited References

Jones, 1975, Roettger, 1981

Acknowledgements

This project involved help and support from many people. We are especially grateful to Michael Smith, Shane Dillon, Adrian Murphy, Daniel O'Connor, Jacqui Nelson, Anna Hocking, Suzanne Hocking, David Hocking and Jeffrey Hocking. Useful discussions with Peter Brown and Jim Jones are also acknowledged. Support from Alan Manson and Chris Meek during an installation at Saskatoon is also acknowledged, as is the help from the staff at Starfire Optical Base in New Mexico during an installation of a SKiYMET radar at that site. Interactions with Kerry Ellis and Alan Webster are also recognized.

References

- Arlt, R., Rendtel, J., Brown, P., Velkov, V., Hocking, W.K., Jones, J., 1999. The 1998 outburst and history of the June Bootid meteor shower. *Monthly Notices of the Royal Astronomical Society* 308 (3), 887.
- Avery, S.K., Riddle, A.C., Balsley, B.B., 1983. The Poker Flat, Alaska, MST radar as a meteor radar. *Radio Science* 18, 1021–1027.
- Avery, S.K., Vincent, R.A., Phillips, A., Manson, A.H., Fraser, G.J., 1989. High latitude tidal behaviour in the mesosphere and lower thermosphere. *Journal of Atmospheric and Terrestrial Physics* 51, 595–608.
- Briggs, B.H., 1980. Radar observations of atmospheric winds and turbulence: a comparison of techniques. *Journal of Atmospheric and Terrestrial Physics* 42, 823–833.
- Briggs, B.H., 1984. The analysis of spaced sensor records by correlation techniques. In: *Handbook for MAP, Vol. 13, Ground Based Techniques*. Univ. of Illinois, Urbana, pp. 166–186.
- Brown, P., 1999. The Leonid meteor shower: historical visual observations. *Icarus* 138, 287–307.
- Brown, P., Hocking, W.K., Jones, J., Rendtel, J., 1998a. Observations of the Geminids and Quadrantids using a stratosphere-troposphere radar. *Monthly Notices of the Royal Astronomical Society* 295, 847–859.
- Brown, P., Jones, J., 1995. A determination of the strengths of the sporadic radio-meteor sources. *Earth, Moon and Planets* 68, 223–245.
- Brown, P., Simek, M., Jones, J., 1997. Radar observations of the Leonids: 1964–1995. *Astronomy and Astrophysics* 322, 687–695.
- Brown, P., Simek, M., Jones, J., Arlt, R., Hocking, W.K., Beech, M., 1998b. Observations of the 1996 Leonid meteor shower by radar, visual and video techniques. *Monthly Notices of the Royal Astronomical Society* 300 (1), 244–250.
- Cepkecha, Z., Borovicka, J., Elford, W.G., Revelle, P.O., Hawkes, R.L., Porubcan, V., Simek, M., 1998. Meteor Phenomena and bodies. *Space Science Reviews* 84, 327–471.
- Cervera, M.A., Elford, W.G., Steel, D.I., 1997. A new method for the measurement of meteor speeds: the pre- t_0 phase technique. *Radio Science* 32, 805–816.
- Hecht, E., Zajac, A., 1974. *Optics*. Addison-Wesley, London, p. 565.
- Hocking, W.K., 1997a. System design, signal processing procedures and preliminary results for the Canadian (London, Ontario) VHF Atmospheric Radar. *Radio Science* 32, 687–706.
- Hocking, W.K., 1997b. Recent advances in radar instrumentation and techniques for studies of the mesosphere, stratosphere and troposphere. *Radio Science* 32, 2241–2270.
- Hocking, W.K., 1999a. Temperatures using radar-meteor decay times. *Geophysical Research Letters* 26, 3297–3300.
- Hocking, W.K., 1999b. Real-time meteor entrance speed determinations made with interferometric meteor radars. *Radio Science*, submitted for publication, in press, 2000.
- Hocking, W.K., May, P., Roettger, J., 1989. Interpretation, reliability and accuracies of parameters deduced by the spaced antenna method in middle atmosphere applications. *Pure and Applied Geophysics* 130, 571–604.
- Hocking, W.K., Thayaparan, T., 1997. Simultaneous and co-located observation of winds and tides by MF and Meteor radars over London, Canada, (43°N, 81°W) during 1994–1996. *Radio Science* 32, 833–865.
- Hocking, W.K., Thayaparan, T., Jones, J., 1997. Meteor decay times and their use in determining a diagnostic mesospheric temperature-pressure parameter: methodology and one year of data. *Geophysical Research Letters* 24, 2977–2980.
- Jones, J., 1975. On the decay of underdense radio meteor echoes. *Monthly Notices Royal of the Astronomical Society* 173, 637–647.
- Jones, J., Brown, P., 1993. Sporadic meteor radiant distributions: orbital survey results. *Monthly Notices of the Royal Astronomical Society* 265, 524–532.
- Jones, J., Brown, P., 1994. The radiant distribution of sporadic meteors. *Planetary and Space Science* 42 (2), 123–126.
- Jones, J., Morton, J.D., 1982. A method for imaging radio meteor radiant distributions. *Monthly Notices of the Royal Astronomical Society* 200, 281.
- Jones, J., Webster, A.R., 1992. Forward-scatter radiant mapping: Asteroids, Comets, Meteors. Lunar and Planetary Institute, Houston, pp. 273–276.
- Jones, J., Webster, A.R., Hocking, W.K., 1998. An improved interferometer design for use with meteor radars. *Radio Science* 33, 55–65.
- Jones, W., Jones, J., 1990. Ionic diffusion in meteor trails. *Journal of Atmospheric Terrestrial Physics* 52, 185–191.
- Larsen, M.F., Palmer, R.D., Fukao, S., Woodman, R.F., Yamamoto, M., Tsuda, T., Kato, S., 1992. An analysis technique for deriving vector winds and in-beam incidence angles from radar interferometric measurements. *Journal of Atmospheric and Oceanic Technology* 9, 3–14.
- Larsen, M.F., Roettger, J., 1991. VHF radar measurements of in-beam incidence angles and associated vertical-beam radial velocity corrections. *Journal of Atmospheric and Oceanic Technology* 8, 477–490.
- McKinley, 1961. *Meteor Science and Engineering*. McGraw-Hill, Toronto.

X

Editor
2.A.
Vincent

- Nakamura, T., Tsuda, T., Tsutsumi, M., 1997. Development of external interferometer for meteor wind observation attached to the MU radar. *Radio Science* 32, 1203-1214.
- Norton, A.P., 1973. Norton's Star Atlas, 16th Edition. Gall and Inglis, Edinburgh, p. 153.
- Roper, R.G. (Ed.), 1987. Handbook for MAP, Vol. 25. Scostep Secretariat, University of Illinois, Urbana, IL, USA, 422 pp.
- Roettger, J., 1981. Investigations of lower and middle atmosphere dynamics with spaced antenna drifts radars. *Journal of Atmospheric Terrestrial Physics* 43, 277-292.
- Roettger, J., Ierkic, H.M., 1985. Postset beam steering and interferometer applications of VHF radars to study winds, waves and turbulence in the lower and middle atmosphere. *Radio Science* 20, 1461-1480.
- Tsuda, T., Nakamura, T., Kato, S., 1987. Mean winds observed by the Kyoto Meteor radar in 1983-1985. *Journal of Atmospheric and Terrestrial Physics* 49, 461-466.
- Tsuda, T. et al., 1995. A preliminary report on observations of equatorial atmospheric dynamics in Indonesia with radars and radiosondes. *Journal of the Meteorological Society of Japan* 73, 393-406.
- Tsutsumi, M., Tsuda, T., Nakamura, T., 1994. Temperature fluctuations near the mesopause inferred from meteor observations with the middle and upper atmosphere radar. *Radio Science* 29, 599-610.
- Woodman, R.F., 1985. Spectral moment estimation in MST radars. *Radio Science* 20, 1185-1195.
- Zrnić, D.S., 1979. Estimation of spectral moments for weather echoes. *IEEE Transactions on Geoscience Electronics* GE-17, 113-128.

Simultaneous and colocated observation of winds and tides by MF and meteor radars over London, Canada (43°N, 81°W), during 1994–1996

W. K. Hocking and T. Thayaparan

Department of Physics, University of Western Ontario, London, Ontario, Canada

Abstract. Simultaneous and colocated comparisons of winds and tides by MF and meteor VHF radars have been made in the 85–94 km height range from July 1994 to June 1996 over London, Ontario, Canada. Results have been obtained for every month of the year. From these comparisons it is concluded that, in general, the MF spaced antenna technique and the meteor method both provide reliable means for synoptic studies of neutral air motions in the height range 85–94 km, at timescales of greater than 12 hours, and therefore are valuable tools in middle atmospheric research. However, we do find that some parameters seem to be estimated with greater precision than others. In particular, the measurements of the zonal long-term wind variations, and the semidiurnal tide in both the zonal and meridional directions, seem particularly robust and reliable, while there is somewhat less consistency between measurements of the zonal diurnal tide and the meridional monthly mean winds. The former problem is very likely to be an artifact of the strong diurnal variation in meteor count rates. However, we cannot claim that our meridional monthly mean wind agreement is always good, and these discrepancies deserve further investigation.

1. Introduction

Atmospheric winds in the mesosphere and lower thermosphere have been observed routinely for many years with radars using the spaced antenna technique. This technique (hereinafter referred to as the SA technique) was originally used for total reflection experiments, in which case the incident radio waves were totally reflected from layers of ionization in the upper atmosphere. The method was subsequently modified for *D* region work using partial reflections [e.g., Awe, 1961; Fraser, 1965, 1968; Fraser and Kochanski, 1970; Briggs, 1977, 1984; Hocking *et al.*, 1989], and later still used for tro-

pospheric and stratospheric wind measurements with VHF radars [e.g., Röttger and Vincent, 1978; Röttger, 1981]. The received signals are due to reflection and scatter from weakly ionized irregularities in the mesospheric *D* region and from neutral air and humidity fluctuations in the troposphere and stratosphere. Extensive observational studies of winds, waves, and turbulence have been made with this technique, but doubts have been expressed in the past as to the type of motion actually measured in such experiments, which might be the motion of turbulence carried along by the wind, atmospheric wave motions, or ionization drifts of electromagnetic origin [e.g., Hines and Rhagava Rao, 1968; Hines *et al.*, 1993].

The best way to test for possible biases in wind estimates when using the SA technique is by comparisons with other different techniques at the same place and time. Extensive compar-

Copyright 1997 by the American Geophysical Union.

Paper number 96RS03467.

0048-6604/97/96RS-03467\$11.00

isons and tests of the SA technique have been carried out with rocket, satellite, and radar measurements. For example, *Fraser and Kochanski* [1970] and *Gregory and Rces* [1971] initially showed that SA measurements at MF and HF in the *D* region produced reliable winds. In many such comparisons the two sets of data were separated in space and time. *Stubbs* [1973] and *Stubbs and Vincent* [1973] compared the SA wind with the meteor measurement of the neutral wind, where the two sets of equipment were at nearby locations. They showed that SA winds agreed well with meteor measurements of winds in the 80-100 km region and concluded that the partial reflection experiment was capable of measuring the neutral air motion in the *D* region. More recently, *Cervera and Reid* [1995] compared MF SA wind velocities in the 80-98 km height range with meteor measurements. The agreement between the two techniques was generally good below 90 km, while above 90 km they found that the SA technique yields smaller wind speeds than the meteor drift technique.

Vincent et al. [1977] compared neutral wind measurements in the *D* region made by rocket techniques with drift observations made by the SA technique, and again good agreement was obtained. *Labitzke et al.* [1987] made a comparison between direct wind observations based on the MF SA technique and geostrophic winds based on satellite-derived height fields (approximately 78-80 km) in 1979-1982 and found very good agreement for most of the year. *Lloyd et al.* [1990] compared the winds measured by an optical Fabry-Perot interferometer system and by an MF SA radar system during the autumn and early winter in 1987. When data were available, the results from the two instruments were consistent with each other, both in wind direction and amplitude. Similar investigation was later carried out by *Phillips et al.* [1994], and once again, strong similarities in the MF SA radar and Fabry-Perot interferometer Doppler wind fields were observed, although some differences existed (possibly due to auroral contamination).

The above extensive comparisons, which include a large body of data at a variety of locations, strongly suggest close agreement between winds measured by the SA technique and neutral air motions. While there is much accumulating evidence that the SA technique yields a reliable means of estimation of the motion of the neutral air, nevertheless, a few report disagreements, including *Wright* [1968], *Rossiter* [1970], and *Hines et al.* [1993]. At least some of the disagreements (e.g., *Wright* [1968] and *Rossiter* [1970]) are understandable as defects of the experimental arrangement and as a consequence of spatial or temporal sampling distinctions between the measurements [e.g., *Stubbs*, 1973; *Stubbs and Vincent*, 1973].

However, *Hines et al.* [1993] recently conducted intercomparisons among wind measurements using MF radar, incoherent scatter radar, and meteor radar during the AIDA'89 (Arecibo Initiative in Dynamics of the Atmosphere) campaign in April 1989 with the fundamental objective of testing the wind interpretation of MF/HF partial reflection drift measurements in the lower ionosphere. On the basis of comparisons of the different sets of observations they concluded that MF/HF partial reflections systems are capable of measuring the neutral air motion below 80 km, and above 80 km they fail to give consistently reliable measurements of the neutral winds. It is important to point out here that these results are limited to a single site over a limited period (7 days) of observations. *Hines et al.* [1993] suggested that the discrepancies revealed during the AIDA'89 experiments may be a result of the contamination of wind estimates by the phase velocity of the internal gravity waves because the MF scattering process is modulated by the passage of such waves through the scattering volume. This is a recurring suggestion put forward by *Hines and Rhagava Rao* [1968]. Originally, it was proposed that the SA method might be actually measuring the motion of the waves themselves and thus be measuring the phase speeds of the waves. This suggestion seems unlikely because it requires that the received signals are due to reflection from ex-

tended partially reflecting planar surfaces which have been modulated by the presence of gravity waves, and it is now largely believed that this suggestion is improbable. For example, *Hocking et al.* [1989] have discussed this possibility and have suggested that extended specular reflectors are unlikely, being probably broken up into short sections and thereby restricting any biases produced by this "specular reflection" model. However, more subtle models which involve gravity wave contamination have recently been developed. For example, *Hines* [1991] has proposed that the biases may be due to preferential selection of the wind field when using the MF method, something similar to the proposal of *Nastrom and VanZandt* [1994] but applied to horizontal velocities. This is to say that when there is an anisotropic gravity wave field, turbulence will be preferentially generated at times and wave phases when the instantaneous wind field at any location bears certain systematic relationships to the general direction of propagation of the wave field. In particular, instances when the instantaneous winds are generally in the same direction as the overall mean sense of propagation of the asymmetric wave field will be more inclined to generate turbulence. At other times, when the instantaneous winds have different relationships to the mean wave phase speed, there will be a tendency for greater stability and hence less formation of turbulence. Thus, while any individual measurement of the wind might be a true representation of the wind at that point and time, once one starts forming averages, then the means will be weighted toward those occasions when the instantaneous wind has directions commensurate with the preferred direction of phase speeds of the wave field.

A very different explanation for the AIDA'89 campaign results was given by *Kudeki et al.* [1993]. These authors pointed out that SA wind estimation errors due to wind field inhomogeneities in the presence of vertical velocity fluctuations within the scattering volume may account for the discrepancies observed in the AIDA campaign. *Kudeki et al.* [1993] proposed a wave-induced fluctuations model and showed

that systematic wind estimation errors should be expected to result from spatial variation in the vertical component of the perturbation wind field associated with gravity waves. The fluctuation biases may be large in instantaneous velocity estimates but will average to zero mean in a long-term temporal average, suggesting that estimates of tidal and longer-period waves should be relatively accurate. This explanation was further substantiated and supported by more detailed numerical simulation results presented by *Sürücü et al.* [1995]. Only isotropic scattering was considered by *Kudeki et al.* [1993], but the numerical simulations were carried out for both isotropic and specular scatterers with different sets of gravity wave parameters by *Sürücü et al.* [1995]. The numerical results of *Sürücü et al.* [1995] are summarized as follows. First, the individual horizontal SA wind estimates are very well predicted by the model of *Kudeki et al.* [1993], as long as the gravity wave has a horizontal wavelength larger than the horizontal dimension of the MF radar scattering volume. When the scatterers are highly anisotropic ("specular"), the estimated winds averaged over one period of the perturbing gravity wave exhibit statistically significant biases from the model of *Kudeki et al.* [1993], but the bias is not necessarily toward the phase speed of the gravity wave. The largest biases were obtained for large amplitude (~ 10 m/s) waves with small horizontal wavelengths (< 40 km) and were of the order of 15 m/s. On the basis of these results, *Sürücü et al.* [1995] concluded that wind estimation biases of the magnitude observed in the AIDA campaign results are unlikely to result from the mechanism suggested by *Hines et al.* [1993] but are more likely to result from the systematic measurement errors described by *Kudeki et al.* [1993]. Finally, we note that a reanalysis of the AIDA data by *Turek et al.* [1995] suggests that the agreement between MF, meteor, and incoherent scatter is actually fairly reasonable, at least up to 90 km altitude.

However, nagging doubts remain about the motions which are detected by the SA type of experiment. Hence further tests of the SA method

have been carried out over London, Ontario, and the results are presented in the following sections. The strength of our comparison is its extended nature, having been made over a 2-year period and covering every month of the year, and the fact that our two instruments are essentially colocated, being less than 400 m apart on the ground. We will concentrate our studies on tidal and larger periods in order to avoid the types of problems described by *Sürücü et al.* [1995], but we will also present some instantaneous comparisons later in the paper.

The two techniques that we consider here are the MF SA and the VHF meteor interferometer radar technique. These are of particular interest because they are both used to measure winds and tides in the mesosphere and lower thermosphere (80-100 km). In the following section the MF and VHF meteor radar systems are described. The comparisons of the two experimental techniques are described in section 3. Section 4 describes two different data analysis methods used to analyze the meteor data, together with the method of analyzing the MF data and its statistical uncertainties. Following this, a comparison of winds and tides measured by the two techniques is described in section 5. The discussions and conclusions of this study are presented in sections 6 and 7, respectively.

2. Instrumentation and Basic Techniques

A VHF interferometric meteor radar and a MF radar have been used to produce simultaneous and colocated observations of the horizontal winds in the mesosphere and lower thermosphere (82-94 km) at the Environmental Science Western Facility near the University of Western Ontario (UWO) in London, Canada (43°N, 81°W). The two sets of equipment were at locations about 400 m apart. Both systems have been operating simultaneously since July 1994, with the MF system running continuously. The VHF system only operates as a meteor radar for typically 10 days per month, since for the rest of the time it is used as a wind profiler radar for

studies of tropospheric dynamics. These colocated radars provide a unique opportunity to check the consistency of parameters measured by the MF and meteor experimental techniques. Results of these comparisons are presented and discussed in the following sections. In this section we only describe the main features of the two radar systems. The detailed description of the design strategy and the system implementation of the radars are given by *Hocking* [1993], *Hocking* [this issue], *Thayaparan et al.* [1995a], and *Thayaparan* [1995].

2.1. VHF Meteor Radar

Since July 1994 the Canadian (London, Ontario) VHF atmospheric radar (CLOVAR) [*Hocking*, this issue] has been used to measure horizontal winds by utilizing radio reflections from meteor trails. This radar has been designed to provide nearly all-sky coverage, and measures Doppler shifts in the frequency of meteor echoes and meteor locations (angular position and range) as its fundamental quantities. Meteor locations are calculated using standard interferometric procedures, with meteors being located to an accuracy of $\pm 3^\circ$ in zenith and azimuth. This section describes the main characteristics of the radar when used in meteor mode.

The VHF radar operates at a frequency of 40.68 MHz, corresponding to a wavelength of 7.375 m. Peak power was 5 kW until September 1995 and was subsequently increased to 10 kW in that month. The duty cycle used was normally $\sim 1.47\%$, and the pulse length was 13.33 μs , which is equivalent to 2-km range resolution. A pulse repetition frequency (PRF) of 1100 Hz was used in the earlier experiments (from July 1994 to December 1994), and this was later (from January 1995) increased to 2143 Hz in order to increase the meteor echo detection sensitivity by allowing increased coherent integration. The PRF of 2143 Hz was carefully chosen so that there was a range ambiguity at 70 km, but since very few meteors are detected below 70 km in altitude, this was not a drawback. Rather, we deliberately sampled at altitudes of 10-58 km and relied on the fact that the mete-

ors were known to exist at ranges of greater than 70 km and so were known to be range-aliased. For example, an echo at a true range of 80 km will appear at an apparent range of 10 km, and one at a true range of 140 km will appear at 70 km. Thus by recording from 10 to 58 km we in fact recorded all echoes at ranges between 80 and 128 km. This procedure worked well but required that extra selection criteria be incorporated into our software to ensure that we did not confuse aircraft and other short-lived tropospheric phenomena with meteors. By starting our sampling at 10 km, we were able to largely avoid any real atmospheric echoes. However, in order to be quite sure we had real meteors, our selection criteria were designed to seek out only underdense meteors, as will be seen shortly.

One problem does exist with this strategy, and that is the fact that some meteors (at angles beyond about 50° from zenith) could be at ranges in excess of 150 km, and so be range-aliased into the recorded data by a triple-range alias. Such meteors were typically no more than about 5% of the data but could become more important during meteor showers. We will reconsider these special cases later.

When transmitting at 1100 Hz, an eight-point coherent smoothing was performed on the raw data to improve the signal-to-noise ratio, while a 16-point coherent integration was used when transmitting at 2143 Hz. We use a single receiver which had the ability to multiplex signals from four separate input receivers (see *Hocking* [1993] for more details). Therefore we attained a sampling time interval of ~ 29 ms when using 1100 Hz PRF and ~ 30 ms when using 2143 Hz PRF.

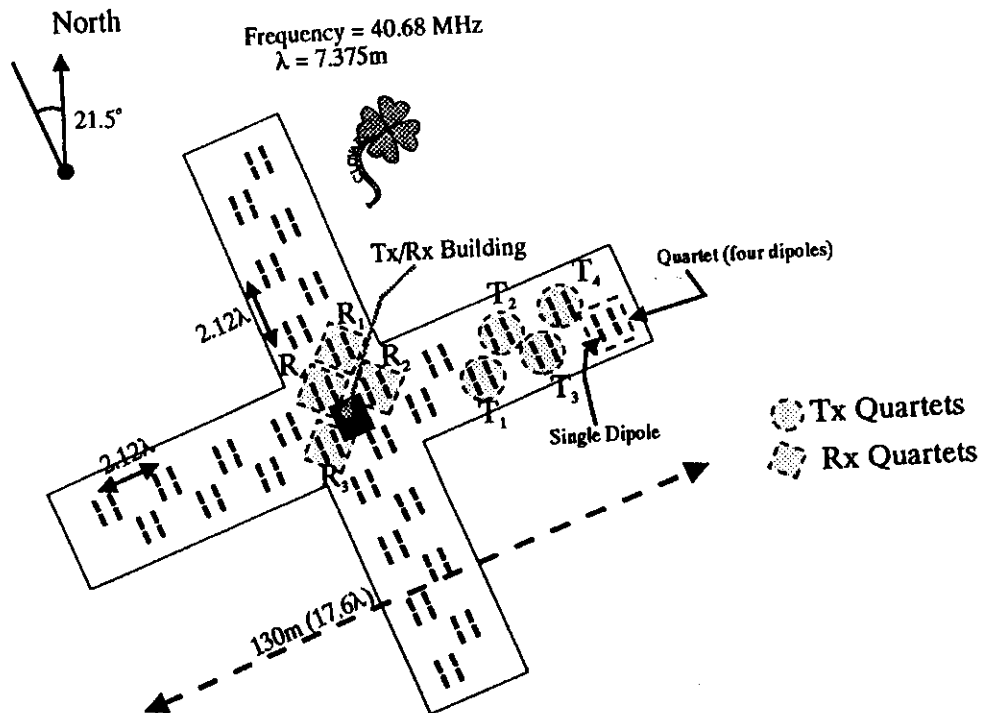
The configuration for the antenna system of the UWO VHF radar is sketched in Figure 1a. Each antenna group (denoted a "quartet") consists of four half-wave dipoles at the corners of a square. The dipoles are suspended $\lambda/4$ above the ground plane, where λ is the radar wavelength. The distance between each dipole of a quartet is $\lambda/2$. This arrangement ensured minimal ground wave radiation of RF (radio frequency) energy along directions parallel and per-

pendicular to the dipoles. The quartets labeled as T_1 , T_2 , T_3 , and T_4 were used simultaneously for transmission, and quartets R_1 , R_2 , R_3 , and R_4 were used for reception. By phasing antennas T_2 and T_4 to be π out of phase with respect to T_1 and T_3 , we forced the transmitter polar diagram to look like four separate, broad beams pointing about 25° off-zenith to the north, south, east, and west (see Figure 1b). Each such beam has a half width of about 25° . This arrangement ensures that maximum power is radiated in these four directions, but we emphasize that all meteor direction determinations were done by interferometry.

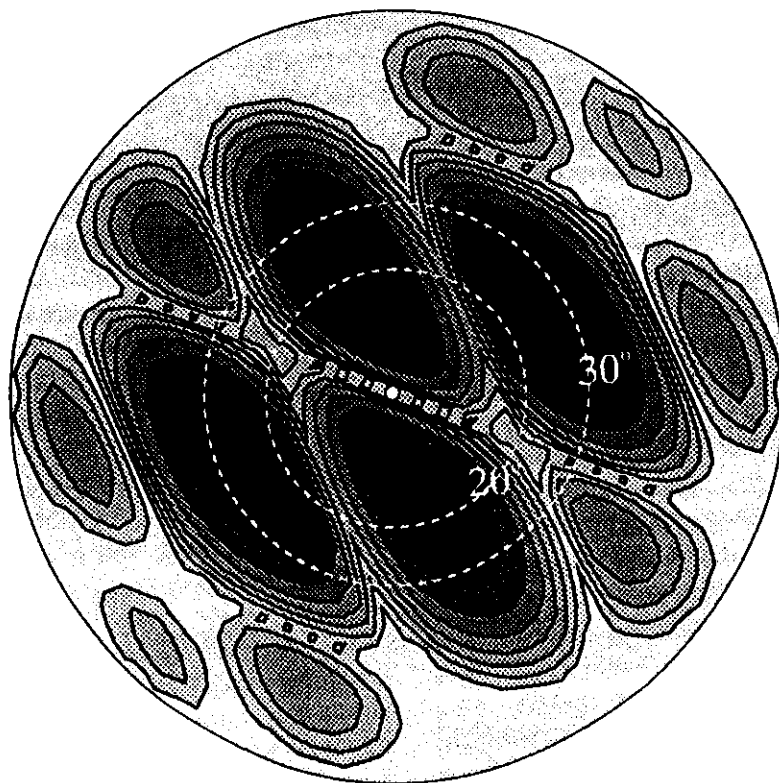
Another advantage of this configuration is that receiving antennas R_1 and R_2 are only 0.53λ apart in the east-west direction, and R_2 and R_3 are only 0.53λ apart in the north-south direction, but at the same time the antennas are sufficiently far apart ($>1.5\lambda$) that antenna coupling is not significant. The more conventional meteor receiver antenna spacing of $\lambda/2$ can involve some degree of antenna coupling, and such coupling can lead to errors in determination of the phase difference between adjacent antennas. Even small errors can be very important when the antenna separations are so small. Not only is the coupling reduced with our arrangement, but also, errors in phase determinations are less severe when a longer baseline (like ours) is used.

Despite the advantages of this larger spacing, there are also some disadvantages. To begin, there is some angular ambiguity with this particular set of antennas; that is, meteors at angles beyond about 50° from the zenith cannot have their directions unambiguously resolved. One set of phase differences between receiver antennas can correspond to two possible angles in the sky. For example, a meteor at a true position of, say, 60° from zenith in the west direction could give the same set of phase differences as perhaps a meteor at 45° in the southeast direction. However, by drawing on the fact that we know the normal height range of the meteors, we can largely remove this ambiguity. For example, it often turns out that for one of these possible positions the combination of position and range

(a) Meteor Antenna Layout



(b) Transmission Polar Diagram



results in an unrealistic meteor height, so that this possibility can be eliminated. The only exception to this rule is for meteor echoes which are triple range-aliased; in those cases, we can produce erroneous meteor direction determinations. However, experiments at lower PRFs have shown that such cases occur less than about 5% of the time. Elimination of these low-angle meteors is especially helped by the polar diagrams of the transmitter beams (see Figure 1) and the receiver antennas, which have low gain at low elevation angles; the half-power half width of the receiver antenna polar diagram is about $\pm 25^\circ$. However, the fraction of low elevation angles can increase during major meteor showers, so we generally avoid such time intervals for our wind determinations.

Meteor detection and direction determination are performed in real time at the radar. Prior to May 1996, data collection and analysis were performed on the same computer, and data collection ceased while analysis proceeded. Typically, data were recorded for about 1 min, and then this data set was searched for meteors. The data search took typically 30 s, and then the sequence was repeated. After May 1996, the single computer was replaced by two personal computers networked together, so that one computer was used for data collection while the other was used for data analysis. In this way, the total downtime for data collection was reduced to about 3%, with the analysis computer working on data just acquired by the data acquisition computer, and the data acquisition computer proceeding to record the next data set (see *Hocking* [this issue] for more details).

The meteor detection algorithm basically searches for a place in the time series where two

successive amplitude points exceed a threshold value compared with the mean noise level of the time series. After several trial and error tests, we have adopted the following criteria. If the average amplitude of a pair of successive points exceeds about 3σ , where σ is the root-mean-square (RMS) amplitude of the typical "noise" (i.e., when there are no meteors present), then the amplitudes following these initial two larger successive peaks are examined, and if the elevated values are sustained (i.e., are not impulsive spikes), then the corresponding interval in the time series is identified as being a possible meteor. It is also required that no secondary peaks occur in a region up to 2.5 s after the original large amplitudes. Overdense echoes exist and can last for up to tens of seconds, but it was decided to use the time interval of 2.5 s in order to eliminate false detections such as aircraft, man-made impulsive noise, etc., in the meteor-detection procedure. Once the meteor is detected, the algorithm also checks a few points back from the maximum amplitude of the location of the meteor trail to test whether the echo is characterized by a very rapid initial rise in amplitude. This procedure successfully rejected the data if there was any beating present in the echo or any other irregularities present due to trail distortion. After several tests, it turns out that the maximum amplitude is generally reached within 0.1 s, and it was decided to use this value as a reliable time limit in the meteor detection procedure. Any slower-rising echo is rejected by the program. As an additional test, the signal in the 1-s interval prior to the main peak of the meteor is also studied for coherence; if it is coherent, it indicates that the current peak is probably not a real meteor, but if

Figure 1. Graphs showing the layout of the transmitter and receiver antennas and the polar diagram for transmission. Contour levels in Figure 1b are at 4-dB steps. The locations of the transmission quartets within the main Canadian (London, Ontario) VHF atmospheric radar (CLOVAR) array are shown by shaded circles, and these were fed with successive phase differences of π . This produced four main lobes in the transmission polar diagram at $20^\circ - 30^\circ$ from overhead. The four receiving quartets are indicated by shaded diamonds. The ground plane of the array is not shown.

this preceding data set shows evidence of being noise (erratic rates of change of phases at the origin of the autocorrelation function), then it truly indicates that this peak has risen abruptly out of the noise and is very likely a meteor. This procedure successfully rejected overdense meteors, aircraft, *E* region echoes (e.g., sporadic *E*), and possible turbulence scatter. Visual inspection of the output signals of several hundred meteor observations using this algorithm showed it to be a reliable discriminator of meteors.

Toward the end 1996, we also found that we could improve our sensitivity by incoherently averaging the amplitudes received on all four antennas. We found this gave us much better meteor-detection capabilities, and this was a major advantage. Often the location of the meteor is the most difficult part of the procedure. Once a meteor had been located in the time series, it is relatively easy to form complex cross-correlation functions for subsequent analysis. Indeed, many of these procedures discussed above evolved during the development of the system, so that as time went by we found we were achieving better and better count rates. In July 1994 we typically detected 200 meteors per day, while by the beginning of 1996 the typical count rate was up to 400 per day. Further into 1996 (particularly with the advent of the two-computer system and the use of incoherent averaging of receiver amplitudes for the initial meteor detection) we were able to achieve count rates in excess of 800 and more per day.

Auto-correlation and cross-correlation functions were formed using data from typically a 2- or 3-s window around the meteor peak, where the window length is different for each meteor but is always greater than the time it takes for the meteor signal to disappear into the noise again. Direction determination and radial velocities are calculated by standard interferometric techniques [e.g., Hocking *et al.*, 1989], in which we use phase differences between pairs of antennas to determine direction. The phase difference recorded on two receiver antennas at position vectors \vec{R}_i and \vec{R}_j is given by $\phi_{ij} = (2\pi/\lambda)(\vec{R}_i - \vec{R}_j) \cdot (\vec{I}_m)$, where \vec{I}_m is the unit vec-

tor in the direction of the meteor. By considering three antennas at \vec{R}_1 , \vec{R}_2 , and \vec{R}_3 , and finding phase differences between all pairs, it is possible to invert the phase differences to determine the direction \vec{I}_m . More specific details are given by Thayaparan [1995]. We should emphasize that when we determine directions, we allow for the phase differences to have various multiples of 2π added and subtracted, in order to check for all possible angular ambiguities. The initial tests are done using only receive antennas 1, 2, and 3, and this gives several possible positions in the sky. Anticipated phase differences between antenna 4 and antennas 1, 2, and 3 are then determined for each possible meteor location, and then these are compared with the actual phase differences measured. As a rule, all but one position is ruled out by this cross-check strategy, thereby giving the actual position of the meteor in the sky. Only meteors which can be located absolutely unambiguously are used in subsequent analysis.

Rates of change of phase of the autocorrelation and cross-correlation functions at zero lag are used to determine radial velocities [Hocking *et al.*, 1989] through the relation $v_{\text{radial}} = (\lambda/(4\pi))(d\phi/dt)$ evaluated at zero lag. We ensure that the radial velocities estimated by rates of change of phase from all autocorrelation functions of all receivers, as well as the crosscorrelations of all pairs of receivers, are self-consistent; if there are significant differences, the data set is rejected. This procedure very effectively removes lightning echoes, for example, which tend to have erratic phase variations near zero lag of the correlation functions. Once all these tests have been satisfied, the relevant information (time of occurrence, radial velocity, position, degree of ambiguity (if any), and meteor lifetime) are stored to file for subsequent analysis.

2.2. MF Radar

The MF radar operates at a frequency of 2.219 MHz and transmits 20 kW of peak power at a duty cycle of 0.12%. The pulse repetition frequency is 60 Hz with 32-point coherent integra-

tion. This gives an effective sampling interval of 0.533 s. Since November 1992 the radar has been used to measure horizontal winds with the spaced antenna method in the 49-142 km height range. We emphasize, however, that we only consider the MF winds to be reliable estimates of neutral winds in the region below 95 km and will not make any use of the higher-level data. Wind measurements are made at time intervals of 5 min and at 3 km height intervals, although the vertical pulse length is closer to 4-5 km. The configuration for the receivers is three antennas in an equilateral triangle with a spacing of 225 m. The transmitter uses a 3×3 array of dipoles with 150-m spacing. The complex autocorrelation and cross-correlation functions obtained with 512-point time series are parameterized to obtain true velocity estimates using full correlation analysis (FCA) [e.g., Briggs, 1984; Hocking *et al.*, 1989]. A more detailed description of the MF radar system is given by Thayaparan *et al.* [1995a] and Thayaparan [1995].

3. Comparison of the Experimental Techniques

Before we can make any comparison between the results obtained with the two different techniques, we must recognize that the two methods are strongly influenced by many factors unique to each particular system, such as beam width, antenna design, scatterer characteristics, and temporal and spatial distinctions. The purpose of this paper is essentially to test the validity of the SA MF method, and we are implicitly assuming that the meteor winds form a reliable reference. However, the assumption that the meteor measurements provide accurate wind data in the 85-94 km height region needs to be discussed; there are exceptions to this rule. For example, when a meteor trail shows strong alignment with the direction of the Earth's magnetic field, the meteor trail can drift in directions which may be unrelated to the neutral wind motions [Kaiser *et al.*, 1969]. The degree of alignment required decreases with height and is about 2° at 114 km; a much tighter alignment is re-

quired at altitudes of around 90 km, where most of our analysis applies. It can therefore be assumed with confidence that the large majority of meteor trails observed move with the neutral wind. However, there are other important factors. For example, the rate of incidence of meteors is a strong function of time of day, with a large maximum at around 0600 LT. There are also variations in daily meteor rates from day to day, and certain regions of the sky can receive preferentially more or fewer meteors than others.

It is also of interest to compare the regions of the sky over which each technique effectively averages its data. The volume from which information is received by the MF SA system can be approximately determined from the effective pulse width (equivalent to height resolution) and the beam width of the polar diagram of the radar. The half-power half width of the polar diagram is $\sim 20^\circ$ and the effective pulse width is ~ 3 km. This implies that measurements at a nominal height of 90 km must be an average result for a horizontal area ~ 72 km in diameter, with a 3-km uncertainty in height. Therefore, for the MF partial reflection experiment, the bulk of the returned power comes from within a volume of $\sim 10,000 \text{ km}^3$ ($\sim \pi r^2 h$, where $r \approx 36$ km at $h = 3$ km) centered at 90 km. Because the partial reflection process often involves scattering from a considerable volume, the wind field obtained by the SA technique is effectively a spatial smoothing (or averaging) over the volume from which information is obtained. Additionally, the 5 min record time length may result in some degree of smoothing (or averaging) of the drift motion.

In contrast, with the VHF meteor wind technique the short lifetime of a meteor trail (typically ≤ 0.4 s) means that the radial component of the wind velocity obtained is essentially an instantaneous measurement and the wind measurement is made over a time interval of 2.5 s or less. The pulse width (equivalent to range resolution) of the VHF meteor radar is ~ 2 km. In meteor studies the radio reflection from a meteor trail is specular, with the majority of the reflected power coming from the first Fresnel zone.

This quantity is given by $\sim 2(R\lambda/2)^{1/2}$, where R is the meteor range from the observatory site and λ is the operating radio wavelength. The size of the first Fresnel zone is of the order of 1 km near 90 km for $\lambda = 7.375$ [McKinley, 1961]. Therefore the majority of the returned power comes from a relatively small volume of ~ 2.5 km³. However, the need to combine data from many meteors to make useful estimates of the mean wind in fact means that the meteor winds produced are determined over a longer time period and larger effective volume than the SA method. The effective volume of the sky from which meteors are drawn in a period of 1 hour is typically 90,000 km³, substantially larger than that of the spaced antenna technique.

The VHF meteor radar described here has been designed to provide nearly all-sky coverage, but we have set the maximum limit for the zenith angle which a meteor can have to 53° in our data analysis procedure because there are only a few meteors detected from greater zenith angles. This limitation of the zenith angle also helps to reduce the degree of ambiguity of meteor detection which was discussed earlier, except for the relatively rare occurrence of triple-range-aliased meteors, which can sometimes be erroneously located in angle. On average, the locations of a typical meteor and the MF radar volume are separated by ~ 50 km, but the meteor points are spread out across the sky. Hence it is noteworthy that the comparisons to be presented were actually made using broadly simultaneous MF and meteor measurements from the same height rather than the same volume, and fluctuations due to turbulence or gravity waves can lead to notable differences. It is also important to note that the successive trails observed with the meteor radar may be separated by horizontal distances of up to 250 km in extreme cases. Since it is therefore possible that the line-of-sight velocities measured from successive meteor trails occurring at the same height but separated by large horizontal distances will be inconsistent, any meteor wind determinations from only a few widely spaced meteors within a given time interval should be suspect, and this

is another reason why we have concentrated our studies on tidal periods. Nevertheless, we will later also look at some instantaneous comparisons.

4. Data Analysis Methods

Different procedures were applied and tested to estimate the mean winds and tides between 82 and 94 km with our MF and meteor radars. The errors of the mean winds and tides have also been studied. We will concentrate on the data between 85 and 94 km since meteor count rates were very low at 82 km, but the 82 km data will be shown for completeness.

We will consider first the procedures used with the meteor radar. Two algorithms have been applied; the first analysis procedure was developed by ourselves in-house, and the second one is that of Groves [1959]. These two types of analysis will be discussed in the following sections. The two procedures have differences and similarities, but because they were developed independently we can use intercomparison between them to check the data quality. Good data should produce consistent results between the two techniques, while poor data (such as data with erratic tidal variability) will show substantial differences which we can use to identify such occasions. Both procedures will be outlined in more detail shortly.

Because the meteor count rate was quite low, it was necessary to "bin" data from successive days according to time of day, thus making an "equivalent" day for analysis. Thus we have used a superposed epoch analysis to estimate the mean winds and tidal oscillation. For a given height, all echoes occurring during a given data run (typically 5-15 days of data) are superimposed into either 24×1 hour bins (one for each hour of the day), or alternatively, into 12×2 hour bins, to produce an "equivalent day" for that data run. This "typical day" is then analyzed for mean and tidal components. All our subsequent data were produced by this superposed epoch analysis procedure.

With regard to the MF method, our proce-

dures are similar to those presented by *Thayaparan et al.* [1995a], but at the same time we have made some changes in order to produce greater consistency with the meteor procedures. For example, we have only selected MF data for days during which the meteor system was running. In addition, and despite the higher data rates available with the MF method, we have chosen to bin the MF data in an identical way to the meteor data. Thus we also use a superposed epoch analysis for our MF data, for consistency with the meteor analysis.

Once we have formed our typical day for either the meteor or the MF data, we routinely fit and analyze the data using classical harmonic analysis techniques with mean, 24-, 12-, and 8-hour components [e.g., *Manson et al.*, 1989; *Thayaparan et al.*, 1995a; *Thayaparan et al.*, 1996]. The zonal (u) and meridional (v) components were represented as a function of time (t) by

$$u(t), v(t) = a_0 + \sum_{i=1}^{i=3} a_i \sin\left(\frac{2\pi}{T_i}t + \Phi_i\right) \quad (1)$$

where a_0 is the prevailing mean wind and a_i and Φ_i give the mean amplitude and phase for the 24-hour ($i = 1$), 12-hour ($i = 2$), and 8-hour ($i = 3$) tidal components (in fact, any number of higher-order harmonics could be included by simply continuing the Fourier series). When there were short breaks in the data, these were simply omitted from the least squares fitting routine without seriously affecting the results. A fit is only performed if at least 20 (10) different hours are represented in the 24 hourly (12×2 hour bins) data set for a given height. In fact, there were no gaps in either superposed epoch data sets in any heights used in this study. We will now turn to a more detailed discussion of the two main analysis methods used in our meteor determinations.

4.1. The UWO Meteor-Wind Analysis Method

The meteor data have been analyzed for the mean winds and tides over the observing period using a standard UWO analysis procedure,

which is discussed in detail by *Thayaparan* [1995]. Briefly, we have used either 1-hour or 2-hour bins of data at each height of observation, making the assumption that the wind is constant within the data interval. Data are also binned according to height; for example, data from below 83.5 km altitude are binned together and treated jointly as "82" km data. Other groupings are 83.5-86.5 km (treated as 85 km), 86.5-89.5 km (88 km), 89.5-92.5 km (91 km), 92.5-96.5 km (94 km) and >96.5 km (treated as 98 km). This grouping gives reasonable data rates as well as an approximate vertical resolution of 3 km, roughly similar to the vertical resolution of the MF system. An all-sky least squares algorithm is then used in each bin to convert the ensemble of radial velocities to an average zonal and meridional component. The main points of this procedure will now be outlined.

Within any height-time data bin, we might have typically 10-50 meteor records, all from different positions in the sky and at different times within the temporal width of the bin. We have records of their radial velocities and positions, but no more. We therefore assume that the average (model) wind over this region of space and time is given by $\vec{V} = (u\vec{i} + v\vec{j} + w\vec{k})$, and then write that the "model" radial velocities are given by $v_{r(\text{model}),i} = \vec{V} \cdot \vec{I}_{\text{met},i}$, where $\vec{I}_{\text{met},i}$ is the unit vector toward the (known) location of the meteor number i . We then proceed to minimize the function

$$\epsilon^2 = \sum_{i=1}^N [v_{r(\text{model}),i} - v_{r(\text{met}),i}]^2 \quad (2)$$

with respect to u , v , and w . In some cases we allowed all three velocity components to be variable (a three-dimensional (3-D) wind evaluation), while in others we forced w to be zero (a two-dimensional (2-D) wind determination).

We can minimize ϵ^2 by differentiating ϵ^2 with respect to u , v , and w separately and setting each derivative to zero. This produces three equations:

$$u \sum l_i^2 + v \sum l_i m_i + w \sum l_i n_i = \sum v_{r(\text{met}),i} l_i \quad (3)$$

$$u \sum l_i m_i + v \sum m_i^2 + w \sum m_i n_i = \sum v_{r(\text{met}),i} m_i \quad (4)$$

$$u \sum l_i n_i + v \sum n_i m_i + w \sum n_i^2 = \sum v_{r(\text{met}),i} n_i \quad (5)$$

where l_i , m_i , and n_i are the direction cosines of the i th meteor. Solution of these equations allows estimates of u , v , and w to be made for each height-time bin. These values are then later used in the harmonic fitting analysis procedure which has been outlined earlier.

When calculating these mean motion vectors, we used two additional restrictions. First, we did not use meteors which lay within 12° of zenith, since small errors in the radial velocities of these meteors can lead to large errors in the horizontal velocities. Second, we developed an additional criterion for rejection of outliers, which removed meteors having radial velocities which were significantly inconsistent with all the others in their bin. This especially helped remove spurious meteors which might have been wrongly located, such as those which were triple-range aliased (see earlier). This latter procedure will now be outlined.

First, we applied the algorithm described above (equations (3)-(5)) to all our available data and thereby found a first estimate of the mean wind \vec{V} for this bin. Then, for each meteor position, we calculated an estimate of the expected radial velocity at each point by using the relation $v_{r,\text{expected}} = \vec{V} \cdot \underline{I}_{\text{met},i}$. We then examined the difference between this quantity and the actual measured radial velocity, and if this quantity exceeded 30 m/s then we rejected this meteor as an outlier. The value of 30 m/s was chosen as a cutoff after inspecting many distributions. It is also consistent with the expected RMS velocities expected due to gravity waves; gravity waves have typical RMS values of around 10-30 m/s, and we observe a component of these motions equal to about one half of the horizontal value (taking the typical zenith angle to be 30°). Hence we should expect variations of radial velocities of the order of 5-15 m/s within a small region of space on the timescale of an hour or so. Allowing up to 30 m/s allows for more ex-

treme fluctuations and ensures that we are not too severe with our rejection criteria.

Note that the quantity

$$v_{r\sigma} = \sqrt{\frac{\sum_{i=1}^N [v_{r,\text{expected}} - v_{r(\text{met}),i}]^2}{N}} \quad (6)$$

represents a measure of the RMS value of these residuals. Typical values of $v_{r\sigma}$ were in the range 5-20 m/s, consistent with our expectations described above. As a final step in our procedure, and after we have rejected all outliers, we repeat the all-sky least squares fitting exercise outlined above (see equations (3)-(5)) to produce a set of new, improved estimates of the mean wind, \vec{V} , for each bin. It is this new set of vectors which we then use for all our subsequent harmonic fitting analyses.

It is also important to recognize the impact of the residuals $v_{r\sigma}$ on our determinations of tidal amplitudes. Values of $v_{r\sigma}$ of the order of 5-20 m/s correspond (assuming mean zenith angles of the order of 30°) to fluctuations in the horizontal winds of the order of 10-40 m/s. We therefore need of the order of 100 points or more at any one height to obtain accuracies in tidal amplitudes of the order of 4 m/s, so we should not be surprised when our MF and meteor wind estimates show some disagreements. Clearly, when performing our comparisons, we will need to be very careful about our error estimations, and we will discuss this issue shortly.

It should be noted here that each 1-hour or 2-hour averaged mean wind could be obtained by using both 2-D and 3-D least squares fitting procedures. Different ways to deduce the wind field are denoted by Me_{12} , Me_{13} , Me_{22} , and Me_{23} , where the first subscript denotes the time bin (either 1-hour or 2-hour) and the second subscript denotes the type of least squares fitting procedure (either 2-D or 3-D). This allows us to perform four different optional estimations of the mean winds and tides.

4.2. Groves Analysis Method

An alternative procedure for analyzing the meteor data is given by *Groves* [1959]. *Groves*

applied a multiparameter least squares method to all the meteor wind data from a given observing period to determine specified parameters which characterize the tidal structure. The data are usually analyzed in 24-hour periods by fitting a prevailing wind plus 24-, 12-, and 8-hour harmonic components. We again bin our data to form an equivalent day. The values of the meridional and zonal components are assumed to simultaneously have polynomial variations with height, plus tidal variations in time. The method also allows for vertical components of velocity; it does not force w to be zero. However, the validity of the vertical velocities derived is questionable, and we will not use them anywhere in our analyses. Groves' analysis has been used by several groups [e.g., Rossiter, 1970; Stubbs and Vincent, 1973; Roper, 1966, 1975, 1978; Aso *et al.*, 1979; Tsuda *et al.*, 1980].

The accuracy of these profiles depends on the number of data points available, the distribution of echoes in space and time, and the number of degrees of freedom allowed in the polynomial height profiles. In our routine analysis, cubic (or third degree) polynomial variations with height in the zonal and meridional components were used. The Groves [1959] analysis can accommodate gaps of up to 4 hours in the data, although best results are obtained when echoes are evenly distributed throughout the day. The wind profiles are least reliable near the limits of the meteor height range, where the echoes occur less frequently; often the velocities derived from the Groves analysis then tend to be very large. The best results are likely to be obtained near 88-91 km. The Groves analysis will not detect changes in the wind with timescales less than 8 hours, and no attempt has been made in this work to extract periodicities less than semidiurnal.

4.3. Comparisons of the Different Methods

As noted, there are four different ways (Me_{12} , Me_{13} , Me_{22} , and Me_{23}) to estimate the winds and tides from the meteor data using the UWO analysis method. These four different proce-

dures were applied and used for the estimation of winds and tides and their uncertainty. All these analysis methods were performed at each height. This leads to a better feel for the accuracy of our fits of winds and tides with the meteor radar.

The graphs in Figure 2 illustrate the accuracy of our fitting procedure between 85 and 94 km in August 1994 by showing the tidal fits performed on the 2-hour bins of MF and meteor data. Statistical analysis of uncertainty in winds and tides showed that the UWO harmonic fit performed on the 2-hour bins of data deduced by the 2-D least squares fitting procedure (i.e., Me_{22}) generally agrees well with the harmonic fit of the Groves [1959] analysis (i.e., Gr in the figure), although we have found differences. Therefore, to improve our statistics, the mean wind and the amplitude and phase of the tidal oscillation for each month are estimated by taking a vector average of the two methods (i.e., vector average of Me_{22} and Gr; see Figure 2). From this type of data analysis, the tidal amplitude and phase structure are calculated for the meteor data and then subsequently compared with the MF data.

Figure 3 illustrates the typical behavior as a function of height for the amplitude and phase of the semidiurnal tide during April 1995, obtained by the UWO (i.e., Me_{22}) and Groves [1959] (i.e., Gr) least squares fitting analysis procedures performed on the meteor data, and these are compared with the MF data. The various profiles in each graph represent different realizations; 8 days have been selected at random out of the 15-day period and used to perform fitting by the three procedures. Each selection of day-groups is then plotted as a separate graph. We have done this to demonstrate the inherent variability contained in the data and to demonstrate that there is no "perfect" solution to the fitting procedure. The error bars on the graphs will be discussed later. It can be seen that generally the UWO least squares fitting procedure agrees well with the harmonic polynomial fit of the Groves analysis. However, on occasions (less than about 10% of the total number) we have found that there are significant differences be-

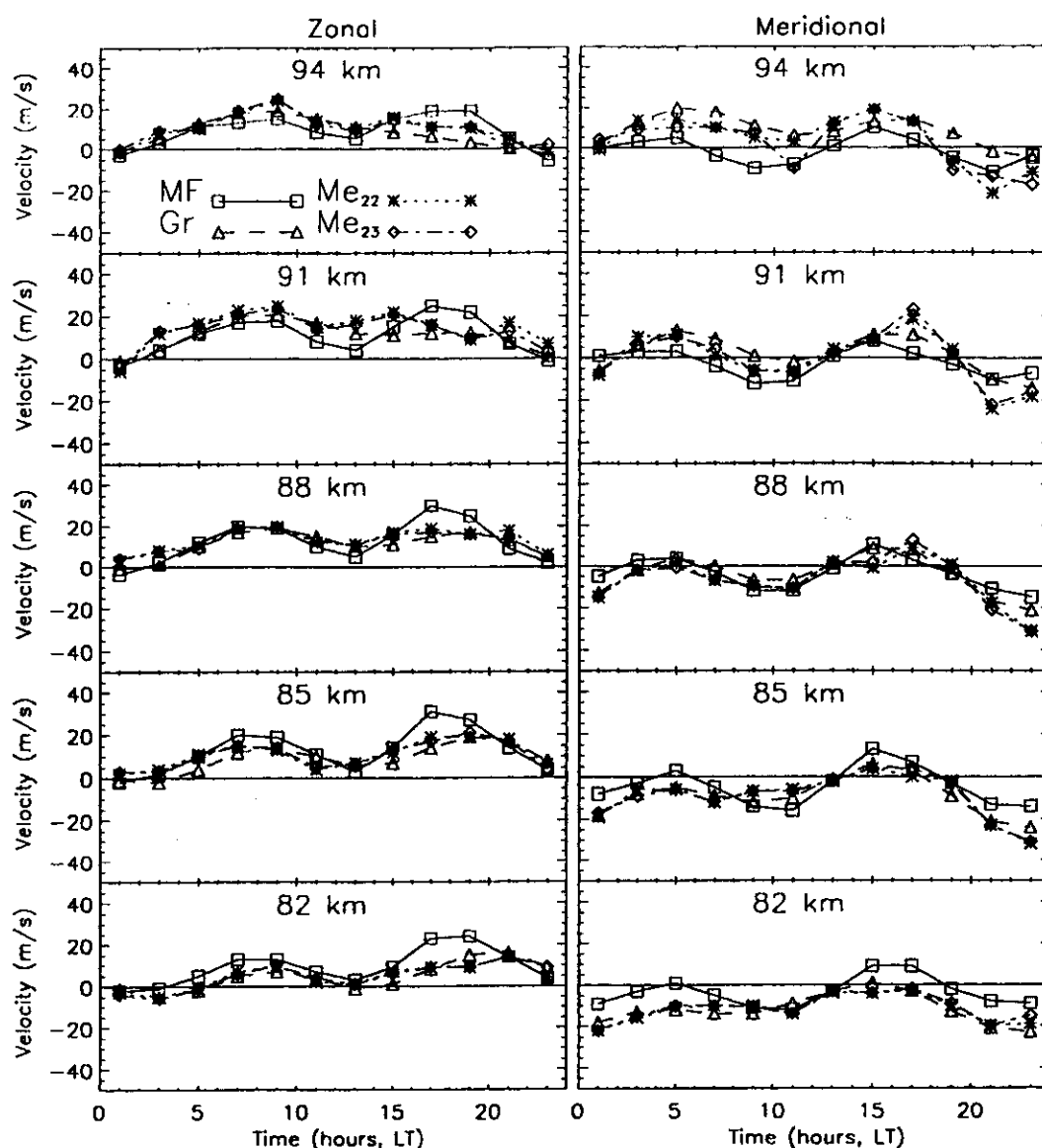


Figure 2. Two-hourly means and tidal fits for the zonal and meridional winds between 82 and 94 km in August 1994 for three different procedures (University of Western Ontario (UWO) algorithm, Groves [1959], and MF). See the text for more details.

tween these two types of analysis methods. This effect is especially noticeable when the tides are erratic and/or variable, and on such occasions it is even possible that the MF method agrees better with one or other of the meteor methods than agreement between the meteor results. However, in the main, the Groves and UWO algorithms produce broadly consistent results and

are simply different interpretations of the same data. Thus we can consider the two sets of results to be different samples from the same population and so can average the two methods in order to (marginally) improve the uncertainties associated with our meteor winds. More importantly, examination of the differences between the methods serves as a useful estimate of the

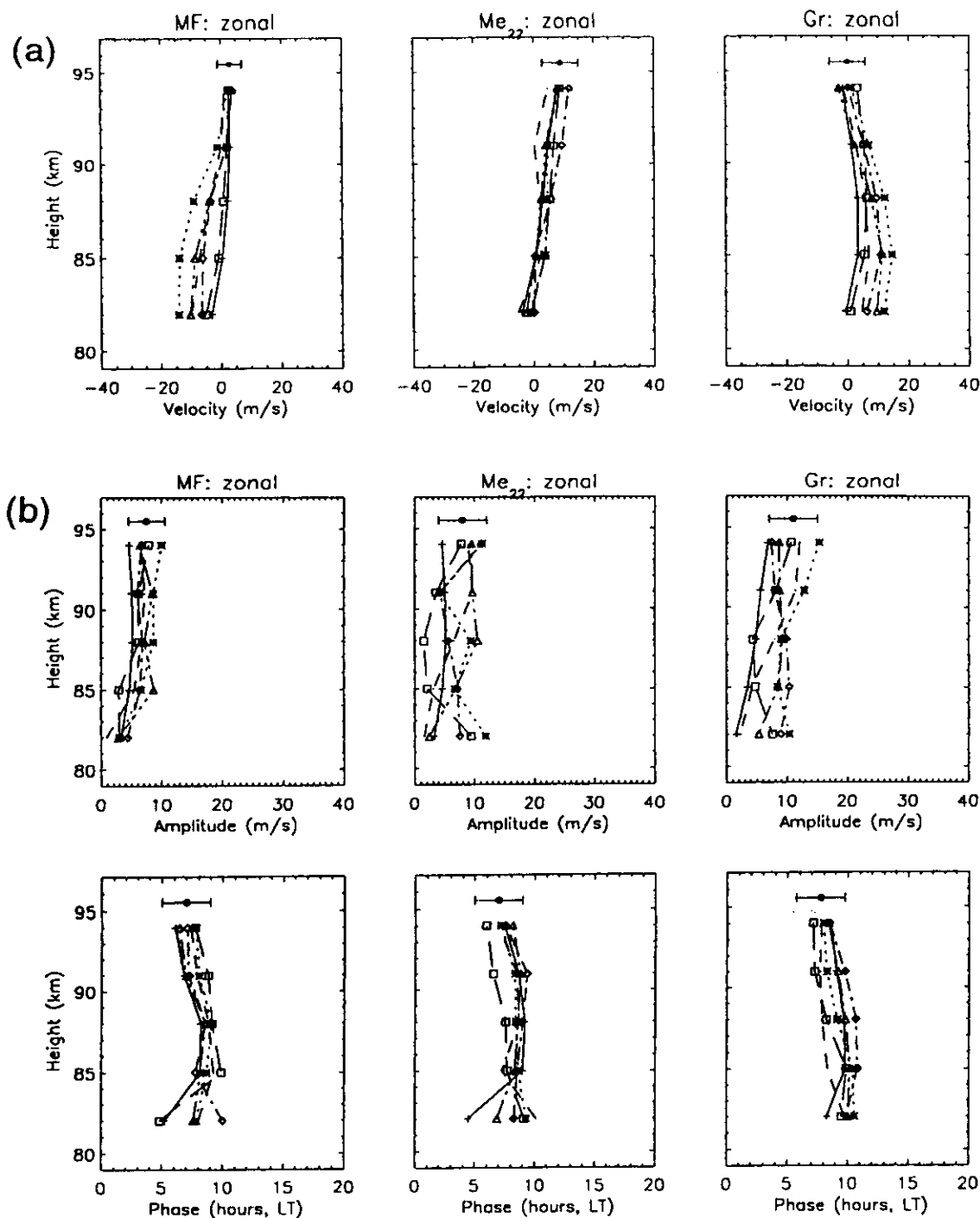


Figure 3. Shown is the mean behavior as a function of height of the monthly mean winds, and amplitudes and phases of the tides during April 1995 obtained by the MF method, and the UWO (i.e., Me_{22}) and *Groves* [1959] (i.e., Gr) least squares fitting procedures performed on the meteor data. Each profile corresponds to data collected from a group of 8 days from within the 15-day observing period, where different groups of 8 days are used for each profile. Figure 3a shows the zonal monthly means, Figure 3b shows the zonal semidiurnal tide, and Figure 3c shows the meridional diurnal tide. See the text for more details.

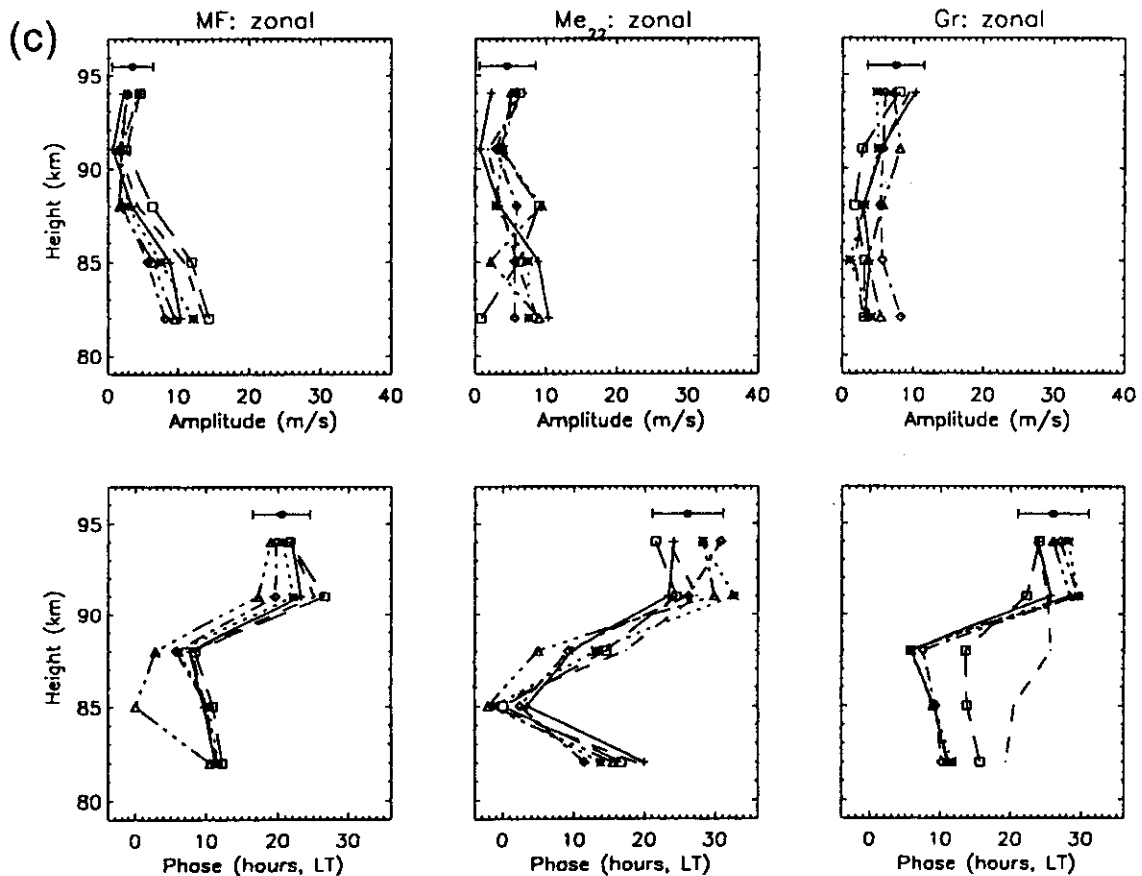


Figure 3. (continued)

errors in the basic method, and we will see this in the following section.

4.4. Statistical Analysis of Uncertainty

In general, the error of any measurement system depends on nonideal characteristics, for example, nonlinearity, environment, and statistical effects of elements [Taylor, 1982]; i.e., uncertainty is a function of several variables. Our purpose in this section is to obtain reasonable estimates of the error in our meteor and MF data. We will do this by performing internal comparisons within each group; we will at no stage use comparisons between the MF and meteor winds as a means of establishing error estimates. Once we have established our error estimates, however, we will use these estimates as the basis of our comparisons between the two methods.

In discussing the measurement accuracy, one needs to consider the statistical uncertainties associated with the measurement. Not all types of experimental uncertainties can be assessed by statistical analysis based on repeated measurements. For this reason, uncertainties are classified into two groups: the random uncertainty and the systematic uncertainty. Almost all derived wind measurements are subject to both random and systematic uncertainties. The systematic uncertainties are associated with imperfect knowledge of the radar system measurement inaccuracies. Systematic errors may arise for the MF system if the aerial separation is too small relative to the scale of the diffraction pattern; the calculated "true" velocity is often too small [e.g., Golley and Rossiter, 1970]. Care must therefore be taken to ensure that the tri-

angle used is sufficiently large, but if it is too large the analysis frequently breaks down. The aerial separation for our work is 225 m and this has been shown to be appropriate for reliable wind estimates [Meek, 1990; Thayaparan, 1995, and references therein]. As another example, in our analysis (e.g., 2-D least squares fit), a nonuniform distribution of scatterers in the volume, together with a strong vertical wind, could contaminate the measurement of the horizontal wind and lead to a systematic error in horizontal wind speed. There is no definitive method to tell us what to do about systematic uncertainties. In addition, other biases may be introduced by echoes from nearby transmitters, weak ground clutter echoes, etc., within a range gate. From the point of view of our meteor studies, sources of error include the fact that meteors have a bias in their count rates to certain times of day and even to certain days. Spatial variability of meteor count rates over the sky can also be a problem. These problems can be compounded when we realize that the MF data can also have a bias to certain times of day, which generally do not match the biases in meteor count rates. In addition, within any typical 10-day observing period, different days may produce preferentially more data for one or other of the techniques, even though the overall time interval of the observations corresponds to the same days. Thus events which occur on certain days may be accentuated in one technique and not the other. Great care has been taken for the MF and meteor radars in system calibrations and processing to reduce the systematic errors as far as possible, but some of the above problems must remain unresolved and will show themselves in the errors.

The random errors can be estimated by comparing results obtained simultaneously by quasi-independent methods and/or by analyzing data from different parts of the same data run. We will discuss various ways in which to determine these errors.

As a first estimate of the errors, we have broken the data recorded over, say, a 10- or 15-day period into smaller subgroups of typically 5-8 days and intercompared results. For exam-

ple, Figure 3 shows the results of such a process. We show here profiles obtained by clustering different days within the 15-day period and applying our procedures. In this case, we use data in groups of days which included April 8, 9, 12, 13, 15, 16, 19, and 20 and then April 9, 11, 13, 15, 17, 19, 21, and 23, etc.; some groupings were periodic, some were random selections. This procedure has some connections with the "Shake test" described by Rüster *et al.* [1996]. We could then find the standard deviations at each height and average to get some idea of the spread. We then multiplied by 1.96 to give something comparable to the 95% confidence widths of the distributions. This procedure represents the first way we could use to get error estimates, although we have to note that the method may not give the full error because the different realizations are not completely independent; the estimates are probably underestimates of the errors. However, this will simply force our subsequent MF-meteor comparisons to be more stringent, not less so.

With the meteor data, we can also use comparisons between the different meteor algorithms (Me₂₂, Me₂₂, Me₂₂, Me₂₂ and Groves [1959]) as another means to estimate the errors associated with any one estimate. While the UWO and Groves methods are certainly not independent, since they use the same data, it is still true that they view the same data using somewhat different assumptions. We do not feel that any one method is superior to the other, so that any differences in their respective results can be taken as lower limits of the errors intrinsic in the various fitting procedures. Therefore, as another estimate of uncertainties in the estimates of monthly mean winds, tidal amplitudes, and tidal phases, we look at the distribution of differences in the estimates produced by each procedure. We also clustered the recorded data into three height groups; i.e., 82-85, 88-91, and 94-98 km, in order to get some idea of the vertical structure of the random errors. When we examine differences in these height groups and for all seasons for monthly means, tidal amplitudes, and phases and plot them as histograms, we see

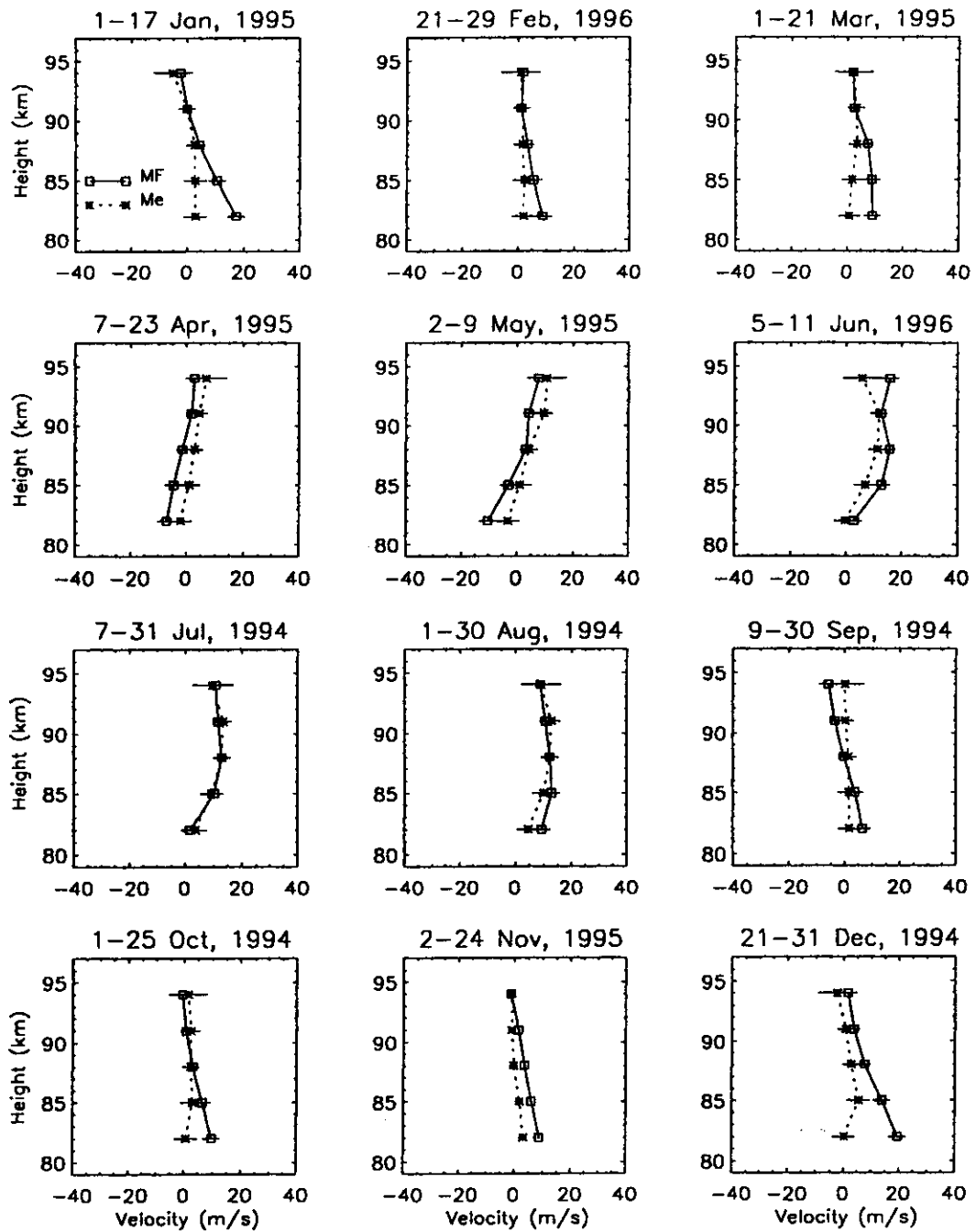


Figure 4. A comparison between the monthly mean winds measured by the MF and meteor radar systems for the zonal component. The MF winds are displayed by squares connected by a solid line, and the corresponding meteor winds are displayed by asterisks connected by a dotted line.

a broadly Gaussian shape peaking around zero. The 95% confidence limits correspond to 1.96σ , where σ^2 is the variance of the distribution.

If the two techniques being differenced were completely independent, then the 95% confidence limits in the above distributions would have been $\sqrt{2}$ times the 95% confidence limits of the distribution of measurements by one technique alone. Thus the 95% confidence limits for any one technique can be found as $1/\sqrt{2}$ times the value calculated from the differences. This estimate is again something of an underestimate, since the two methods are not entirely independent. The errors associated with the average of the UWO and Groves [1959] methods are $1/\sqrt{2}$ times less again. We have followed the above procedure to estimate our errors associated with our meteor data and have used these intercomparisons between different techniques as a check on our error estimations by the first technique. Results were similar, and the overall errors deduced from all methods are shown in Figures 4-9 (to be discussed shortly). We also show the mean uncertainties as column 2 in Table 1; note that these are averages over all data, and we have combined the zonal and meridional estimates. In reality we found that the meridional component could not be estimated with quite as good an accuracy as the zonal component in many cases, so these errors are probably underestimates for the meridional component.

The uncertainties associated with the MF SA mean wind velocities were calculated primarily by the first procedure outlined above. All of our estimated uncertainties are shown as error bars on all graphs to be shown later. However, in order to give some feel for typical values, Table 1 shows the average values of the 95% confidence limits for the uncertainties estimated by the MF ($\bar{\sigma}_{0.95}(\text{MF})$) in column 1. The meteor ($\bar{\sigma}_{0.95}(\text{Me})$) techniques between July 1994 and June 1996 are shown in column 2, as discussed. In each case we have only taken accuracies of one significant figure. These overall accuracies are also shown superimposed on Figure 3. Note that the widths of the bars are comparable to the spread of the data, although not always in per-

fect agreement since these particular error bars are actually averages over the whole year, while the various profiles are just for April. The main point to notice is simply that the data spread is certainly not incommensurate with the error bars. Subsequent figures (Figures 4-9) use error bars as calculated for each data set separately.

We finally combine these two error estimates to give an error value which we can use for our tests. We define a "test parameter" for tests between the MF and meteor parameters as $\sigma_{\Delta 0.95} = (\bar{\sigma}_{0.95}^2(\text{MF}) + \bar{\sigma}_{0.95}^2(\text{Me}))^{1/2}$. These values are tabulated as the third column in Table 1, and will be discussed again shortly.

5. Comparison of Winds and Tides Measured by the Two Techniques

In the present section, results obtained by the MF and meteor techniques at the same time and place will be compared, with a view to investigating whether the measured velocities detected by the partial reflection SA type of experiment are truly indicators of neutral air motions. Simultaneous MF and meteor measurements were made during the following periods: July 7-31, August 1-30, September 9-30, October 1-25, and December 23-31 in 1994; January 1-17, March 1-21, April 7-23, May 2-9, and November 2-24 in 1995; and February 21-29 and June 5-11 in 1996.

When both the height distribution and diurnal variations are considered, it is clear from our long time observation that there is a general decrease of available meteor numbers detected below 85 km and above 94 km [e.g., Thayaparan, 1995]. Therefore the profiles are most reliable between 85 and 94 km as far as the available meteor rate is concerned, on which the reliability of a wind measurement ultimately depends. Furthermore, it should be also noted that the summer MF radar echoes received above 95 km are contaminated by some degree of group retardation [e.g., Namboothiri *et al.*, 1993] and *E* region echo spreading. Therefore we have greatest confidence in our data for heights between 85 and 94 km (both MF and meteor radars) but show the data between 82 and 94 km for com-

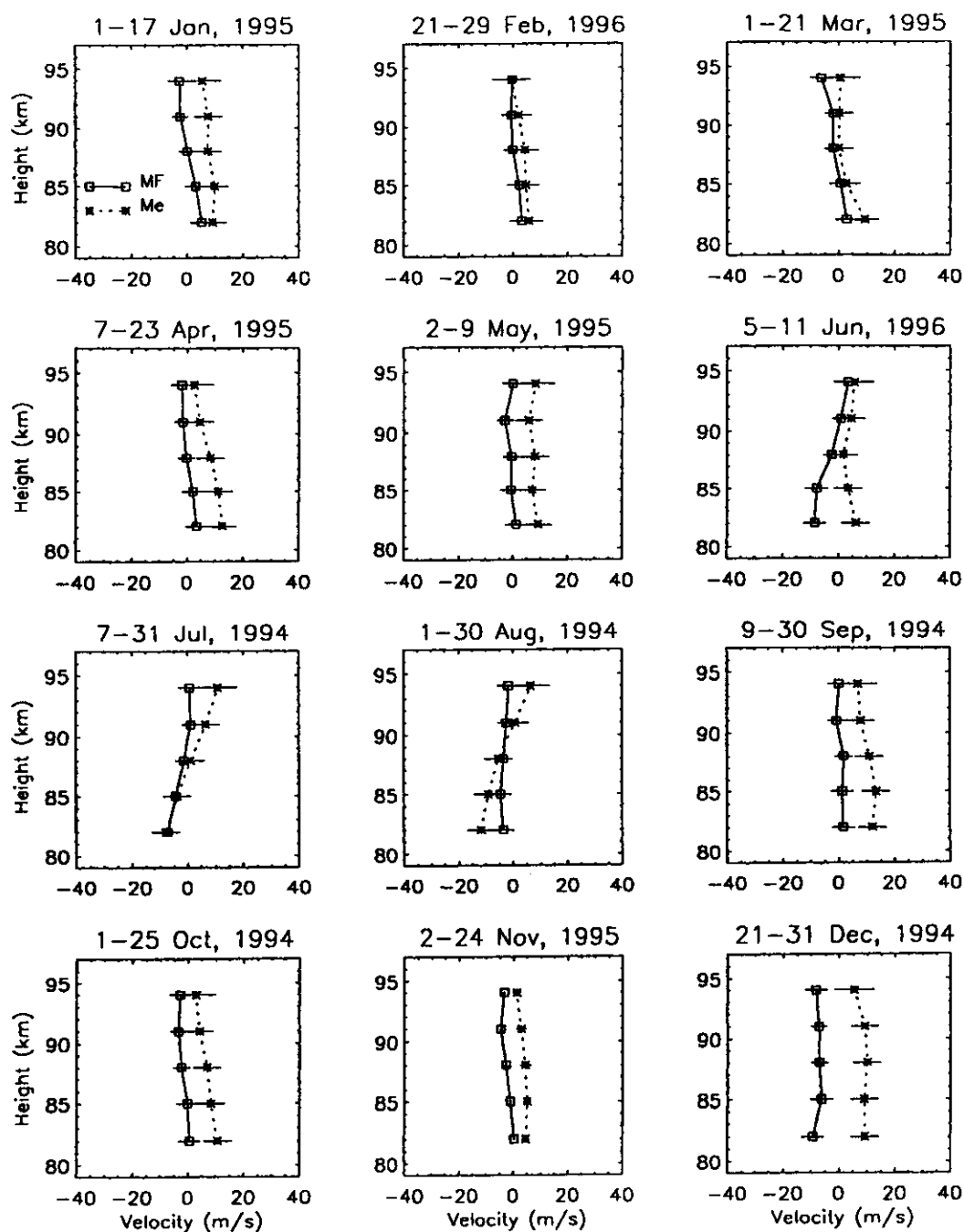


Figure 5. A comparison between the monthly mean winds measured by the MF and meteor radar systems for the meridional component. The MF winds are displayed by squares connected by a solid line, and the corresponding meteor winds are displayed by asterisks connected by a dotted line.

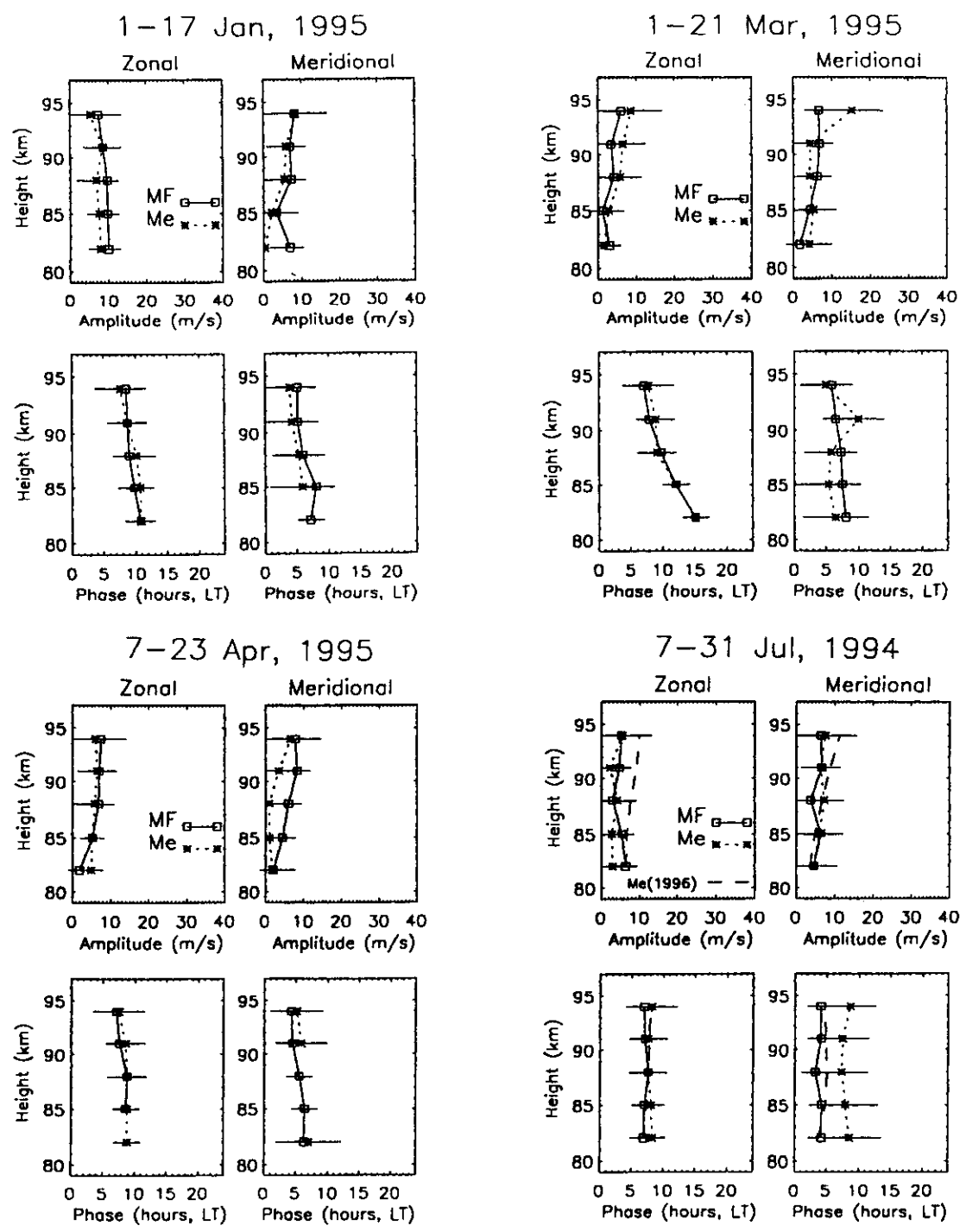


Figure 6. Height profiles of the amplitude and phase of the zonal and meridional components for the semidiurnal tide observed by the two techniques for the months of January, March, April, and July. The squares with the connecting solid line indicate the MF SA wind profile, and the asterisks with the dotted line indicate the meteor wind profile. Note also a line made of long dashes in the meridional phases for July 1994; this line refers to the phases measured very recently in 1996, when a much better data rate was available. We ignore the phase estimates when the amplitudes are small (<3 m/s). See the text for more details.

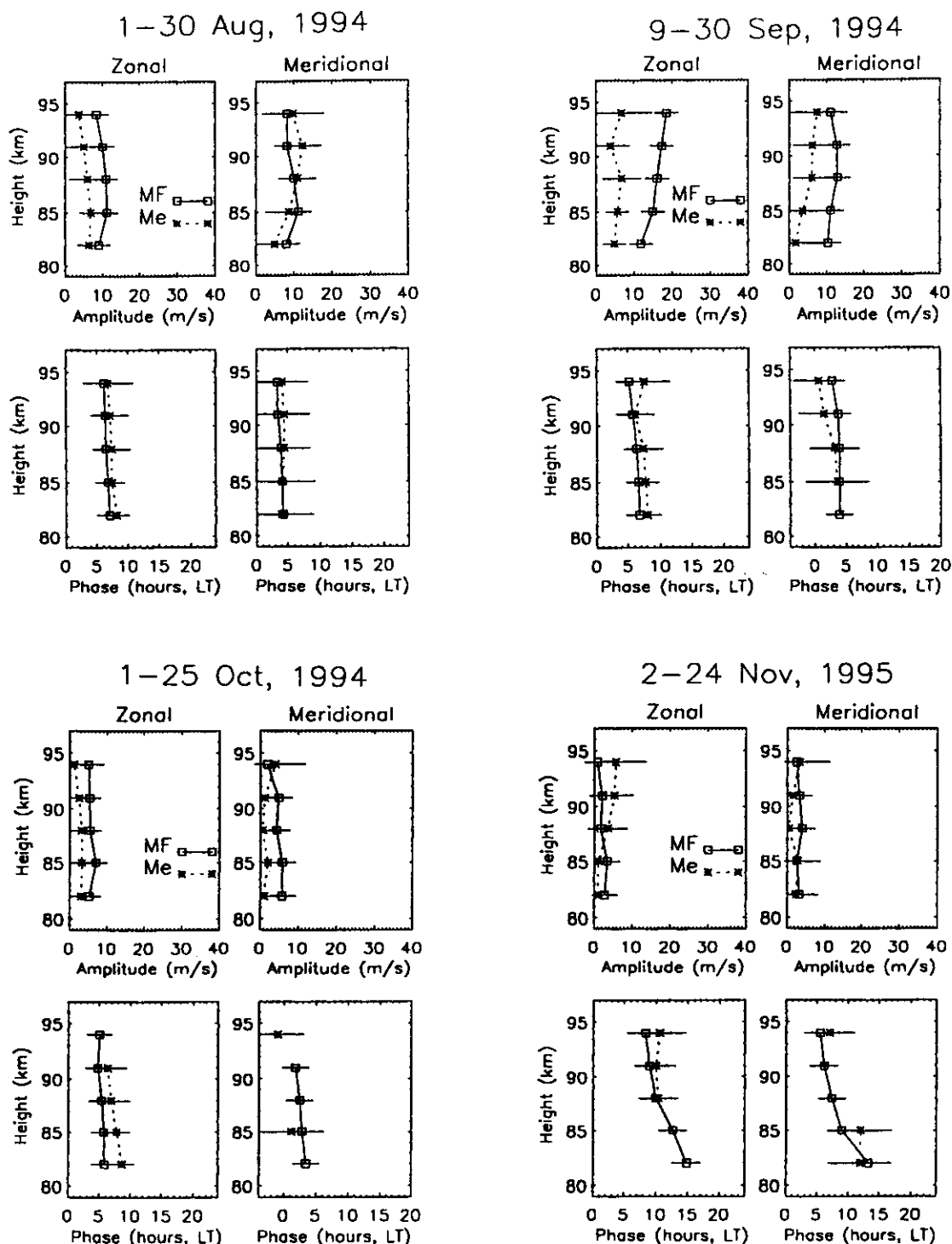


Figure 7. Height profiles of the amplitude and phase of the zonal and meridional components for the semidiurnal tide observed by the two techniques for the months of August, September, October, and November. The squares with the connecting solid line indicate the MF SA wind profile, and the asterisks with the dotted line indicate the meteor wind profile. Note that we ignore the phase estimates when the amplitudes are small (<3 m/s). See the text for more details.

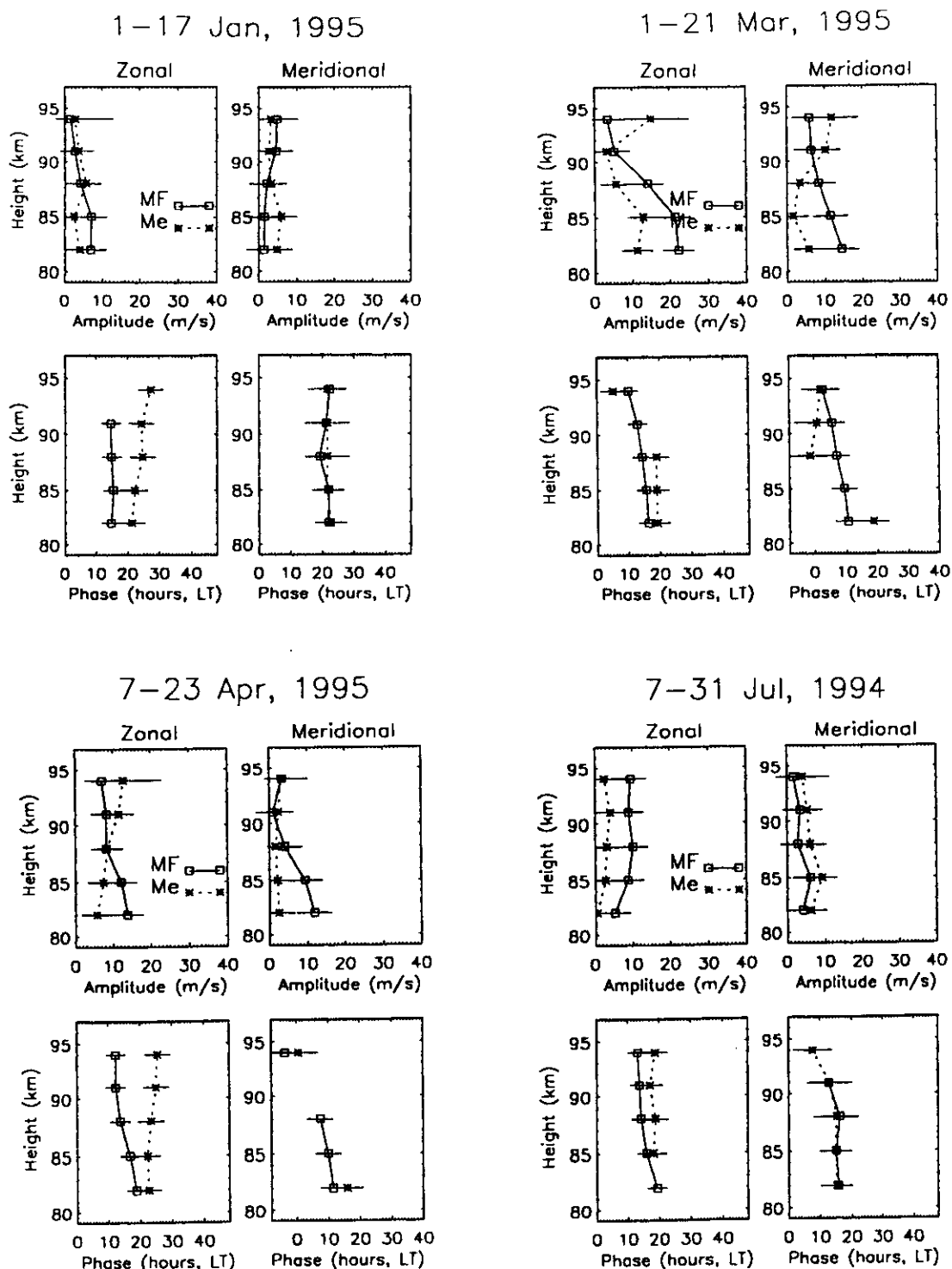


Figure 8. Height profiles of the amplitude and phase of the zonal and meridional components for the diurnal tide observed by the two techniques for the months of January, March, April, and July. The squares with the connecting solid line indicate the MF SA wind profile, and the asterisks with the dotted line indicate the meteor wind profile. Note that we ignore the phase estimates when the amplitudes are small (<3 m/s). See the text for more details.

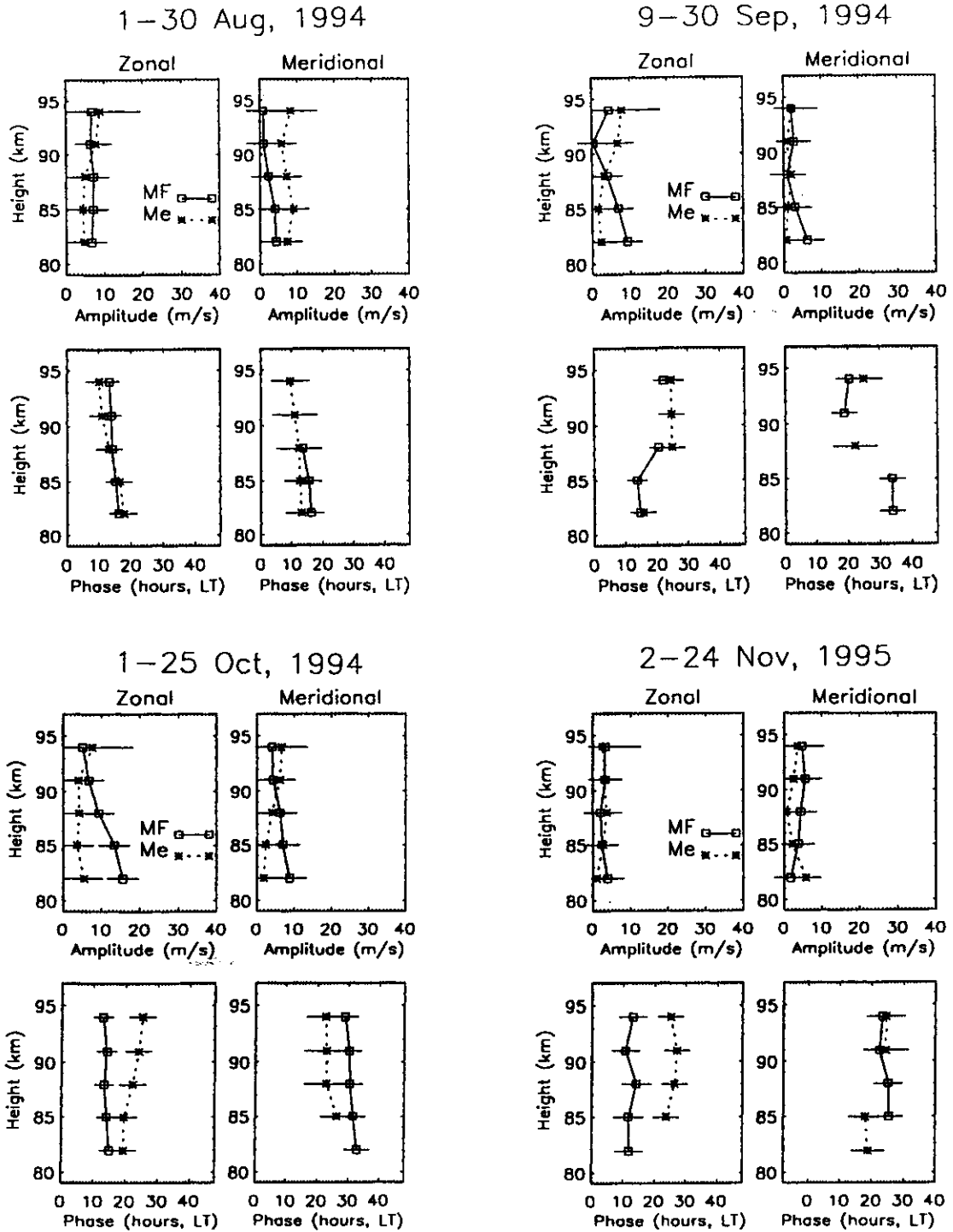


Figure 9. Height profiles of the amplitude and phase of the zonal and meridional components for the diurnal tide observed by the two techniques for the months of August, September, October, and November. The squares with the connecting solid line indicate the MF SA wind profile, and the asterisks with the dotted line indicate the meteor wind profile. Note that we ignore the phase estimates when the amplitudes are small (<3 m/s). See the text for more details.

Table 1. Mean Uncertainties Estimated by the MF and Meteor Systems

	$\bar{\sigma}_{0.95}(\text{MF})$, m/s	$\bar{\sigma}_{0.95}(\text{Me})$, m/s	$\sigma_{\Delta 0.95}$, m/s
Mean wind	4	6	7
Semidiurnal			
Amplitude	3	4	5
Phase	2	2	3
Diurnal			
Amplitude	3	4	5
Phase	4	5	6

Here $\bar{\sigma}_{0.95}(\text{MF})$ and $\bar{\sigma}_{0.95}(\text{Me})$ are the average values of the 95% confidence limits for the uncertainties estimated by the MF and meteor techniques, respectively, between July 1994 and June 1996. The resultant uncertainty of the two systems is defined as $\sigma_{\Delta 0.95} = (\bar{\sigma}_{0.95}^2(\text{MF}) + \bar{\sigma}_{0.95}^2(\text{Me}))^{1/2}$ (see the text for more details).

pleteness. We will focus on the comparison of the mean winds (Figures 4 and 5), tides (Figures 6, 7, 8, and 9) and instantaneous (Figure 10) wind comparison by the two techniques; the general characteristics of the mean winds and tides over London are given by *Thayaparan et al.* [1995a, b] and *Thayaparan* [1995].

In Tables 2 and 3, we have classified our comparisons as either excellent (E), good (G) or poor (P) according to how the mean differences over each profile relate to the term $\sigma_{\Delta 0.95}$ in Table 1. The average behavior of the profile between 85 and 94 km is found as follows. Average

values χ of the difference (between the two techniques) for each profile are calculated through the expression $\chi = \sum_{i=1}^4 |\text{MF} - \text{meteor}|$, where $i = 1$ (85 km), $i = 2$ (88 km), $i = 3$ (91 km), and $i = 4$ (94 km), and where χ can be either the monthly mean wind or the amplitude or phase of either of the tidal periods. Then these means are compared to the criteria shown in Table 1.

In detail, the comparison is classified as good (denoted by G) if the mean wind difference measured by the two techniques is less than 7 m/s, if the amplitude difference of the tidal (semidiurnal or diurnal) oscillation measured by the

Table 2. Monthly Classification of the Simultaneous Comparison of the Mean Winds and Tides Measured by the Two Techniques for the Zonal Component

Month	Mean Wind	Semidiurnal		Diurnal	
		Amplitude	Phase	Amplitude	Phase
Jan. 1-17, 1995	E	E	E	E	P
Feb. 21-29, 1996	E	G	G	G	E
March 1-21, 1995	G	G	E	P	G
April 7-23, 1995	G	E	E	G	P
May 2-9, 1995	G	P	G	E	P
June 5-11, 1996	G	E	E	E	P
July 7-31, 1994	E	E	E	P	G
Aug. 1-30, 1994	E	G	E	G	E
Sep. 9-30, 1994	G	P	G	G	G
Oct. 1-25, 1994	E	G	G	P	P
Nov. 2-24, 1995	E	G	G	E	P
Dec. 23-31, 1994	G	E	G	E	P

The behavior for each month in which comparison between the two techniques is possible has been classified into one of three types: excellent (E), good (G), and poor (P) (see the text for more details).

Table 3. Monthly Classification of the Simultaneous Comparison of the Mean Winds and Tides Measured by the Two Techniques for the Meridional Component

Month	Mean Wind	Semidiurnal		Diurnal	
		Amplitude	Phase	Amplitude	Phase
Jan. 1-17, 1995	P	E	G	G	E
Feb. 21-29, 1996	E	G	G	E	E
March 1-21, 1995	G	G	G	P	G
April 7-23, 1995	P	G	E	G	G
May 2-9, 1995	P	G	P	E	G
June 5-11, 1996	G	G	G	E	G
July 7-31, 1994	G	E	P*	G	E
Aug. 1-30, 1994	G	G	E	P	E
Sep. 9-30, 1994	P	P	G	E	G
Oct. 1-25, 1994	P	G	G	G	G
Nov. 2-24, 1995	G	E	G	G	G
Dec. 23-31, 1994	P	G	G	G	G

The behavior for each month in which comparison between the two techniques is possible has been classified into one of three types: excellent (E), good (G), and poor (P).

*Although we have denoted this as poor and will leave it so, there seems strong evidence that this was simply a result of a very poor data rate in July 1994; recent tests in 1996 suggest that in fact, agreement is normally good (see Figure 6). See the text for more details.

two techniques is less than 5 m/s, and if the phase difference of the semidiurnal (diurnal) oscillation measured by the two techniques is less than 3 (6) hours (see Table 1). However, a data set is upgraded to excellent (denoted by E) if the monthly mean wind difference measured by the two techniques is ≤ 2 m/s, if the amplitude difference of the tidal (semidiurnal or diurnal) oscillation measured by the two techniques is ≤ 2 m/s, and if the phase difference of the semidiurnal (diurnal) oscillation measured by the two techniques is $\leq 1(2)$ hour (hours). The comparison is classified as poor (denoted P) if the mean wind difference measured by the two techniques is > 7 m/s, if the amplitude difference of the tidal (semidiurnal or diurnal) oscillation measured by the two techniques is > 5 m/s, and if the phase difference of the semidiurnal (diurnal) oscillation measured by the two techniques is $> 3(6)$ hours. Note that these criteria are actually a little too strict for the meridional component since these could not be measured as precisely as the zonal data with the meteor technique. However, we will still use the same criteria for both components, even though this may be a little harsh for our meridional comparisons. We will now turn

to a brief discussion of the results for the various parameters.

5.1. Mean Winds

This section presents a comparison between the monthly mean winds measured by the MF and meteor radar systems for both the zonal and meridional components (Figures 4 and 5). The results reveal that the zonal mean winds are measured with a higher degree of consistency by the two techniques than the meridional mean winds during this period of observation. Tables 2 and 3 show that all 12 comparisons for the zonal component correspond to either type E or G, while only six comparisons correspond to either type E or G for the meridional component. Indeed, the comparisons in December and January are almost opposite, which is worrisome. Further comparisons are needed in other years to determine if these differences are real, although we do note that a northward flow in December and January (as seen with the meteor winds) is more consistent with current understanding about the gravity-wave forced upper level flow in these months [e.g., Garcia and Solomon, 1983].

Overall, zonal comparisons show remarkable

agreement between the MF and meteor winds during all months of observation, and there are only a few instances of disagreement (>5 m/s; e.g., below 88 km during March and December) at certain heights. However, we do not feel the meteor winds at the lowest heights are all that reliable, due to low meteor count rates below 85 km. It is interesting to note here that the agreement may be a little better after January 1995; this is when we increased the PRF from 1100 Hz to 2143 Hz in order to increase the meteor echo rate, on which the reliability of a wind measurement ultimately depends. In general, the meridional winds are relatively much more variable than the zonal winds over London [e.g., *Thayaparan et al.*, 1995a], and this may also contribute to our differences. It is also true that a higher percentage of meteors are found in the east-west vertical plane, which may also explain why the zonal agreement is better.

5.2. Tides

Both the meteor and the MF method regularly show diurnal and semidiurnal tidal components to be present in the winds in the 80-100 km height range [e.g., *Tsuda et al.*, 1983; *Manson et al.*, 1989; *Thayaparan et al.*, 1995a]. Our purpose here is to measure these simultaneously and intercompare the results.

In this section, a comparison is made of the amplitude and phase of the monthly tidal oscillation determined by the MF and meteor radar systems for both the zonal and meridional components. Figures 6-9 only present a comparison between the two techniques for months where more than 15 daily simultaneous meteor and MF observations are available. However, Tables 2 and 3 summarize the monthly behavior of the comparison for all 12 months. We found that the influence of the terdiurnal tide is very small during these periods of observation, and therefore it will not be discussed in this paper. The phase corresponds to the hour after midnight, local time, at which the amplitude is maximum.

The phases of the tidal oscillation will only be presented in the figures when the amplitudes of the tidal oscillation are greater than 3 m/s,

which is considered as a reasonable cutoff value after several tests (and as also determined from Table 1). This is because the highest reliability of the phase estimates is associated with reasonably large tidal amplitudes. When amplitudes are small, the phase determinations are of dubious quality, reflecting more random phases.

5.2.1. Semidiurnal tide. Figures 6 and 7 illustrate the mean behavior as a function of height of the amplitude and phase of the semidiurnal tide observed by the two techniques, and we see a relatively good overall agreement in phase in both the zonal and meridional components. Both techniques show excellent agreement, particularly between 85 and 94 km in all months for the zonal component. For the meridional component, very good agreement is observed in all months except during July. However, it should be made clear that the month of July in 1994 was the very first month for which the meteor system was even run, and our meteor-detection criteria were not fully developed. It is therefore quite likely that this may have been an anomalous result, and indeed subsequent tests in July 1996, using our improved system, produced a phase profile for the meridional component which quite closely matched the MF data. This is shown by the long dashes in the meridional phase for that curve, which represent the 1996 meteor phases. The MF phases were pretty much unchanged for 1996 compared with 1994. These 1996 data were only just available at the time of writing of this paper, so we will not dwell on them, save to say that we are fairly convinced that the anomaly here for 1994 was a result of inadequate data.

Distinct tidal rotations are evident in both techniques during most of the months. The phases of the zonal and meridional of the semidiurnal tide generally show the form of a propagating tide, with the meridional component leading the zonal by ~ 3 hours. This behavior is consistent with the expected clockwise rotation of the wind vector in the northern hemisphere. In general, downward phase progression (as inferred by the negative phase gradients, i.e., earlier phases at upper height) of the semidiurnal

tides is observed during most of the months. During the summer months (e.g., July and August) the phase profiles are constant with height, suggesting the presence of evanescent or long vertical wavelength behavior. These structures are simultaneously observed by both techniques, and these characteristics are typical over London [e.g., *Thayaparan et al.*, 1995a].

The comparisons of the amplitude of the semidiurnal tide by the two techniques often show good agreement for the zonal and meridional components. It is also clear that there is a tendency for the MF winds to be larger (>5 m/s) than the meteor winds in both the zonal and meridional components during September. In contrast, the meteor winds show larger values than the MF winds in the zonal (e.g., above 85 km during March and above 88 km during November) and meridional (e.g., at certain heights during March and August) components during certain months. One point which is worth making is that despite the poor agreement in amplitude during September, the phase still shows relatively good agreement between the two techniques. The fact that there is overall good agreement in amplitude and an excellent agreement in phase for the two techniques clearly show that the two techniques are measuring the same phenomenon, which we assume to be the true 12-hour tide of neutral wind fluctuations.

5.2.2. Diurnal tide. Figures 8 and 9 present the mean behavior as a function of height of the amplitude and phase of the diurnal tide observed by the two techniques. The two techniques show relatively better overall agreement in phase for the meridional component than for the zonal component. Although the comparisons show that on the average, there is good overall agreement between the two techniques, it is nevertheless true that there are some disagreements in phase. The disagreement is evident during January, April, October, and November for the zonal component.

The phases of the diurnal tides are generally less organized and show greater variability than the semidiurnal tide. In general, downward

phase progression of the diurnal tides are observed during most of the months, but on occasions the phase profiles of the diurnal tide show evanescent or long vertical wavelength behavior (e.g., during July for the zonal and during January for the meridional).

With respect to the diurnal tidal amplitudes, the two techniques again show reasonable agreement, but again some disparities are also observed. The disagreements are clearly seen during March, July, and October for the zonal component. For the meridional component the disagreements are apparent during March and August. It is important to point out that despite poor agreement in amplitude during March and July by the two techniques, good agreements are noted in phase during those months for the zonal component. Similarly, for the meridional component, in spite of the poor agreement in amplitude during March and August, excellent agreement in phase during August and good agreement during March are observed.

We therefore see that our comparisons are not completely satisfactory in some aspects in relation to the diurnal tide, especially in the zonal component. This may be due to the general decrease of available meteor numbers for about 12 hours centered at 1800 LT [e.g., *Thayaparan*, 1995], and this could lead to a poor harmonic fits. The meteor analysis methods also depend on the number of points available, and the best results are obtained when echoes are evenly distributed throughout the day. Similar behavior is also noted by other stations [e.g., *Cervera and Reid*, 1995].

5.3. Instantaneous Wind Comparison

Despite our emphasis on long-term oscillations, it is also of interest to check some instantaneous meteor winds. The velocity determined from an individual meteor is only a component of the true wind, so the comparison must be made by projecting the individual MF wind velocities onto the meteor line-of-sight relating the reflection point to the receiving station. In this manner, a direct comparison was made with the line-of-sight velocity determined from individual

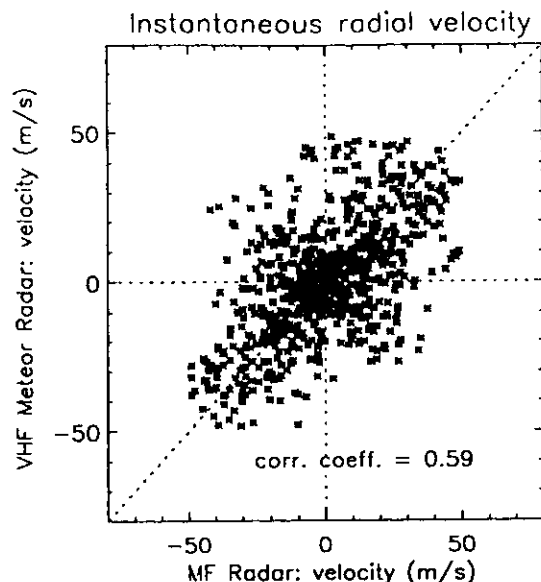


Figure 10. Projection of instantaneous horizontal MF drift velocities on the meteor line-of-sight compared with the line-of-sight velocity derived from meteor trails occurring simultaneously at the same height. See the text for more details.

meteors. In practice, meteor and MF records obtained within 5 min of each other were compared. Figure 10 shows the results of more than 800 such comparisons randomly selected from different days throughout the 12 months. The line-of-sight velocity, determined from the motion of the meteor trail, is plotted along the vertical axis, and the projection of the MF wind velocity is plotted along the horizontal axis. The line-of-sight velocities are regarded as positive if they were approaching the station.

Figure 10 shows a scatterplot of the instantaneous meteor wind radial velocities versus the equivalent radial velocity deduced from the MF SA winds. If there were perfect agreement between the two techniques, all points would lie along the straight dotted line bisecting the angle between the axes. In fact, the agreement is not perfect. However, a statistical relationship does exist between the two sets of data, as the correlation coefficients have the values of 0.59, and the points tend to lie in the correct quadrants. The 95% confidence limits are 0.54 and

0.63. These correlation coefficients do not imply that either method is defective. Such discrepancies can be expected because the MF radar volume and the meteor locations are often separated by substantial distances and certainly often by several tens of kilometers and more.

6. Discussion

Of all our 120 comparisons in Tables 2 and 3, only 23 (19%) were poor. (This figure of 23 includes the July meridional semidiurnal phases, which we have already demonstrated were probably poor simply because of inadequate data rates. We feel instinctively that this profile should not be included as poor, but we want to concentrate our analysis period to be in the interval July 1994 to June 1996, so have not corrected this anomaly). None of the other 97 profiles could be rejected as different at the 95% confidence level, and any differences can be ascribed solely to statistics. Of these remaining acceptable profiles, 38 were excellent and 59 were good. Thus, overall, the agreement is probably acceptable.

Our results reveal that the agreement is often relatively worse during the fall and spring periods, especially in May, September, and October. As has been shown in our previous observations [Thayaparan *et al.*, 1995a], strong variations of the phase of the diurnal tide are usually observed during changes of the circulation in the mesosphere and lower thermosphere. Thus it may be quite natural that the agreement between the two techniques is not as good during times such as stable circulation. In addition, the meteor rate and the MF echo strength undergo seasonal and diurnal variations, and these variations are rarely correlated between the two techniques. Thus the MF data in any observing period may be weighted to one day in the data set, when results were especially good, while the meteor method may have weightings to different days. These variations may therefore play a role in the quality of agreement between the two techniques. For example, the relatively poorer agreement with respect to the diurnal tide when

compared with the semidiurnal tide comparisons very likely relates to the diurnal variation in meteor count rate, coupled with an asymmetry in meteor count rates in the east and west directions.

Observational results found in earlier studies [Thayaparan *et al.*, 1995b] strongly suggest that significant interaction between the diurnal tide and gravity waves occurs over London at certain times of the year. Such interactions may be an important source of short-term tidal variability in the mesosphere and lower thermosphere. These observations showed that propagating gravity waves with periods less than 2 hours can significantly modulate the tidal amplitudes, and the reverse is also true. Furthermore, our observations show that the tidal amplitudes are reduced by 2-6 m/s and the phase differences are of the order of 1 hour compared with the mean of the month, when mutual interaction between the tides and the gravity waves exists in the 85-94 km height range [Thayaparan *et al.*, 1995b]. Therefore it is possible that differences between the tidal amplitudes determined by the two techniques are also affected by spatial and temporal variations related to such phenomena. For example, if the MF radar happened to detect strong echoes in association with such interactions, and if these occurred during times of day when the meteor count rate was low, we could expect substantial differences in tidal estimates by the two techniques. More observations and comparisons of this kind should be done in order to study these causes; in particular, an increase in the number of meteors is needed, and we are looking at ways to achieve this increase.

Thus many of the differences can be ascribed to undiscovered systematic errors which can occur as much in the meteor data as in the MF data. At the same time, however, we note that on occasions, there are some differences between the results of the two measuring techniques which are too large to be explained by random or systematic errors of the two methods. This is especially true of the meridional monthly mean wind, where fully one half of the comparisons were described as poor. We see that often

the meteor wind is more positive than the MF wind for the meridional component (Figure 5). Particularly prominent differences can be seen in December and January, where the meridional winds are in opposite directions. As noted earlier, the meteor data seem to agree best with theoretically expected flow directions.

The results of the instantaneous comparison between the two techniques show that on the average, the MF radar using the SA technique provides moderate agreement with winds determined by the VHF interferometer meteor radar technique. The majority of the differences are explainable, as discussed previously, in terms of geometry of the experiment, the wave-induced fluctuations model given by Kudeki *et al.* [1993], and temporal and spatial distinctions between the two techniques. It should be remembered that although we have used a common method of data analysis for both the MF and meteor data, the fundamental principles of measuring and determining the velocities are quite different. We noted previously that the MF SA wind velocities are essentially a spatial and temporal average, while in contrast, the meteor wind velocities are essentially instantaneous measurements from a relatively small region combined together over a larger time and larger spatial area. (It is also important to note that on occasions the collecting regions of the two techniques could be separated horizontally by up to 50-100 km and vertically by 3 km.) Obviously, differences in the sizes and locations of the MF and meteor observing volumes may be partially responsible for differences in the winds near these regions and subsequently may lead to differences in the velocities. Differences in the winds could possibly be due to turbulence and gravity waves.

At present, the observational material obtained in this experiment is not yet sufficient to allow us to decide on the relative importance of the diverse possibilities which could explain those few differences which we have found. A detailed clarification of the occasional differences between the results of meteor wind measurements and MF SA measurements in the same height region must therefore be the object of

special investigations and will require more observations through longer periods of time.

7. Conclusion

Simultaneous and colocated comparisons between winds and tides measured by an MF SA radar and by a VHF interferometer meteor radar have been made in the 85-94 km height range from July 1994 to June 1996 over London, Ontario, Canada. From the results of this comparison it is concluded that in general, the MF SA technique provides a reliable means for synoptic studies of neutral air motions in the height range 85-94 km at periods ≥ 12 hours. This conclusion is particularly well illustrated by Tables 2 and 3. In general, the phases of the tides (both the semidiurnal and diurnal) show relatively better agreement for the two techniques than the amplitude. Overall, the semidiurnal tide shows relatively better agreement between the two techniques than the diurnal tide, possibly due to biases introduced by the diurnal variation in meteor count rate which can affect the meteor estimates of the diurnal tide. It is also noteworthy that there is better agreement between the winds and tides deduced by the two techniques in the summer, and the worst agreement is in May, September, and October (fall and spring). This may be due to the fact that the seasonal changes occur during the fall (summer to winter circulation) and spring (winter to summer circulation) periods, and consequently, the wind fields in the upper atmosphere are considerably more variable during these periods than other seasons. However, there are some notable exceptions to the overall general agreement. In particular, it is evident from our observations that the zonal mean winds are measured with a higher degree of consistency between the two techniques than the meridional mean winds. In addition, there can be significant differences in the meridional winds, especially in midwinter. The meteor winds seem to be more consistent with theoretical expectations in this case. The reason for the difference here is unresolved and deserves further scrutiny in the future.

Acknowledgments. We wish to thank R. G. Roper for supplying us with the Groves algorithm and J. MacDougall for his support of the MF system. The system and these studies were supported by grants from NSERC (the Natural Science and Engineering Research Council) of Canada.

References

- Aso, T., T. Tsuda, and S. Kato, Meteor radar observations at Kyoto University, *J. Atmos. Terr. Phys.*, **41**, 517-525, 1979.
- Awe, O., The fading of radio waves weakly scattered at vertical incidence from heights near 90 km, *J. Atmos. Terr. Phys.*, **21**, 142-156, 1961.
- Briggs, B. H., Ionospheric drifts, *J. Atmos. Terr. Phys.*, **39**, 1023-1033, 1977.
- Briggs, B. H., The analysis of spaced sensor records by correlation techniques, *Handbook for MAP 13*, 166-186, Univ. of Ill., Urbana, 1984.
- Cervera, M. A., and M. I. Reid, Comparison of simultaneous wind measurements using colocated VHF meteor radar and MF spaced antenna radar systems, *Radio Sci.*, **30**, 1245-1261, 1995.
- Fraser, G. J., The measurement of atmospheric winds at altitudes of 64-120 km using ground-based radio equipment, *J. Atmos. Sci.*, **22**, 217-218, 1965.
- Fraser, G. J., Seasonal variation of southern hemisphere mid-latitude winds at altitudes 70-100 km, *J. Atmos. Terr. Phys.*, **30**, 707-719, 1968.
- Fraser, G. J., and A. Kochanski, Ionospheric drifts from 64-108 km altitudes at Birdlings Flat, *Ann. Geophys.*, **26**, 675-687, 1970.
- Garcia, R. R., and S. Solomon, A numerical model of the zonally averaged dynamical and chemical structure of the middle atmosphere, *J. Geophys. Res.*, **88**(c2), 1379-1400, 1983.
- Golley, M. G., and D. E. Rossiter, Some tests of methods of analysis of ionospheric drift records using an array for 89 aerials, *J. Atmos. Terr. Phys.*, **32**, 1215-1233, 1970.
- Gregory, J. B., and D. T. Rees, Wind profiles to 100 km near 53° N during 1969, *J. Atmos. Sci.*, **10**, 1079-1082, 1971.
- Groves, G. V., A theory for determining upper atmosphere winds from radio observations on meteor trails, *J. Atmos. Terr. Phys.*, **16**, 344-356, 1959.
- Illies, C. O., The saturation of gravity waves in the middle atmosphere. Part III. Formation of the turbopause and of turbulent layers beneath it, *J. Atmos. Sci.*, **48**, 1380-1385, 1991.
- Hines, C. O., and R. Bhagava Rao, Validity of three station methods of determining ionospheric motions, *J. Atmos. Terr. Phys.*, **30**, 979-993, 1968.
- Hines, C. O., G. W. Adams, J. W. Brosnahan, F. T. Djuth, M. P. Sulzer, C. A. Tepley, and J. S. Van Baelen, Multi-instrument observations of mesospheric mo-

- tions over Arecibo: Comparisons and interpretations, *J. Atmos. Terr. Phys.*, **55**, 241-287, 1993.
- Hocking, W. K., The University of Western Ontario VHF atmospheric radar, Solar-terrestrial energy program, in *Proceedings of the Sixth Workshop on Technical and Scientific Aspects of MST Radar*, pp. 349-356, STEP handbook, SCOSTEP Secretariat, Natl. Oceanic and Atmos. Admin., Boulder, Colo., 1993.
- Hocking, W. K., System design, signal-processing procedures, and preliminary results for the Canadian (London, Ontario) VHF atmospheric radar, *Radio Sci.*, this issue.
- Hocking, W. K., P. May and J. Röttger, Interpretation, reliability and accuracies of parameters deduced by the spaced antenna method in middle atmosphere applications, *Pure Appl. Geophys.*, **130**, 571-604, 1989.
- Kaiser, T. R., W. M. Pickering, and C. D. Watkins, Ambipolar diffusion and motion of ion clouds in the earth's magnetic field, *Planet. Space Sci.*, **17**, 519-552, 1969.
- Kudeki, E., P. K. Rastogi, and F. Sürücü, Systematic errors in radar wind estimation: Implications for comparative measurements, *Radio Sci.*, **28**, 169-179, 1993.
- Labitzke, K., A. H. Manson, J. J. Barnett, and M. Corney, Comparison of geostrophic and observed winds in the upper mesosphere over Saskatoon, Canada, *J. Atmos. Terr. Phys.*, **49**, 987-997, 1987.
- Lloyd, N., A. H. Manson, D. J. McEwen, and C. E. Meek, A comparison of middle atmospheric dynamics at Saskatoon (52°N, 107°W) as measured by a medium-frequency radar and a Fabry-Perot interferometer, *J. Geophys. Res.*, **95**(D6), 7653-7660, 1990.
- Manson, A. H., C. E. Meek, H. Teitelbaum, F. Vial, R. Schindler, D. Kurschner, M. J. Smith, G. J. Fraser, and R. R. Clark, Climatologies of semidiurnal and diurnal tides in the middle atmosphere (70-110 km) at middle latitudes (40-55), *J. Atmos. Terr. Phys.*, **51**, 579-593, 1989.
- McKinley, D. W. R., Meteor science and engineering, McGraw-Hill, New York, 1961.
- Meek, C. E., Triangle size effect in spaced antenna wind measurements, *Radio Sci.*, **25**, 641-648, 1990.
- Namboothiri, S. P., A. H. Manson, and C. E. Meek, E region real heights and their implications for MF radar-derived wind and tidal climatologies, *Radio Sci.*, **28**, 187-202, 1993.
- Nastrom, G.D., and T.E. Vanzandt, Mean vertical motions seen by radar wind profilers, *J. Appl. Meteorol.*, **33**, 984-995, 1994.
- Phillips, A., A. H. Manson, C. E. Meek, and E. J. Llewellyn, A long-term comparison of middle atmosphere winds measured at Saskatoon (52°N, 107°W) by a medium-frequency radar and a Fabry-Perot interferometer, *J. Geophys. Res.*, **99**D6, 12,923-12,935, 1994.
- Roper, R. G., The semidiurnal tide in the lower thermosphere, *J. Geophys. Res.*, **71**, 5746-5748, 1966.
- Roper, R. G., The measurement of meteor winds over Atlanta (34°N, 84°W), *Radio Sci.*, **10**, 363-369, 1975.
- Roper, R. G., Winds from the Atlanta (34°N, 84°W) radio meteor wind facility, *J. Atmos. Terr. Phys.*, **40**, 891-894, 1978.
- Rossiter, D. E., A comparison of ionospheric drifts with radio meteor measurement of the neutral wind, *Aust. J. Phys.*, **23**, 103-117, 1970.
- Röttger, J., Investigations of lower and middle atmosphere dynamics with spaced antenna drift radars, *J. Atmos. Terr. Phys.*, **43**, 277-292, 1981.
- Röttger, J., and R. A. Vincent, VHF radar studies of tropospheric velocities and irregularities using spaced antenna techniques, *Geophys. Res. Lett.*, **5**, 917-920, 1978.
- Rüster, R., P. Czechowsky, P. Hoffman and W. Singer, Gravity wave signatures at mesopause heights, in *Proceedings of the Seventh Workshop on Technical and Scientific Aspects of MST Radar*, pp. 58-61, STEP Handbook, SCOSTEP Secretariat, Natl. Oceanic and Atmos. Admin., Boulder, Colo., 1996.
- Stubbs, T. J., The measurement of winds in the D-region of the ionosphere by the use of partially reflected radio waves, *J. Atmos. Terr. Phys.*, **35**, 909-919, 1973.
- Stubbs, T. J., and R. A. Vincent, Studies of D-region drifts during the winters of 1970-72, *Aust. J. Phys.*, **26**, 645-660, 1973.
- Sürücü, F., S. J. Franke, and E. Kudeki, On the influence of specular reflections in MF radar wind measurements, *Radio Sci.*, **30**, 1229-1244, 1995.
- Taylor, J. R., *An Introduction to Error Analysis*, Univ. Sci., Mill Valley, Calif., 1982.
- Thayaparan, T., Large and medium-scale dynamics in the mesosphere and lower thermosphere measured by MF and meteor VHF radars, Ph.D. thesis, Dep. of Phys., Univ. of Western Ont., London, Ont., Canada, 1995.
- Thayaparan, T., W. K. Hocking, and J. MacDougall, Middle atmospheric winds and tides over London, Canada (43°N, 81°W) during 1992-1993, *Radio Sci.*, **30**, 1293-1309, 1995a.
- Thayaparan, T., W. K. Hocking, and J. MacDougall, Observational evidence of gravity wave-tidal interactions using the UWO 2 MHz radar, *Geophys. Res. Lett.*, **22**, 381-384, 1995b.
- Thayaparan, T., W. K. Hocking, and J. MacDougall, Amplitude, phase, and period variations of the quasi 2-day wave in the mesosphere and lower thermosphere over London, Canada (43°N, 81°W) during the two years of 1993 and 1994, *J. Geophys. Res.*, in press, 1996.
- Tsuda, T., T. Aso, Y. Takashima, R. Ito, and S. Kato, Meteor radar observations at Kyoto in two C.T.O.P. periods, *J. Atmos. Terr. Phys.*, **42**, 461-469, 1980.
- Tsuda, T., T. Aso, and S. Kato, Seasonal variation of solar atmospheric tides at meteor heights, *J. Geomagn. Geoelectr.*, **35**, 65-86, 1983.
- Turek, R. S., K. L. Miller, R. G. Roper, and J. W. Bros-

- nathan, Mesospheric wind studies during AIDA Act 89: Morphology and comparison of various technique, *J. Atmos. Terr. Phys.*, 57, 1321-1343, 1995.
- Vincent, R. A., T. J. Stubbs, R. H. O. Pearson, K. H. Lloyd, and C. H. Low, A comparison of partial reflection drifts with winds determined by rocket techniques - I, *J. Atmos. Terr. Phys.*, 39, 813-821, 1977.
- Wright, J. W., The interpretation of ionospheric radio drift measurements - I., Some results of experimental comparisons with neutral wind profiles, *J. Atmos. Terr. Phys.*, 30, 919-930, 1968.

W. K. Hocking and T. Thayaparan, Department of Physics, The University of Western Ontario, London, Ontario N6A 3K7, Canada. (e-mail: whocking@danlon.physics.uwo.ca; paran@danlon.physics.uwo.ca)

(Received June 18, 1996; revised October 25, 1996; accepted November 12, 1996.)

Meteor decay times and their use in determining a diagnostic mesospheric temperature-pressure parameter: methodology and one year of data

W. K. Hocking, T. Thayaparan, and J. Jones

Department of Physics, The University of Western Ontario, London, Ontario, Canada, N6A 3K7

Abstract. Ambipolar diffusion coefficients in the meteor region have been measured using meteor decay times determined with the CLOVAR radar [Hocking, 1997]. This parameter may then be used to infer information about atmospheric temperatures or pressures in that region. In particular, we show annual variations in the parameter T/\sqrt{P} . Our procedures, together with the underlying assumptions, are described, and our results are compared to the CIRA (1986) empirical model as well as other experimental data. These successful measurements have been possible because of our use of a new 5-element interferometer which has minimal inter-element coupling and has an angular location accuracy of better than $\pm 2^\circ$, together with new algorithms which introduce important corrections to the decay time height profile. We concentrate in this paper on monthly averages, but higher temporal resolutions are possible.

1. Introduction

Meteors entering the earth's atmosphere produce ionized plasma trails which persist for life-times of typically a few hundredths of a second out to several seconds. If a radio wave impinges on such trails at an angle normal to the trail, then a portion of the wave energy is scattered back along the direction from which it has come. The strength of the backscattered radiation depends among other things on the free electron density within the trail and the radius of the trail relative to the radar wavelength. After the trail has formed, it begins to dissipate by, among other processes, ambipolar diffusion, eddy diffusion, recombination, and chemical reactions. It is generally true that ambipolar diffusion is the dominant factor in the early stages of trail growth, and therefore primarily determines the echo intensity for underdense trails near mesopause heights [e.g., Jones, 1975]. The backscattered radio amplitude from an underdense trail decreases exponentially with time due to ambipolar diffusion [e.g., McDaniel and Mason, 1973] in the manner

$$A(t) = A_0 e^{-16 \pi^2 D_a t / \lambda^2} \quad (1)$$

where λ is the radar wavelength, D_a is the ambipolar diffusion coefficient, and t is time. $A(t)$ is the radio wave amplitude at time t and A_0 is the value at $t=0$, (typically the time at which the exponential decay begins).

Decay times have been used in several studies to investigate temporal variability of the diffusion coefficient D_a [e.g., Tsutsumi et al., 1994; Reddi et al., 1993; Chilson et al., 1996]. However, recent theory [e.g., Jones and Jones, 1990; Jones, 1995] has shown that D_a is proportional to T^2/P , where T is a temperature and P is a pressure, so if either

T or P is known, the other parameter can be deduced. In this work, we present not D_a but rather T/\sqrt{P} ($\propto \sqrt{D_a}$) and discuss its usefulness in the atmosphere. This approach has not been undertaken previously, although Chilson et al. [1996] have made provisional experimental investigations of the relationship. We also demonstrate new instrumental techniques and design, as well as new software, which have all been important in allowing us to achieve the accuracy necessary to undertake these studies.

2. Experiment

A 10 kW peak power VHF (very high frequency) radar operating at a frequency of 40.68 MHz was used in pulsed mode to detect and record meteor trail echo. Individual pulses had a length of 13.3 μ s (2 km resolution) and pulses were transmitted at a pulse repetition frequency (PRF) of 2143 Hz. This produced range aliasing of our meteors, but as we will see we were generally able to locate unambiguously a meteor's angular position to within an accuracy of $\pm 2^\circ$. Hence, provided that it was assumed that all meteors lie in the height range between 70 and 110 km, it was possible to de-alias most signals and determine the true range and altitude. Further details can be found in Hocking [1997] and Hocking and Thayaparan [1997] (henceforth HT97).

Careful selection criteria were developed to isolate only underdense meteors and reject aircraft, lightning, and man-made interference. Visual inspection of several thousand records showed that our rejection criteria were successful on over 99% of occasions. A more detailed description of the meteor detection algorithm is given by HT97.

Figure 1 shows the arrangement of interferometric antennas used in our experiment. Note that this arrangement differs from that described in HT97. We have made these adjustments because the new interferometer has better directional detection capabilities and fewer angular ambiguities than the older receiving system. The new antenna separations of more than two wavelengths also reduce antenna coupling [Jones and Webster, 1992; Jones et al., 1997]. Ad-

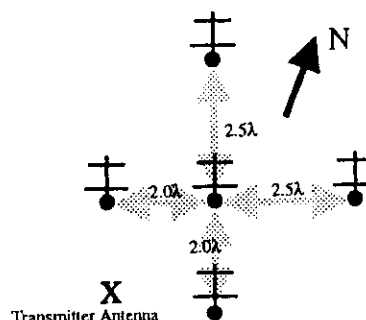


Figure 1. Arrangement of transmit and receive antennas used in our experiments. The 5 receiver antennas form an interferometer (see the text for more details).

ditionally, by using only a single transmit antenna we have been able to feed it with very low loss cable (1/2 inch heliax), thereby optimizing our transmitted power.

With the arrangement shown in Figure 1, we use the following procedure. Pulses of radio waves were transmitted from the antenna marked "X" and the returned signals (in-phase and quadrature components) were recorded separately for each of the 5 receive antennas. We also recorded a sixth channel for noise checks. These signals were multiplexed on a pulse-to-pulse basis through a single receiver. Thus the effective PRF for a single antenna was $2143/6 = 357.166$ Hz. To further enhance the signal to noise ratio, coherent integration over 4 successive pulses was used, giving an effective PRF of 89.29 Hz. The shortest meteor decay time which can be reasonably detected with our system is 0.025 s. Because the decay time decreases with height, the theoretical upper limit for our system is ~ 105 km (up to 110 km for very strong meteor trails and overdense trails).

These channels were then digitized for subsequent analysis. For any meteor detection, a 4-second window of data around the meteor was recorded at the range of detection. This corresponds to about 360 in-phase and quadrature point-pairs per receiver. The cross-correlation functions (CCFs) between all pairs of receiving antennas were then found. By determining phases at zero time lag, it was possible to use standard interferometry procedures [e.g., see Hocking et al., 1989] to determine unambiguously the angular location of the meteor trail in the sky. For an exponential amplitude function like (1), the auto- and cross-correlation functions are also exponential with the same decay time. Thus we can say that the time for the cross-correlation functions (averaged over all pairs) to fall to one half the peak value of the correlation function is given by

$$\tau_{1/2} = \frac{\lambda^2 \ln 2}{16 \pi^2 D_a} \quad (2)$$

We use primarily the cross-correlation functions, rather than the auto-correlation functions, because they do not have a troublesome noise spike at zero lag. Our system therefore acts as an all-sky meteor radar, locating meteor trails to an accuracy of $\pm 2^\circ$ in azimuth and zenith, and recording range, altitude, radial velocity, peak amplitude, $\tau_{1/2}$ and other pertinent parameters. The figure of $\pm 2^\circ$ has been determined both from numerical studies of antenna coupling and by determination of meteor radiants during shower conditions [Jones et al., 1997]. We record typically 800 meteors per day in non-shower conditions and up to 1500 meteors per day during strong meteor showers. As a point of interest we note that often the hardest part of the analysis is the initial meteor detection. We have found that by using incoherent addition of all 5 receive antennas we have significantly improved our ability to make an initial identification of a meteor. Once a meteor has been detected, the above-noted coherent procedures are then applied. We will not illustrate a typical meteor detected with this system - ours are generally quite similar to those illustrated by other authors [e.g., Chilson et al., 1996].

Our procedures unambiguously locate the position of most meteors, although there can be ambiguities either in angle or in height at low elevations. Meteors with ambiguous locations (e.g., two or more possible heights or angles) are removed from subsequent analysis. Generally most meteors above 30° in elevation are used.

3. Analysis

3.1 Theory

Our analysis for calculation of T/\sqrt{P} follows partly that of Chilson et al. [1996], with some adjustments. We employ

(2) to determine D_a , and then use the expression

$$D_a = \frac{2kT}{q_e} \left(\frac{T}{273.16} \right) \left(\frac{1.013 \times 10^5}{P} \right) K_0 \quad (3)$$

where k is the Boltzmann constant, q_e is the electronic charge ($= 1.6 \times 10^{-19}$ C), and T and P are the temperature and pressure of the neutral gas, respectively. K_0 is a constant related to the nature of the plasma in the trail. If metallic ions (M^+) are the main ionic constituent and N_2 is the main neutral species, then $K_0 = 2.5 \times 10^{-4} \text{ m}^2 \text{ s}^{-1} \text{ V}^{-1}$. It should be noted that this is an "average" value representative of ions having mass numbers between those of Mg^+ and Fe^+ . If N_2^+ is the main ion, $K_0 = 1.9 \times 10^{-4} \text{ m}^2 \text{ s}^{-1} \text{ V}^{-1}$ [e.g., Chilson et al., 1996; Jones and Jones, 1990; Jones, 1995]. Chilson et al. [1996] found that they should use the latter value of K_0 . We have adopted the more usual assumption that the main ions are M^+ and our subsequent results will verify this assumption (i.e., $K_0 = 2.5 \times 10^{-4}$).

Then combining (2) and (3)

$$\frac{T}{\sqrt{P}} = \sqrt{\frac{q_e}{2k} \left(\frac{273.16}{1.013 \times 10^5 K_0} \right) \left(\frac{\lambda^2 \ln 2}{16 \pi^2 \tau_{1/2}} \right)} \quad (4)$$

With our choice of wavelength, this becomes

$$\frac{T}{\sqrt{P}} = 1.93 \sqrt{\frac{1}{K_0}} 10^{x/2} \quad (5)$$

where $x = \log_{10}(\frac{1}{\tau_{1/2}})$, and $K_0 = 2.5 \times 10^{-4} \text{ m}^2 \text{ s}^{-1} \text{ V}^{-1}$.

3.2 Analysis Procedure

Figure 2a shows a scatter plot of some ten thousand or so values of decay time plotted as a function of height. The data were actually from a 14 day period, namely November 13-26, 1996. The scatter is not unusual, being similar to that shown by Chilson et al. [1996] and Tsutsumi [1994]. Despite the scatter, there is a clear band of high density extending from the bottom left to top right of the figure. We emphasize that our spread is also partly natural, since we include data from a 2-week period, so variations in temperature and pressure will enhance the spread over this time.

At this point, it has been common in the past to treat height as the independent variable and fit some form of function to the data [e.g., Chilson et al., 1996] in order to deter-

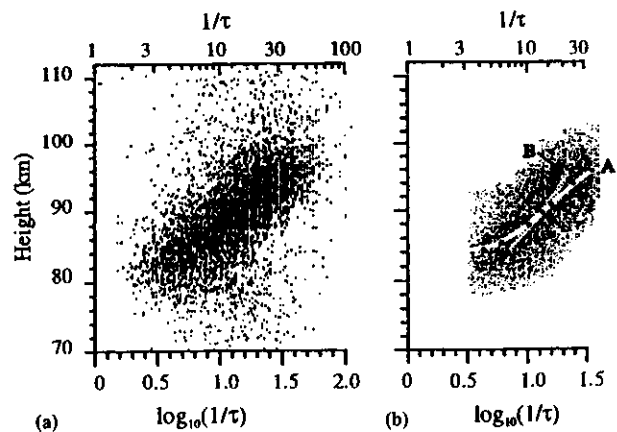


Figure 2. (a) Scatter plot of height versus $x (= \log_{10} \frac{1}{\tau_{1/2}})$ for all meteors recorded in the interval from November 13 to November 26, 1996. (b) As for (a), but with exclusion criteria and median filter applied (see text). Note also that this figure is plotted with higher resolution than (a).

mine a representative curve of $\tau_{1/2}$ versus height. We have not done this; rather we chose $x = \log_{10}(\frac{1}{\tau_{1/2}})$ as our independent variable, because we have found that this generally had less error than the height. We then grouped the data in bins of $x = (0.5-0.7)$, $(0.7-0.9)$, $(0.9-1.1)$, $(1.1-1.3)$, $(1.3-1.5)$, and $(1.5-1.7)$. We rejected data with decay times greater than 0.1 s above 96 km and less than 0.05 s at ≤ 84 km. We also excluded all data with $\tau_{1/2} \leq 0.025$ or $\tau_{1/2} \geq 0.3$ s at any height. Note that these restrictions are not terribly severe - only a few points lie outside this range anyway. Within each bin, we then applied a median filter and rejected the upper and lower 3% of our data (i.e., highest and lowest heights). The resultant data set is shown in Figure 2b. We then fitted a fifth order polynomial to the data, as shown by the line (A) in Figure 2b.

As a check, we also repeated a similar procedure, treating height as the independent variable. This produced the line (B) in Figure 2b. Subsequent calculations of T/\sqrt{P} were performed using both fitted lines, but we have found that when we treated x as the independent variable our T/\sqrt{P} values were always more consistent with data in the current literature. This confirmed that x was the best variable to treat as independent, at least for our system.

3.3 Bias Adjustment

Before turning to calculation of T/\sqrt{P} values, we need to recognize one extra adjustment which needs to be made to our fitted profile. Consider a population of meteors which have the same decay time. If we make measurements of a large population of such meteors, then due to various instrumental errors we will obtain a spread of measured heights. We can approximate this as a Gaussian distribution of the form $\exp\{-(h-h_r)^2/(2\sigma_r^2)\}$, centered at a height h_r .

Now consider all meteors, with all possible decay times. It is well known that the measured flux of meteors peaks at around 90 km altitude when the radar wavelength is around 40-50 MHz. The distribution can be broadly approximated as a Gaussian function of the form $\exp\{-(h-h_p)^2/(2\sigma_p^2)\}$. We can (and do) measure this distribution.

As a consequence, if we were to use our measured data to determine a mean height for all our data with a selected fading time, it will be a weighted average of the product of these two functions, i.e.,

$$h_{\text{measured}} = \frac{\int_{h=-\infty}^{\infty} h e^{-(h-h_r)^2/2\sigma_r^2} e^{-(h-h_p)^2/2\sigma_p^2} dh}{\int_{h=-\infty}^{\infty} e^{-(h-h_r)^2/2\sigma_r^2} e^{-(h-h_p)^2/2\sigma_p^2} dh} \quad (6)$$

where h_r is the true height corresponding to decay time τ and h_p is the height of peak meteor count rate. Similarly, our fitted polynomial will have errors in the height as a function of $\tau_{1/2}$ and needs to be adjusted to compensate for this bias.

We therefore include in our analysis algorithms a procedure to correct for this effect, and solve equation (6) by inverting the equation to extract h_r . We do this for all points on the profile. The parameter h_p is measured by finding the peak of the distribution of all our data and σ_p is found as the standard deviation of our distribution. The only uncertain parameter is σ_r , but this has reasonable limits. It is essentially the uncertainty in meteor height, which relates directly to the pulse length and angular uncertainty. For meteors directly overhead, we expect σ_r to be of the order of the pulse length. For off-vertical angles, the pulse length effect is reduced but the angular uncertainty contributes an extra error. We have therefore assigned a value for σ_r of ≈ 2 km. Numerical experiments showed that our inversion was moderately insensitive to the choice of σ_r provided it was within the reasonably expected limits of 2 to 3.5 km.

This inversion formed the final process in our analysis, enabling us to plot T/\sqrt{P} versus height. Some typical corrected data showing this adjustment can be seen by the large solid isolated points in Figure 2, close to line (A). Having thus finally obtained a reasonable profile of $\tau_{1/2}$ versus height, we were then able to apply equation (5) to produce a height profile of T/\sqrt{P} . Because our data tend to be less reliable at 85 km altitude due to the small number of meteors at that height, we have only catalogued T/\sqrt{P} at 88, 91, and 94 km.

4. Results

Figure 3 summarizes the results of our monthly mean values for T/\sqrt{P} for heights of 88, 91, and 94 km. Each determination for each month was made with typically 10,000-20,000 meteors. On the same graph, we show the the values of T/\sqrt{P} presented in the CIRA (1986) empirical model [Fleming et al., 1988] for our latitude of 43°N. We also compare our values with values deduced from climatological means provided by Na lidars [Senft et al., 1994] and satellite [Clancy et al., 1994] values, where the relevant pressures in these latter cases were taken from CIRA (1986).

Agreement is reasonable, but we do note some systematic differences in certain months. In principle, it would be possible to use these values to determine atmospheric temperatures directly by using CIRA (1986) pressures. Conversely, we could use known temperatures to determine pressures. However, pressure is a rapidly changing function of height and only a 1 km shift in height changes the pressure in the meteor region by $\sim 15\%$. The CIRA (1986) pressures are given only to 5 km accuracy, and we therefore feel reticent about using them to measure temperatures - a 15% error in pressure produces a 7% temperature error, which is more than we can tolerate. However, the recent Na lidar temperatures due to Senft et al. [1994] are very accurate, and so we may use our measurements of T/\sqrt{P} to measure pressure using these temperatures. Figure 4 shows pressure versus month compared to CIRA (1986), where the CIRA (1986) temperatures have been interpolated to the correct height. The data for 88 km altitude are not shown due to lack of space, but were equivalent in quality. Note that whilst there is general absolute agreement, there are also minor differences.

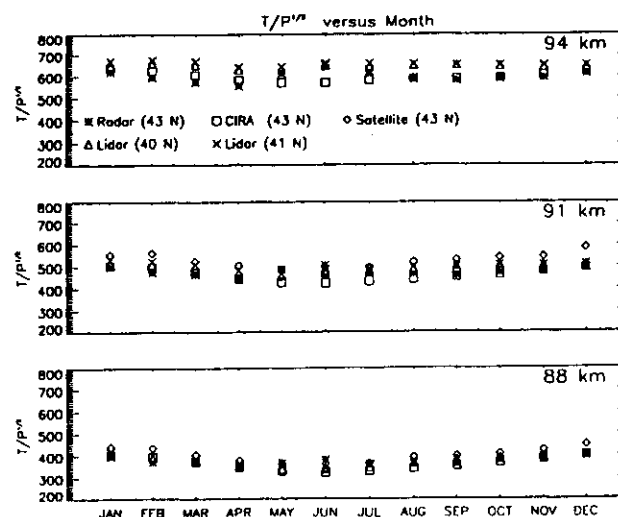


Figure 3. Monthly mean values of T/\sqrt{P} as a function of month as measured during our campaign. These values are compared with Na lidars, satellite, and the CIRA (1986).

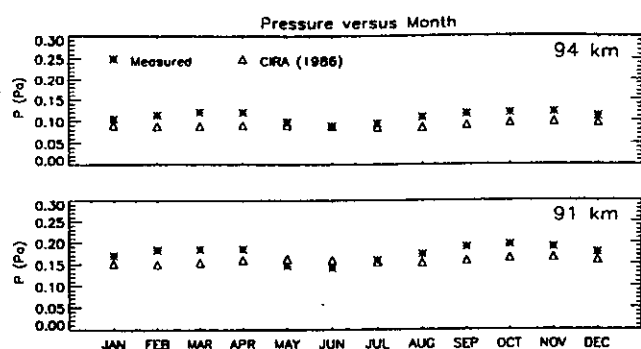


Figure 4. Monthly mean pressures as a function of month. The CIRA (1986) pressures are shown as a reference. Note that measured pressure is estimated by using our measurements of T/\sqrt{P} together with the average temperatures of two lidars [Senft et al., 1994].

In view of recent comparisons of Na lidar and CIRA (1986) temperatures, which suggest that the CIRA temperatures are in error [e.g., Senft et al., 1994], we are not surprised to see that the CIRA (1986) pressures may also be in error as shown by Figure 4. We consider that our pressure data may be more reliable than the CIRA (1986) values. We especially note a pressure minimum in summer which is not evident in the CIRA (1986) data.

5. Conclusion

Meteor decay times have been used to deduce the parameter T/\sqrt{P} and have been compared to calculations by other methods. The parameter T/\sqrt{P} can be used to determine (a) temperature if pressure is accurately known or (b) pressure if temperature is known accurately. Since the pressure is a sensitive function of height, it must be precisely known in order to measure the temperature accurately. The CIRA (1986) pressures may not be accurate enough to do this. We therefore used our measurements of T/\sqrt{P} together with Na lidar temperatures to measure P . Calculations show that there are some differences (15–25%) between the estimated and model (CIRA) pressure values. However, we also note that T/\sqrt{P} is an important parameter in its own right, and can be compared to numerical values for verification of computer models, for example. We anticipate that meteor measurements of T/\sqrt{P} may be a useful tool in future atmospheric studies, and subsequent work will include examination of this parameter at tidal and planetary wave scales.

Acknowledgments. We thank the Canadian Natural Sciences and Engineering Research Council for grant support.

References

Chilson P. B., P. Czechowsky, and G. Schmidt, A comparison of ambipolar diffusion coefficients in meteor trains

using VHF radar and UV lidar, *Geophys. Res. Lett.*, **23**, 2745–2748, 1996.

Clancy, R. T., D. W. Rusch, and M. T. Callan, Temperature minima in the average thermal structure of the middle mesosphere (70–80 km) from analysis of 40- to 92-km SME global temperature profiles, *J. Geophys. Res.*, **99D9**, 19,001–19,020, 1994.

Fleming, E. L., S. Chandra, M. R. Schoeberl and J. J. Bernett, Monthly mean global climatology of temperature, wind, geopotential height and pressure from 0–120 km, *NASA Technical Memorandum 100697*, 85 pp, 1988.

Hocking, W., System design, signal-processing procedures, and preliminary results for Canadian (London, Ont.) VHF atmospheric radar, *Radio Sci.*, **32**, 687–706, 1997.

Hocking, W. K., and T. Thayaparan, Simultaneous and co-located observations of winds and tides by MF and meteor radars over London, Canada (43°N, 81°W) during 1994–1996, *Radio Sci.*, **32**, 835–867, 1997.

Hocking, W. K., P. May, and J. Röttger, Interpretation, Reliability and accuracies of parameters deduced by the spaced antenna method in middle atmosphere applications, *Pure Appl. Geophys.*, **130**, 571–604, 1989.

Jones, J., On the decay of underdense radio meteor echoes, *Mon. Not. Roy. Astr. Soc.*, **173**, 637–647, 1975.

Jones, J., and A. R. Webster, Forward-scatter radiant mapping, *Asteroids, Comets, Meteors*, pp. 273–276, Lunar and Planetary Institute, Houston, 1992.

Jones, J., and A. R. Webster, and W. K. Hocking, An improved interferometer design for use with meteor radars, in press, *Radio Sci.*, 1997.

Jones, W., The decay of radar echoes from meteors with particular reference to their use in the determination of temperature fluctuations near the mesopause, *Ann. Geophysicae*, **13**, 1104–1106, 1995.

Jones, W., and J. Jones, Ionic diffusion in meteor trails, *J. Atmos. Terr. Phys.*, **52**, 185–191, 1990.

McDaniel, E. W., and E. A. Mason, The mobility and diffusion of ions in gases, John Wiley and Sons, NY, 1973.

Reddi, C. R., K. Rajeev, and G. Ramkumar, Annual and semiannual temperature oscillations at the mesopause levels over Trivandrum (8.5°N, 78°E), *J. Geophys. Res.*, **98(D5)**, 8925–8931, 1993.

Senft, D. C., G. C. Papen, C. S. Gardner, J. R. Yu, D. A. Krueger, and C. Y. She, Seasonal variations of the thermal structure of the mesopause region at Urbana IL (40°N, 88°W) and Ft. Collins, CO (41°N, 105°W), *Geophys. Res. Lett.*, **21**, 821–824, 1994.

Tsutsumi, M., T. Tsuda, and T. Nakamura, Temperature fluctuations near the mesopause inferred from meteor observations with the middle and upper atmosphere radar, *Radio Sci.*, **29**, 599–610, 1994.

W. K. Hocking, T. Thayaparan, and J. Jones, Department of Physics, The University of Western Ontario, London, Ontario, Canada, N6A 3K7.

(received June 12, 1997; revised September 4, 1997; accepted October 9, 1997.)

An improved interferometer design for use with meteor radars

J. Jones

Department of Physics and Astronomy, University of Western Ontario, London, Ontario, Canada

A. R. Webster

Department of Electrical and Computer Engineering, University of Western Ontario, London, Ontario, Canada

W. K. Hocking

Department of Physics and Astronomy, University of Western Ontario, London, Ontario, Canada

Abstract. The measurement of the directions of radio meteors with an interferometric system is beset by two problems: (1) The ambiguity in the measured directions for antennas spaced by more than $\lambda/2$ and (2) the effects of mutual impedance when the antennas are spaced at $\lambda/2$ and less to avoid these ambiguities. In this paper we discuss the effects of mutual impedance between spaced antennas and describe an interferometer which both minimizes these effects and avoids the ambiguities associated with spacings larger than $\lambda/2$. We have modeled a version of this design numerically and show that under ideal conditions an interferometer of total span 4.5λ can yield directions accurate to about 0.3° with a signal-to-noise ratio of 20 dB. Finally, we have tested the design with observations from the 1996 Geminid and 1997 Quadrantid meteor showers and find that even without a ground plane, the interferometer provides unambiguous directions to an accuracy of the order of 1.5° .

1. Introduction

The measurement of the echo directions of radio meteors is important in several fields of study. Since the reflection process of radio waves from meteor trains is predominantly specular for underdense meteors, the direction of the echo contains important information about the trajectory of the associated meteoroid and the extraction of this directional information has been at the core of most of the methods for deducing the orbits of the meteoroids [Weiss and Elford, 1963; Morton and Jones, 1982; Baggaley et

al., 1993.]. The Doppler shifts of the frequencies of radio-meteor echoes are also routinely used to measure winds in the upper atmosphere [Spizzichino et al., 1965; Roper, 1975; Nakamura et al., 1995; Valentic et al., 1996; Hocking, 1997], and when coupled with range and directional information, this provides a description of the wind field. More recently measurements of the ambipolar diffusion coefficients using the decay times of underdense radio-meteors has enabled the variation of atmospheric temperature with height as determined from the range and elevation of the meteor echo to be monitored on a daily basis [Tsutsumi, et al., 1994; Hocking et al., 1997]. Clearly, it is important to be able to measure the echo directions accurately.

Before microcomputers became widely used in data acquisition systems, echo directions were

Copyright 1998 by the American Geophysical Union.

Paper number 97RS03050.

0048-6604/98/97RS-03050\$11.00

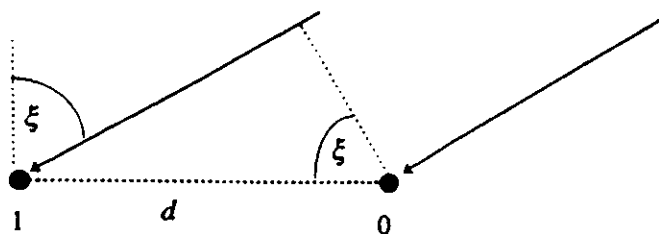


Figure 1. Measurement of angle of arrival, ξ , from the signal phase on spaced antennas.

difficult to measure, and whereas elevations could usually be estimated using range and heights, the azimuth of the echo was usually uncertain to within the width of the antenna beam. Certainly, it was possible to measure directions using the phase differences between elements of an interferometer, but the amount of data reduction required when several antennas were used was daunting. Nowadays this is no longer a problem, and interferometers are used routinely to obtain the directions of meteor echoes.

The use of interferometers, however, has its problems. In order to measure the echo direction unambiguously over the visible hemisphere down to low elevation angles, the antennas of a two-element interferometer must be separated by no more than 0.5λ if no information other than phase is used. If range information is available, it is often possible to resolve this ambiguity, since the meteors usually occur in the height range 80-120 km; but for systems with high pulse-repetition frequencies this may not be possible because of range aliasing. An important consideration is the mutual coupling between the antennas, which increases as their spacing decreases, so that there is the likelihood that the phase difference between the signals from the two antennas is seriously in error.

In this paper we discuss the errors resulting from the effects of mutual coupling of the antennas and show that they cannot be neglected for small antenna spacings. We then present a design for a three-element interferometer which avoids the effects of mutual coupling while at the same time resolves the directional ambiguity. We present the results of numerical experiments

which show that this design can yield very accurate directions, and finally, we present some results of observations of radio meteors using such an interferometer.

2. The Effects of Mutual Coupling on the Measured value of Angle of Arrival using Linearly Spaced Antennas

In principle, the angle of arrival (AOA) of radio waves at a receiving site can be determined by measuring the phase angle difference ϕ_{10} between two antennas spaced by distance d as shown in Figure 1, the angle ξ being measured relative to the normal to the axis of the array. Angular measurements in three dimensions can be obtained from two such arrays arranged orthogonally.

The phase ϕ_{10} of the signal on antenna 1 relative to antenna 0 in Figure 1 is given by,

$$\phi_{10} = -2\pi \frac{d}{\lambda} \sin \xi \quad (1)$$

Since ϕ_{10} is measured in the range $\pm\pi$, the value of ξ is determined unambiguously in the range $\pm\pi/2$ only if $d \leq 0.5\lambda$. On the other hand, larger values of d result in a better estimate of ξ . A common arrangement to accommodate both of these desirable features is an array of several elements spanning a large aperture with adjacent elements spaced $\lambda/2$. A problem does arise, though, with mutual coupling between adjacent closely spaced elements so that the measured value of ϕ can be significantly in error; these mutual coupling effects diminish as the spacing is increased, i.e., as the mutual impedance (Z_m) decreases. For identical antennas (with impedance Z_a in isolation, each connected to matched loads ($Z_L = Z_{in}^*$), the equivalent circuit is shown in Figure 2. Expressions for the calculation of mutual impedance can be found in several standard textbooks [e.g., see Balanis, 1982].

The phase of the currents I_0 and I_1 flowing into the loads are the measured phases, whereas the required phases are those of the open cir-

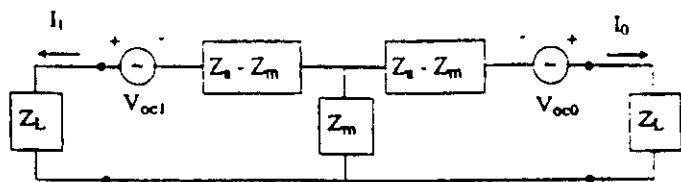


Figure 2. Electrical equivalent circuit for closely spaced identical antennas.

circuit voltages induced in the antennas as given above; it will be noted that if Z_m is zero, then the measured phase is that required.

For two half-wave dipoles spaced $\lambda/2$, as shown in Figure 3, the coupling is significant so that the measured phase (ϕ_{10}) is modified from that which would be obtained in isolation. If this phase is inserted into equation (1), then the inferred value of the angle of arrival is in error, as shown in Figure 4.

Although the collinear arrangement produces the greater error at such close spacing, the mutual impedance decreases much more rapidly with increasing separation than the side-by-side case. The zero error for directions orthogonal to the array axis is always found at any separation, but the zero error along the array axis is only found at separations which are multiples of $\lambda/2$. This is because at angles of arrival close to the axis of the array, the generators are in antiphase at such spacings, and thus the currents are also in antiphase, as may be seen by inspection of Figure 2. At any other spacing, the errors in phase can produce large angular errors for echo directions close to the array axis, since for a given finite phase error, $\Delta\phi_{10}$, the error $\Delta\xi$ in AOA is given by

$$\Delta\xi \approx -\frac{\lambda\Delta\phi_{10}}{2\pi d \cos \xi} \quad (2)$$



Figure 3. Half-wave dipoles spaced by $\lambda/2$; (a) side by side and (b) collinear.

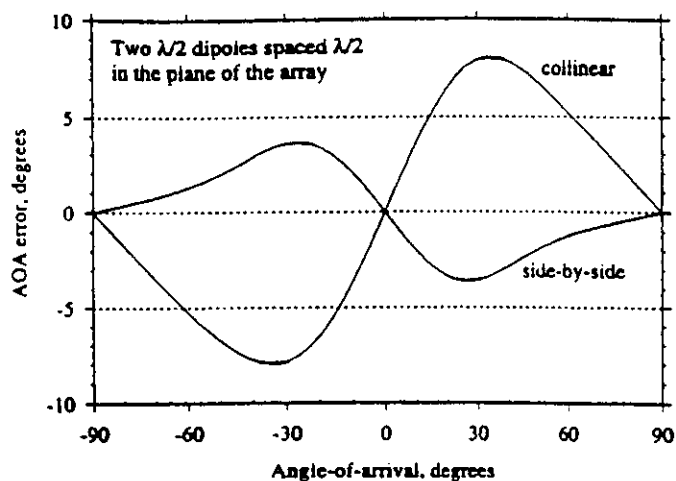


Figure 4. The error in angle of arrival (AOA) for the closely spaced dipoles in Figure 3.

A plot of the error in AOA (i.e., $\Delta\xi$ versus AOA) is shown in Figure 5 for separation in the range $0.5 - 1.0\lambda$. We see that for separation close to 0.75λ , the error increases as the array axis is approached, while the error at large ξ for a separation of 0.5λ and 1.0λ approaches zero as in Figure 4; these phenomena, albeit with diminishing amplitude, are repeated at intervals of $\lambda/2$. As a consequence it is clear that the separation between such dipoles should be set at a multiple of $\lambda/2$ to minimize the angular error at larger values of ξ , and separations of $(2m+1)\lambda/4$, where m is an integer, should be avoided. In fact, in Figure 5 the range in ξ is restricted to $\pm 65^\circ$ since outside the range $\pm 70^\circ$, the estimate of the true value of ξ is inaccessible due to the errors introduced by the mutual coupling effects. This effect is shown to better advantage in Figure 6, which relates to a spacing of 0.75λ ($m=1$).

As the separation between antennas increases, the mutual effects diminish, so that for a given acceptable error in the echo direction a suitable spacing may be chosen. Spacings of $n\lambda/2$ are desirable, and Figure 7 shows the errors introduced in measured echo directions due to the mutual coupling effects over the range $0.5-2.5\lambda$. From this, it can be seen that for spacings greater than about 1.5λ , the effects are quite small, with errors less than 0.5° .

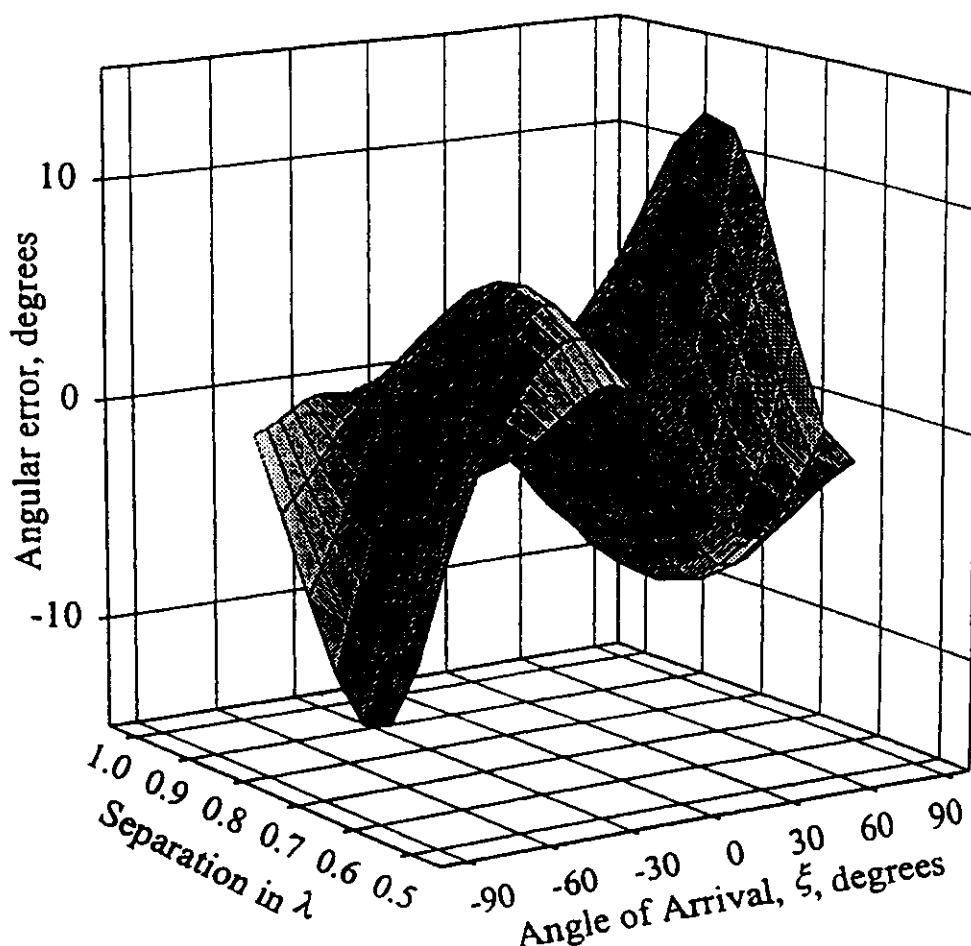


Figure 5. Angular error (in angle-of-arrival) versus angle-of-arrival (range $\pm 65^\circ$ shown for side-by-side dipoles with separation in the range $0.5 - 1.0\lambda$).

3. An Improved Meteor Radar Interferometer

In order to obtain an accurate estimate of the angle of arrival using two spaced antennas it is desirable to use a spacing of several wavelengths, but this introduces ambiguities due to the uncertainty of the number of multiples of 2π introduced. Additional antennas separated by $\lambda/2$ are still needed to resolve these ambiguities, but, as has been shown, the mutual coupling produces significant errors at such close spacing. A solution to this problem is to use three antennas arranged to be spaced by distances differing by $\lambda/2$; for example, in Figure 8, values of $d_1 = 2.5\lambda$ and $d_2 = 2.0\lambda$ might be used. Phase measurements ϕ_{10} and ϕ_{20} relative to the center

antenna then allow unambiguous determination of the angle of arrival since

$$\phi_{10} = -\frac{2\pi d_1}{\lambda} \sin \xi \quad (3)$$

$$\phi_{20} = +\frac{2\pi d_2}{\lambda} \sin \xi \quad (4)$$

so that essentially two estimates of ξ are available:

$$\sin \xi = -\frac{\lambda}{2\pi} \frac{(\phi_{10} - \phi_{20})}{(d_1 + d_2)} \quad (5)$$

$$\sin \xi = -\frac{\lambda}{2\pi} \frac{(\phi_{10} + \phi_{20})}{(d_1 - d_2)} \quad (6)$$

The first giving an accurate, but ambiguous answer, while the second gives a less accurate answer but resolves the ambiguity since $(d_1 - d_2)$

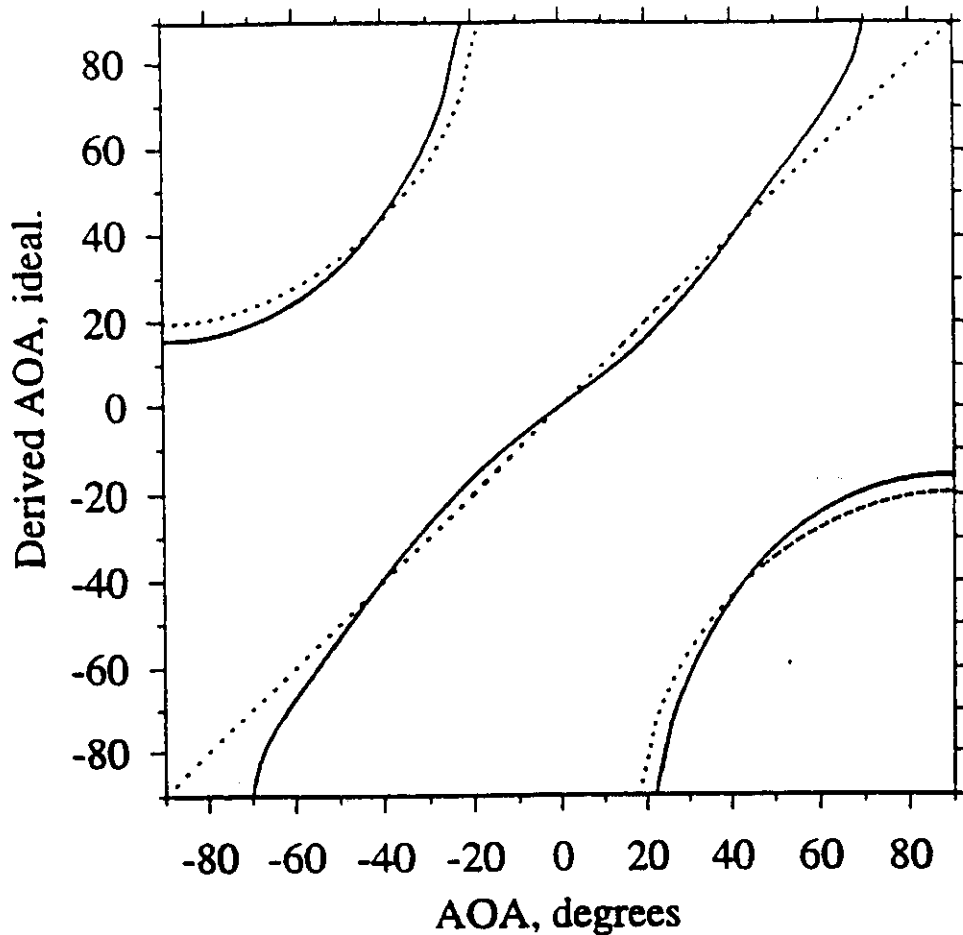


Figure 6. The AOA derived from the phase measurements from side-by-side $\lambda/2$ dipoles spaced by 0.75λ ; the dotted lines are for the ideal case of no mutual coupling effects while the solid lines allow for these effects, and illustrate the errors introduced. Note the fact that for $\xi > \pm 70^\circ$ a good estimate of the AOA is not available.

is equal to $\lambda/2$ and the multiples of 2π cancel in the numerator. For example, with $d_1 = 2.5\lambda$ and $d_2 = 2.0\lambda$ and with $\xi = -40^\circ$, we measure $\phi_{10} = +141.5^\circ$ and $\phi_{20} = +102.8^\circ$ so that the quantities $(\phi_{10} - \phi_{20})$ and $(\phi_{10} + \phi_{20})$ evaluate to -38.7° and -115.7° , respectively. This is illustrated in Figure 9, where the measured phase associated with $(d_1 + d_2)$ gives multiple accurate possibilities from which the correct value of ξ is determined by the measurement associated with $(d_1 - d_2)$. The shaded bands cover a representative phase uncertainty of $\pm 15^\circ$, and the points raised above regarding ambiguities and accuracy are apparent; note that from equation (2), a

phase uncertainty of $\pm 15^\circ$ at $\xi = -40^\circ$ translates into respective errors of $\pm 6^\circ$ and $\pm 0.7^\circ$ for the close and wide spacings in this example.

The uncertainty in the phase measurements is directly affected by the signal-to-noise ratio, and in relation to this, two points are worth noting from Figure 9:

1. As the echo direction becomes closer to the array axis, the phase uncertainty results in a larger uncertainty in the measured echo direction and the echo direction may become indeterminate if the phase uncertainty is too large.

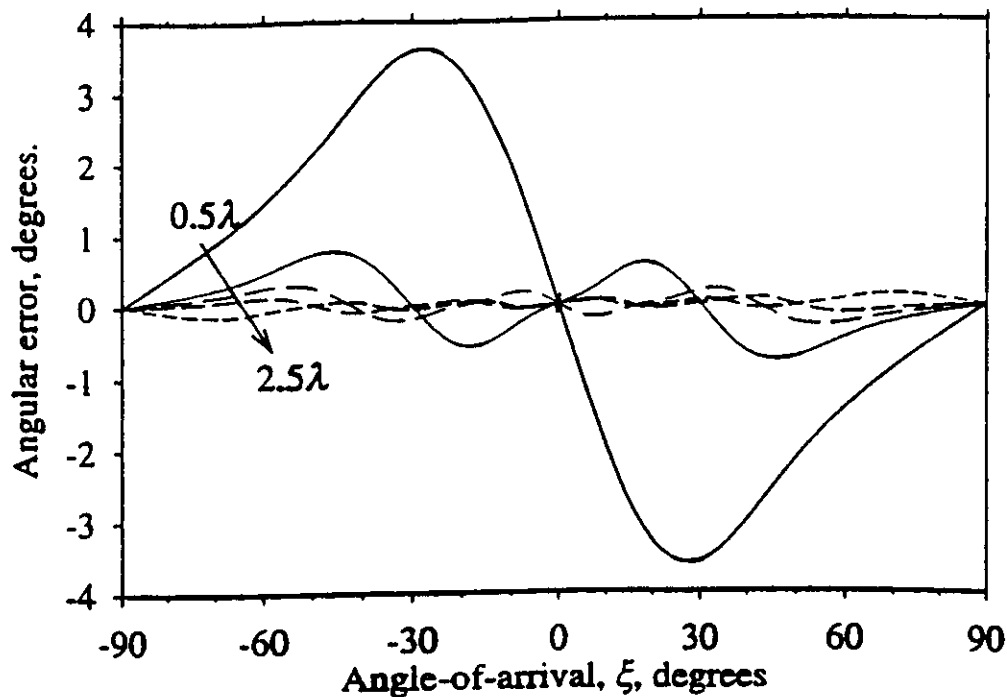


Figure 7. Errors in AOA for side-by-side dipoles with spacings at $\lambda/2$ intervals.

2. The separation of the multiple estimates in the echo directions for the wide spacing must be greater than the uncertainty in the estimate from the close spacing. In other words, it is not practical to extend the separations indefinitely in order to gain a corresponding improvement in accuracy.

Although the first part of this exercise involved only two dipoles, in practice, the situation would be much more complex if the antennas have parasitic elements, particularly in the presence of a nearby ground. Nevertheless, it is apparent that the effects of coupling between

the antennas decrease rapidly as the spacing is increased and are likely to be negligible for spacings greater than 2λ .

4. Numerical Modeling

How well can we expect to measure echo directions using this design of interferometer? In practice, the accuracy will be limited by the signal-to-noise ratio, and in this section we describe the results of numerically modeling the direction-measuring procedure. We take our system to be a five-element interferometer as shown in Figure 10, consisting of two orthogonal three-element linear interferometers with a common central element. For the sake of this study we have supposed the antennas to have isotropic gain, and we have ignored the effects of the ground reflections.

Echo directions were generated with a uniform random distribution in direction, and the resulting inphase (I) and quadrature (Q) signals were calculated for each antenna. Gaussian noise corresponding to a specified mean signal-to-noise

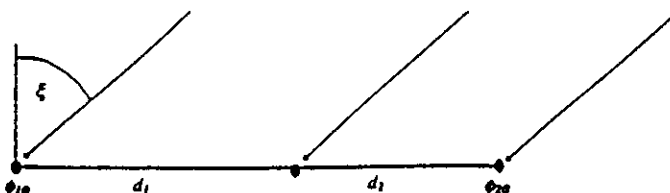


Figure 8. A linear array of three elements with the centre one used as phase reference.

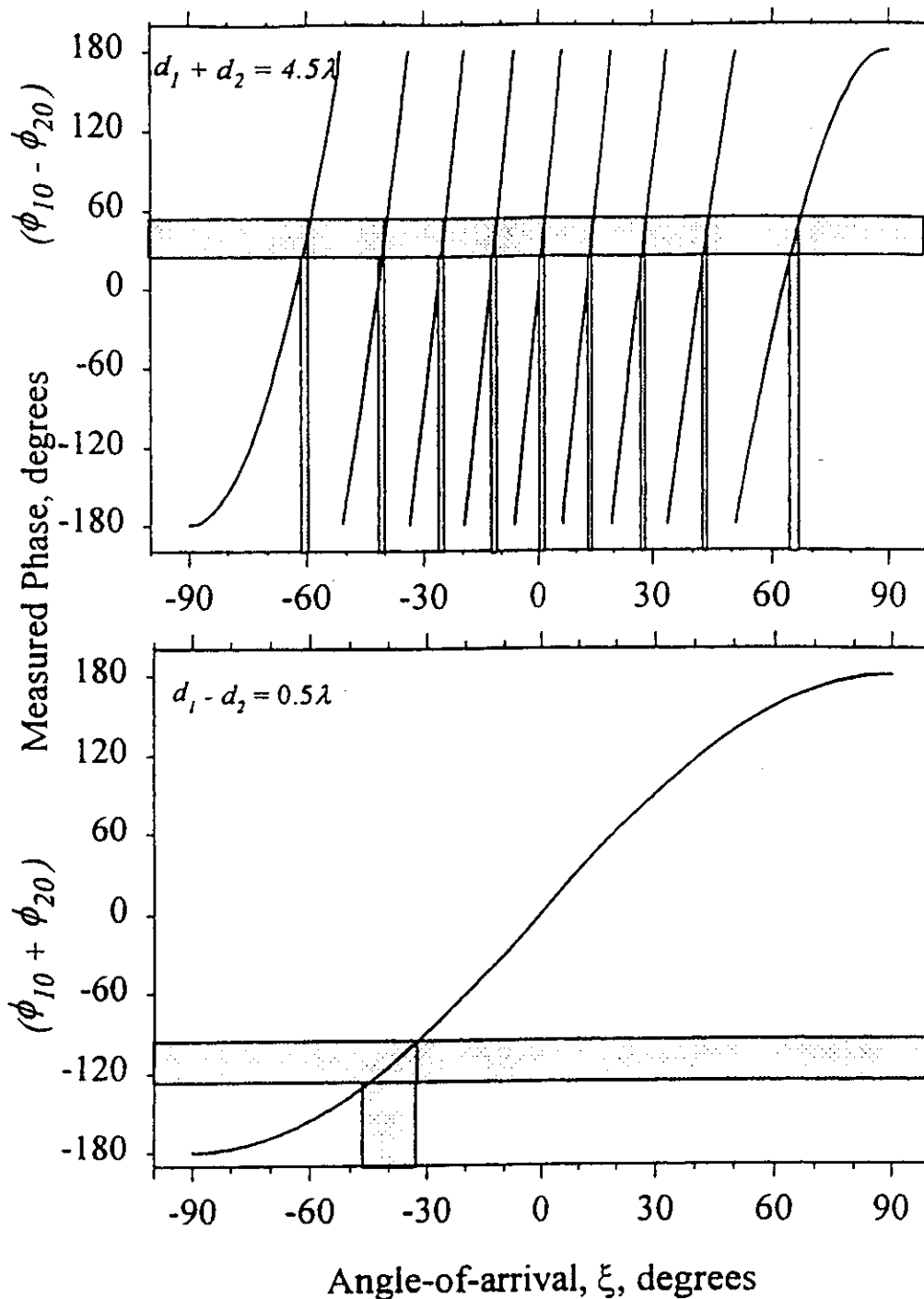


Figure 9. The relationship between the measured phase angles and derived angle of arrival, where the phases are as indicated in Figure 8. The shaded bands show the effect of uncertainties of $\pm 15^\circ$ in the total phases.

ratio was then added to each of the I and Q signals and the resultant phase calculated. We then were able to calculate the apparent direction cosines to each of the interferometer axes

using equation (6) to get an initial estimate and then refining it using equation (5). For each of these trials the angle between the original and apparent directions were calculated, and a plot

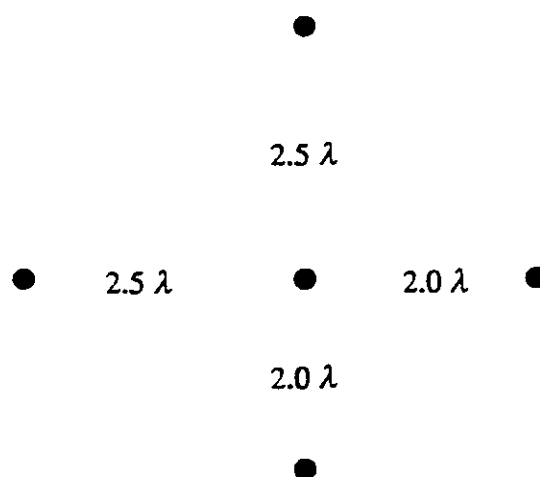


Figure 10. Interferometer configuration for the numerical model.

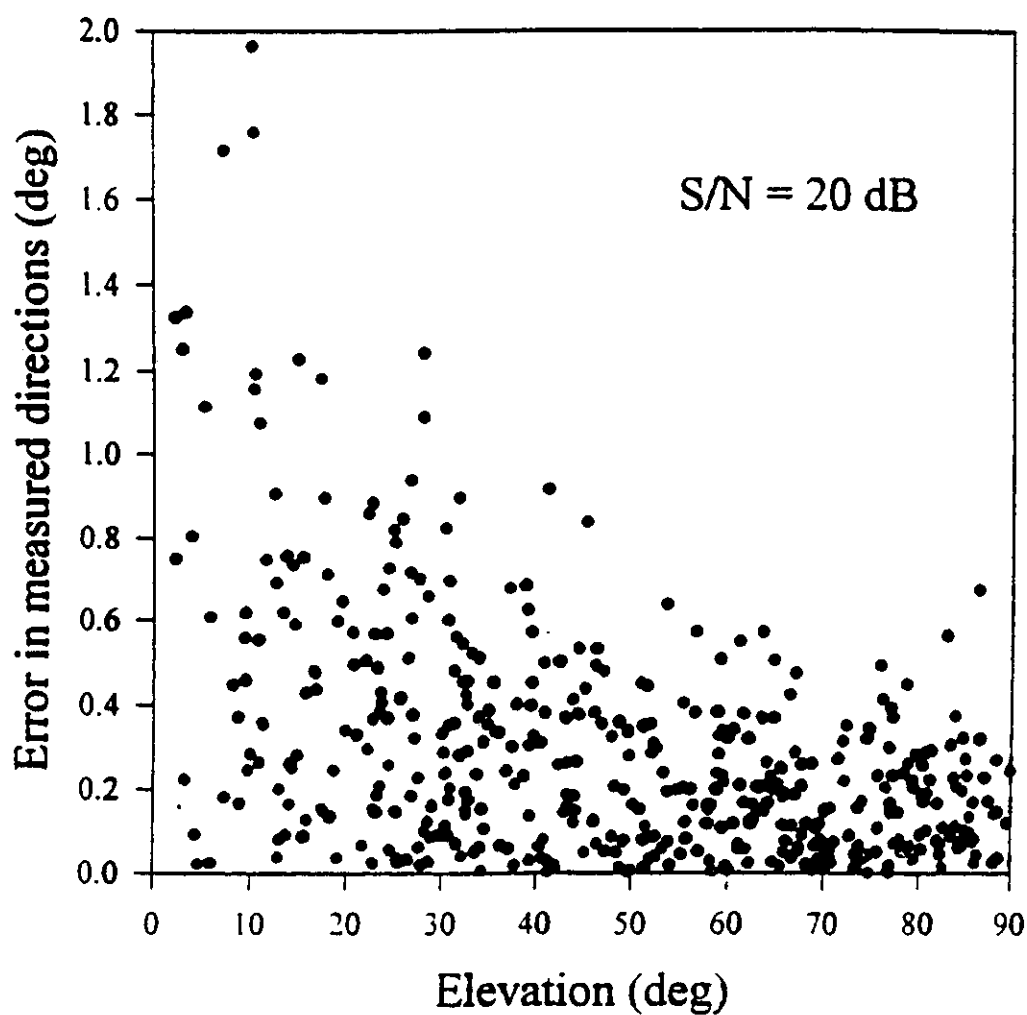


Figure 11. Error in direction as a function of angle of elevation for numerical model. Note that the elevation angle is derived from the angle of arrival ξ used earlier.

of these directional errors as a function of echo elevation for one such numerical experiment involving 500 trials in which the mean signal-to-noise ratio was 20 dB is shown in Figure 11.

The mean error in directions for elevations above 30° is 0.31° . For smaller elevations the error increases rapidly with decreasing elevation angle; for example, at an elevation of 20° the average error in the directions is about 1.8° . We have investigated the model at length and find, as would be expected, that increasing the signal to noise ratio improves the measurements even more: Doubling the signal-to-noise ratio to 26 dB reduces the error in direction by approximately a factor of 2. There seems to be little advantage in increasing the antenna spacing, but the accuracy can be increased by an order of magnitude by adding two extra antennas spaced at, say, 30λ from the center. We have also modeled the situation with smaller signal-to-noise ratios and find that below 17 dB the method starts to produce grossly incorrect apparent echo directions even for elevations greater than 30° , but the fraction of these is small even for signal-to-noise ratios as small as 10 dB. This, of course, applies only to the case when a single phase measurement is made at each antenna; when several measurements are available which can be averaged, the accuracy is improved accordingly.

5. Observational Results.

We have incorporated a five-element interferometer similar to that used in the model above into the Canadian London Ontario VHF atmospheric radar (CLOVAR) located at 43°N , 81°W , which has been described by *Hockins* [1997]. The end antennas were placed at 2.0 and 2.5λ from the central antenna as in the model, but whereas the model did not have to include the effects of the ground, the actual interferometer was built on uneven terrain and was also close to some trees, both of which introduce phase errors whose magnitude it is difficult to estimate. The performance of the interferometer was investigated using observations made

with CLOVAR in its meteor mode during the Geminid and Quadrantid meteor showers in December 1996 and January 1997, respectively.

We estimated the directional errors using two methods: (1) from the residual phase error after the signal direction was determined and (2) from the apparent scatter in the directions of echoes belonging to meteor showers. The first method indicated that the measurement error in direction is approximately 2° for echoes with elevations greater than 30° .

Shower meteors (Geminids and Quadrantids, in this case) have essentially parallel trajectories, and the specular reflection condition dictates that the echo directions are perpendicular to this direction. We were therefore able to select those meteors which fulfilled this condition to within a specified tolerance, $\pm\theta$, and Figure 12 shows how the number of such meteors varied with θ . For a Gaussian distribution in signal direction resulting from a small dispersion in the directions of the meteor trajectories, as well as measurement errors in the echo directions, the number N of echoes satisfying a given specular tolerance condition is given approximately by

$$N = A \operatorname{erf}(\theta/\sqrt{2}\sigma) + B\theta \quad (7)$$

where σ is the composite dispersion in the echo directions and the linear term is to take account of contamination by sporadic meteors which becomes more severe as θ increases. The coefficients A and B are proportional to the shower and sporadic activity. We have verified that this approximation is valid and that accurate values of σ are obtained by using a least squares method to fit this formula to with simulated data. Applying this method to the observational Geminid and Quadrantid data, we find that the apparent scatter in echo directions is 1.5° and 1.7° , which represents an upper limit to the measurement error since it also incorporates the intrinsic scatter in the meteoroid trajectories, which is probably the reason that the scatter is somewhat greater for the Quadrantids than for the Geminids.

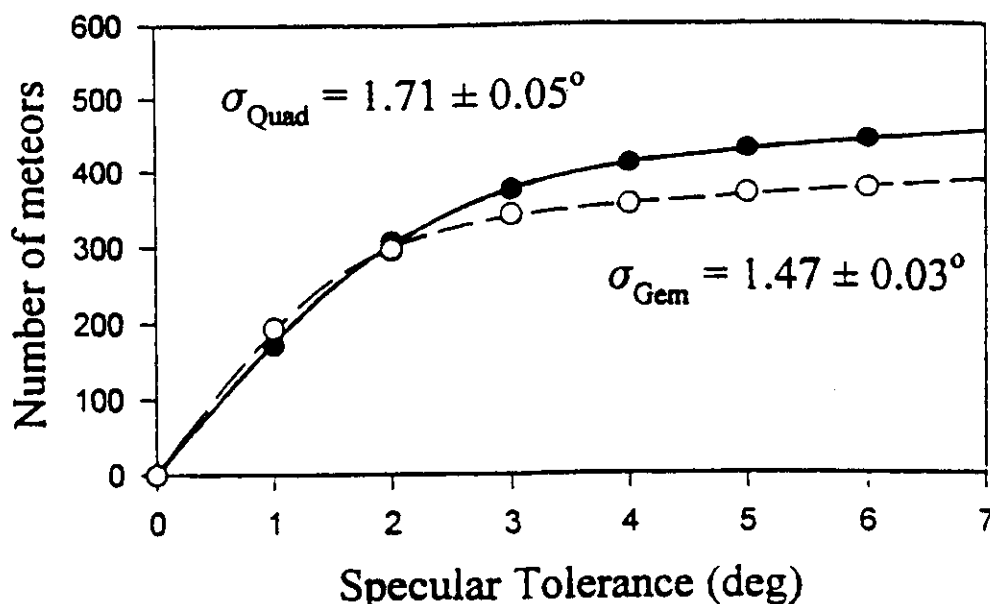


Figure 12. Fit of equation (7) to observational data to obtain apparent scatter in echo direction. Solid circles indicate Quadrantids 1997, and open circles indicate Geminids 1996.

The value of $\pm 1.5^\circ$ obtained observationally is much greater than the 0.31° accuracy that the method is capable of, and we attribute the difference to the effects of uneven terrain and trees. It is clear that care must be taken to reduce such effects to realize the potential accuracy of the interferometer, and this may take the form of a carefully constructed ground plane or the use of antennas with polar diagrams that minimize ground reflections. For many applications such heroic efforts are not warranted, and it is sufficient to measure directions to an accuracy of a degree or two without the worry of possible ambiguities.

Acknowledgments. The authors gratefully acknowledge the funding of this project by the National Science and Engineering Research Council of Canada.

References

- Baggaley, W.J., A.D. Taylor, and D.I. Steel, The Southern Hemisphere Meteor Orbit Radar facility: AMOR, in *Meteoroids and their Parent Bodies*, edited by J. Stohl and I.P. Williams. pp. 245-248, 1993. Atron. Inst. of the Slovak Acad. of Sci., Bratislava.
- Balanis, C.A., *Antenna Theory - Analysis and Design*, Harper Collins, New York, 1982.
- Hocking, W. K., System design, signal-processing procedures and preliminary results for the Canadian (London, Ontario) VHF atmospheric radar, *Radio Sci.*, 32 (2) 687-706, 1997.
- Hocking, W. K., T. Thayaparan, and J. Jones., Meteor decay times and their use in determining a diagnostic mesospheric temperature-pressure parameter: Methodology and 1 year of data. *Geophys. Res. Lett.*, 24, 2977-2980, 1997.
- Morton, J. D., and J. Jones., A method for imaging radio meteor radiant distributions. *Mon. Not. R. Astron. Soc.*, 198, 737-746, 1982.
- Nakamura, T., T. Tsuda, and M. Tsutsumi, Meteor wind observations with the MU radar., *Radio Sci.*, 26 (4) 857-869, 1991.
- Roper, R. G., The measurement of meteor winds over Atlanta., *Radio Sci.*, 10 (3) 363-369, 1975.
- Spizzichino, A., J. Delcourt, A. Giraud, and I. Revah, A new type of continuous wave radar for the observation of meteor trails, *Proc. IEEE*, 53, 1084-1086, 1965.
- Tsutsumi, M., T. Tsuda, T. Nakamura, and S. Fukao, Temperature fluctuations near the mesopause inferred from meteor observations with the middle and upper atmosphere radar, *Radio Sci.*, 29 (3), 599-610, 1994.
- Valentic, A., J. P. Avery, S. K. Avery, M. A. Cervera, W. G. Elford, R. A. Vincent, and I. M. Reid. A comparison of meteor radar systems at Buckland Park, *Radio Sci.*, 31 (6) 1313-1329, 1996.
- Weiss, A. A., and W. G. Elford, An equipment for combined geophysical and astronomical measurements of meteors., *Proc. Inst. Radio Eng. Aust.*, 24 197, 1963.

W. K. Hocking and J. Jones Department of Physics and Astronomy, University of Western Ontario, London, Ontario, Canada. N6A 3K7 (e-mail: whocking@danlon.physics.uwo.ca; jim.jones@julian.uwo.ca)

A. R. Webster, Department of Electrical and Computer Engineering, University of Western Ontario, London, Ontario, Canada. N6A 5B9 (e-mail: awebster@engntadmin.engga.uwo.ca)

Received June 23, 1997; revised October 21, 1997; accepted October 29, 1997)

424

Temperatures using radar-meteor decay times.

W. K. Hocking

Department of Physics, The University of Western Ontario, London, Ontario, Canada, N6A 3K7

Abstract. Experimental studies of the temperature and pressure dependence of the ambipolar diffusion coefficient in the mesopause region have been undertaken by studying meteor trail decay times with radars at a variety of sites in North America, with latitudes between 75N and 35N. The site at Resolute Bay, Canada, has proven especially useful, due to the wide range of mesopause temperatures experienced at that site between summer and winter. Theoretical predictions have been confirmed, and an algorithm is outlined which permits meteor decay times to be used to determine absolute measurements of mesospheric temperatures.

1. Introduction

As meteoroids enter the Earth's atmosphere, they form approximately cylindrical plasma trails with considerable electron content. These trails are capable of reflecting radio waves which impinge upon them, and so a suitably configured radar can be used to detect and interrogate them. The trail forms quickly and then expands radially as time progresses. Assuming that ambipolar diffusion is the main trail expansion mechanism in the early stages of growth, then the backscattered radar signal for an underdense meteor appears as a sudden leap in amplitude to an initial value A_0 , followed by an amplitude decay according to

$$A(t) = A_0 e^{-(16\pi^2 D_a t)/\lambda^2} = A_0 e^{-\ln 2 \frac{t}{\tau_{1/2}}} \quad (1)$$

where t is time, λ is the radar wavelength, D_a is the "ambipolar diffusion coefficient", and $\tau_{1/2}$ is the time for the amplitude to fall to one half of its maximum value. $A(t)$ is the received field strength at time t , with $t=0$ being the time at which the meteor signal first appears. The value $\tau_{1/2}$ is typically in the range 0.01 to 0.5 seconds for a radar operating at a frequency in the range 30 to 50 MHz. (e.g. see Hocking *et al.*, 1997, and references therein). This paper deals exclusively with such underdense meteors.

By measuring the half-amplitude decay time $\tau_{1/2}$ of the meteor signal, it is possible to estimate the parameter $D_a = \lambda^2 \ln 2 / (16\pi^2 \tau_{1/2})$. This parameter in turn depends on the atmospheric temperature and pressure, and Jones and Jones [1990] have predicted that D_a can be determined as

$$D_a = K_{amb} \frac{T^2}{P} \quad (2)$$

Specific details about K_{amb} have been outlined in Hocking *et al.*, [1997] and Chilson *et al.*, [1996]. Hocking *et al.* have demonstrated application of this theory to determination of the parameter $\chi^\circ = T/\sqrt{P}$, and shown that experimental measurements of this parameter using meteor decay times agree reasonably well with CIRA (Cospar International Reference Atmosphere) estimates of χ° .

However, despite the good progress in determination of D_a and thence χ° , as demonstrated by Hocking *et al.* [1997],

the methods discussed there do not produce an absolute measure of temperature. It is possible to convert χ° to a temperature if model pressures are used, like those specified by Fleming *et al.*, [1988] (hereafter *F88*), but these can at times have insufficient accuracy or reliability. We therefore seek a technique which allows absolute determination of temperatures, independent of knowledge of P . In addition, the assumed relation (2) is still a largely theoretical derivation, and needs stronger confirmation.

Two objectives are addressed. We demonstrate using data from a meteor radar installed at Resolute Bay in Northern Canada (75N, 95W) that D_a is indeed consistent with (2), and then we show that this knowledge allows us to develop a strategy for absolute determination of the temperature at the height of maximum meteor count rates (typically 86-90 km, depending on radar frequency, season and location).

2. Instrumentation

We utilize data from three separate meteor radars, operating at four separate sites distributed throughout North America in the years 1997-1999. The first was the CLOVAR instrument situated at London, Ontario, which has been described by Hocking *et al.*, [1997]. Its frequency of operation was 40.68 MHz. The second was a similar radar to the CLOVAR instrument, but it used 5 receivers, one for each receiving antenna (in contrast to CLOVAR, which multiplexed 5 antenna signals through one receiver). Called SKiYMET (allSKy interferometric METeor radar), this second radar operated at a frequency of 35.24 MHz and was installed at London, Ontario, from November 1997 to February 1998, then at Saskatoon (52° N, 117° W) from April to July 1998, and finally at Albuquerque, N.M. (35° N, 107° W) from September 1998 to the present. The third radar was a system similar to that described by Hocking and Thayer [1997], but sited at Resolute Bay. It differed from the other two radars primarily in receiver antenna layout and frequency. For reception it utilized only four receiving antennas, with signals being multiplexed through a single receiver. Although inferior to the improved 5-antenna interferometer used with the SKiYMET systems, it was still quite adequate for the studies described here-in. In the case of the newer 5-antenna interferometer, angular accuracies of $\pm 1-2^\circ$ in meteor angular location were possible, whilst the 4-antenna system has a resolution of typically $\pm 2-3^\circ$.

In all experiments, our objectives were the same: to locate as many meteors as possible, calculate their angular position in the sky, use their known range for determining their height, and then use correlation techniques to determine their decay times. Typically the Resolute Bay radar detected 150-600 meteors per day, the CLOVAR radar typically 600-1200 per day, and the SKiYMET radar typically 1000-2500 per day, depending on background noise level and general meteor activity. Using these data, scatter plots of height (z) vs $\log_{10}(1/\tau_{1/2})$ were prepared, as demonstrated in Fig. 1. These particular graphs were produced using data from the Resolute Bay radar, for typical winter and summer conditions. Similar graphs for the CLOVAR radar were also shown in Hocking *et al.*, [1997]. The subsequent analysis will now be described.

Copyright 1999 by the American Geophysical Union.

Paper number 1999GL003618.
0094-8276/99/1999GL003618\$05.00

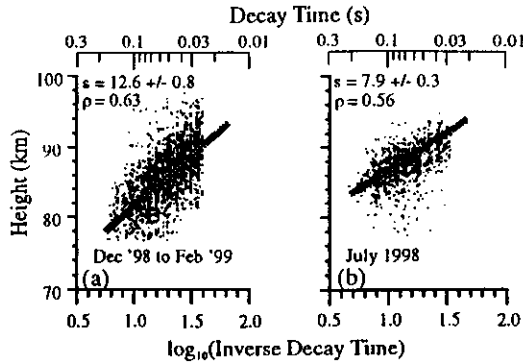


Figure 1. Scatter plots of meteor heights vs. logs of inverse decay times for Resolute Bay for (a) Winter 1998-9 and (b) July 1998. The slope of the best fit line is s , and the correlation coefficient is ρ .

3. Test of the dependence of D_a on Temperature and Pressure

Our first agenda here will be to perform a test of equation (2), and then use the results of that test to develop a new method for determination of absolute temperatures.

To begin, it is clear from figs. (1a) and (1b) that the slopes of the best fit straight line for these two scatter-plots are very different; indeed they differ by almost a factor of 2. The errors in the slopes are of the order of 4-6%. We will demonstrate that these different slopes relate to the mean temperature at the height of maximum meteor activity. At many sites, the differences in slope between winter and summer can be slight, but because high northern latitudes exhibit a large temperature range (from 210 K to 130 K) between seasons [e.g. see Lübken and von Zahn, 1991; hereafter LV91] the difference is very substantial. We utilize this feature to demonstrate that D_a is proportional T^2/P to within experimental error. To do this we presume that $D_a \propto \frac{T^2}{P}$. Then

$$\log_{10} D_a = \Omega \log_{10} T - \iota \log_{10} P + c_1, \quad (3)$$

where c_1 is a constant. If one moves downward over a height interval of about one scale height (about 7 km), P changes by typically a factor of 2.7, whereas even in extreme circumstances T will change by at most a few percent. Hence we recognize that P is a rapidly changing function of height relative to T , so we may write

$$\log_{10} D_a = -\iota \log_{10} P + c_2(z, T) \quad (4)$$

where c_2 is a relatively weakly varying function of height and temperature relative to the pressure term. For an isothermal atmosphere, $P = P_0 e^{-\frac{mg}{kT}z}$, where g is the acceleration due to gravity (9.49 ms^{-2} at 90 km altitude), m is the mass of a "typical" atmospheric molecule, k is Boltzmann's constant and T is the temperature. If we utilize this, and also recognize that D_a is proportional to $1/\tau_{1/2}$ (equation (1)), we may then write

$$z = \frac{1}{\iota} \frac{1}{\log_{10} e} \frac{kT}{mg} \log_{10} \left(\frac{1}{\tau_{1/2}} \right) + c'_3(T, z) \quad (5)$$

where c'_3 is a weakly varying function of T and z . We will write this as

$$z = S_m \log_{10} \left(\frac{1}{\tau_{1/2}} \right) + c'_3(T, z). \quad (6)$$

We therefore see that, to a reasonable approximation,

$$T \simeq \iota \frac{\log_{10} e \, mg}{k} S_m \simeq 14.3 \iota S_m \quad (7)$$

It should also be recognized that the best-fit lines in fig. 1 are simple fits to the raw data. However, Hocking et al., [1997] demonstrated that this is not the best estimate of the true mean profile of height vs. $\log_{10}(1/\tau_{1/2})$, due to natural biases which occur in the detection process. In section 3.3 of that paper, a procedure was outlined which applies a deconvolution bias adjustment. When this procedure is applied, it steepens the slope by typically 10% to 20%. We have applied a least-squares fit to the raw data, without bias adjustment, in fig. 1, solely for display purposes. However, in all future discussions we utilize a best-fit line which has this adjustment incorporated. It is this bias-adjusted slope which we consider to be S_m in equation (7).

Fig. 2 shows a scatter plot of T vs. S_m for 11 different months using the Resolute Bay data (10 months from 1998, and one from July 1997). We have used the values of temperature as determined by LV91 at 69°N for those months for which those authors had data, and the values from the model of F88 for those months in which LV91 did not make measurements. The months of March and November in 1998 were not used due to unavailability of meteor data. We have then fitted a further least-squares line to fig. 2.

The best-fit slope for the data shown in fig. 2 was 14.09 ± 1.7 , which corresponds, after comparison with (7), to a value for ι of 0.99 ± 0.12 . Thus this is consistent with the assumption that $\iota = 1$. We therefore consider that these data demonstrate experimentally that D_a is inversely proportional to pressure, as predicted by (2): we shall henceforth take $\iota = 1$.

Our next step is to determine the value of Ω . We return now to equation (3), but assume $\iota = 1$. Then we see that if $\log_{10}(T)$ is plotted as a function of $\log_{10}(D_a P)$, we expect a slope of $\frac{1}{\Omega}$. We can determine D_a experimentally by determining $\tau_{1/2}$ and thence D_a through equation (1), and we can use the same temperatures as those used in fig. 2. However, we need absolute measurements of the pressure P , which represents an area of uncertainty.

In order to ascertain a suitable pressure model, we have examined pressure data from other sources as a function of month. We have used two sources: firstly the empirical model of F88, and secondly the experimental data of LV91. Using 88 km altitude as an example, the Fleming model shows a summer maximum of about 0.35 to 0.4 Pascals, and a winter minimum of about 0.2 Pa. In contrast, LV91 shows a generally constant value of pressure throughout all seasons, with all values being confined between 0.2 and 0.25 Pa. These are therefore very different in behaviour, and we need to decide which is best to use for Resolute Bay. When

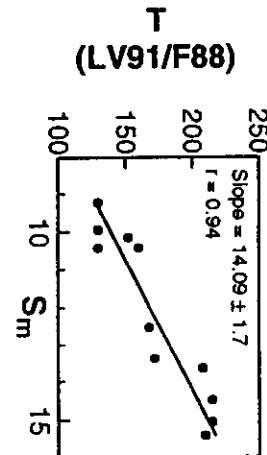


Figure 2. Bias-adjusted slopes of the best-fit lines to scatter-plots like those shown in fig. 1, relative to known 88 km temperatures, for 1998 at Resolute Bay.

we plot T vs $(D_a \cdot P)$, we get the two "scatter plots" shown in Fig. 3. Remarkably, the *F88* profiles trace out an ellipse as a function of season. This is very significant - it suggests that T and $(D_a \cdot P)$ show a generally sinusoidal variation as a function of season, but are out of phase by 90° . This is unreasonable, so we cannot use these pressures. In contrast, the data using *LV91*'s pressures (fig. 3b) show a straight line trend, with slope 0.56 ± 0.07 . The 95% confidence interval limits are 0.41 and 0.71. This corresponds to a value of Ω of 1.8 ± 0.2 , with 95% confidence of being in the range 1.4 to 2.4. We therefore surmise that (i) the *F88* (and CIRA) pressures at Resolute Bay are a poor representation of the true seasonal cycle, (ii) *LV91*'s values of pressure are reasonable, and (iii) Ω is consistent with a value of 2 within expected error. We therefore claim that our results support the original modeling results of Jones and Jones [1990], and we accept that $D_a \propto T^2/P$.

4. Absolute Temperatures

We now use these results to determine T . However, extra care is needed if we require good accuracy, so we no longer assume that the atmosphere is isothermal. Rather, we let $T = T_0(1 + \alpha z')$, where the quantity α relates to the mean temperature gradient. We should emphasize that ignoring this term altogether produces errors in the absolute temperature of less than 5-10%, but we can improve our estimates of T if we include it. We therefore now examine the expected temperature gradients as a function of season and latitude.

During much of the year, especially the non-summer months, the mesopause at mid to high latitudes is above the region of peak meteor activity, so that the temperature profile through that region is moderately linear, with a fairly well defined gradient, at least when averaged over periods of days. In summer, occasions exist when the mesopause dips below the meteor peak height, so that $\frac{dT}{dz}$ becomes positive. By studying these gradients using the model of *F88*, and also from experimental rocket and lidar studies [*LV91*, States and Gardner, 1999], we have found that the following expression gives a generally reasonable estimate of the gradient as a function of latitude and time at the height of peak meteor count rates;

$$\left[\frac{dT}{dz}\right]_{av} = -1.5 - [-2.5 \exp\{-(\theta - 45)^2/200\}] + 1.5 \exp\{-(\theta - 90)^2/1350\}] \times \exp\{-\#^2/3200\} \quad (8)$$

where θ is the latitude in degrees, and $\#$ is the temporal displacement in number of days from mid-June in the northern hemisphere (or displacement in days from mid-December in the southern hemisphere). This embodies a mean temperature gradient of about -1.5 K/km in winter (and the equinoctial months closest to winter) at all latitudes, a gradient of about -1.5 K/km in the equatorial regions in summer,

a tendency to zero or positive gradients at mid-latitudes in summer (low mesopause height), and a tendency to very steep negative gradients in the polar regions in summer.

Having developed an expression for the gradient, we now utilize it in the following way. Assuming for generality that $D_a = K_\Omega T^{\Omega}/P$, and defining a vertical coordinate z' which is zero at the height of peak meteor activity, and recognizing that generally $P = P_0 \exp\{-\int_0^{z'} \frac{mg}{kT} dz''\}$, we may write

$$\log_{10}(D_a) = \Omega \log_{10}[T_0(1 + \alpha z')] + \log_{10} e \frac{mg}{k} \int_0^{z'} \frac{1}{[T_0(1 + \alpha z'')] } dz'' + \text{constant}. \quad (9)$$

where $\alpha = \frac{1}{T_0} \frac{dT}{dz}$. If we now differentiate this equation with respect to height, and evaluate it at $z' = 0$, we have

$$\frac{1}{S_m} = \log_{10} e \Omega \alpha + \log_{10} e \frac{mg}{k} \frac{1}{T_0}. \quad (10)$$

S_m is the slope of the graph of z' versus $\log_{10} D_a$, or equivalently the slope of the graph of z' versus $\log_{10}(1/\tau_{1/2})$, after bias adjustment. Solution of (10) with $\Omega = 2$, and α determined from (8), allows determination of T_0 .

5. Results

We have determined S_m and thence T_0 from (10) for all of our radars, and compared our results to other experimental data measured at similar sites. For example, our measurements at London, Ontario, have been compared to spectrometer and lidar measurements of She and Lowe, [1998], as well as lidar measurements from Urbana [Senft et al., 1994]. Our measurements at Resolute Bay have been compared to those of *LV91* at Andoya (69 N). Our measurements at Saskatoon and Albuquerque have been compared to *F88*, after addition of about 5K to the *F88* data. This addition was included to compensate for a bias in *F88* and CIRA temperatures which seems to occur at mid-latitudes, as evidenced by She and Lowe, [1998], and Senft et al., [1994]. A graph of our monthly data vs. these other measurements is shown in fig. 4a. Clearly the data are closely aligned along the line of zero offset and unit slope. However, there is also a tendency for the meteor radar to underestimate the "true" value at low temperatures, and overestimate (very slightly) at higher ones. A best-fit line shows that

$$T_{true} = 0.774 T_{meteor} + 42.8. \quad (11)$$

The reason for this slightly skewed line is not clear. If α were not exactly unity, or Ω was not exactly 2.0, this could alter the fits. This is possible, since the errors on these exponents deduced earlier were of the order of 10 to 20%. We cannot fine-tune our procedures to any higher degree, so we recognize equation (11) as a "calibration curve". The fit has a correlation coefficient of 0.9 and a typical vertical scatter about the line of $\pm 7K$. At least some of this scatter is due to the fact that the reference temperatures are from different sites and different years, so the intrinsic error in our data must be considerably less than $\pm 7K$.

Therefore, as a final step, we apply equation (11) to our meteor temperatures to produce our final estimates of T . Given that the typical vertical spread of points about this best-fit line is $\pm 7K$ (only part of which is due to our technique), it is evident that it is possible to make measurements of monthly mean temperatures using this procedure with precision of the order of 4 to 8 K.

As justification for this statement, we present fig. 4b, which shows monthly mean temperatures measured at London, Ontario, as averaged over the period March 1997 to February 1999 inclusive. Superposed are temperatures for

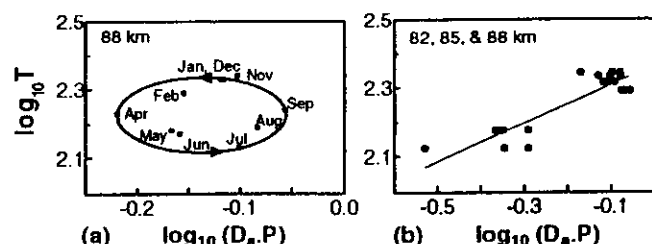


Figure 3. Log-log graphs of $(D_a \cdot P)$ vs. temperature for Resolute Bay, using two different estimates of pressure, for the heights indicated. In (a), the pressures of *F88* were used whereas in (b), the pressures presented in *LV91* were used.

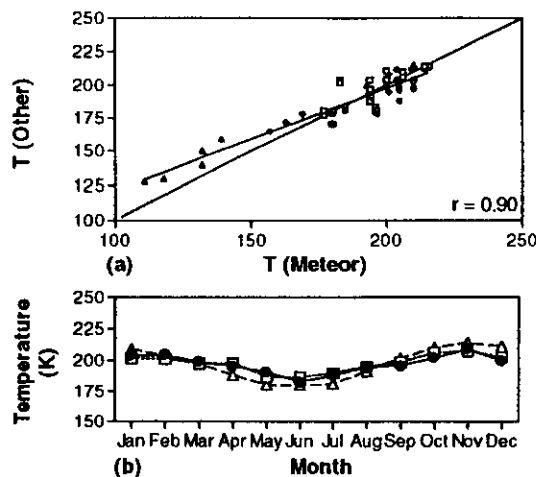


Figure 4. (a) Scatter plot of the "temperature" deduced from equation (10) (abscissa) compared to temperatures at similar sites from other techniques like spectrometers, lidar and empirical models (ordinate), for ~88 km altitude. The solid triangles refer to Resolute Bay (75N, 1998-9) compared to LV91 (69N), the diamonds to Saskatoon (April - July 1998) compared to F88, and the inverted triangles refer to Albuquerque, NM (Dec 1998 - Feb 1999) compared to F88 for 35N. The CLOVAR data (London, Ont: 43N) were compared to OH data from London for 1993 and lidar data from Fort Collins (41N) for 1993 [She and Lowe, 1998], and lidar data from Urbana (40N) for 1992-3 [Senft et al., 1994]. The open circles use CLOVAR data from 1997, and the open squares are for 1998. For some months comparisons were not possible for certain instruments, due to unavailability of data; the graph contains 75 points in total.

(b) Monthly mean temperatures at ~88 km over London, Ont. (43N), for 1997-8, after application of the calibration equation (11) (solid circles). For reference the lidar temperatures at 40N for 1992-3 [triangles: Senft et al., 1994] and 1996-7 [squares: States and Gardner, 1999] are also shown.

Urbana (40N) as a comparison. These data were produced during 1992-3 [Senft et al., 1994] and 1996-8 [States and Gardner, 1999]. She and Lowe, [1998] showed similar values. It should be emphasized that the data due to States and Gardner, [1999] were not used in the original calibration, so to some extent this comparison is independent of the earlier calibration. Absolute values are clearly very similar. Differences between lidar and meteor temperatures are no worse than differences between lidar measurements which used different sampling strategies in different years.

6. Discussion

Previous ground-based temperature determinations have often used optical methods (lidar, spectrometers), and these can have better precision than the accuracies cited above. However, they suffer because (i) they can generally only obtain useful data at night, during cloud-free and low moonlight conditions, and (ii) in the case of passive optical techniques like spectrometers, the actual height of the emissions can be unknown to within 5-10 km altitude. Daytime optical instruments are rare and expensive [e.g. States and Gardner, 1999]. In the case of the meteor technique, the mean height at which the temperature is determined is well known, and measurements are possible at all times, including daytime and during cloudy periods. Given that tidal variations can have amplitudes as high as 15K, and are often locked to local time, this can mean that the "daily average" temperatures determined by optical methods can have systematic errors

as high as 10 K [e.g. see States and Gardner, 1999]. Thus we consider that the methods outlined here-in can serve a useful role as atmospheric temperature monitors in the future. The 24-hour coverage available, and the relatively low cost of meteor systems, are distinct advantages.

7. Conclusion

It has been illustrated that it is possible to use underdense meteor decay times collectively to make reasonable estimates of the temperature at the height of maximum meteor detectability, which is in the range 86 to 92 km (depending on frequency) and is easily measured. The typical accuracy of these measurements is of the order of 4 to 10 K, depending on circumstances. The method is more accurate in the non-summer months, when the temperature gradient can be better and more reliably represented. A strong advantage of the method lies in its ability to make daytime measurements.

Acknowledgments. The support of the Natural Sciences and Engineering Research Council of Canada is recognized. Thanks also to Anna Hocking for support with diagrams and statistical analyses. I am grateful for discussions with Dr. J. Jones of UWO. Preliminary comparisons with some of the unpublished lidar data of R. Sica and S. Argall are also appreciated. The support of Alan Manson and Chris Meek during the Saskatoon installation is appreciated.

References

- Chilson P. B., P. Czechowsky, and G. Schmidt, A comparison of ambipolar diffusion coefficients in meteor trains using VHF radar and UV lidar, *Geophys. Res. Lett.*, **23**, 2745-2748, 1996.
- Fleming, E. L., S. Chandra, M. R. Schoeberl and J. J. Barnett, Monthly mean global climatology of temperature, wind, geopotential height and pressure from 0-120 km, *NASA Technical Memorandum 100697*, 85 pp, 1988.
- Hocking, W. K., and T. Thayaparan, Simultaneous and co-located observations of winds and tides by MF and meteor radars over London, Canada (43°N, 81°W) during 1994-1996, *Radio Sci.*, **32** 835-867, 1997.
- Hocking, W. K., T. Thayaparan and J. Jones, Meteor decay times and their use in determining a diagnostic mesospheric temperature-pressure parameter: methodology and one year of data, *Geophys. Res. Lett.*, **23**, 2977-2980, 1997.
- Jones, W., and J. Jones, Ionic diffusion in meteor trails, *J. Atmos. Terr. Phys.*, **52**, 185-191, 1990.
- Lübken, F.-J., and U. von Zahn, Thermal structure of the mesopause region at polar latitudes, *J. Geophys. Res.*, **96**, 20841-20857, 1991.
- Senft, D. C., G. C. Papen, C. S. Gardner, J. R. Yu, D. A. Krueger, and C. Y. She, Seasonal variations of the thermal structure of the mesopause region at Urbana IL (40°N, 88°W) and Ft. Collins, CO (41°N, 105°W), *Geophys. Res. Lett.*, **21**, 821-824, 1994.
- She, C.Y., and R.P. Lowe, Seasonal temperature variations in the mesopause region at mid-latitude: comparison of lidar and hydroxyl rotational temperatures using WINDII/UARS OH height profiles, *J. Atmos. Solar-Terr. Phys.*, **60**, 1573-1583, 1998.
- States, R.J., and C.S. Gardner, Thermal structure of the mesopause region (80-105 km) at 40° N latitude: 1. Seasonal variations, *J. Atmos. Sci.*, in press, 1999.

W. K. Hocking, Department of Physics, The University of Western Ontario, London, Ontario, Canada, N6A 3K7.

(Received June 18, 1999; accepted August 10, 1999.)

Real-time meteor entrance speed determinations made with interferometric meteor radars

W. K. Hocking

Department of Physics and Astronomy, University of Western Ontario, London, Ontario, Canada

Abstract. Previously developed methods for determination of meteor entrance speeds into the Earth's atmosphere are extended and unified and applied to a real-time radar system. A Fourier transform approach, using a rescaled time axis, is employed, permitting entrance speed determinations with accuracies of the order of 0.5 km s^{-1} . After the method is described, it is demonstrated by using it to determine the entrance speeds of several major streams, including the Zeta Perseids, the Arietids, the Beta Taurids, the June Bootids, meteors from within the Piscids complex, and the Geminids. Values are consistent with previous optical measurements, but in some cases the radar measurements have higher accuracy. The possibility of detection of space debris, or perhaps dust in Earth orbit, is also considered.

1. Introduction

Knowledge about the speeds of meteors as they enter the Earth's atmosphere has always been important for astronomical purposes, such as determination of meteor orbits [e.g. McKinley, 1961; Baggaley *et al.*, 1997]. However, many measurements of entrance speeds are based on optical studies, and these methods are difficult to employ and are applied only infrequently. Radar measurements have also existed, but the very earliest ones relied on photographic film for data recording and storage. Data were subsequently digitized, and computer algorithms have been developed to speed up data analysis, but until now many of these algorithms have been performed off-line, after collection of raw data to storage media. Exceptions include the work of Baggaley *et al.* [1997]. Furthermore, many studies of meteors used radars with pulse repetition frequencies of only a few hundred cycles per second, or even less, and this often limits the capability of radars to determine meteor entrance speeds.

In an important recent paper, Cervera *et al.* [1997] have shown how the weak signals just prior to the rapid onset of a meteor echo detected with a radar can be used to determine entrance speeds. This weak signal occurs because of Fresnel interference effects within the trail. This contrasts with earlier methods,

which used Fresnel oscillations just after the occurrence of the main peak [e.g. McKinley, 1961; Baggaley *et al.*, 1997]. The method of Cervera *et al.* [1997] will be called the "pre- t_0 " method in this paper, and the method that employs oscillations that occur after the peak will be called the "post- t_0 " method.

Fresnel oscillation methods are not the only radar procedures for measuring meteor entrance speeds; for example, another important method is a technique using meteor rise times, described by Baggaley *et al.* [1997]. Multiple station radar studies may also be used, which were also described by Baggaley *et al.* [1997]. However, the rise-time method is prone to larger errors than the Fresnel method, and the multiple stations are often technically complex to implement. In contrast, the pre- t_0 method produces higher accuracy but is capable of being used in a smaller percentage of cases. We choose in this paper to concentrate on the method associated with the Fresnel oscillations of the meteor echoes, especially the pre- t_0 method. We will demonstrate that this can be optimized numerically and can also be combined with the post- t_0 method to produce a unified result that employs the best features of each technique.

Previous applications of the pre- t_0 method have relied on visual procedures to "unwrap" the phase information in the signal prior to the meteor peak; the process was not automated. Our purpose here is to show how the method can be efficiently employed in a Fourier-analysis algorithm. We also demonstrate that this method may be applied to the Fresnel oscillations that occur both before and after the

Copyright 2000 by the American Geophysical Union.
Paper number 1999RS002283.
0048-6604/00/1999RS002283\$11.00

peak, therefore substantially improving our signal-to-noise ratio compared with use of either case alone. The methods described produce good accuracy and fast numerical computation. We also describe the radar used for these studies and demonstrate how it achieves pulse repetition frequencies of sufficient rate that these methods may be gainfully employed. The method is demonstrated by applying it to data from several meteor streams in both the Northern and Southern Hemispheres.

2. Equipment

The primary radar used in these studies is a special new interferometric radar specifically designed for meteor studies of a variety of types. Called the SKiYMET meteor radar, it is an all-sky interferometric meteor radar with a simple design, good portability, and sophisticated technological design, which has been developed jointly by Genesis Software Pty. Ltd., of Australia and Mardoc Inc., of Canada.

The system uses five two-element vertically directed Yagi antennas arranged at the center and the ends of an asymmetric cross on the ground. This arrangement is shown in Figure 1 [also see *Hocking et al.*, 1997]. Two of the arms are 2.5 wavelengths long, and two are 2.0 wavelengths long. This allows interferometry to be performed to determine the position of the meteor trail in the sky, without ambiguities in angle of arrival, but at the same time assures minimal coupling between the different antennas [*Jones et al.*, 1998]. Five separate receivers are used for data acquisition, one for each antenna, and cable lengths and receiver delays are carefully measured.

Data are recorded by a high speed digital recording system controlled by a Pentium personal computer operating under Free-BSD UNIX. The system is configured so that data processing occurs while the data are streamed into the system, permitting near-real-time data analysis. Indeed, all meteor parameters are generally determined within a few seconds of meteor detection and written to both binary and ASCII data files. Additionally, all the digitized data for a 4s interval surrounding the meteor are saved to a separate file for subsequent retrospective analysis (if required) at a later date.

The system is capable of unattended operation and, indeed, generally operates in this mode. However, because it uses the UNIX operating system, it

SKiYMET antenna ground plan

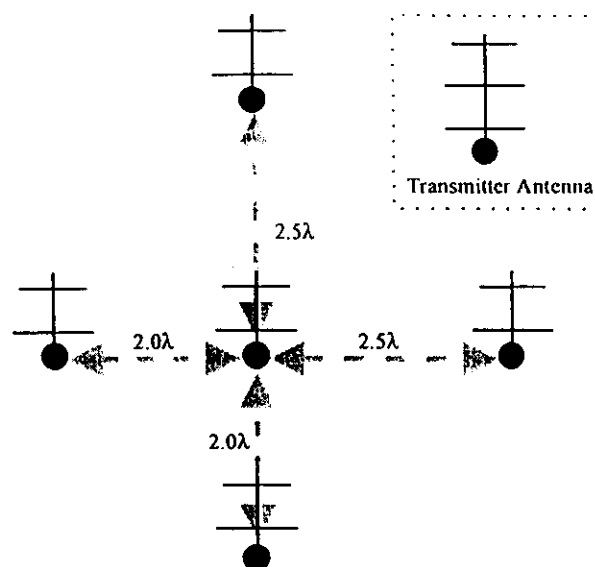


Figure 1. Plan view of the transmitter and receiving antennas used in the all-sky interferometric meteor (SKiYMET) system. The location of the transmitter is not critical, but the receiver antennas should be maintained in this arrangement. However, the receiver antenna plan may be rotated at an arbitrary angle with respect to north.

can be interfaced to a network or accessed through a dial-in modem. This allows the operator to monitor the system output and adjust system parameters remotely.

Data from two radars are used in this study. The first was operated at two Northern Hemisphere sites during different parts of 1998, and the second was operated in the Southern Hemisphere. The first was operated at London, Ontario, Canada (43°N, 81°W), in late 1997 and early 1998 and then then moved to Saskatoon, Canada (52°N, 107°W), for 3 months from April to July 1998. The second has been operated by Genesis Software Pty. Ltd., of Australia at a site near Adelaide, Australia (35°S, 138.5°E), from September 1998 until the present time.

Both radars transmitted pulsed radiation with a pulse length of 2 km, at a pulse repetition frequency of 2144 Hz. Peak power was 6 kW, and the carrier frequency was 35.24 MHz in all cases. The pulse

repetition frequency (PRF) of 2144 Hz produces an aliasing range of 70 km, but it is possible to determine the true range by combining the measurements of angular position and the knowledge that the radio meteors almost always produce trails in the region between 70 and 110 km altitude. Meteors exist at higher altitudes but cannot generally be seen by the radars at 35.24 MHz due to the rapid trail expansion that follows the meteoroid entry and plasma-trail creation. A four-point coherent integration was used in order to optimize the signal-to-noise ratio, giving an effective PRF of 512 Hz.

The system is also capable of more refined analyses, such as determination of meteor radiant and upper atmosphere wind speeds, using a point-and-click user interface. However, our major concern here is with its ability to determine meteor entrance speeds. We emphasize that like all monostatic meteor radars, the system only detects meteor trails orientated perpendicularly to the radial direction from the radar to the meteor, and this will be assumed throughout.

3. Meteor Entrance Velocity Determinations

The technique we use for our meteor velocity determinations follows and expands the principles espoused by *Cervera et al.* [1997]. This method makes use of the fact that if a meteor trail being formed in the atmosphere is illuminated by radio waves impinging from a direction perpendicular to the direction of alignment of the trail, then a Fresnel diffraction pattern is produced at the radar by the backscattered radio waves. This pattern sweeps past the radar as the front of the trail moves forward. The pattern actually moves at twice the speed of the head of the echo, due to the so-called "point source" effect, which arises because the transmitter is essentially a point source. Figure 2 shows a schematic of a trail forming in a region of the radar beam and the resultant diffraction pattern that forms near the radar. This pattern has a well-known shape, related to the so-called "Cornu spiral" [e.g., *Hecht and Zajac*, 1974],

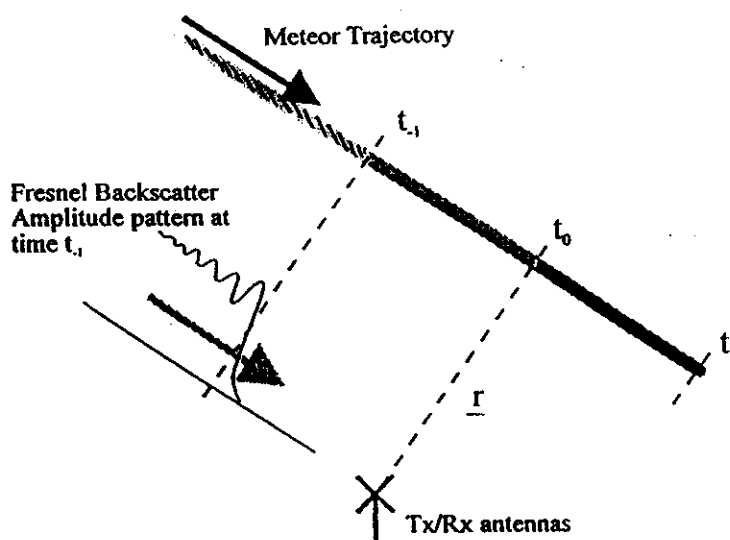


Figure 2. Schematic illustration of a meteor entering the Earth's atmosphere and forming a trail behind it. The dashed lines labeled t_{-1} , t_0 and t_1 indicate the position of the head of the trail at three time steps. The radial expansion of the trail with time is not shown. A visualization of the diffraction pattern produced by radio waves impinging from a direction perpendicular to the trail, and reflected back from whence they came, is shown as well. As the trail-head passes the broken line indicated by t_0 , this diffraction pattern moves past the antennas. As shown, the diffraction pattern oscillates in amplitude on the trailing side but appears to simply fall gently away from the t_0 position on the leading side. However, this pre- t_0 section does in fact contain phase variations (not shown), so the inphase and quadrature parts of the echo are oscillatory in nature. It is this oscillatory characteristic prior to the meteor peak that we employ in our studies.

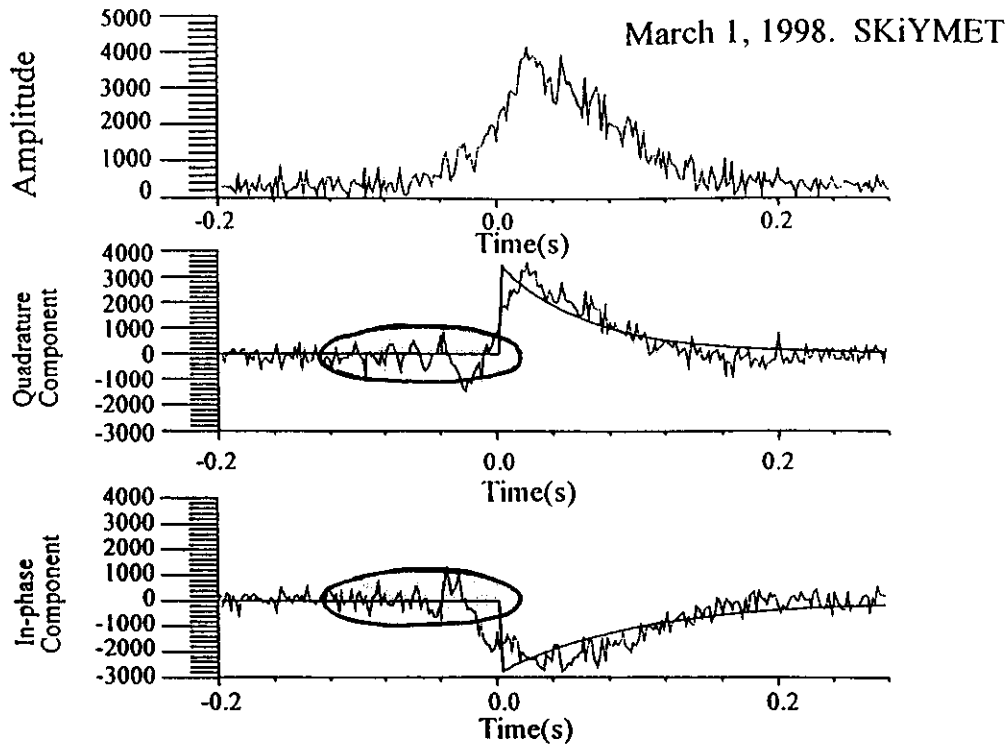


Figure 3. An example of a meteor signal recorded with a SKiYMET radar (light lines). Oscillations of the inphase and quadrature components of the amplitude are indicated by shaded ellipses, and these represent the pre- t_0 signal utilized in this paper. The bold lines show the results of fitting an exponential function with rapid turn-on to these data.

so that by measuring the complex amplitude as a function of time at a single receiver antenna, one can measure the speed of the patterns and hence that of the meteor itself. The Cornu spiral is also discussed by *Baggaley et al.* [1997]. It should be emphasized that this diffraction pattern first appears before the meteor signal peaks in amplitude and then persists after the peak. In the past, the amplitude oscillation occurring just after the peak has been used to measure the meteor speeds [e.g., *McKinley*, 1961], while more recently, *Cervera et al.* [1997] have used the oscillations in complex amplitude prior to the peak. An example of a meteor signal as it is detected by the SKiYMET radar is shown in Figure 3. The pre- t_0 component is indicated by the shaded areas. Figure 4 shows a numerical simulation of such a signal and demonstrates the oscillations in more detail. We will return to this model in due course.

To good order, the oscillation that results as the meteor enters the general region perpendicular to the radar line of sight is a sinusoidal function in t^2 , where t is the temporal displacement and where $t = 0$ oc-

curs at the precise point where the meteor trail-head passes perpendicular to the radar line of sight [e.g. see *Baggaley et al.* 1997]. The value of t can be both positive and negative, and we will employ this functional dependence in our analysis algorithms. This $\sin(\omega t^2)$ dependence is evident in both Figures 3 and 4, where the oscillations can be seen to occur at a lower frequency when closest (in a temporal sense) to the peak. The dependence is shown even more strongly in Figures 5a and 5b. Figure 5a shows a particularly clear example of the so-called pre- t_0 oscillations, together with the atmospheric oscillations that occur after the amplitude peak. Figure 5b shows the pre- t_0 complex amplitudes plotted as a function of the square of time, and it is quite clear that the oscillations are periodic in t^2 .

Our objective here is to use this information relating to the diffraction patterns in an optimal manner and implement it in real time on the radar controller previously described. We will use the diffraction characteristics both prior to and after the amplitude peak.

Before proceeding further, we make one more observation. Because the meteor trail drifts, the real and imaginary amplitudes (also called the inphase and quadrature amplitudes) after the meteor peak show sinusoidal oscillations that are linear in time, not in the square of time. This part of the signal is usually used to determine the radial component of the drift speed of the wind in the region in which the meteor trail occurs. An example of this oscillation has already been shown in Figure 5a. Any post- t_0 Fresnel oscillations would be superimposed on this oscillation. We therefore used a least squares filtering procedure to remove these oscillations caused by atmospheric drift (as well as any mean offset of the oscillations) before proceeding with the next stage of our analysis.

4. Model

Before developing our technique further, a numerical model of a typical meteor entry is introduced. This model was developed in order to simulate the effects of meteor entry into the atmosphere and is an important tool in the developments described herein. In the model the meteor trail was assumed to comprise a large number of scattering centers stretched out in a line, to simulate the meteor trail. The signal produced at the radar was deduced by adding the signal backscattered from each of these centers, including phase information, to produce a numerical sum. Inverse range-squared factors were included for both transmission to the trail and after scatter from it. The trail was allowed to drift with

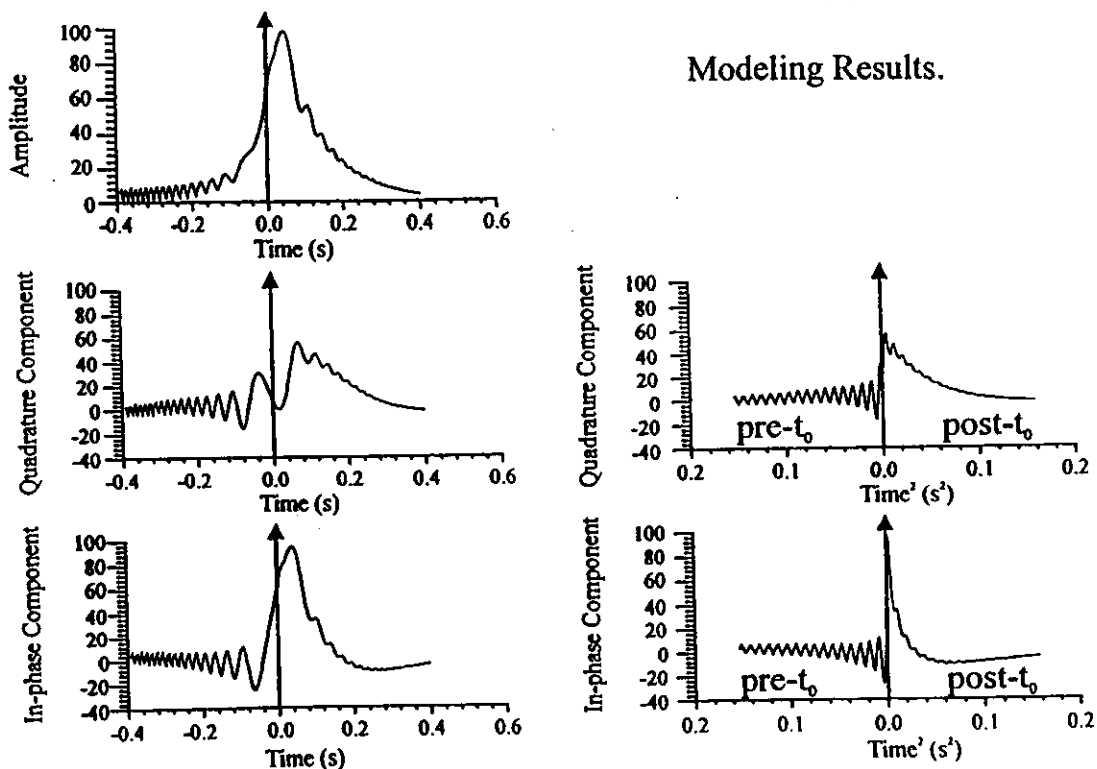


Figure 4. Three graphs showing the total amplitude, and inphase and quadrature components, of the signal received from a meteor as a function of time, as determined from a numerical simulation. In this case the meteor was assumed to be at a range of 80 km and had an assumed speed of about 8 km s⁻¹. The half-amplitude decay time was 0.1 s, and the radial drift speed was chosen to be small but non-zero. The radar frequency was assumed to be 40.68 MHz, corresponding to a wavelength of 7.375 m. The graphs on the right-hand side show the inphase and quadrature components when plotted as a function of t'^2 , where t is the time from the $t = 0$ point.

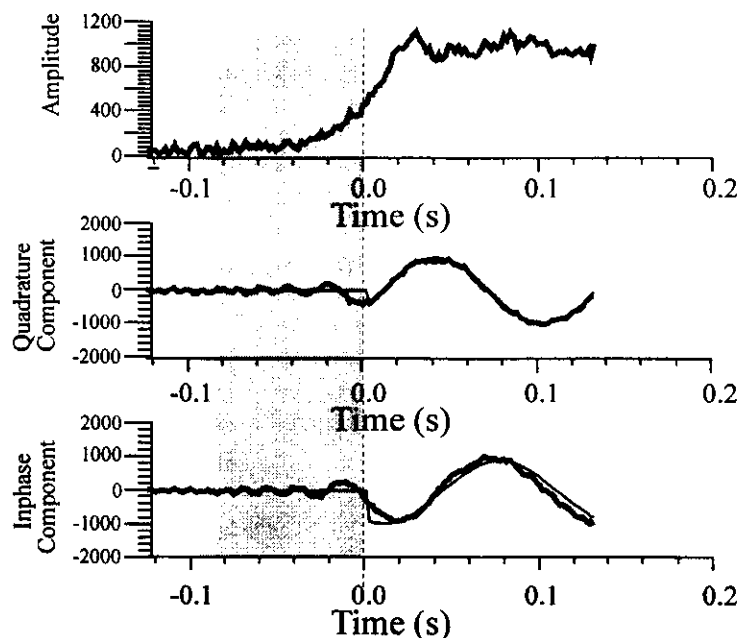


Figure 5a. Another example of a meteor signal demonstrating pre- t_0 oscillations, but concentrating on the region around $t=0$. The recorded signal is shown by the bold shaded line. The pre- t_0 signal can be seen in the shaded vertical band. In this case the meteor had a long lifetime, so the exponential decay in amplitude (top graph) after " $t = 0$ " is not apparent in this short section of the record. The sinusoidal oscillations after $t = 0$, due to the radial drift of the trail as it is carried by the wind, are apparent in the lower two graphs. The thin solid line shows the results of fitting a sinusoid with a (weak) exponential decay to the post- t_0 portion of the meteor.

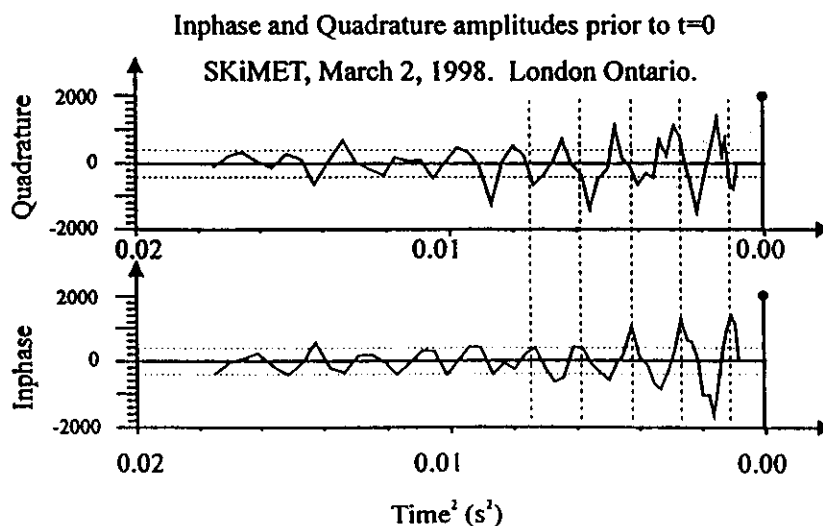


Figure 5b. Graph showing the pre- t_0 component of Figure 5a, but rescaled and plotted as a function of t^2 . The vertical dashed lines are placed at regular intervals on the time axis and clearly coincide with maxima in the inphase component, indicating that the oscillations are periodic in t^2 . These same vertical lines also co-incide quite closely with zero-crossings of the quadrature component, indicating that the inphase and quadrature components are out of phase by 90° .

the mean wind, and parameters like entrance speed, mean wind speed, and trail decay time could be entered as input.

Figure 4 shows a sample output from this program, where in this case it was assumed that the mean wind speed (and therefore the perpendicular drift of the trail) was very small. The meteor trail was assumed to be at a range of 80 km, and the radar frequency was taken to be 40.68 MHz. This radar frequency was used for these initial simulations because it matched the frequency of the "Canadian (London Ontario) VHF atmospheric radar" (CLOVAR), which was the instrument used for the initial studies relating to this work [Hocking, 1997; Hocking and Thayaparan, 1997]. The two right-hand graphs show the same complex amplitude plotted as a function of t^2 ; the regular oscillations in t^2 are now very apparent.

Our next step was to Fourier analyze such model data, where the independent parameter was chosen to be t^2 , not t . We define the point where the amplitude reaches about one half of its peak value as " $t = 0$ " and rescale our axis proportionally to $\xi = t^2$. Thus the complex amplitude now obeys the relation

$$a = a_R \cos(\omega \xi + \phi) + i a_I \sin(\omega \xi + \phi), \quad (1)$$

where $i = \sqrt{-1}$. Hence the system is linear in ξ and can be subject to standard Fourier analysis.

The time series of data around the meteor peak were then divided into two halves: that prior to " $t=0$ " and that after. A small interval of data around $t = 0$ was removed altogether, in order to avoid problems with the very rapid rise in amplitude in this interval. For the data prior to $t = 0$, Fourier analysis was simple. For the data after this point, it was first necessary to remove the exponential decay and any oscillation associated with radial drift. This latter step was done in the time domain before storing the data as a function of t^2 . The residual was then stored as a function of t^2 and Fourier analyzed. In each case, the Fourier transformation produced a very narrow spike at one select frequency. However, the two halves of data produced spikes at frequencies that were opposite in sign, as would be expected from knowledge of the behavior of the resultant Cornu spiral. In order to optimize the signal-to-noise ratio, the sign of the spectra from one of the data halves was reversed, and then this spectrum was added to the other. This gave a very clean and narrow spectral spike.

It should be noted that the "frequency" in this case actually has units of t^{-2} , not t^{-1} . Therefore it is not clear how to relate these units to the entrance speed of the meteor. In order to be able to know the meaning of any peak, we therefore used our model and performed many simulations with different meteor entrance speeds and plotted the resultant frequency in t^2 as a function of the meteor entrance speed squared. The result is shown in Figure 6, after normalization to a range of 80 km.

The frequency in t^2 , which we will denote as f , can be used to determine the entrance speed for a meteor at 80 km range, as observed with a 40.68-MHz radar, through the relation

$$v_{80} = \sqrt{(f + 15.8)/1.674}. \quad (2)$$

Upon further, more careful investigation, it was found that the above expression could be marginally improved if 0.35 were subtracted from v_{80} whenever the first estimate exceeds 15 km s^{-1} . A value of 0.45 should be subtracted if the first estimate lay between 10 and 15 km s^{-1} , and 0.6 should be subtracted if the value was below 10 km s^{-1} . The method was found to give unreliable estimates if the entrance speed was less than 5 km s^{-1} but was quite reliable at 6 km s^{-1} and above. The failure at very low speeds relates to the fact that the rise time becomes fairly large, and the pre- t_0 oscillations can become comparable in period to oscillations associated with radial drift, leading to confusion for the software.

In order to determine the speed at any other range, it is simply necessary to modify the speed determined from Figure 6 by the relation

$$v_{\text{entrance}} = \sqrt{(r\lambda)/(80 \times 7.375)} \times v_{80}, \quad (3)$$

where the conversion arises because the Fresnel zone sizes change as a function of range r and wavelength λ . The range r is assumed to be in kilometers, and the factor 7.375 refers to the wavelength of a 40.68-MHz radar (which was used in the simulations). This relation is therefore quite valid for all meteor radars, since it takes into account both the meteor range and the radar wavelength.

Thus we have demonstrated the main features of the Fresnel diffraction pattern using our model and have also developed a protocol we will employ shortly for analyzing real-time data. Figure 6, and the equations above, form important parts of our technique.

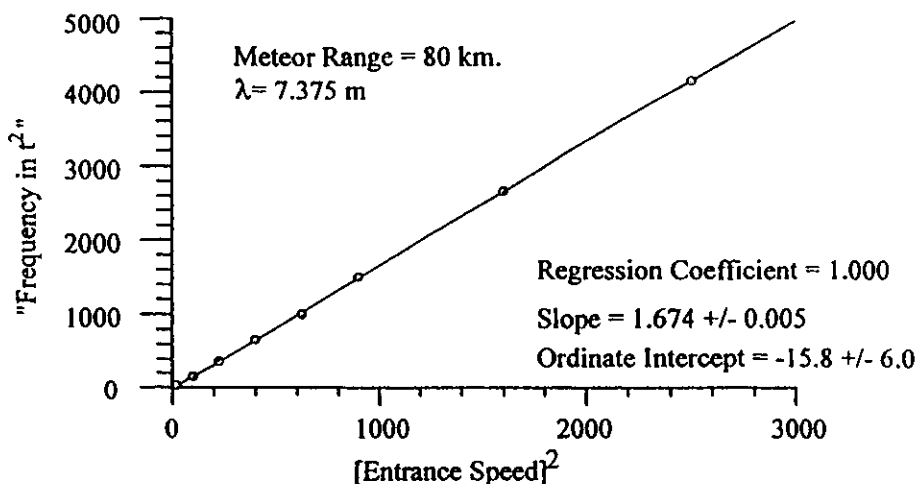


Figure 6. Modeling results showing the "frequency" of the pre- t_0 signal after it has been rescaled as a function of t^2 , versus the actual entrance speed of the meteors used in the simulation.

5. The Analysis Algorithms

We now turn to analysis of real data. Meteor signals like that shown in Figure 3 were analyzed in a way similar to that described above for the model. First, the $t=0$ position was found by determining a point corresponding to a time at which the amplitude reached about half its maximum value. This point occurs during the rapid ascent in amplitude of the received signal. Accurate location of this point is important for further analysis. In practice, we found the point where a three-point running mean passed one half the value of the three-point mean at the amplitude peak.

Our next step was to remove any sinusoidal oscillations in time, and any exponential decay, from the post- t_0 complex signal. Then the pre- t_0 and post- t_0 oscillations were stored as a function of t^2 and Fourier analyzed. We should emphasize that it was not always possible to analyze the post- t_0 data, especially if the radial drift speed was high, or the fitting procedures gave large errors. In such cases, entrance speed determinations were made using only the pre- t_0 data.

The Fourier analysis was again performed on data for which the independent variable was t^2 . Separate spectra were formed using data from each of the five receivers, and then these spectra were averaged, in order to improve the signal-to-noise ratio and therefore optimize determinations of the entrance speeds.

It should be emphasized that the Fourier transformations were not fast Fourier transforms (FFTs). FFTs were not possible because the points were not at equal steps of the parameters $\xi = t^2$. Because of this consideration, care had to be taken in choosing the frequency step size in our Fourier transforms. We in fact opted for a multiwindowed procedure. To begin, we chose a window of points within ± 0.2 s of the $t = 0$ points. We then chose a frequency step designed to search for relatively short period oscillations in ξ . If no significant peaks were found, the window size was increased and the Fourier process was repeated, this time at higher-frequency resolution and going to lower frequencies. This process was repeated four times, each time increasing the window widths and searching at lower frequencies and at finer frequency steps. The rationale behind this was twofold. First, if the oscillations were of high frequency, then they were only significantly above the noise level close to the $t = 0$ position. Therefore by choosing a short data window, we remove the outer sections that are largely noise and therefore improve our signal-to-noise ratio. If no peak is now found, we increase the window size, thereby allowing a search to lower frequencies. We assume that if the frequency is less, the pre- t_0 oscillations will be evident farther from the $t=0$ position and therefore will require a larger time window to enable the full behavior of the pre- t_0 signal to be captured. In each case, a search was performed for a single dominant peak. If no peak

was found, we moved to the next window size. In all, up to four windows were used; if no dominant peak was found after this, it was concluded that determination of a meteor entrance speed was not possible, and the analysis was aborted.

A typical sequence of spectra is shown in Figure 7. In this case only two trials are shown. The first trial (top panel) uses the narrowest window (0.2 s) and examines the highest "frequencies". For this trial the frequency range covered the values between 1500 and 5000, in steps of 28 Hz^2 . (In all cases the unit used in the time-squared domain was s^2 , so the unit of "frequency in t^2 " was Hz^2 .) Although some minor peaks are apparent in attempt 1, none are really dominant. The program therefore progressed to the next attempt and produced the bottom panel in Figure 7. In this case a data window of 0.2 s in length was again used, and frequencies were stepped from 300 to 2000 in steps of 16 Hz^2 . Clearly, there is one strong, dominant peak, and the program concludes that this is the true one. It does not go on to

investigate the next window, in order to save computer time. If further searches had been required, a window length of 0.35 s would have been used, and frequencies would have been stepped from 15 to 500. If there had been no success then, the frequencies would have been stepped from 0 to 15, with even finer resolution.

Our final step is to convert these frequencies in t^2 into velocities. To do this, we used the results of our model simulation as shown in Figure 6, together with (2) and (3). Thus we were finally able to convert our spectral peaks to entrance speeds.

Figure 8 shows a typical distribution of meteor entrance speeds from the radar that ran in London, Ontario, in 1997 and 1998. Unfortunately, the efficiency of measurement is not high if there is substantial radio interference, so in spite of collecting some 20,000 meteors in the period covered by the figure, only about 860 (4.5%) useful entrance speeds were determined. In low noise sites, higher efficiencies are possible, reaching as high as 10%. *Baggaley*

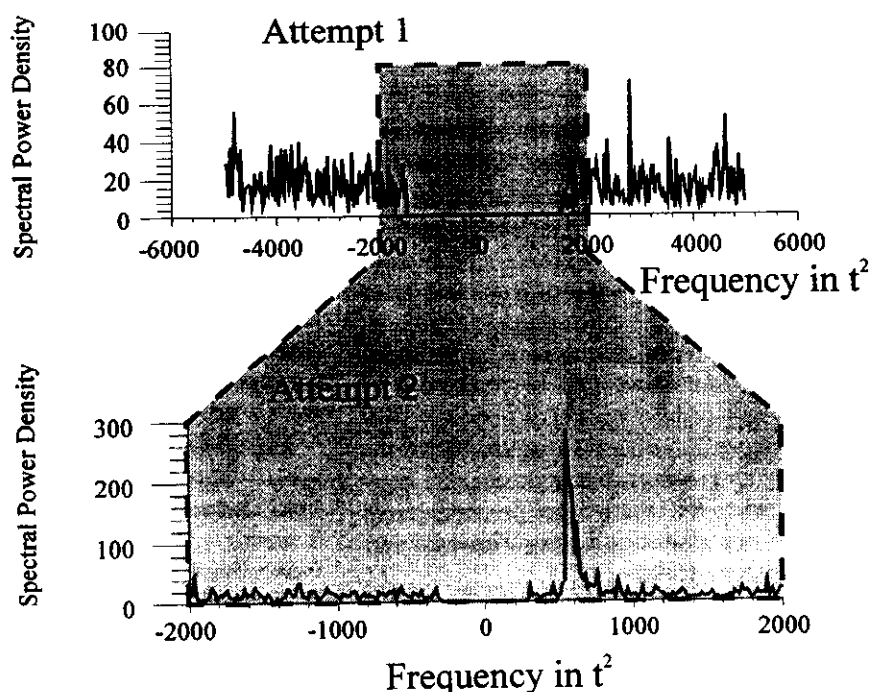


Figure 7. Demonstration of the stages of spectral analysis. The upper graph shows the spectrum produced when a window of width 0.2 s is used, and the frequencies are stepped from -5000 to -1500, and 1500 to 5000, in steps of about 28. No dominant peak occurs, so the process is repeated using a frequency range of 300-2000, with steps of about 16. At this stage, a strong peak is found (shown).

Meteor Entrance Velocities, 19 February 1998 to 02 March 1998.

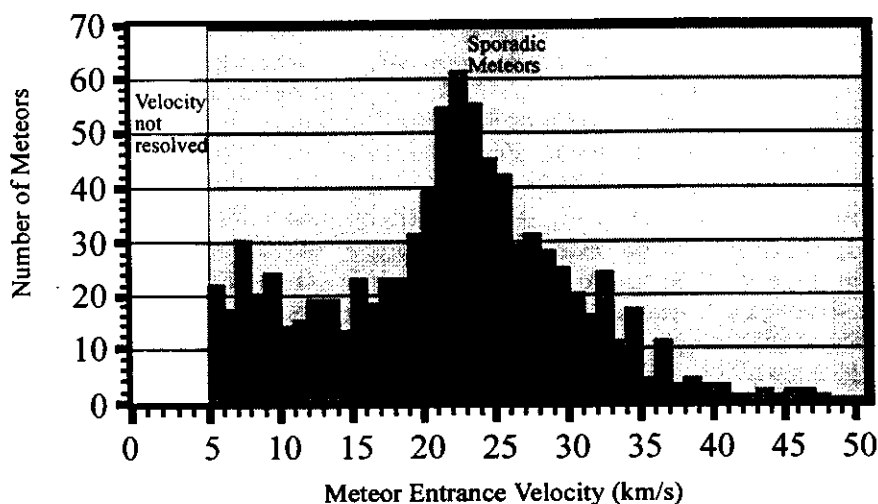


Figure 8. Distribution of 860 meteor entrance speeds recorded near London, Ontario, during a 2-week period in 1998, using a SKiYMET radar.

et al. [1997] have suggested that the maximum expected rate of echoes that display Fresnel oscillations would be about 20%, with all other echoes being contaminated by effects like trail distortion and meteor fragmentation. It should also be emphasized that we have deliberately set our acceptance tests to be very rigorous, so that we have a very low probability of false measurements. This is because we are more interested in accuracy than in large numbers of doubtful measurements. Nevertheless, this rate of detection is still orders of magnitude greater than that which can be achieved by photographic means, where even a single measurement is very difficult. Note also that our maximum speeds are around 40 km s^{-1} ; larger speeds can be measured if we use two-point coherent integration of our data, instead of the usual four-point. Our detectability decreases, however, so this is a trade-off which must be considered. We will now turn our attention to experimental verification of our measurements.

6. Experimental Verification

We now turn our attention to considering whether our measurements really make sense. To do this, we employ several strategies. We examine both sporadic meteors and meteor streams and compare our data with optical measurements.

6.1 Sporadics

Over the course of several months, "sporadic" meteors are cumulatively the most common of all meteors. Therefore we will begin our verification by examining the characteristics of all the meteors recorded over a non shower period and comparing our measurements to other, earlier observations.

To begin, Figure 9a shows the height distribution of meteor entrance speeds measured with dual-camera optical techniques by *Sarma and Jones* [1985]. These data were recorded over a period of several years and required careful dual-station photography and extensive analysis. In all, 454 meteors were studied in their program.

Figure 9b shows the height distribution of meteor speeds determined by a SKiYMET radar at London, Ontario (43°N , 81°W), during a period of only 2 weeks. Figure 9b contains 860 meteors, almost twice the number of optical observations presented by *Sarma and Jones* [1985]. Superimposed on Figure 9b, as well as on Figure 9a, is the mean profile of meteor speeds versus height determined during a major survey with the Jodrell Bank radar [see *McKinley*, 1961]. The Jodrell Bank survey was accomplished using post- t_0 measurements, generally by person-intensive analysis of photographic traces.

It is clear that the optical data, the Jodrell Bank survey, and our own data are in good agreement be-

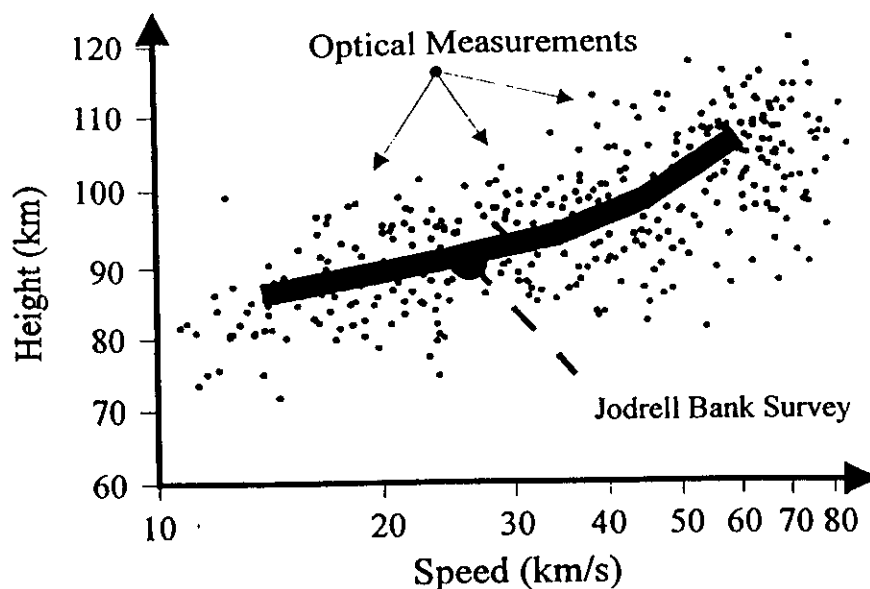


Figure 9a. Adaptation of a graph from *Sarma and Jones* [1985], showing the distribution of entrance speeds into the atmosphere measured with dual-station optical observations (dots). Superimposed on the graph is the mean profile deduced during a radar-meteor survey performed with the Jodrell Bank radar [from *McKinley*, 1961].

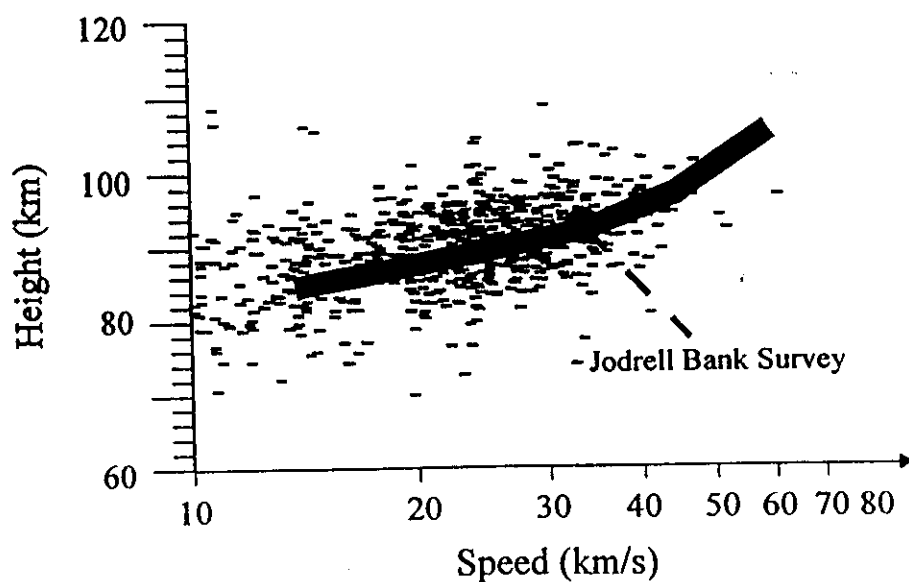


Figure 9b. Distribution of entrance speeds into the atmosphere measured with the SKIYMET radar and using the techniques discussed in this paper (shaded rectangles). Superimposed on the graph is the same Jodrell Bank mean profile as that shown in Figure 9a.

low 100 km altitude. Our data in Figure 9b have an upper level cutoff at about 100 km altitude, where the meteor entrance speeds exceed $\sim 45 \text{ km s}^{-1}$. This limit arises because of our choice of a four-point coherent integration in our data-collection strategy, as was discussed earlier. However, the striking fact about the graphs is that the points in Figure 9b were determined in near-real-time (less than 1s per calculation), and over 860 measurements were obtained in a period of only 2 weeks. This contrasts with 454 points in about 3 years for the data shown in Figure 9a. The new algorithms have therefore vastly improved the rate at which meteor entrance speed determinations can be made.

The comparisons in Figure 9 show that the entrance speeds determined in this study have the correct general characteristics. However, it is also desirable to determine the accuracy of the method in more detail. For this, we turn to studies of meteor showers.

6.2 Shower Studies

Figure 10 shows a typical meteor entrance speed distribution during the occurrence of a meteor shower. The data were recorded with a SKiYMET radar at Adelaide, Australia, during the period of December 11-13, 1998. This particular radar was owned and operated by Genesis Software Pty., Ltd. While the broad distribution is similar in shape to Figure 8, there are also two "spikes" in the histogram

at speeds of 14 and 35 km s^{-1} . These spikes are due to showers. We will show that the increased occurrence at 35 km s^{-1} is due to the Geminid meteor stream. The increase in occurrence at 14 km s^{-1} is also due to a simultaneous meteor shower with a radiant that appears to be at a right ascension of 15 hours and 10 min ($\pm 20 \text{ min}$) and a declination of 60° south ($\pm 3^\circ$). This source determination is only approximate and needs further confirmation. We therefore do not consider this stream further, and because we cannot be fully sure of its radiant, we do not include it in Table 1. In the next section we will concentrate on the Geminids, since they are a well-studied source and their entrance speeds are well known from optical studies. They therefore represent an excellent reference for us to check the quality of our method.

Before doing this comparison, however, we need to first provide confirmation that these meteors were indeed due to the Geminids stream. In order to do this, we need to recognize that meteors are only detected by the radar when their trails are aligned perpendicular to the vector r , where r is aligned in the direction from the radar to the trail. The meteor will have entered from some radiant direction, which we cannot determine. However, we do know that the radiant must have originated somewhere on a great circle in the sky defined by the set of all the directions perpendicular to the vector r . While we cannot know where on this great circle the radiant lay, we can draw a map of this "great circle of possible radi-

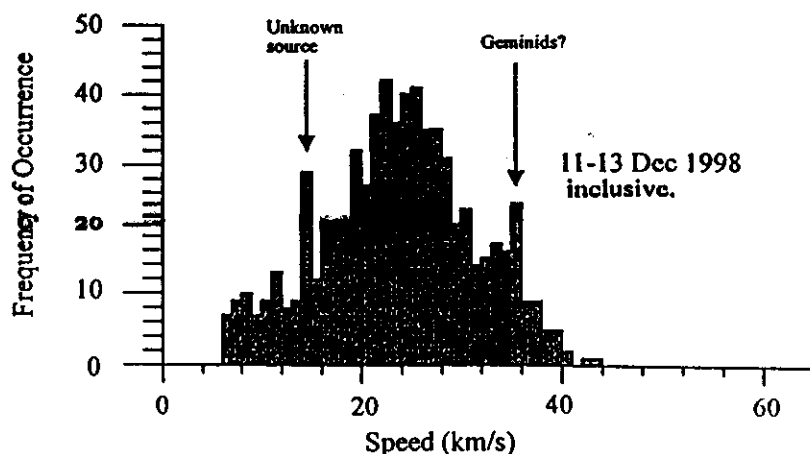


Figure 10. Histogram of frequencies of occurrence of different entrance speeds observed with a SKiYMET radar during the period December 11-13, 1998, at Adelaide, Australia. Velocities associated with two possible meteor streams are indicated.

Table 1. Presentation of Meteor Entrance Speeds Measured With SKiYMET Radars, Compared With Known Optical Measurements (Where Available)

Showers	Date	Right Ascension; Declination	Optical Speed, km s^{-1}	Radar Speed, km s^{-1}	Number of Meteors
ζ Perseids	June 5-11, 1998	4 hours 10 min; 24°	29	28.8 ± 0.4	23
Arietids	June 5-11, 1998	3 hours 0 min; 23°	39	40.95 ± 0.4	12
β Taurids	June 26-29, 1998	5 hours 50 min; 20°	31	30.5 ± 0.2	28
June Bootids	June 27, 1998	15 hours 10 min; 61°	—	17.65 ± 0.15	18
Northern Piscids	Oct. 1-3, 1998	1 hour 50 min; 8°	—	22.1 ± 0.3	13
Southern Piscids	Oct. 1-3, 1998	23 hours 20 min; -3°	—	14.1 ± 0.3	10
Unnamed Source	Oct. 1-2, 1998	21 hours 0 min; -40°	—	16.85 ± 0.2	22
Geminids	Dec. 11-13, 1998	7 hours 32 min; 32°	35	35.3 ± 0.2	33

The radiant of the showers are taken from various references [e.g. *McKinley*, 1961, table 6.1; *Norton*, 1973], but were also confirmed by our radar measurements of shower sources. The errors in the entrance speeds quoted above are standard deviations for the mean. The number of meteors refers to the number of radio meteors used in our determinations.

ants" on a galactic grid. For each meteor detected, such a great circle was plotted. We were then able to reject non-Geminid meteors in the following way. If the aforementioned great circle did not pass close to the known Geminids radiant at right ascension (RA) = 07 hours 28 min, declination = 32° , then it could be rejected as definitely non-Geminid. If, on the other hand, the great circle passed close to the known Geminid source, then it may have been

a Geminid. Of course, it may not have been, too, and non-Geminids which have radiant on great circles that pass close to the Geminid radiant cannot be removed by this process. However, this filter will at least remove a large number of meteors that are clearly not Geminids. A more detailed discussion of this process has been given by *Hocking et al.* [2000], where the above strategy is extended to allow actual source radiant determinations.

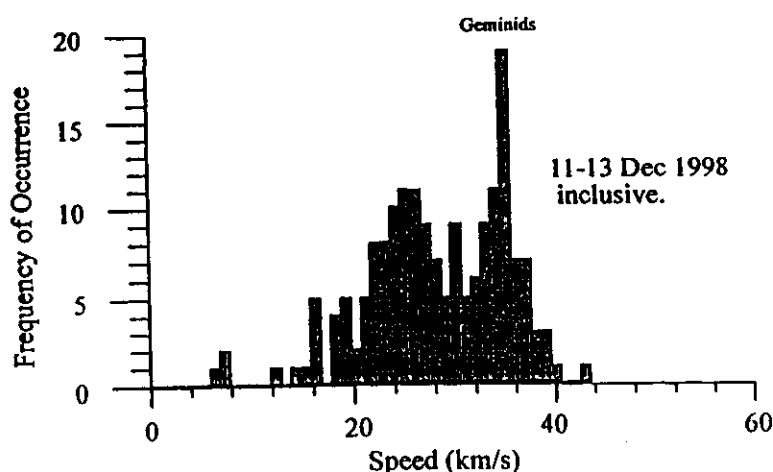


Figure 11. Same histogram as that shown in Figure 10, but filtered to remove any meteors that could not have had radiant within about $\pm 2.5^\circ$ declination and ± 30 min right ascension of the Geminids source.

Figure 11 shows the speed distribution of meteors that had great circles that passed through the region with declination between 30°N and 35°N and right ascension between 7 hours 0 min and 8 hours 0 min. Clearly, the peak at $\sim 35 \text{ km s}^{-1}$ has persisted, but the rest of the histogram has seriously diminished in value by about 80%. The spike at 35 km s^{-1} in fact remains at about 10-12 points above its base level (where "base level" refers to the point where the spike meets the general level of the histogram). This figure therefore acts as very strong confirmation that the spike is indeed due to the Geminids.

Our next step was to find the mean value associated with this spike. We found the average of all speeds in the range $34 - 37 \text{ km s}^{-1}$, which delineates the spike region. The mean value so determined was $35.30 \pm 0.21 \text{ km s}^{-1}$. This compares to a known speed for the Geminids of 35 km s^{-1} [McKinley, 1961, Table 6.1]. Agreement is therefore very good, although we have not taken account of the deceleration of the meteors due to the Earth's atmosphere. We consider the latter conversion to be outside of the scope of our current study.

We have repeated this procedure for many known shower sources (again without atmospheric deceleration calculations incorporated). Table 1 shows our meteor entrance speed determinations for eight such sources, compared with known optical speeds (where available). Agreement is generally good, and indeed in some cases the radar provides better accuracy than the optical measurements. The errors quoted are standard deviations for the mean.

One shower of particular interest is the June Bootids. This source has been analyzed in some detail by Arlt *et al.* [1999]. By measuring entrance speeds and simultaneously determining the source radiant (also achieved by the SKiYMET radar), it was possible to determine the orbit parameters of this meteoroid stream and hence associate it with the comet Pons-Winecke. This was the first time this correlation was confirmed, coinciding with a similar determination by optical methods (also discussed by Arlt *et al.*).

We have obtained meteor entrance speeds with two meteor radars operating side by side at different frequencies (P. Brown and J. Jones, private communication, 1999). These were both SKiYMET radars, supplied commercially and operated at frequencies of 29.85 and 38.0 MHz. Meteor entrance speeds were accumulated with these radars on occasions when

a meteor was detected simultaneously on both systems. It was found that of 45 coincident meteors detected, 43% had speed differences of less than 0.4 km s^{-1} , and 70% had speed differences of less than 0.8 km s^{-1} . The distribution of speed differences was non-Gaussian, with highest probabilities near 0 km s^{-1} , and with a broadly exponential falloff. The standard deviation of differences was 1.1 km s^{-1} . Assuming that the errors in each measurement were equal for the two radars, then the standard deviation for the errors in a single measurement are $1.1/\sqrt{2}$, or about 0.75 km s^{-1} . Values are likely to be more accurate than 0.3 km s^{-1} on 43% of occasions and better than 0.55 km s^{-1} on 70% of occasions. Notice that these errors are mainly random errors, rather than systematic errors, so the accuracy of our measurements of stream speeds can be substantially improved by using averaging over many meteors. This explains why the errors in Table 1 are significantly less than the values quoted here.

Figure 12 shows a time evolution of meteor entrance speed histograms from both Adelaide and Saskatoon, showing an interesting perspective of the meteor entrance speeds over extended time intervals. One point of significant interest in these graphs is a band of speeds in the region $7 - 10 \text{ km s}^{-1}$. This band has been highlighted by a vertical shaded bar extending from the bottom of both columns in the figure. Observations of meteors with such low speeds is not new (e.g., Sarma and Jones [1985]) measured speeds down to 11 km s^{-1} , and the radar can see meteors with weaker intensity than optical measurements), but the local maximum in their frequency of occurrence in this speed range has not been reported before. It is clear that on occasions the number density of meteors in this region rises above the normal background level, and it seems that the entrance speeds in this band have a "time evolution." For example, at Adelaide the effect is strongest in December and January, while at Saskatoon the effect is most noticeable in the months from May to July. This speed range corresponds to the speeds that debris orbiting the Earth would have, and therefore these "meteor trails" could possibly be produced by Earth-orbiting dust, or even space debris from former Earth-orbiting satellites, entering the Earth's atmosphere. We consider that this band of entrance speeds to be of particular interest. We admit that the nature of these entities is still indeterminate, and further investigations into their cause are still needed, but we consider

443

METEOR ENTRANCE SPEED STUDIES : month by month details.

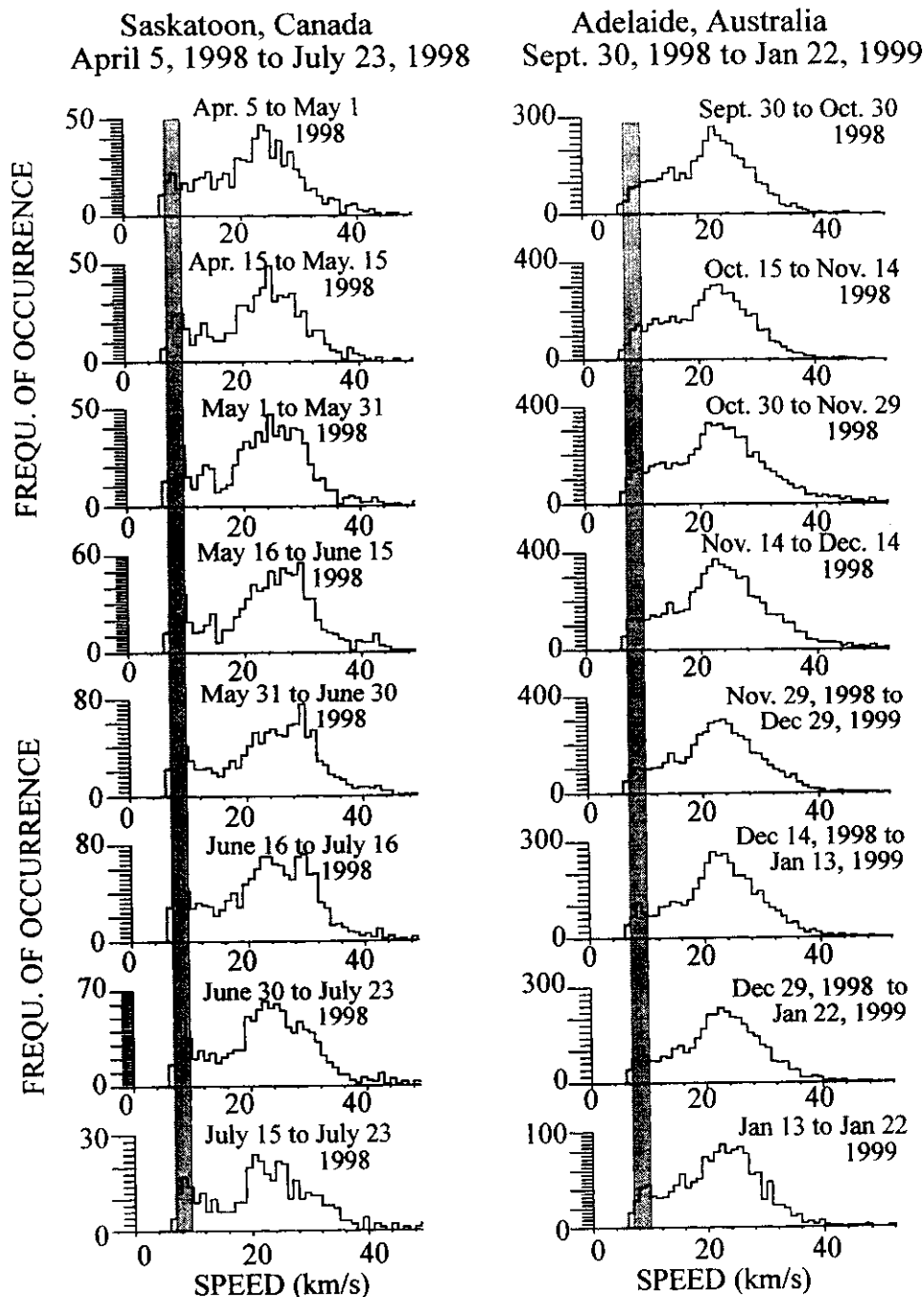


Figure 12. Monthly histograms of the distributions of meteor entrance speeds into the atmosphere, stepped at intervals of half-months. The speed-band between 7 and 10 km s⁻¹ is highlighted.

the very existence of this peak to be a noteworthy phenomenon. We intend to dedicate further study to these particular trails in the future.

7. Conclusions

An automated procedure for determination of meteor entrance speeds with an interferometric meteor radar has been presented. The procedure permits real-time calculation of entrance speeds and has been applied on a new-generation SKiYMET radar. Results have been presented for a variety of meteor streams and have shown good agreement with previous optical measurements. Because of the simplicity of its operation, this instrument, coupled with the technique outlined, should permit many studies of previously poorly known meteor streams. The possibility of space debris, or some form of Earth-orbiting dust, being detected has also been outlined.

Acknowledgments. The author acknowledges the support given to this project by MARDOC Inc., and for the data supplied by Genesis Software Pty., Ltd. He is also grateful for the support and assistance of Chris Meek and Alan Manson during the installation of the SKiYMET radar at Saskatoon. Discussions with Peter Brown and Jim Jones are appreciated. This work has also been supported in part by the Natural Sciences and Engineering Research Council of Canada.

References

- Arlt, R., J. Rendtel, P. Brown, V. Velkov, W.K. Hocking, and J. Jones, The 1998 outburst and history of the June Bootid meteor shower, *Mon. Not. R. Astron. Soc.*, **308**(3), 887 - 896, 1999.
- Baggaley, W.J., R.G.T. Bennet, and A.D. Taylor, Radar meteor atmospheric speeds determined from echo profile measurements, *Planet. Space Sci.*, **45**, 577-583, 1997.
- Cervera, M.A., W.G. Elford and D.I. Steel, A new method for the measurement of meteor speeds: The pre- t_0 phase technique, *Radio Sci.*, **32**, 805-816, 1997.
- Hecht, E., and A. Zajac, *Optics*, Addison-Wesley-Longman, Reading, Mass., 1974.
- Hocking, W.K., System design, signal processing procedures and preliminary results for the Canadian (London, Ontario) VHF atmospheric radar, *Radio Sci.*, **32**, 687-706, 1997.
- Hocking, W.K., and T. Thayaparan, Simultaneous and colocated observation of winds and tides by MF and meteor radars over London, Canada, (43°N, 81°W), during 1994-1996, *Radio Sci.*, **32**, 833-865, 1997.
- Hocking, W.K., T. Thayaparan and J. Jones, Meteor decay times and their use in determining a diagnostic mesospheric temperature-pressure parameter: Methodology and one year of data, *Geophys. Res. Lett.*, **24**, 2977-2980, 1997.
- Hocking, W.K., B. Fuller and B. Vandepeer, Real-time determination of meteor-related parameters utilizing new digital technology, *J. Atmos. Solar-Terr. Phys.*, in press, 2000.
- Jones, J., A.R. Webster, and W.K. Hocking, An improved interferometer design for use with meteor radars, *Radio Sci.*, **33**, 55-65, 1998.
- McKinley, D.W.R., *Meteor Science and Engineering*, McGraw-Hill, New York, 1961.
- Norton, A.P., *Norton's Star Atlas and Reference Handbook*, 16th ed., Gall and Inglis, Edinburgh, 1973.
- Sarma, T., and J. Jones, Double-station observations of 454 TV meteors, *Bull. Astron. Inst. Czech.*, **36**, 9-24, 1985.
- W.K. Hocking, Department of Physics and Astronomy, University of Western Ontario, London, Ontario, N6A 3K7, Canada. (whocking@julian.uwo.ca)

(Received November 2, 1999; revised March 31, 2000; accepted April 20, 2000.)

Meteor Analysis Laboratory.

The following notes pertain to a meteor analysis "hands-on" session.

They are extracted from a commercial manual kindly provided by MARDOC INC.

The software is copyrighted, and is loaned to this school. Some pages have been deliberately removed, so you should not be surprised to see missing pages.

THE SOFTWARE MAY NOT BE COPIED

OR EXTRACTED FOR USE AFTER THE SCHOOL.

IT IS ILLEGAL FOR YOU TO USE IT IN

ANY WAY OUTSIDE THIS LABORATORY, UNLESS

YOU PURCHASE THE PACKAGE.

Please respect this arrangement, and recognize that Mardoc Inc. has been very generous to permit this software to be used free-of-charge by the school.

W. Hocking

SKiYLINE

Introduction

The SKiYLINE analysis package is a series of programs designed to allow intensive analysis of the data produced by the SKiYMET radar system. It improves on some of the on-line analysis, and also introduces a large number of additional options, including composite day studies, harmonic analysis, Fourier transform and spectral studies, and meteor shower investigations.

The package works from a series of menus, and can operate under MSDOS, WINDOWS3.xx, WINDOWS95 and WINDOWS98 environments. At present, the program does not use the mouse to select options - it is keypad driven.

In WINDOWS mode, it operates as a DOS sub-window. It is necessary that ANSI.SYS be loaded by the config.SYS file. The DOS window is selected by clicking on the MSDOS icon, and you can toggle between a full screen mode and a smaller window within WINDOWSXX by pressing "alt + enter". You can select your window size with the selection option at the top right-hand corner of the window box. (If such a selection does not appear, click on the MSDOS icon in the top lefthand corner and select "toolbar" ; then choose your window size.) Often users find that a window size of 5 x 9 or 6 x 10 are good choices, and that the characters are large enough to read, but the window is small enough that it does not dominate the whole screen. To create a "shortcut" to MSDOS, select start, go to "programs", find MSDOS, right-click, and then select "create shortcut". Then drag the mouse down to the lower left hand corner of the screen and release. The MSDOS icon will now appear at the base of the screen, and you need only to click on this icon to enter MSDOS. If you are using WINDOWS and the Tcl-Tk option, plots may be terminated by clicking the "quit" button, whereupon you will be transferred to the next graph, or returned to the menu box. If using a DOS environment, return to the menu by simply pressing any key after you have finished surveying the graph. (See appendix E for installation of Tcl-Tk)

WELCOME TO SKIYLINE - Please select an option below.

1. Manipulation of *.mpd files (sort, merge, compress, expand).
 2. Plot Meteor Flux distributions vs. height, time and angle.
 3. Wind Analyses (time series, composite day, FFT, harmonic fit).
 4. Diffusion Coeff, Temperature (incl. Composite day, harmonics).
 5. Meteor Shower studies, source maps.
 6. Meteor Entrance Speed studies
 7. Plotting: user-selected windows, hard copies (PS or HPGL).
- E. EXIT PROGRAM.

MARDOC Inc.

Enter a selection:

The following pages will discuss the various menus available within the Skyline software.

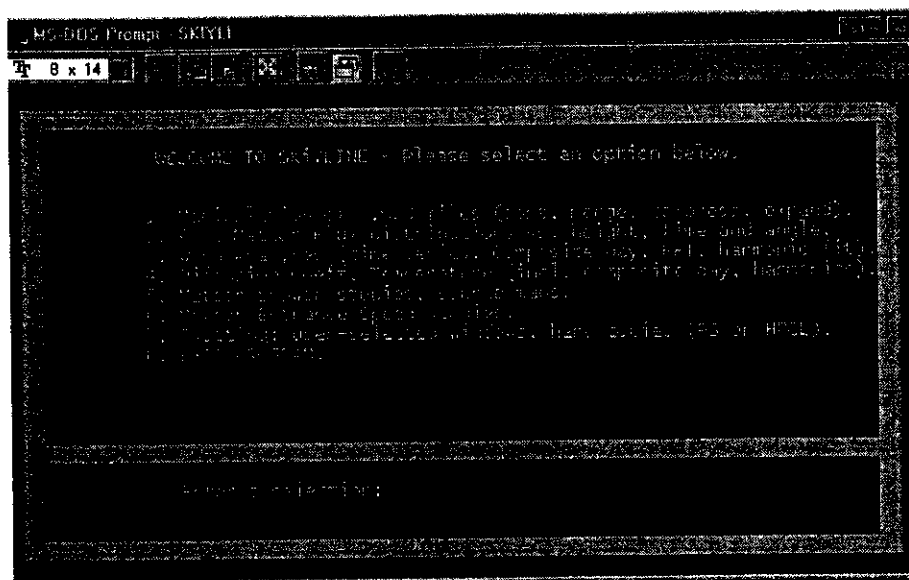
For each menu, a representative menu will be shown, like the one above. In reality, the menus look something like the picture on the next page, with different colour schemes being used for different menus. We will not produce pictures of *all* the screens. Actions are initiated by typing the number indicated (1 – 7 above or E to exit) followed by the return key. The selections shown above lead you to a group of secondary menus which allow a variety of analysis options.

The next few pages will sequentially follow through the various analyses available, discussing what they mean, what options are available, and showing sample graphs. Note that the graph will be produced for you by default, but if you want to display them again after the analysis is complete then you should use *option 7* and follow the instructions. *Option 7* may also be used to produce files which may be easily printed – either postscript or HPGL. It is the user's responsibility to transfer these files to the printer, but if you have a postscript printer, then a postscript file "file.ps" can be printed simply by typing "copy files.ps prn". If you use the HPGL files, a program like "Print-a-plot.Pro" can be used.

Note that if you are using the WINDOWS-based Tcl-Tk package, you can resize and move all plots by clicking and dragging with the mouse.

MARDOC Inc.

228



Sample selection menu.

The example shown above illustrates the selections available for the main menu. When the appropriate number is entered, the program will then progress to a second menu, which will allow the user to select various "local" options. These different "secondary" menus will now be described.

Special note in regard to plotting

You have a choice of various plotting options, which include DOS-type plots and Tcl-Tk plots. The former are generally much faster, and we recommend using DOS, EGA, VGA, SVGA or XGA. See appendices B and C for more details about how to select your option. If you work in DOS under WindowsXX, you will use a plotting display that automatically uses the full screen (though you can make it into a box within windows if you use alt-enter). If you use Windows and the Tcl-Tk option, you will use a plotting program that allows you to resize the window. See appendix E for installation of Tcl-Tk.

If you are using the Tcl-Tk option, the default background colour is green. If you prefer, you can change this to black or white. To do this, alter the file backgrnd.txt in c:\...\skiylin. In addition to being able to reset the size of the window you observe, you can also readjust the initial "startup size" to something of your own preferences. To do this, edit the file winsiz.txt in c:\...\skiylin and adjust lines 6 and 7 to suit (the first lines describe the changes needed).

MARDOC Inc.

In using the Windows-based Tcl-Tk plotting package you may find that there are occasional error messages, and at times the window re-sizing fails. These occurs due to problems in WINDOWS 95/98. You can fix them (at least in part) by altering the system performance and mouse response time.

To do this, you need to go to "Settings" and alter various features. To get to "Settings", right click on the background window and go to the "Active Desktop" and then "Customize My Desktop". Select "Settings" and follow through to "Performance". Alter the mouse performance to use less features. Alternatively, go to the "Start" menu button in the left-hand corner, and find "Settings" from there. You can also alter the mouse to have a slightly slower response time. Consult your Windows "Help" menu for more information about altering these features. None of these changes are needed if you use the DOS, VGA, SVGA or XVGA modes.

You may also find it useful to load a commercial program like XV or HYPERSNAP. These are available at quite low cost from a software source like www.download.com. They permit the user to "capture" any part of the screen, and save to jpg or bmp files. This can sometimes be useful if you want to send "quick-look" pictures across the internet, or post them on the web. So if you want this package, go to www.download.com igo to the "Search" bar, and type in

hypersnapDX

You can then download the file, and install it.

If you like the program, then you can order a full version (which avoids the system displaying a little advertisement tag everytime you capture something) by clicking on the "register" option in hypersnap. It really is quite cheap - about \$30 or so, I think. You can order it across the web.

Do not forget that you may also use **option 7** in the main menu to produce hardcopy plots.

MARDOC Inc.

How to exit in the event of a wrong entry

The menu tables are structured so that if you enter the wrong sub-menu, you just have to press "M" (lower or upper case) to return to the master menu. Once an operation is completed, the system returns to the master-menu. However, occasionally you may find that you accidentally enter a program by mistake e.g. you might type a "3" in a sub-menu instead of a "4", and suddenly realize that you are in the wrong program. The easiest way to exit is to type ctrl-C, and you will be asked if you wish to terminate the program. Answer yes. If this does not work, press ctrl-C and then ctrl-Z, and then the "return" key. This should also lead to a request from the computer for you to terminate the program. In some cases the program may then try and plot (non-existent) graphs, so you may get a blank screen with a white border. Just press "return" a few times and you should eventually be able to leave the program. You should then be back at the DOS prompt. Now re-type SKiYLINE (case-insensitive) and start again.

We will now turn to a discussion of the various menus, considering each successively.

1. FILE MANIPULATION

1. Show a directory listing.
2. Merge multiple successive files (mp_merge).
3. Sort into chronological order, delete duplicates (mtmsort).
4. Create file with selected zeniths and azimuths (sel_angl).
5. Create file with selected height intervals (sel_ht).
6. Sort into HOURLY order, for composite-day studies (sortid).
7. Compress files into compact-binary format (cmpr_met).
8. Expand files from compact-binary format (exp_met).
- M. Return to main menu.

MARDOC Inc.

Enter a selection: _

1. FILE MANIPULATION

It is possible to sort and organize the files according to different criteria, and this set of menus lets you do this. Firstly, remember that the files produced on the SKiYMET system are daily files – i.e. one for each day. But for processing the data, it is often better to work with monthly files. *Option 2* allows you to create monthly files in a simple manner.

Indeed, *option 2* should ALWAYS be run before starting any serious analysis. This is because the format used for most of the skyline analyses differs slightly from the format used to store the data. For example, the data are stored to milisecond accuracy, but the output of mp_merge is stored only to an accuracy of one tenth of a second. There are also various other subtle differences.

Thus you should always **STORE** the daily files produced by SKiYMET as a backup, but to apply the skyline software you need to first run the files through *option 2* (mp_merge). Alternatively, the monthly files can be created with mp_merge on the SKiYMET system. Either way, mp_merge must be applied to the data.

_____ MARDOC Inc. _____

Option 3 is also important. For strong meteor signals, duplicate detection of meteors can occur in adjacent range gates. It is also possible that the times of detection may not be chronological (e.g., a meteor at time 12 hr 36 min 11.4 s could occur in the original file prior to one at 12 hr 36 min 11.3s). Whilst not a serious issue, it is preferable that meteors appear sequentially in time. The user may specify how far apart in range two meteors must be to be considered as "different meteors".

Option 3 (mtmsort) sorts the data file to produce a chronological listing, and also ensures that each meteor is only listed once – if a meteor occurs at two adjacent range gates, for example, the one with the largest signal is chosen and the other one is removed.

Thus it is important to run mtmsort before any serious analysis is started.

Option 4 produces a similar output to **option 3**, but allows you to be more selective. For example, you may wish to generate a file which contains only meteors occurring in the northern sky. **Option 4** allows you to do this.

Option 5 allows further sorting. Whereas **option 4** allows you to specify selected zeniths and azimuths, this option allows you to select data according to chosen height intervals. Note you may combine **options 4 and 5** sequentially to permit selection of special angles and special heights - just use the output of one run as the input of the next.

Option 6 allows you the possibility to sort the data in a somewhat unusual, but very useful manner. Data are sorted into order of increasing hour, irrespective of the actual date. All files are given the same date – namely that of the first meteor detected. This special file then allows you to do a series of studies of so-called "composite days". A composite day gives, in effect, the "average" conditions as a function of time of day during the entire period of the file (or a designated sub-set of it). You will see applications of these files later in the notes.

Options 7 & 8 are compression and expansion utilities. They allow substantial data compression, which means that you can store data efficiently. This can also be important for transferring data from the SKiYMET system, since similar programs to these exist there, and you can transfer the data in a compressed format very quickly. By using **option 6**, and then applying a further generic compression utility like PKZIP, compression ratios of 5 and 6 are possible.

MARDOC Inc. _____

2. FLUX PLOTS

1. Show a directory listing.
2. Rates vs time, angle & height for selected 2 day period (mdis_dos).
3. Just plot meteor positions vs. angle for whole file (mdisn).
4. Position vs angle, but colour-coded for time-of-day (mdiscol).
5. Meteor positions vs. angle, but finer resolution (mdisdot).
6. Contour plot of angular distribution of meteors (met_cntr).
7. Flux rate vs time, user defined intervals/bin-sizes (fluxhres).
8. Save a file (e.g., ANALYS.PLT or MDIS.PLT) to a new name.
- M. Return to main menu.

MARDOC Inc.

Enter a selection: —

2. FLUX PLOTS

The above programs are generally designed for visualizing the meteor count rates in various ways. In general they do not produce files which are used by follow-up programs. There is one exception to this rule, and this arises if these programs are used to plot **unambiguous meteors only**. Then a file of **“unambiguous meteors”** is produced. This can be a useful file to have.

Other than this, the programs mainly produce plot files, with names of either ANALYS.PLT or MDIS.PLT or METCNT.PLT (the file names are usually indicated when you run the programs).

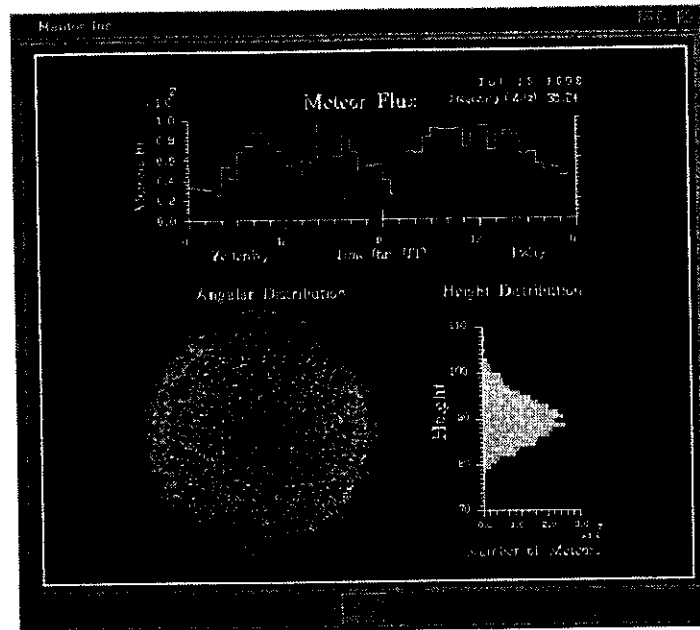
These displays are plotted as part of the process. If for some reason you wish to save any one of these plot files to a new name, use ***option 6*** above as soon as you have finished viewing the graph.

You may also view portions of these plots (i.e., “blow-up” selected sections) by going to ***option 7*** in the main SKiYLINE menu, and follow the instructions.

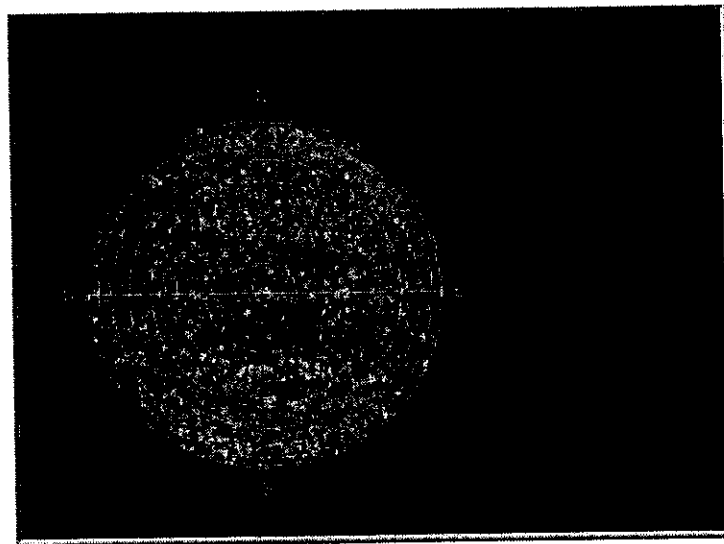
Examples of the types of plots which are available are shown in the following pages. The first picture shows an output of ***option 2***, and the second of ***option 3***. Subsequent pages ***show options 4, 5, 6 and 7.***

It should also be noted that the “fluxes” shown in the figures are **NOT** compensated for radar polar diagram selection effects, or angle of entry effects. Such corrections are often site-specific, and should be implemented by the user.

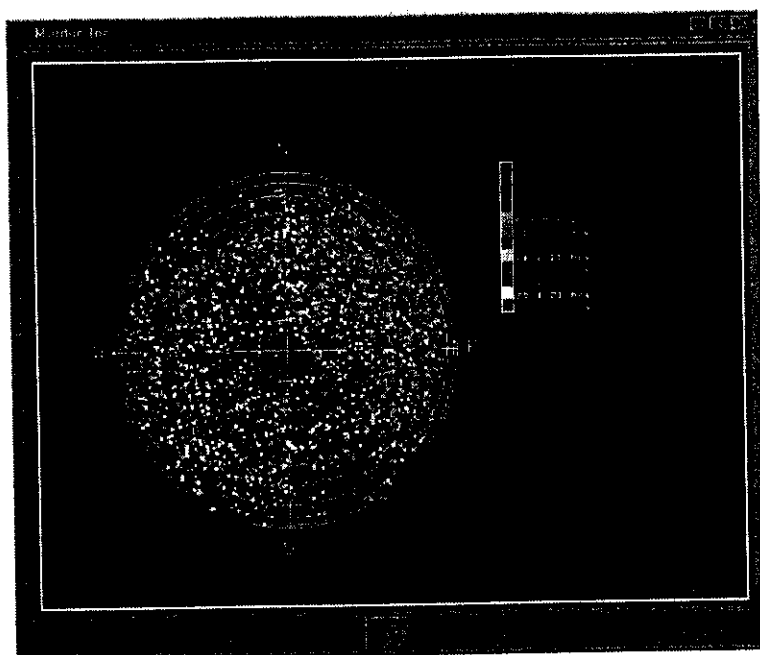
MARDOC Inc. _____



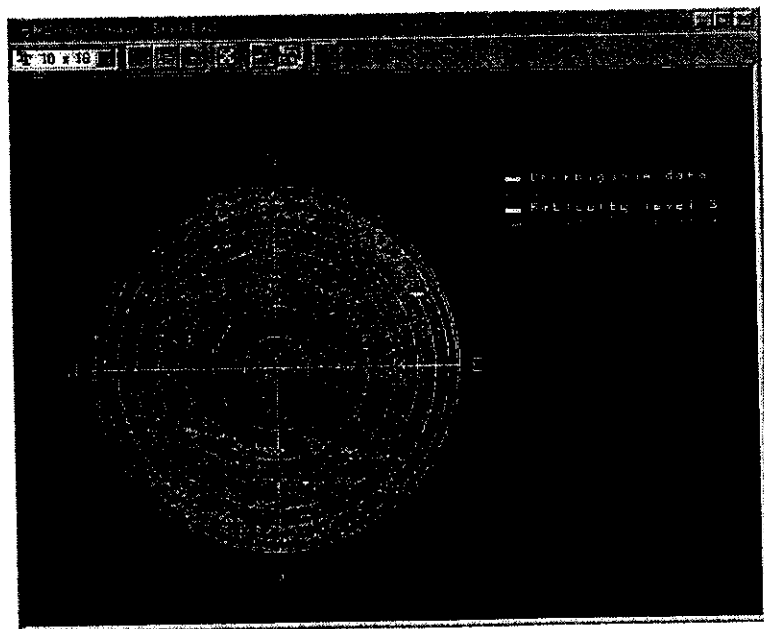
Sample output for *option 2*.



Sample output for *option 3*.



Sample output for *option 4*.

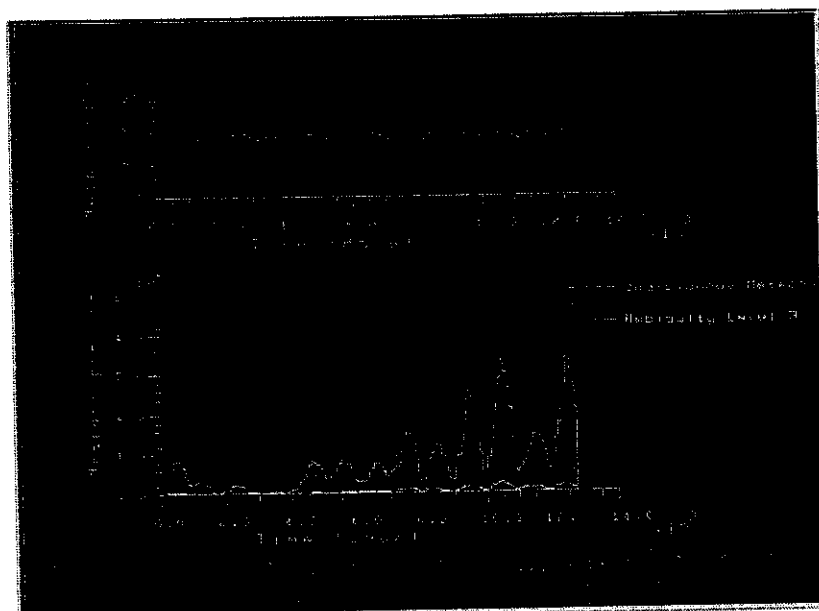


Sample output for *option 5*.

MARDOC Inc.



Sample output for option 6.



Sample output from option 7.

3. WIND ANALYSES

1. Show a directory listing.
2. Hourly winds (up to 1 month at a time: ndaywds).
3. Spectral analyses of winds (wds_fft).
4. Running power spectra (PS) over extended period (wd_runs).
5. Convert running PS-format to monochrome-compatible (wdrcnvt).
6. Composite Day studies of winds (tidal studies: me_tide).
7. Tidal harmonic fits to composite day winds (t_harmnc).
8. Combine all harmonic fit data for year to 1 file (tid_cnsc).
- M. Return to main menu.

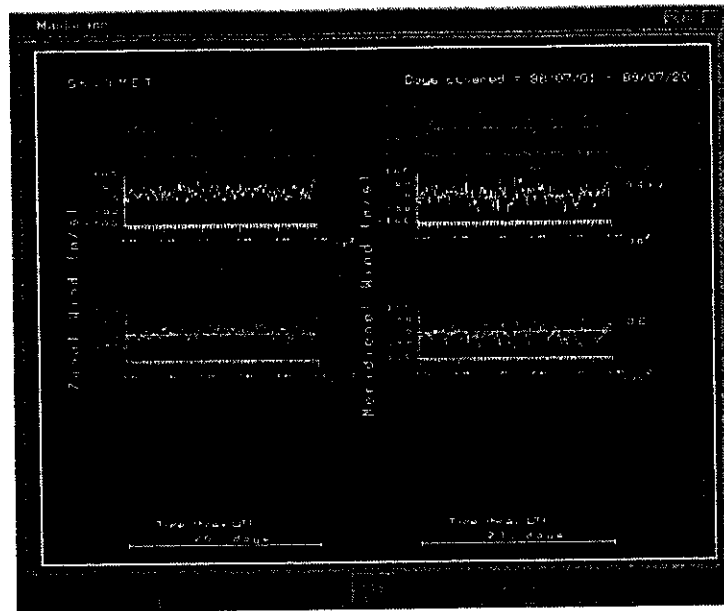
MARDOC Inc.

Enter a selection: _

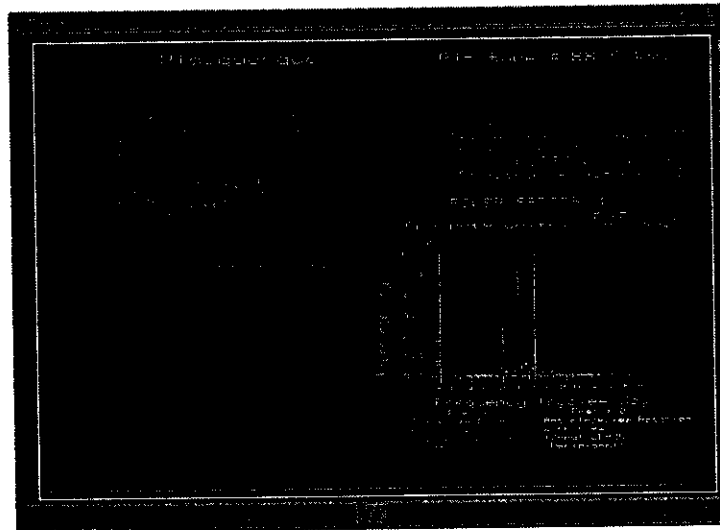
3. WIND ANALYSES

This menu guides you through a variety of analysis routines that are designed to work with wind data. The descriptions in the menu are largely self-explanatory. Typical outputs are demonstrated in the sample plots shown in the following figures. Note that option 2 contains a variety of options in regard to averaging intervals (in height and time), and also offers the possibility to determine vertical winds as well. However, we recommend caution with this parameter, since vertical winds using meteor radar determinations are notoriously unreliable.

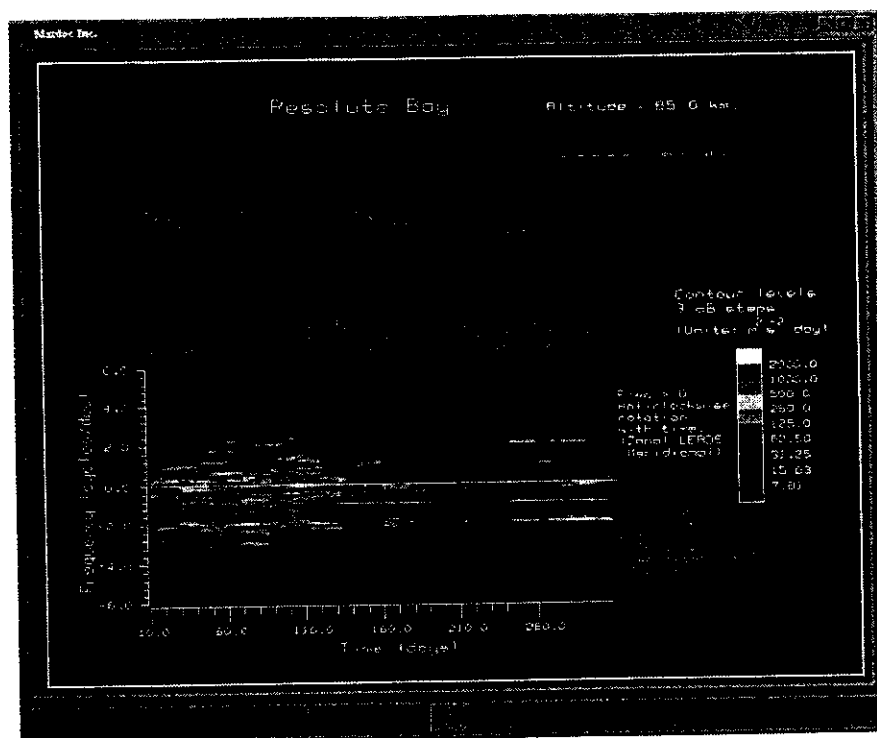
MARDOC Inc. _____



This graph shows a typical plot produced for *option 2*. Zonal winds occur to the left and meridional to the right. Hourly or two-hourly means may be selected. These means are also stored for further analysis on a file that you will name. Possible naming conventions will be offered in the program (see Appendix A).



This graph shows a sample spectral analysis of a discrete set of data (*option 3*). The raw data are shown to the left, and the spectrum occurs on the right. The user may select the height of the data, the window start point, window type, and also has a choice between analyzing components separately or performing rotary spectrum.

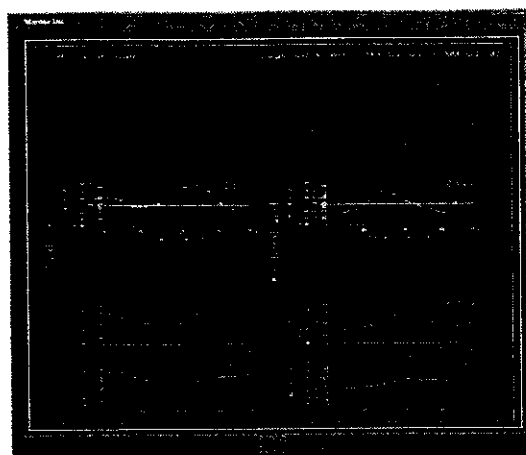


This contour graph shows a “running-power spectrum” of a segment of data at one designated height (*option 4*). The program is similar to *option 3*, but uses a window that slices through the data. A vertical cross-section through this graph gives similar information to that shown for *option 3*, but each new point on the time axis corresponds to a new start position for the window. Thus the user sees a “time-evolution” of the spectra. The user can select the height of the data, the window length, the window type and the step interval between successive windows.

The upper graph shows the mean winds as a function of time determined using the same window as for the spectra.

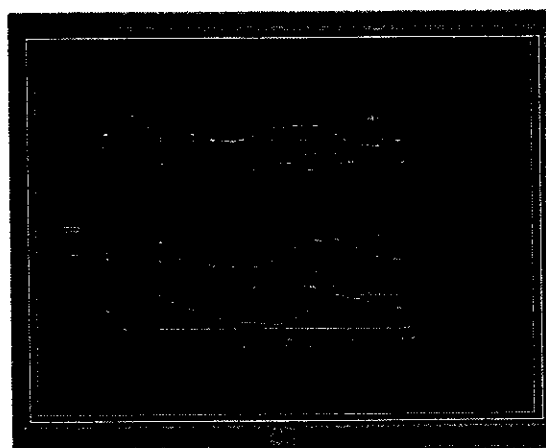
Options 3 and 4 also permit you to *store the processed spectral data*, as well as producing the plots shown above. The power spectral densities are stored in text format on the file *PS_STOR.TMP*. This file is erased and re-written each time these options are re-used, but if you want to save the file you can re-name the file to an appropriate new name of your own choosing, thereby saving the output.

MARDOC Inc.

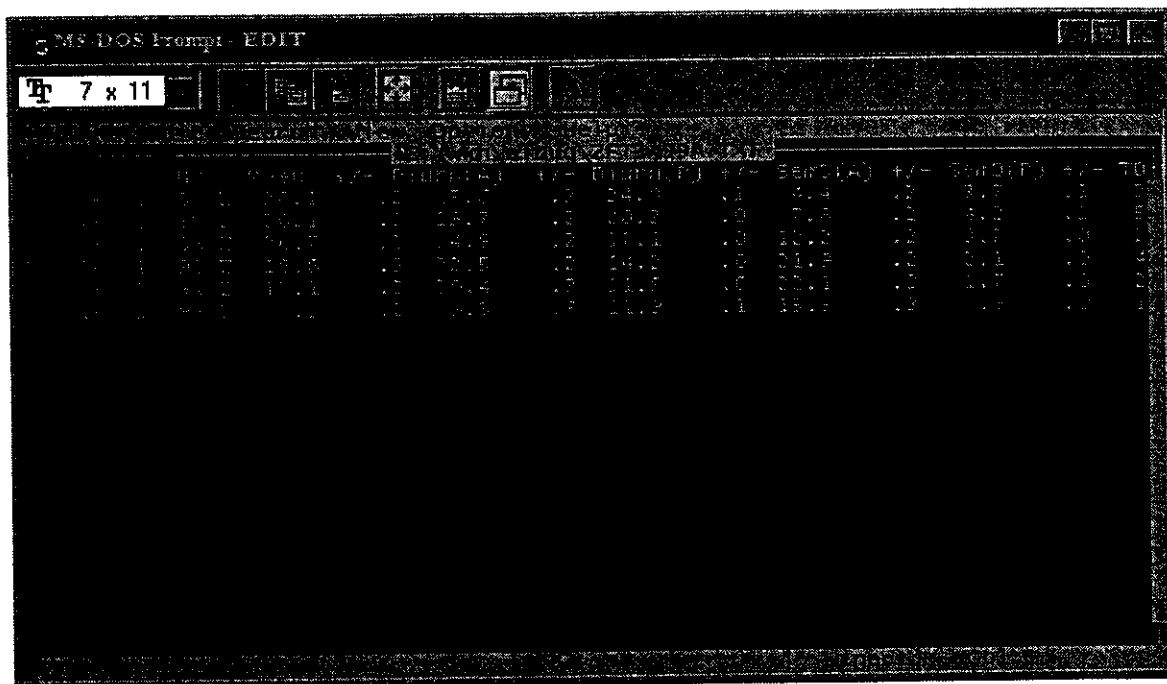


Option 5 does not produce a graph. Its purpose is to produce a grey-scale plot for use in generating a hard copy. The colour template used for this program is somewhat different from the "normal" one employed in the program **hardplt** (**option 7** in the main menu). Therefore, if you want to generate a grey-scale hard-copy of a graph created with **option 4** above, you should run **option 5** to produce a new file as the input to the "hard-copy" option in menu #7.

This set of graphs shows a typical output from **option 6**. It illustrates the mean winds as a function of time of day, averaged over an extended number of days (typically one month, or perhaps 10 days). The user may select the length of time over which such "composite days" are formed. These data can be determined by using the composite-day files that can be generated using menu #1, **option 5**. However, this particular program CAN also work with the original monthly data file – it is NOT necessary to use a composite-day file. (This is in contrast to composite-day studies of temperature related parameters (next menu) which do require this special composite-day file.)



This graph shows a typical output from the harmonic analysis option (*option 7*). The graphs look similar to those in *option 6*, but the output includes a file holding the fitted parameters and also shows an overlay of the best fit curves.



This table shows the results of the tidal fitting discussed in the previous figure. At this point, it is the user's responsibility to take these data and display them or further analyze them. A larger, more detailed file is also produced, but it is not shown here. It is partly described in **appendix A**. The user may choose to examine the outputs using a suitable editor.

Option 8 does not produce a graphical output. Its purpose is to combine all of the useful mean and tidal data into a single file. After you have performed tidal fitting to all the different months of the year, you will have a large number of files, and it can be difficult to usefully manage these data. By running this option, you will combine all this information into one, easily-read, file. This can serve as useful input to subsequent user-written analysis programs. However, in order to use this program, you **MUST** have adhered to the naming convention for the various files described in Appendix A, and within the various programs. If you chose to develop your own naming convention, you will not be able to employ this option. *Note that if you have missing monthly files (e.g. you have missing data for one or more months), the program will still run, but will simply store the data for these months as "missing", usually by using a number like -999 or 999 to store the points.*

The same program discussed above in regard to *option 8* can also be used to perform vector averages of tidal amplitudes and phases over several successive years. If you have a range of years (e.g. 1998 to 2001), the program will automatically find all of the relevant files for all these years (or for the range of years which you designate), and perform vector averages across these years for the tides, and calculate yearly averaged mean winds in both zonal and meridional components.

The output file can also be easily copied into a spread-sheet for further analysis.

4. DIFFUSION COEFFICIENT AND TEMPERATURE ANALYSES

1. Show a directory listing.
2. Time-series of temperature and diffusion coeffs (diffuse).
3. Sort into HOURLY order, for composite day studies (sortid).
4. Composite day studies of temps. (tidal studies) (diffuse).
5. Tidal harmonic fits to composite day data (t_harmnc).
- M. Return to main menu.

MARDOC Inc.

Enter a selection: _

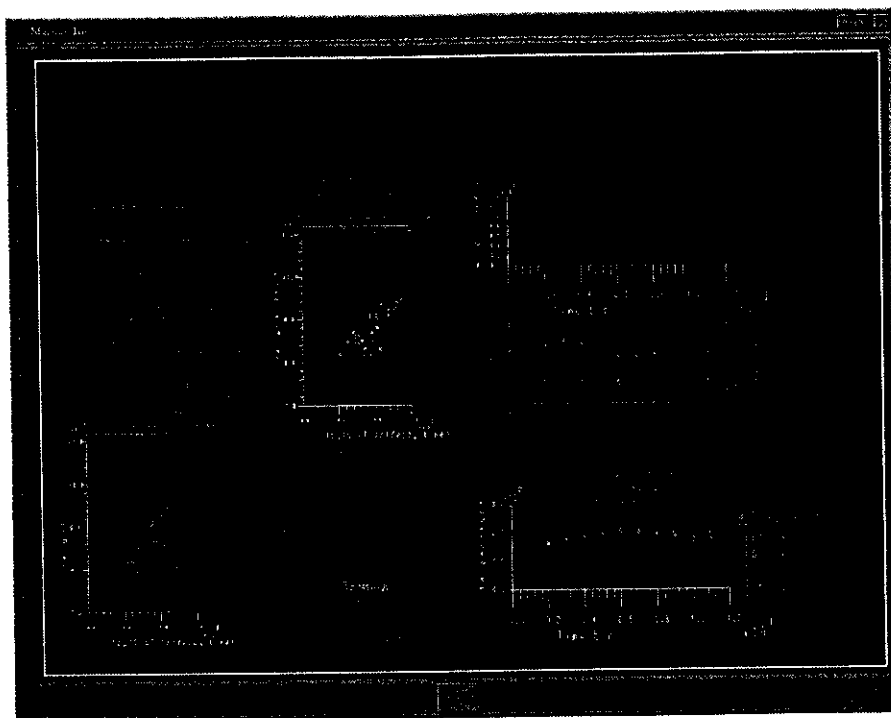
4. DIFFUSION COEFFICIENT AND TEMPERATURE ANALYSES

The following figure (next page) shows the typical output format produced in this class of analyses. It shows graphs of log (inverse decay time) vs height (bottom left), a density plot of the same (upper middle), and then a plot of diffusion coefficient vs height (bottom middle).

Normally the analysis is performed on successive data bins. For example, the bins might cover 4-day groups of data, or they might be composite-day data, with the first bin being the first 2 hours of data; and so forth. The three graphs just described refer ONLY to the data from the FIRST bin in the sequence. The graphs on the right hand side show information pertaining to ALL bins. For example, in the case above, the lower left hand graph shows the temperature as a function of time of day during a composite day. Note the oscillation over the course of the day, which relates to the tidal oscillations in temperature. The middle right-most graphs shows the ambipolar diffusion coefficient as a function of time (in this case time of day) – again, tidal oscillations are apparent. The top graph shows the numbers of meteors in each bin. If you intend to view graphs like the first three for a different bin number, re-run the program but choose your desired bin as the START time.

In the above example, we have demonstrated a typical composite day. This would result when using *option 4* (after first applying *option 3*). If, however, you had used *option 2*, you would have produced similar graphs, but the time axis would now be in days, and you would be able to examine planetary-wave oscillations in temperature.

MARDOC Inc. _____



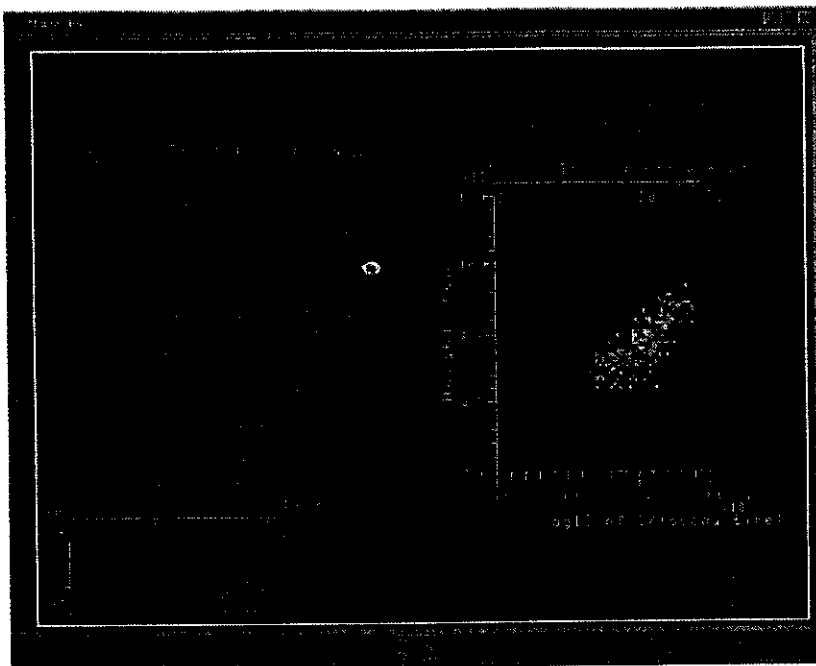
It should be noted that **option 3** here is in fact the same as **option 5** in the "File manipulation" menu: it is included here just to make it easier to access. It MUST be applied if you wish to do composite-day studies of temperature-related parameters.

When you choose one of the **options 2 or 4**, you produce graphs like the one shown above. However, it is often hard to see all the detail in all the graphs. Therefore, the program has been structured so that you will first see the whole set of graphs, as above. But then, after you have closed this plot, the program immediately shows you ANOTHER graph, but this time it is an expanded view of the upper middle graph. When this is closed, you are shown a view of the lower middle graph. When this is closed, you are shown expanded views of the right hand graphs. By using this strategy, you are able to see all the graphs in some detail.

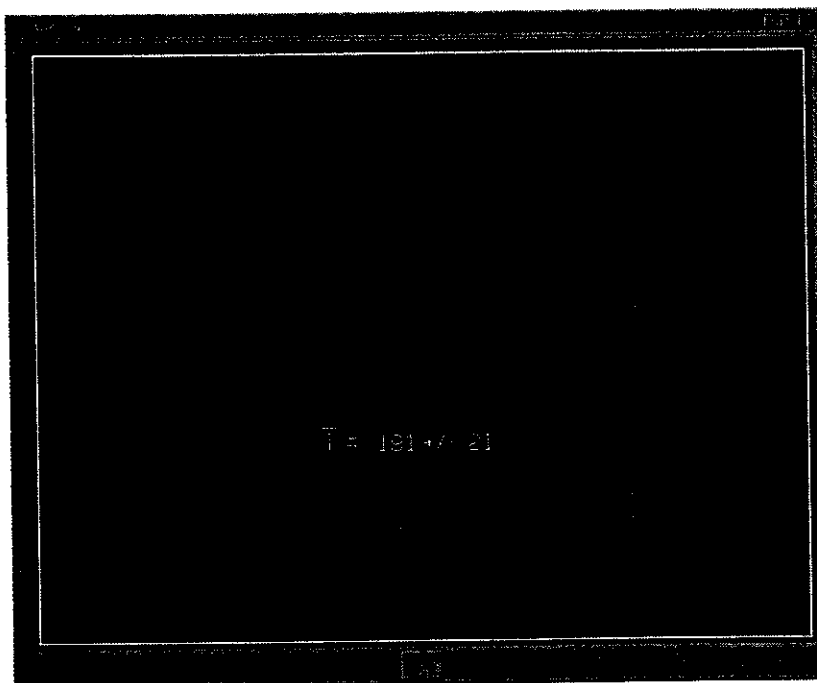
Examples of these "expanded views" are shown in the following figures.

Following these graphs, a text file is opened which holds information about the final diffusion coefficients and parameters. An example of this is shown shortly.

It is also possible to do harmonic fits to the various parameters produced by **options 2 and 4**. These harmonic fits can be produced by running **option 5**. This option also produces graphs, and tables of fitted parameters, but the graphs and tables are similar in format to those demonstrated earlier for harmonic fits to the winds. Hence, we do not show examples explicitly here.



Expanded view of the upper left-hand part of the main plot.



Expanded view of the plot of diffusion coefficient vs. height for the first bin.

MARDOC Inc.

Figure 1 is a scatter plot with a linear regression line. The vertical axis is labeled $\lg R_p$ and has major tick marks at 0, 1, and 2. The horizontal axis is labeled $\lg [I]$ and has major tick marks at 0, 0.4, 0.8, and 1.2. There are 12 data points plotted, showing a clear positive linear correlation. A solid line represents the linear fit, starting at approximately (0, 0.5) and ending at (1.2, 1.5). The equation for the line is $\lg R_p = 0.5 \lg [I] + 0.5$, and the correlation coefficient is $r = 0.99$.

```

MS-DOS Prompt - EDIT
7 x 11

      1. 2. 3. 4. 5. 6. 7. 8. 9. 10.
11. 12. 13. 14. 15. 16. 17. 18. 19. 20.
21. 22. 23. 24. 25. 26. 27. 28. 29. 30.
31. 32. 33. 34. 35. 36. 37. 38. 39. 40.
41. 42. 43. 44. 45. 46. 47. 48. 49. 50.
51. 52. 53. 54. 55. 56. 57. 58. 59. 60.
61. 62. 63. 64. 65. 66. 67. 68. 69. 70.
71. 72. 73. 74. 75. 76. 77. 78. 79. 80.
81. 82. 83. 84. 85. 86. 87. 88. 89. 90.
91. 92. 93. 94. 95. 96. 97. 98. 99. 100.
101. 102. 103. 104. 105. 106. 107. 108. 109. 110.
111. 112. 113. 114. 115. 116. 117. 118. 119. 120.
121. 122. 123. 124. 125. 126. 127. 128. 129. 130.
131. 132. 133. 134. 135. 136. 137. 138. 139. 140.
141. 142. 143. 144. 145. 146. 147. 148. 149. 150.
151. 152. 153. 154. 155. 156. 157. 158. 159. 160.
161. 162. 163. 164. 165. 166. 167. 168. 169. 170.
171. 172. 173. 174. 175. 176. 177. 178. 179. 180.
181. 182. 183. 184. 185. 186. 187. 188. 189. 190.
191. 192. 193. 194. 195. 196. 197. 198. 199. 200.
201. 202. 203. 204. 205. 206. 207. 208. 209. 210.
211. 212. 213. 214. 215. 216. 217. 218. 219. 220.
221. 222. 223. 224. 225. 226. 227. 228. 229. 230.
231. 232. 233. 234. 235. 236. 237. 238. 239. 240.
241. 242. 243. 244. 245. 246. 247. 248. 249. 250.
251. 252. 253. 254. 255. 256. 257. 258. 259. 260.
261. 262. 263. 264. 265. 266. 267. 268. 269. 270.
271. 272. 273. 274. 275. 276. 277. 278. 279. 280.
281. 282. 283. 284. 285. 286. 287. 288. 289. 290.
291. 292. 293. 294. 295. 296. 297. 298. 299. 300.
301. 302. 303. 304. 305. 306. 307. 308. 309. 310.
311. 312. 313. 314. 315. 316. 317. 318. 319. 320.
321. 322. 323. 324. 325. 326. 327. 328. 329. 330.
331. 332. 333. 334. 335. 336. 337. 338. 339. 340.
341. 342. 343. 344. 345. 346. 347. 348. 349. 350.
351. 352. 353. 354. 355. 356. 357. 358. 359. 360.
361. 362. 363. 364. 365. 366. 367. 368. 369. 370.
371. 372. 373. 374. 375. 376. 377. 378. 379. 380.
381. 382. 383. 384. 385. 386. 387. 388. 389. 390.
391. 392. 393. 394. 395. 396. 397. 398. 399. 400.
401. 402. 403. 404. 405. 406. 407. 408. 409. 410.
411. 412. 413. 414. 415. 416. 417. 418. 419. 420.
421. 422. 423. 424. 425. 426. 427. 428. 429. 430.
431. 432. 433. 434. 435. 436. 437. 438. 439. 440.
441. 442. 443. 444. 445. 446. 447. 448. 449. 450.
451. 452. 453. 454. 455. 456. 457. 458. 459. 460.
461. 462. 463. 464. 465. 466. 467. 468. 469. 470.
471. 472. 473. 474. 475. 476. 477. 478. 479. 480.
481. 482. 483. 484. 485. 486. 487. 488. 489. 490.
491. 492. 493. 494. 495. 496. 497. 498. 499. 500.
501. 502. 503. 504. 505. 506. 507. 508. 509. 510.
511. 512. 513. 514. 515. 516. 517. 518. 519. 520.
521. 522. 523. 524. 525. 526. 527. 528. 529. 530.
531. 532. 533. 534. 535. 536. 537. 538. 539. 540.
541. 542. 543. 544. 545. 546. 547. 548. 549. 550.
551. 552. 553. 554. 555. 556. 557. 558. 559. 560.
561. 562. 563. 564. 565. 566. 567. 568. 569. 570.
571. 572. 573. 574. 575. 576. 577. 578. 579. 580.
581. 582. 583. 584. 585. 586. 587. 588. 589. 590.
591. 592. 593. 594. 595. 596. 597. 598. 599. 600.
601. 602. 603. 604. 605. 606. 607. 608. 609. 610.
611. 612. 613. 614. 615. 616. 617. 618. 619. 620.
621. 622. 623. 624. 625. 626. 627. 628. 629. 630.
631. 632. 633. 634. 635. 636. 637. 638. 639. 640.
641. 642. 643. 644. 645. 646. 647. 648. 649. 650.
651. 652. 653. 654. 655. 656. 657. 658. 659. 660.
661. 662. 663. 664. 665. 666. 667. 668. 669. 670.
671. 672. 673. 674. 675. 676. 677. 678. 679. 680.
681. 682. 683. 684. 685. 686. 687. 688. 689. 690.
691. 692. 693. 694. 695. 696. 697. 698. 699. 700.
701. 702. 703. 704. 705. 706. 707. 708. 709. 710.
711. 712. 713. 714. 715. 716. 717. 718. 719. 720.
721. 722. 723. 724. 725. 726. 727. 728. 729. 730.
731. 732. 733. 734. 735. 736. 737. 738. 739. 740.
741. 742. 743. 744. 745. 746. 747. 748. 749. 750.
751. 752. 753. 754. 755. 756. 757. 758. 759. 760.
761. 762. 763. 764. 765. 766. 767. 768. 769. 770.
771. 772. 773. 774. 775. 776. 777. 778. 779. 780.
781. 782. 783. 784. 785. 786. 787. 788. 789. 790.
791. 792. 793. 794. 795. 796. 797. 798. 799. 800.
801. 802. 803. 804. 805. 806. 807. 808. 809. 810.
811. 812. 813. 814. 815. 816. 817. 818. 819. 820.
821. 822. 823. 824. 825. 826. 827. 828. 829. 830.
831. 832. 833. 834. 835. 836. 837. 8
```

MARDOC Inc.

Specifying the Temperature Gradient

The following comments pertain to *options 2 and 4*. In order to deduce temperatures, it is necessary that the program knows something about the mean temperature gradient in the vicinity of the peak in the meteor count-rate profile (see Hocking, *Geophys. Res. Letts.*, 26, 3297-3300, 1999). The program allows this to be determined in various ways. It includes a model as a function of latitude and season, or you may enter your own value. This latter option may be useful if you have other information about the gradient, such as might be obtained from a nearby lidar. Both these options are explained when you run the program. You get offered options of 'E' (for empirical), 'U' (for user-defined) and 'F'. The option 'F' requires some additional explanation.

In option 'F', you create your own, extra, input file which must be called *tgrad.txt*. It must exist in your working (data) directory. This file allows you to enter EITHER the actual gradients, OR the height of the mesopause (which is equally useful).

The file *tgrad.txt* has the following format.

First line either *meso* OR *grad* (ie first 4 letters must be *meso* or *grad*)

Successive lines include dates and a value ..

e.g.

meso

1999,4,15,89.0

1999,4,16,88.5

1999,4,17,87.0

etc

where the fourth element in the line is the parameter - in this case, the MESopause height.

If you want to specify gradients, use

grad

1999,4,15,-1.55

1999,4,16,1.5

etc.

MARDOC Inc.

Thus you may specify a different value of the mesopause height, or the temperature gradient, for each day. If you miss a day, the program will use the empirical formula.

If you want to set ALL data to the same, use

grad

-1,-1,-1,3.4

ie use -1,-1,-1 for year, month, day.

Note that the year is always a 4-digit year (different to the main program).

5. METEOR SOURCE MAPS

1. Show a directory listing.
2. Show source maps for specific period (rsource).
3. Show source maps but allow some data selection (sel_src).
4. Display possible radiants for a single chosen meteor (srce_1).
5. Save a file (e.g. ANALYS.PLT or MDIS>PLT) to a new name.
- M. Return to main menu.

MARDOC Inc.

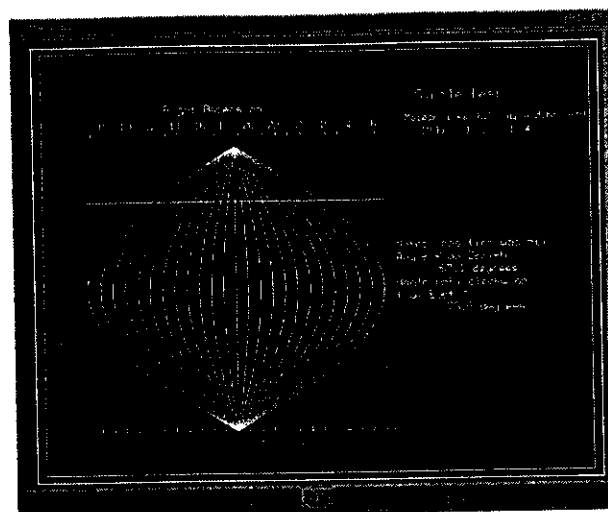
Enter a selection: _

5. METEOR SOURCE MAPS

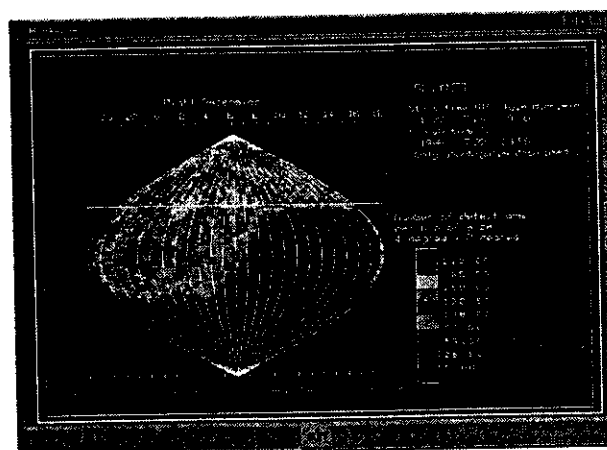
When a meteor is detected by a SKiYMET radar, it is not possible to determine exactly where the meteor came from (i.e., it is not possible to determine the radiant). However, we can determine a "great circle" in the sky, which we know includes the radiant – we just do not know where on the great circle the radiant occurs. **Option 4** allows the user to plot the "great circle". In fact, the program also determines if any of the "great circle" occurred below the horizon, and if it did, it eliminates such sub-sections as possible sources. The result of these determinations is a line that shows all the possible source radiants for a given meteor. **Option 4** displays this line-segment for any user-selected meteor (first figure on the next page). While it is not common for a user to use this plot, it is useful to be aware of this type of display, because it forms the basis for options 2 and 3.

Plotting all possible radiants for any one meteor produces a part-circle. However, if this is done for all meteors in a file, the resultant plots can look like the examples below. If, for example, there are some dominant sources in the sky, then the "great circle" from all these meteors will intersect at a common point – which determines the source radiant. **Option 2 and 3** produce such plots. **Option 2** uses all data, whereas **option 3** only accepts meteors that have "great circles" which pans through a user-specified area of the sky. Sample outputs of **option 2 and option 3** appear as the second and third figure on the following page.

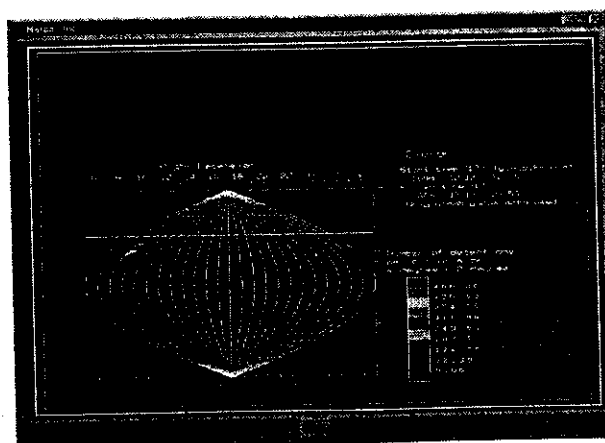
MARDOC Inc. _____



The plot above shows a region of possible source radiants for a particular user-designated meteor.



This is a sample "radiant source map". In this case there are several broad sources in the sky, with the strongest shown as the red and magenta sections below the celestial equator on the left-hand side.



This graph shows an example of an extremely strong meteor source- in this case the Geminids. The source map shows as a very tightly defined source, of very large count-rates, in the upper left of the map. The coordinates of the source are written out in the lower right-hand corner of the display.

6. METEOR ENTRANCE SPEED STUDIES

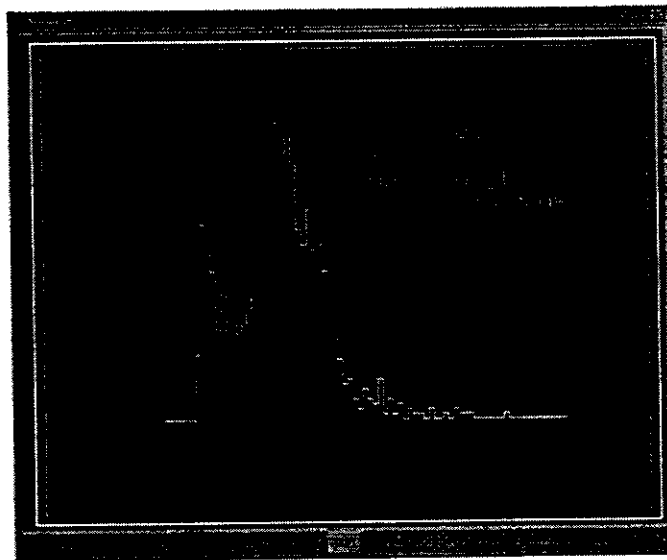
1. Show a directory listing.
2. Show histogram of entrance speeds (srtvmet).
3. Show scatter plot of entrance speeds vs height (srtvmet).
4. Show BOTH histogram and scatter plot (srtvmet).
5. Time evolution of histograms (srtvmet).
6. Save a file (e.g. VELVSHT.PLT) to a new name.
- M. Return to main menu.

MARDOC Inc.

Enter a selection: _

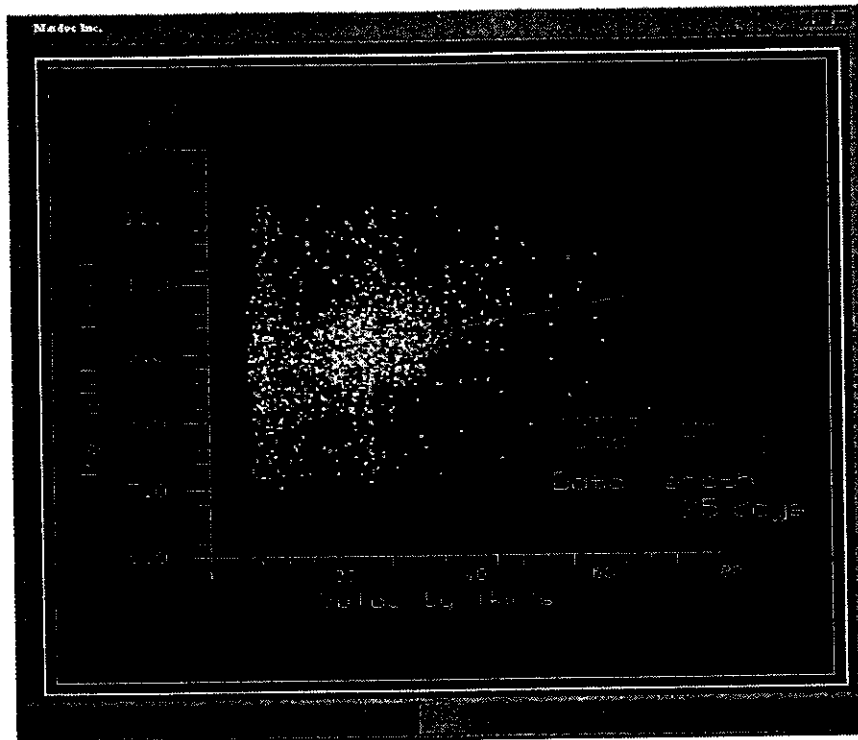
6. METEOR ENTRANCE SPEED STUDIES

These options allow the user to display information about the meteor entrance speeds, for those cases where such determinations were possible. The main forms are histograms and scatter plots. Examples are shown below.



Example histogram of meteor entrance speeds.

MARDOC Inc.



Typical scatter plot of meteor entrance speeds vs. height.

The two previous figures were produced by *options 2 and 3* respectively. If *option 4* is used, both plots are shown simultaneously.

Option 5 produces a variation on the histogram plots, in that it creates a “stacked plot” of successive histograms determined in successive bins of data. No example plot is shown: - the graph consists of a series of plots like that in the first figure, but displaced vertically from each other.

7. PLOTTING AND PRINTING OPTIONS

1. Show a directory listing.
2. Show a graph (*.plt) with user-selected windowing (splotVGA).
3. Produce a hardcopy of a *.plt file (postscript or HPGL).
- M. Return to main menu.

MARDOC Inc.

Enter a selection: _

7. PLOTTING AND PRINTING OPTIONS

These options allow you to:

- re-produce a display of any of the *.plt graphs which you have produced (often altered (usually enlarged) in size) – *option 2*
- and
- Produce files which may be easily transferred to a printer for plotting – *option 3*.

In *option 2*, the user can specify a region of the graph (in user co-ordinates) to be examined. Thus areas of interest can be expanded and viewed in more detail.

It is the users responsibility to transfer the output hard-copy files to the printer. This is often very easy. For example, if you use the postscript option and produce a file called file.ps, you can print it on a postscript printer by typing;

“copy file.ps prn”.

The HPGL file can be graphed in various ways. A commercial package called “print-a-plot pro” can be easily used, for example. Many commercial and drafting packages (e.g., CorelDRAW) accept HPGL files as input too. In fact, by importing these files into a program like CorelDRAW and making cosmetic changes, it is possible to produce very high quality (publication quality) graphs with complete flexibility in regard to adding special labels and annotations. Such operations are the user’s responsibility.

MARDOC Inc. _____

Detailed description of application of the plotting program which produces Post-script hard copies (sub-option 3).

Here is a sample run of the **hardplt** option (option 3) It is the case for production of a POSTSCRIPT output. Note only grey-scale options and black and white options exist in this version - if you want colour, use the HPGL option (see shortly).

I display the questions asked by the program (in italics) ,give typical answers (in bold) , and in some cases also give some description.

Do you want DEFAULT mode?
ie window border drawn, plot all points, fastest plotter
speed, no line segmentation, shading spacings
pre-defined, plot all colours
NOTE.. you will still be offered the option to select
the orientation and size of the plot space on the paper.
1 = YES, 0 = NO

1 <----- You should usually use the DEFAULT mode
 so enter 1 here.

DO YOU WANT Laser-postscript (L), HPGL (H) or Zeta (Z) PLOTTER?

L <----- L (or lower case L ie l) indicate that you want
 a laser-postscript output.

Enter name of file to be plotted (<60 chars)

ffff.plt <----- input file name

file ffff.plt <----- system confirms file name
opened

_____**MARDOC Inc.**_____

*Enter the name of the POSTSCRIPT file to be produced
this MUST have a ".ps" (lower case) extension*

ffff.ps <----- Name of file holding postscript output. Special note: in the HPGL option, the program asks for the OUTPUT file (*.hp) first, then asks for the input file ffff.plt. It is important to note this difference in the options -see later).

1
0
999999

Do you want to

*use program-defined plot-space on plotter page
with abscissa (x-axis) on long edge (horiz pge)[1]
with abscissa (x-axis) on short edge (vertical pge)[2]
or define your own plot-space (size and origin) [0]?
The default has origin as (0,0) with the
lengths as follows...*

long axis = 25.0, short axis = 15.0

*NOTE.. shading is done parallel to the
abscissa in the default*

1 <----- If you choose 1, you get the file printed in LANDSCAPE mode. If you use 2, you get PORTRAIT mode. I recommend just using 1 or 2 for now - avoid option 3.

25.000000 15.000000
*ORIGINS OF WINDOW ON PLOTTER = 0.000000E+00 0.000000E+00
WINDOW LENGTH,HEIGHT (USE SAME UNITS
AS USED IN PREPARING FILE (EG INCHES,CMS))*

50,50 <----- Enter window size here. This may vary between different plots, but I recommend using 50,50 to start with. If you find the output looks tiny, choose the window to be smaller e.g. 20,20. If you find the plot does not all fit on the page, choose a larger window. e.g. 80,50. If you want to decide the window size without printing the file, run menu 7, option 2 first, and experiment with the window size there. When you have it right, then run menu 7, option 3 (ie the program we are discussing here).

MARDOC Inc. _____

476

Note there MAY be times when you deliberately choose a smaller window, and use a non-zero origin, to produce an expanded view of a small part of the plot.

*WINDOW ORIGIN X,Y-----
THESE SHOULD BE COORDS W.R.TO FIRST ORIGIN
USED IN PLOT PROGRAM*

0,0 <----- Generally use 0,0 to begin with, but as you get more experienced, you may want to experiment with different window sizes and different origins (see comments above in relation to window size.

-----OK - that should be it. Now just copy your file to your postscript printer, or you can import it into ghostview if you have that.

Detailed description of application of the plotting program which produces HPGL hard copies (sub-option 3).

Here is a sample run of the *hardplt* option (option 3) It is the case for production of a HPGL output. This option may be in colour.

As in the post-script option, I display the questions asked by the program (in italics) ,give typical answers (in bold) , and in some cases also give some description.

There is a lot of similarity with the postscript version, but a few subtle differences exist too.

*do you want DEFAULT mode?
ie window border drawn, plot all points, fastest plotter
speed, no line segmentation, shading spacings
pre-defined, plot all colours
NOTE.. you will still be offered the option to select
the orientation and size of the plot space on the paper.
1 = YES, 0 = NO*

1 <----- Again, use default mode.

DO YOU WANT Laser-postscript (L), HPGL (H) or Zeta (Z) PLOTTER?

H <----- (or h) ... this chooses the HPGL mode.

You have chosen the HP option..

Do you want to

- A) use eavesdrop mode and print direct to printer*
- B) plot direct to the plotter from a PC via COM1*
- C) store the output on a HP-GL file ?*

C <----- Usually use option C. Options A and B applied when I used to use a pen plotter e.g. HP7470, but that is pretty rare nowadays. Normally one would save to a HP file, and then print the file using an intermediate program. For example,

you could use print-a-plot Pro. My preferred mode is to actually import the file into CORELDRAW!, which is a commercial graphics utility. (I actually use version 3.0, which is very old - dates back to 1994! But it works well. I think they are currently up to version 7.0 or 8.0 or even 9.0.

By using this HPGL option, I can import the file at the highest possible resolution (ie better than using a screen-capture process), and have great flexibility in what I do. I do most of my publications in this way, since I can produce very high quality and have the ability to label, change, shade etc. in any way I like. I find it much more flexible than IDL. I can copy in icons, special symbols, and all sorts of things. But there is a penalty, in that you need to learn how to use coreldraw. You can probably do similar things in other packages like clarisworks etc.

*Enter 1 if this will be printed to a paintjet
or 0 otherwise.*

*If you use 0, all pens (colours) will be set to a
number between 1 and 8, for monochrome plotting, or
for a 8-pen plotter.*

*If you use 1, all pens (ie colours) will be left
unchanged, so you can use up to 99 different colours.*

Enter 0 or 1

1 <----- Generally use 1 here.

Enter name of output HP-GL file

ffff.hp <----- ** Note that I enter the OUTPUT file BEFORE I enter the INPUT file!!
This is the OPPOSITE to the postscript version.

Enter name of file to be plotted (<60 chars)

ffff.plt <----- INPUT file. See note above about
order of input and output file.

file ffff.plt

opened

MARDOC Inc.

You are producing an output file.. it is not clear what device you will send this to, so you will have to set the spacing between lines when doing shading yourself here (e.g. 25 for HP plotter, 5 for HP laserjet laser printer, 6 for the Paintjet printer and 6 for postscript are good values). enter value of ispce1 (ispce2 will be 5x this)

- 6 <----- Generally use 5 or 6 here, for most modern applications. The shading is done as sweeps of a line across the page. There is one exception to using 6. I sometimes use a huge number like 10000. This ensures that a shaded section is NOT shaded! Why would I do this? Well, I do it if I intend to copy the file into coreldraw. I then use the coreldraw polygon-shading facilities to do my shading.

1
0
999999

*Do you want to
use program-defined plot-space on plotter page
with abscissa (x-axis) on long edge (horiz pge)[1]
with abscissa (x-axis) on short edge (vertical pge)[2]
or define your own plot-space (size and origin) [0]?
The default has origin as (0,0) with the
lengths as follows...
long axis = 25.0, short axis = 15.0
NOTE.. shading is done parallel to the
abscissa in the default*

- 1 <----- If you choose 1, you get the file printed in LANDSCAPE mode. If you use 2, you get PORTRAIT mode. I recommend just using 1 or 2 for now - avoid option 3.

25.000000 15.000000
ORIGINS OF WINDOW ON PLOTTER = 1.000000 1.000000
WINDOW LENGTH, HEIGHT (USE SAME UNITS
AS USED IN PREPARING FILE (EG INCHES, CMS))

MARDOC Inc. _____

50,50 <----- See comments in association with postscript version - same comments apply.

WINDOW ORIGIN X,Y-----

*THESE SHOULD BE COORDS W.R.TO FIRST ORIGIN
USED IN PLOT PROGRAM*

0,0 <----- See comments in association with postscript version - same comments apply.

Stop - Program terminated.

APPENDIX A

Proposed file-naming convention

The SKiYLINE package produces a larger number of files holding the various different sorts of processed data. Therefore it is advisable to have a good naming convention. The following is one possible recommendation (although of course you are free to make your own choice).

1. The first step in any analysis is usually to copy the daily files to your own working environment. On the SKiYMET radar system, these daily files are originally called: **mpyyyyymmdd.site.mpd**, where yyyy is a 4-digit year (e.g. 1999), mm is the month (as a number e.g. 08) and dd is the day of the month (e.g. 27).

For most of the analysis performed within SKiYLINE, it is recommended that you work with monthly files. You can either copy the daily files directly to your own working environment, and then merge them into monthly files, *or* you can merge the files into monthly files on the SKiYMET system itself. Either way, you will use the program *mp_merge* to do this. The program *mp_merge* described in association with menu # 1, is part of the SKiYLINE package.

Please note that the output of the program *mp_merge* has a slightly different format to the daily files. The daily files should be retained and stored in their original format, since they contain some extra information which is lost when transformed to monthly files, but nevertheless the monthly files contain all the information that is generally required to run the SKiYLINE software.

If you decide to copy the daily files, you might want to rename them as **MPyymmdd.DAT**, (or **MPyymmdd.MPD**), where yy is a 2-digit year (e.g. 98). Keep files from different sites in different directories. In these notes, we will assume a .DAT extension.

2. Next step is to run *mp_merge* (SKiYLINE menu 1, #2). We recommend that the output file from *mp_merge*, which usually holds all the data for one month, should have a name of the type **MPmmmyyS.DAT**, where mmm is a 2-character string describing the month (JAN, FEB, MAR, APR, MAY, JUN, JUL, AUG, SEP, OCT, NOV, DEC), yy is a 2-digit year (e.g. 98, 03 etc), and S is a character describing the site (e.g. use C for CLOVAR, R for Resolute Bay etc.). Thus a sample name might be **MPFEB98R.DAT**, where R stands for Resolute Bay.

Special Note... In the daily files, we recommend "mm" as a number, like 09 or 11. In all subsequent files, we recommend that the month be described by two or three letters e.g. JAN, FEB, or JA, FB, etc.

MARDOC Inc. _____

3. Although not mandatory, it is highly recommended that you next step is to run *mtmsort* (SKiYLINE menu 1, #3). This removes multiple detection of the same meteor at nearby range gates. The output file should use the same naming convention as described in step 2, but change the extension e.g. MPmmmyyS.DA1. **It is these sorted files which should be used for all subsequent analysis.** (Note that the sorting algorithm, *mtmsort*, also exists on the SKiYMET system, and can be run there).
4. You are now ready to apply the various types of display software, and the following paragraphs describe a proposed naming convention which you might find useful. Before we describe this convention in detail, however, there are various features common to the file-naming convention which need to be described.. We make frequent use of the month, and the following 2-character convention for the month is recommended. As a rule, the month is described by a 3-character alphabetic sequence (e.g. JAN, FEB etc.) for the files we have described up to now, but for all processed files we recommend a two-character descriptor according to the following table.

JA = January
 FB = February
 MR = March
 AP = April
 MY = May
 JN = June

JL = July
 AU = August
 SP = September
 OC = October
 NV = November
 DC = December

We will now describe the file-names recommended for the outputs of the various menus in turn.

5. Fluxes

As a rule, one normally examines the raw fluxes mainly for diagnostic purposes. These fluxes have not been normalized to take account of the polar diagram effects and angle of entry effects. Determination of such normalized fluxes is left to the user, since it is usually a fairly user-specific requirement. As such, the output files are normally only plot files (with standard names ANALYSIS.PLT (for mdis_dos), MSDIS.PLT (for mdisn, mdiscol, and mdisdot). Each new run overwrites any previous files. You are offered the chance to rename these files within the menu, if any particularly take your fancy, but since the programs can recreate these files any time very quickly, we do not offer any special naming convention.

6. Composite Data

Sometimes the data are re-sorted according to hour of day for the whole month (*sortid*). Typical file names are recommended as **HRmmyyS.DAT** or **HRmmyyS.DA1**, where HR stands for hourly data, mm is the 2-character month, yy is a 2-digit year, and S = site. We normally recommend using the same extension as that from which the file was derived. For example, if you produced the new file from MPJAN99R.DA1, make the new file HRJAN99R.DA1, etc.

7. Winds Analysis

We now consider the programs associated with analysis of wind information. We offer the following suggestions for the names. In some cases these names are offered as a suggestion within the various programs themselves.

(a) The first program to consider is *ndaywds*. This produces hourly (or 2-hourly) winds. The recommended file naming format is

WmmyyMS.TXT,

where the first "W" indicates that these are wind data, mm is a 2-character month, yy is a 2-digit year, the last M indicates that these are monthly data, and S is the site descriptor. If you analyze data lengths which are different to one month, you might want to replace the last M with some other indicator. In the main, however, we generally find that users use monthly data when applying *ndaywds*.

(b) Spectral analysis of winds (*wds_fft*)

The spectral analysis of the wind data often becomes a very extensive part of any serious analysis. It is natural to try many different data lengths, window types, heights, and so forth – it would be impractical for us to suggest a methodical scheme for naming these files. Therefore we do not offer any suggestions here.

(c) Running Power Spectra (*wd_runps*)

Similar comments apply as for *wds_fft*. We do not offer any suggested names here – it is just too complex, and user-specific.

(d) Composite day studies of the winds. (*me_tide*)

This program bins all data according to time of day, and produced a so-called "composite" day (sometimes called a daily superposed epoch). Both the Meridional and Zonal components are analysed simultaneously. It is common to analyze all the data from one month, but that is by no means mandatory. Data can be analyzed in lengths from one day to many days. Note that *me_tide* can work on *either* the MP*.DA1 files *or* the HR* files.

MARDOC Inc. _____

For the monthly analyses, we recommend file names

WCmmyyMS.TXT

WCmmyyMS.PLT

where the first W indicates winds, the "C" indicates **composite day** data, mm is the usual 2-character month, yy is the 2-digit year, the "M" indicates that the whole month of data was used to form these composite values, and S is the site-indicator in the usual way.

(e) Harmonic (tidal) fits to composite day data (*t_harmnc*).

Harmonic fits to the data produced by *me_tide* are provided by *t_harmnc* (winds version).

Meridional and Zonal components are analyzed separately. Two separate files are produced in each case - a very brief summary file, holding just the fitting information, and a larger file holding the original composite-day winds, the fitting parameters, and the hourly values which would be expected if the fitted function accurately represented the true winds.

We recommend the following names. Note that as a rule it is normal to analyze monthly data, but you may use other data-lengths. If you do this (e.g. analyze 10-day data strings) then you may need to make some refinements to these names.

The following are the names for the "fitted data files":

MFTmmyyS.TXT and **ZFTmmyyS.TXT**, where the first letter indicates MERIDIONAL or ZONAL winds, "FT" suggests "fitted parameters", mm is the usual 2-character month, yy is the usual 2-digit year, and S is the site-indicator.

The following are the names for the larger, more informative files:

MHCmmyyS.TXT and **ZHCmmyyS.TXT**, where the first letter indicates MERIDIONAL or ZONAL winds, "HC" suggests "HarmoniC" analysis output, mm is the usual 2-character month, yy is the usual 2-digit year, and S is the site-indicator.

The output plot files are recommended to have the same format as these previous *.TXT files, but with different extensions viz.

MHCmmyyS.PLT and **ZHCmmyyS.PLT**

MARDOC Inc.

8. Diffusion Coefficient of temperature studies

We now consider the programs associated with analysis of diffusion information. This relates to parameters deduced using the meteor decay times, and includes ambipolar diffusion coefficients, temperature, and temperature/pressure parameters. We offer the following suggestions for the names. Again we note that in some cases these names are offered as a suggestion within the various programs themselves.

- (a) Time-series of Temperature, Diffusion coefficients etc. (*diffuse*, standard mode).

Program *diffuse* clusters large numbers of decay time values into data-bins, and then performs fitting procedures on these in order to deduce temperatures, diffusion coefficients etc. Bins are usually fairly large in length, often being several days, because of the need for a large number of points (at least several hundred) per bin. This means that we can only use these data to study planetary wave activity and monthly and seasonal variability. More powerful systems may be capable of using bin-lengths of only a few hours if they have high enough count rates.

The output of program *diffuse* is recommended as **DmmyyMS.TXT** for the text output, and **DmmyyMS.PLT** for the plot files. Here, D indicates that these are diffusion-related parameters, mm is the usual 2-character month, yy is the two-digit year, the M following the yy indicates that these are data covering one whole Month, and S is the usual site-indicator.

- (b) Composite day studies of temperature and diffusion (*diffuse*, composite day studies (after running *sortid*))

This group of data is analagous to the winds output produced using program *me_tide*, in that it produces a “composite day” showing the variation over a “typical day” for the month. (As usual, you do not need to choose a full month – you can analyze shorter or longer segments.)

However, in *contrast* to *me_tide*, you *must* run *sortid* on the data to produce an HR* file (see earlier) – this type of output cannot be produced with doing that first.

We recommend the following naming convention.

DCmmyyMS.TXT and DCmmyyMS .PLT,

where the “D” indicates diffusion-related data, the “C” indicates that these are composite data, mm is the usual 2-character month, yy is a 2 digit year, the next “M” indicates monthly data (change it if you use other data lengths), and S is the site-indicator.

MARDOC Inc.

(c) Harmonic fits to composite day studies of diffusion-related measurements.

Harmonic fits to the data produced by *diffuse (composite day version)* are provided by *t_harmnc* (diffusion -version).

Ambipolar diffusion coefficients, temperatures and the parameter T/\sqrt{P} , are analyzed separately. Two separate files are produced in each case - a very brief summary file, holding just the fitting information, and a larger file holding the original composite-day data (be it temperature, ambipolar diffusion coefficient or T/\sqrt{P}), the fitting parameters, and the hourly values which would be expected if the fitted function accurately represented the true values.

We recommend the following names. Note that as a rule it is normal to analyze monthly data, but you may use other data-lengths. If you do this (e.g. analyze 10-day data strings) then you may need to make some refinements to these names.

The following are the names for the "fitted data files":

AFTmmmyS.TXT, **TFTmmmyS.TXT** or **SFTmmmyS.TXT**, where the first letter indicates Ambipolar diffusion coefficient, Temperature, or T/\sqrt{P} , "FT" suggests "fitted parameters", mm is the usual 2-character month, yy is the usual 2-digit year, and S is the site-indicator.

The following are the names for the larger, more informative files:

AHCmmmyS.TXT, **THCmmmyS.TXT**, or **SHCmmmyS.TXT**, where the first letter indicates Ambipolar diffusion coefficient, Temperature, or T/\sqrt{P} , "HC" suggests "HarmoniC" analysis output, mm is the usual 2-character month, yy is the usual 2-digit year, and S is the site-indicator.

The output plot files are recommended to have the same format as these previous *.TXT files, but with different extensions viz.

AHCmmmyS.PLT **THCmmmyS.PLT**, or **SHCmmmyS.PLT**

.....
Final Comment.

It must be emphasized again that the above suggestions cover only a small portion of the many different possible configurations which can be analyzed with this software. Studies of things like 10 day intervals, or 4 day intervals, and many other different combinations, are possible. We have concentrated on monthly data, which we consider is likely to be the most common form of analysis. Obviously there are limitations to the diversity of file names which can be achieved with a DOS operating system, and UNIX or WindowsXX versions of this software will permit greater flexibility with regard to naming conventions. On the other hand, an advantage of the DOS version is that it will run on almost any personal computer, including those with Windows and those without. You can also increase your flexibility by doing different types of analysis in different directories.

MARDOC Inc.

Appendix C

RUNNING THE SOFTWARE.

The following is a very brief summary of how to use the software. A much more extensive discussion (with lots of examples) can be found in the body of this manual, but this is intended as a "quick-start" option.

To run the software, go to the directory in which you have store your data. Open an MSDOS window (I am assuming you are familiar with this process - let Mardoc Inc. know if you are not), go to the data directory, and type **SKIYLINE**.

A menu should appear, which leads to a variety of sub-menus. Hopefully the menus are self-explanatory, but the main body of the manual explains them in much more detail. You then navigate between menus by typing the appropriate numbers.

Also note that I have made recommendations about how you should name the various files. They are described more fully in appendix A of the manual. You do not HAVE to follow these conventions, but it is advisable.

Normally, the following might be a typical sequence of events.

(Extra note - steps A to C can also be done ON THE SKIYMET RADAR, if you have the programs mp_merge and mtmsort on there. Let me know if you do not. It is in fact my own preference to do these processes on the SKiYMET radar itself.)

A. Collect all the data for a month from the radar. These will be separate daily files. They will have names like

mp19991031.sitename.mpd.

You probably should rename them to 8-characters, plus a .dat extension, on your DOS/windows95/98 machine. For example, you might rename the above file to

mp991031.dat

B. Merge all the files into a large monthly file. Use option 1 in the first menu, then option 2 in the next menu, and follow the instructions. Note that you should NOT have to type in all the file names if you make the right choices - you should only need to type the first file name and the number of files.

This will produce a monthly file.

MARDOC Inc._____

IMPORTANT NOTE THE DATA STORAGE FORMAT OF THIS FILE DIFFERS FROM THAT OF THE FILES FROM THE SKIYMET RADAR. THEREFORE YOU MUST ALWAYS FOLLOW THIS PROCESS ON ANY NEW DATA - OTHERWISE THE REST OF THE SOFTWARE WILL NOT RUN!

I recommend naming this file to *mpmmmyys.dat*, where *mmm* is a 3 letter month (e.g. Jun), *yy* is a 2-digit year (e.g. 98), and *s* is a site-indicator e.g. You might use "j" for Juliusruh, or "k" for Kuhlungsborn. Try and decide on a convention and stay with it.

e.g. the data for the month of November 1999 would be

mpnov99j.dat, where "j" stands for Juliusruh. Different users will use an appropriate character from their own site name.

I recommend saving the files from the skiymet radar in the raw form as a backup, but for utilizing the skyline software, you will always use the output files of *mp_merge*.

(If you want to do this step on the skiymet radar itself, simply run the program *mp_merge* on the SKiYMET system. As noted, this is my preference.)

C. The next step is advisable, although not crucial.

Go to the main menu, type 1, and then type 3 (sorting program). When the skiymet radar detects meteors, it sometimes makes duplicate detections of the same meteor at adjacent range gates. If you are using pulse-coding, you can get duplicate detections in the side-lobes. It is a good idea to remove all but the strongest of these multiple detections, and this is exactly what this program does. Just follow the instructions.

As a rule, I use the *mpmmmyys.dat* files as input, and name the output files using the same convention, but with the extension being **.da1**, not **.dat**. You are free to choose another convention here if you like.

MARDOC Inc.

D. OK - you are now ready to do some graphics.

At this stage, just try out some of the software. A good place to start is by pressing "2" at the main menu, which leads you into the flux display software. Choose various options within that submenu to see different types of flux displays. (If you are using the Tcl-Tk option, you can try resizing the windows, and things like that. If you are using the DOS options, try pressing Alt-ENTER - this should enable you to see the plot alternate between full-screen mode and as a window within the main screen.

Once you have played with this for a while, try some of the other menus. Note that menu 1 in the main menu leads to some file manipulation utilities, such as file compression, sorting utilities, selection utilities etc. I recommend you always keep the main mpmmyys.dal files handy, as backup, and create any new files as needed with these utilities.

Note also that some programs require that other programs have been run first. For example, in the winds sub-menu, you cannot run options 3 or 4 without running option 2 first.

I will not guide you through any more of the possibilities. You should just try some of the different options, and learn as you go. Consult the main section of the manual for more details.

Appendix D.

Setting up special files specific to your site.

The following files are crucial for system operation.

INSTRUCT.TXT (this file)

SKIYLINE.BAT

SORTID.BAT

DOS98NT.TXT

BACKGRND.TXT

FK0.TXT

WINSIZ.TXT

NONCOMMC.TXT

COMMERC.TXT (actually this is crucial for commercial operation, but can be removed for non-commercial operation).

1. Create a skiylin directory. It may be anywhere on any disk. e.g. it might be c:\master\skiylin or e:\skiylin or f:\master\skiylin etc.
2. Edit the following files, and change as described below.

Then copy the file skiyline.bat to EACH directory in which you intend to operate. If you create other analysis directories at a later date, also copy **skiyline.bat** to there.

a. skiyline.bat

skiyline.bat listing...

.....

```
@echo off
:loop
if exist semafor.txt del semafor.txt
rem *** the last 6 characters in the next line (skiyli) must be lower case!!!
c:\skiylin\skiyli
if exist semafor.txt goto exit
c:\skiylin\diskch
if exist semafor.txt goto exit
rem run runit.bat in the current directory
call runit
if exist semafor.txt goto exit
goto loop
:exit
if exist runit.bat del runit.bat
if exist semafor.txt del semafor.txt
@echo on
```

Action:

Change all occurrences of c:\
to the name of the directory above the skiylin directory
e.g. c:\ -----> d:\master
or whatever.

MARDOC Inc.

b. sortid.bat

sortid.bat listing...not listed

.....

but find the line

c:\skiylin\sorthrly

and change the sequence c:\
to the name of the directory above the skiylin directory
e.g. c:\ -----> d:\master
or whatever.

c. DOS98NT.TXT

Here is the file listing: alter the key line as described in the comments.

** Write DOS, EGA, VGA, SVGA, X VGA, 98 or NT below to indicate which operating
** system and screen resolution you have. This tells the program which plotting
** program to use. You CAN use DOS or EGA in all 3 cases, - they produce very
** fast, but lower resolution graphs, but can be reduced to a window. VGA, SVGA
** & X VGA produce high res., but cannot be reduced to a window. Use 98 & NT for
** windows (either - experiment). If you add 'RB' after the 98 or NT, you get
** a colour palette using only reds and blues... otherwise you get the default
** palette (more common). In DOS/*GA modes, you do not get a colour-palette
** choice. All text must be continuous (no blanks), CAPITALIZED, and left-
** justified. (maximum of 4 characters). All these comment lines must start
** with ** .. the program reads the first line which does NOT have a **.

XVGA

MARDOC Inc.

d. BACKGRND.TXT

Alter as described in comments. This is ONLY used if you use tcl-tk plotting (SPLOT98 or SPLOTNT).

Green

*** Specify the colour of the background used in SPLOT98 above.

*** Use either Green, Black or White.

*** First letter must be in the first column.

e. FK0.TXT

Here is the file listing. Alter as described.

File FK0.TXT - holds frequency and K0.

Next line is frequency (MHz) (line 4)

35.24

Next line is K0 (line 8)

2.5e-4

Parameter Description:

The radar frequency is self-explanatory.

Parameter K0: (see Hocking et al., GRL, Dec., 1997). The purpose of K0 is to relate the ambipolar diffusion coefficient, the pressure and the temperature through the relation $D_a = .0639 \cdot K0 \cdot (T^2/P)$. The quantity $.0639 \cdot K0$ is called K_{Ω} . The factor .0639 arises as a combination of terms involving the electronic charge, Boltzmann's constant, and standard temperature and pressure. In theory, the value should be about $K0 = 2.5e-4$, but in reality it seems to differ a bit from system to system. This is probably because pressure is such a strong function of height. There may also be some variation due to different ionic concentrations in different types of meteors.

MARDOC Inc.

4/4/24

The user should try and optimize this value of K0 for their own radar by adjusting it in such a way that the estimates of temperature produced

in the output file of the program DIFFUSE (menu 2, sub-menus 2 and 4), combined with the ambipolar diffusion coefficients produced there-in, produce pressures broadly compatible with the CIRA pressures at that height. (See the comments at the bottom of the output files from "diffuse").

f. WINSIZ.TXT

(This file is only used if you use the tcl-tk plot option.)

Comment: Alter the numbers below to alter the default WIDTH & HEIGHT (line 6)
Comment: and ORIGIN (line 8) of the window FIRST used in SPLOT98 or SPLOTNT.
Comment: (The origin co-ordinate is the position of the top left corner of
Comment: the window relative to the top left of the screen)
Comment: **** Do NOT remove these comment lines *****
800,600
50,50

END

